

Role of nuclear metabotropic glutamate receptor 5 in rat models of persistent pain

Kathleen Vincent

Department of Psychology

Faculty of Science

McGill University

Montreal, Quebec, Canada

December 2017

A thesis submitted to McGill University Faculty of Graduate and Postdoctoral Studies Office in partial fulfillment for the degree of Doctor of Philosophy in the Department of Psychology

© Kathleen Vincent, 2017

Table of Contents

Table of Figures.....	v
Abbreviations.....	vii
Abstract.....	xi
Résumé.....	xiii
Acknowledgements.....	xv
Contributions of authors.....	xvii
Introduction.....	1
Background.....	1
Metabotropic glutamate receptor structure and subtypes.....	3
Group I mGluR splice variants.....	4
Group I mGluR-linked intracellular messengers.....	5
DAG-mediated signalling pathway.....	7
IP ₃ -mediated signalling pathway.....	8
JNK pathway.....	8
G protein-mediated calcium oscillations.....	9
G protein-independent signalling.....	10
Group I mGluR scaffolding interactions.....	11
Group I mGluR agonists.....	13
mGluR5 antagonists and inverse agonists.....	16
Localization of mGluRs in the SCDH.....	20
Expression and regulation of mGluR5 following injury.....	21
Intracellular GPCRs.....	23
Nuclear mGluR5.....	25
Activating nuclear mGluR5.....	27
Excitatory amino acid transporters.....	27
Membrane permeability.....	30
Nuclear mGluR5 implications for pain.....	31
Involvement of EAATs in pain.....	33
EAAT inhibitors: Development and subtype selectivity.....	33

EAAT inhibitors and nociception	35
EAAT expression following injury	35
EAATs inhibitors in animals with persistent pain	37
Background on methodologies selected.....	42
Animal models of neuropathic pain	42
Animal models of inflammatory pain	45
Testing methods for assessing pain hypersensitivity	48
Methods.....	53
Animals.....	53
Neuropathic model: Spared nerve injury (SNI).....	54
Inflammatory model: Complete Freund’s adjuvant (CFA)	55
Materials	56
Drug administration	56
Nociceptive testing.....	57
Glutamate-induced pain behaviors	57
Mechanical allodynia testing.....	57
Conditioned place preference – SNI.....	58
Conditioned place preference – CFA.....	59
Immunohistochemistry	60
Tissue preparation	60
Staining protocol.....	60
Cell counting	61
Subcellular fractionation and western blot analysis.....	62
Tissue collection	62
Western blot.....	63
Microdialysis Sampling.....	64
Statistical analysis.....	64
Results.....	67
mGluR5 is increased in nuclear-enriched SCDH fractions of rats with neuropathic pain	67
mGluR5 is increased in nuclear-enriched SCDH fractions of rats with inflammatory pain	70
Nuclear mGluR5 increased by one day following SNI surgery.....	74

Nuclear mGluR5 increased by one day following CFA injection	76
Spinal glutamate induces pain behaviors in rats	79
Glutamate induces greater Fos expression in the SCDH of rats with persistent pain	82
Glutamate induces greater Jun expression in the SCDH of rats with persistent pain	84
Blocking neuronal glutamate uptake is antinociceptive in animals with neuropathic pain	86
Blocking neuronal glutamate uptake is antinociceptive in animals with inflammatory pain	89
Neuronal EAAT inhibitors attenuate mechanical allodynia in neuropathic animals	91
Neuronal EAAT inhibitors produce conditioned place preference in SNI and CFA animals, but not naïves.....	92
EAAT3 inhibitors attenuate glutamate-induced Fos expression	97
EAAT1 and 2 inhibitors potentiate glutamate-induced Jun expression in inflamed and control animals	99
Permeable mGluR5 antagonists are effective at attenuating glutamate-induced pain in neuropathic animals	101
Permeable mGluR5 antagonists are effective at attenuating glutamate-induced pain in inflammatory animals	103
Permeable mGluR5 antagonists reduce mechanical allodynia in neuropathic animals more effectively than non-permeable mGluR antagonists.....	106
Permeable mGluR5 antagonists produce conditioned place preference in neuropathic and inflamed animals	107
Permeable mGluR5 antagonists attenuate glutamate-induced Fos expression	110
Permeable and non-permeable mGluR antagonists attenuate glutamate-induced Jun expression .	112
Discussion.....	114
Selective upregulation of nuclear mGluR5 following persistent pain	115
Functionality of nuclear mGluR5	119
Inflammatory and neuropathic pain is associated with glutamate hyperalgesia.....	121
Intracellular glutamate is pronociceptive in persistent pain conditions	124
Pronociceptive effect of glial EAAT inhibitors	124
Antinociceptive effect of neuronal EAAT inhibitors	125
TBOA	129
Alternative hypotheses for the EAAT inhibitor paradox.....	130
Inverse EAAT hypothesis	130

Glutamate-induced neurotoxicity hypothesis.....	131
Presynaptic glutamate hypothesis	132
Antagonizing intracellular mGluR5 is antinociceptive in persistent pain	133
LY393053 and Fenobam: Permeability.....	133
Behavioral differences between permeable and non-permeable antagonists	135
Fos and Jun expression following permeable and nonpermeable antagonists	138
Location-dependent signaling of mGluR5	139
Intracellular glutamate	141
Origin of nuclear mGluR5	142
Homer1 proteins as mGluR scaffolds	143
Nuclear mGluR5: Involvement in other pathologies?.....	145
Experiment Limitations	146
Future directions	149
Conclusions.....	153
References	156
Appendix I: Vincent et al. 2016.....	177

Table of Figures

Figure 1. mGluR5 signalling cascade.....	6
Figure 2. Scaffolding proteins interacting with mGluR5.....	11
Figure 3. Orientation of mGluR5 on cell surface and nuclear envelope.	25
Figure 4. Ion coupling in EAATs.....	27
Figure 5: Neuronal versus glial glutamate transporter inhibitors.	40
Figure 6. Permeable versus non-permeable mGluR5 antagonists.	42
Figure 7. Conditioned place preference apparatus..	52
Figure 8. Spared Nerve Injury Model.....	55
Figure 9. mGluR5 is increased in nuclear fractions in SNI animals.....	69
Figure 10. mGluR5 is increased in nuclear fractions in CFA animals.....	73
Figure 11. Time course of the changes in subcellular localization of mGluR5 following SNI.....	75
Figure 12. Time course of the changes in subcellular localization of mGluR5 following CFA.....	78
Figure 13. Dose Response curve of glutamate on nociceptive behaviors in SNI and CFA animals.....	81
Figure 14. Glutamate-induced Fos expression in SNI and CFA SCDH.....	83
Figure 15. Glutamate-induced Jun Expression in SNI and CFA SCDH.....	85
Figure 16. EAAT3-specific inhibitors are analgesic in SNI animals.....	88
Figure 17. EAAT3-specific inhibitors are analgesic in CFA animals.....	90
Figure 18. Neuronal EAAT inhibitors reduced mechanical allodynia in SNI rats and glial EAAT inhibitors produce mechanical allodynia in sham rats.....	92
Figure 19. Conditioned place preference of neuronal and glial EAAT inhibitors on SNI and naïve animals.....	94
Figure 20. Conditioned place preference of neuronal and glial EAAT inhibitors in naive and CFA animals.....	96
Figure 21. Neuronal, but not glial, EAAT inhibitor attenuates glutamate-induced Fos expression.....	98
Figure 22. Glial EAAT inhibitor potentiates glutamate-induced Jun expression in control and inflamed rats.....	100
Figure 23. Permeable mGluR5 antagonists attenuate glutamate-induced pain behaviors in neuropathic animals more effectively than non-permeable mGluR5 antagonists.....	102

Figure 24. Permeable mGluR5 antagonists attenuate glutamate-induced pain behaviors in inflamed animals.....	105
Figure 25. Permeable mGluR5 antagonists attenuate mechanical allodynia in neuropathic animals more effectively than non-permeable group I mGluR antagonists.	107
Figure 26. Permeable, but not non-permeable, mGluR5 antagonists produce conditioned place preference in neuropathic and inflamed animals.	109
Figure 27. Permeable, but not non-permeable, mGluR5 antagonists attenuate glutamate-induced Fos in the SCDH.	111
Figure 28. Permeable and nonpermeable mGluR antagonists attenuate glutamate-induced Jun in the SCDH.....	113
Figure 29. Schematic summary illustrating the effect of targeted mGluR5 treatments on neuropathic and inflammatory pain.....	154

Abbreviations

AMPA	α -amino-3-hydroxy-5-methyl-4-isoxazolepropionic receptor
AP-1	Activator protein 1
Arc/arg3.1	Activity-regulated cytoskeleton-associated protein
ATP	Adenosine triphosphate
C-terminus	Carboxyl terminal end
Ca ²⁺	Calcium
CaM	Calcium-modulated protein, calmodulin
CaMK	Calcium/calmodulin-dependent kinases
CaMKII	Calcium/calmodulin-dependent kinase II
cAMP	Cyclic adenosine monophosphate
CCI	Chronic constriction injury
CFA	Complete Freund's adjuvant
CNS	Central nervous system
CPP-I	Conditioned place preference index
CREB	Cyclic adenosine monophosphate responsive element binding protein
CT	Complete transection
DAG	Diacylglycerol
DHK	Dihydrokainate
DRG	Dorsal root ganglion
EAAT	Excitatory amino acid transporter

EGF	Epidermal growth factor
EPSP	Excitatory post-synaptic potential
ER	Endoplasmic reticulum
ERK1/2	Extracellular signal-regulated kinase 1 and 2
GAPD	Glyceraldehyde 3-phosphate dehydrogenase
GDP	Guanosine diphosphate
GPCR	G protein-coupled receptor
GTP	Guanosine triphosphate
HDAC-1	Histone deacetylase 1
i.p.	Intraperitoneal injection
i.pl.	Intraplantar injection
i.t.	Intrathecal injection
IFA	Incomplete Freund's adjuvant
iGluR	Ionotropic glutamate receptor
IP ₃	Inositol 1,4,5-trisphosphate
JNK	c-Jun N-terminal kinase
kDa	Kilo Dalton
L4,L5,L6	Lumbar segment 4,5,6
L-TBA	L- β - <i>threo</i> -benzyl-aspartate
MAPK	Mitogen activated kinase
MEK	Mitogen activated kinase kinase
mGluR	Metabotropic glutamate receptor

mRNA	Messenger RNA
N-terminus	Amino terminal end
NMDA	N-methyl-D-aspartate receptor
N-Cad	N-Cadherin
PIP ₂	Phosphatidylinositol 4,5-biphosphate
PKA	Protein kinase A
PKC	Protein kinase C
PLC	Phospholipase C
pSNL	Partial spinal nerve ligation
PWT	Paw withdrawal threshold
RACKs	Receptors for activated C kinases
RASGRP	RAS guanyl-releasing protein 1
RGS	Regulators of G protein signaling
s.c	Subcutaneous injection
SCDH	Spinal cord dorsal horn
SNI	Spared nerve injury
SNL	Spinal nerve ligation
SNT	Spinal nerve transection
Src	Sarcoma
TBOA	DL- <i>threo</i> - β -hydroxyaspartate
VGLUT	Vesicular glutamate transporters
VRT	Ventral root transection

WAY/UCPH	WAY213613 and UCPH-101
X_{ct}	Cysteine/glutamate exchanger

Abstract

Metabotropic glutamate receptor 5 (mGluR5) is an excitatory G protein-coupled receptor present in the spinal cord dorsal horn (SCDH), where it has a well-established role in pain. In addition to its traditional location on the cytoplasmic membrane, recent evidence shows that this receptor is present on intracellular membranes, and in particular, on the nucleus. Importantly, previous *in vitro* studies reveal nuclear mGluR5 is capable of binding glutamate following its intraneuronal transport through the neuronal glutamate transporter, excitatory amino acid transporter 3 (EAAT3), and producing nuclear calcium responses, implicating it in cell signaling. This thesis presents evidence that mGluR5 is present on the nuclear membranes of SCDH neurons, and is selectively increased on nuclear membranes in rodent models of inflammatory and neuropathic pain, where it has a functional role in nociceptive signaling. This hypothesis is defended using a program of studies involving the pharmacological manipulation of binding at these intracellular receptors. It is demonstrated that blocking glutamate transport into neurons with an EAAT3 inhibitor attenuates glutamate-induced pain behaviors and *c-fos* expression, alleviates mechanical allodynia, and produces a conditioned place preference in inflamed and neuropathic animals. In contrast, preventing glutamate reuptake through glial EAATs has the opposite effect in both persistent pain and control conditions. Importantly, these results also provide an explanation for previous paradoxical effects of the non-selective EAAT inhibitor, TBOA, in persistent pain. It is also demonstrated that permeable mGluR5 antagonists are more effective than non-permeable antagonists at attenuating glutamate-induced pain behaviours and *c-fos* expression and alleviating mechanical allodynia in inflamed and neuropathic animals. Interestingly, antagonizing plasma membrane receptors attenuates glutamate-induced *c-jun* expression, indicating the importance of diverse location-dependent mGluR5 signaling pathways. Taken together, these findings implicate a

novel, intracellular pool of mGluR5 in nociceptive signaling under persistent pain conditions, which presents a potential therapeutic target for chronic pain.

Résumé

Le sous-type mGluR5 du récepteur glutamatergique métabotrope est un récepteur excitateur, associé à la protéine G et présent dans la corne dorsale de la moelle épinière où il a un rôle bien établi dans la douleur. En plus de son emplacement connu sur la membrane cytoplasmique, des observations récentes indiquent que ce récepteur est également présent sur les membranes intracellulaires, et en particulier sur la membrane du noyau cellulaire neuronal. Il est important de noter que des études *in vitro* ont révélé que le mGluR5 nucléaire se lie avec le glutamate après son transport intracellulaire par le transporteur de glutamate, le transporteur d'acide aminé excitateur 3 (EAAT3) et affecte le calcium nucléaire, démontrant ainsi son rôle dans la signalisation cellulaire. Cette thèse soutient que le mGluR5 intracellulaire exerce un rôle dans la signalisation nociceptive en démontrant que le mGluR5 est présent sur les membranes nucléaires des neurones de la corne dorsale de la moelle épinière et que sa présence est accrue de façon sélective sur les membranes nucléaires chez des animaux souffrant de douleur inflammatoire et neuropathique. Cette hypothèse est aussi vérifiée par la manipulation pharmacologique de l'accès du glutamate à ces récepteurs mGluR5 intracellulaires, qui démontre que le blocage du transport du glutamate dans les neurones par des inhibiteurs EAAT3 atténue les comportements nociceptifs et l'expression de c-fos induite par l'application de glutamate, qu'il atténue aussi l'allodynie mécanique et qu'il produit une préférence de place conditionnée chez des animaux en état de douleur inflammatoire ou neuropathique. Par contre, la prévention du recaptage du glutamate par l'antagonisme des transporteurs membranaires de glutamate gliaux produit une réponse nociceptive chez des animaux sains ou en état de douleur. Il est important de noter que ces résultats fournissent une explication des effets paradoxaux de l'inhibiteur non sélectif du transporteur de glutamate, le TBOA, sur la douleur. Il est aussi démontré que des antagonistes du mGluR5 perméables à la membrane

plasmique sont plus efficaces que des antagonistes non perméables à atténuer les comportements douloureux induits par le glutamate et l'expression de c-fos, à soulager l'allodynie mécanique et à produire une préférence de place conditionnée chez des animaux en douleur inflammatoire ou neuropathique. Il est intéressant de noter que l'antagonisme des récepteurs membranaires plasmatiques atténue l'expression du c-jun induite par le glutamate, ce qui indique que l'importance des voies de signalisation liées au mGluR5 dépend de la localisation cellulaire du récepteur. Globalement, ces résultats identifient un nouveau pool intracellulaire de mGluR5 impliqué dans la signalisation nociceptive reliée aux conditions de douleur persistantes. Celui-ci présente une cible thérapeutique potentielle pour la douleur chronique.

Acknowledgements

I would like to extend my thanks to the many people who made this dissertation possible. First and foremost, I would like to acknowledge my supervisor, Dr. Terence Coderre, for his academic support and guidance over the course of my graduate studies. I am sincerely grateful to have had the opportunity to be a member of his lab. His encouragement and enthusiasm for research has kept me motivated throughout this journey. I would also like to thank my PhD committee members, Dr. Alfredo Ribeiro-da-Silva and Dr. Jeffrey Mogil, for sharing their insights and invaluable feedback throughout the various stages of this project. I would also like to thank Dr. Alfredo Ribeiro-da-Silva for allowing me the use of his lab space and equipment for the better part of three years.

Over the past six years I have also had the pleasure of working alongside many talented people in the Coderre lab. I am very thankful to Dr. Virginia Cornea, without whom this project would not exist, and who's guidance from day one was central to my learning. Our laboratory technician André Laferrière has kept the lab running smoothly and has been my go-to person for advice on experiments, and for that I am hugely appreciative. He is also accredited for the French translation of my abstract. Special thanks go out to Dr. Vaigundaragavendran Jegadeesan, a.k.a Rags, for not only spending months optimising and then teaching me subcellular fractionation and western blotting, but also for the constant positive attitude and advice on life after a PhD. I would also like to acknowledge the tremendous help from several students who have been a part of this project over the years including Aiste Mickeviciute, Jollee Fung, Shu-Fan Wang, and Pouya Bandegi. Their hard work and long hours in the lab really pushed this project forward, and each one has been a pleasure to work with.

Thank you to my parents, Jack and Cyndy Vincent for encouraging me every step of the way and for getting me here in the first place. Christina Blair and Caroline Vincent, my sisters and best friends, thank you for being my cheerleaders. Lastly, it is because of this degree that I met my perfect match, Marcel Montrey. Thank you for your love, friendship and support.

Contributions of authors

This dissertation is an original intellectual product of the author, Kathleen Vincent. The mechanical allodynia experiments were designed by myself and the data was collected by visiting medical student Aiste Mickeviciute. Our laboratory technician André Laferrière assisted in drug preparation and administration. The conditioned place preference data for the neuropathic model was collected by visiting summer undergraduate student, Jollee S.T. Fung, and André Laferrière assisted again in drug preparation and administration. The conditioned place preference experiment for the inflammatory model was designed, run and analyzed by myself and data collected with assistance from undergraduate summer student Shu-Fan Wang. Microdialysis data was largely the work of research associate Naresh Kumar and undergraduate summer student Pouya Bandegi, and I assisted in the surgical procedures for the SNI model and data analysis. I was responsible for major areas of concept formation, data collection and analysis, as well as the thesis composition. Dr. Terence Coderre was the supervisory author on this project and was involved throughout the project in concept formation and thesis edits.

A large portion of the data in this thesis has also been presented in the publication “Intracellular mGluR5 plays a critical role in neuropathic pain”, which is included as an appendix. Permission from each author has been obtained to reprint the publication in this thesis. Many people were involved in the preparation of this publication. The co-first authors, Dr. Virginia Cornea and I contributed equally to the study. Dr. Cornea performed the electron and confocal microscopy experiments and assisted with spinal cord collection for the *in vitro* experiments. I conducted the behavioral and immunohistochemical experiments. Yuh-jiin Jong conducted cell-culture, glutamate-uptake/binding, calcium imaging and biochemical experiments. Dr. Naresh Kumar and Pouya Bandegi conducted *in vivo* microdialysis and

HPLC experiments; Aiste Mickeviciute, Jollee S.T. Fung, and André Laferrière performed behavioral experiments. Dr. Alfredo Ribeiro-da-Silva supervised immunohistochemistry experiments and edited the manuscript. Dr. Karen O'Malley, Dr. Terence Coderre, Dr. Virginia Cornea and I wrote the paper.

Introduction

Background

The sensory percept of pain serves a critical, protective function in organisms. Pain alerts us to the presence of noxious environmental stimuli and motivates the initiation of self-protective behaviors. Typically, the sensation of pain is transient and subsides when the noxious stimulus is removed or the damage to tissues has healed. However, when the pain persists beyond the point of healing, it transitions from an informative physiological response to a debilitating disorder. Thus, persistent pain is a pathological process, and it is characterized by an increase in pain sensitivity, such that normally painful stimuli become more painful (hyperalgesia), and those usually associated with non-noxious sensations evoke pain (allodynia). The neural basis for these sensory phenomena has been explored extensively over the years, and both peripheral [1] and central [2] mechanisms have been proposed. While there exists a large body of evidence implicating threshold reduction in nociceptors [3-5], it is generally accepted that sensitization in the central nervous system (CNS), at least in part, contributes to pathological nociceptive signaling. Central sensitization refers to activity-dependent changes in the excitability of the central nervous system (CNS) neurons, and is predominantly characterized by increased spontaneous activity, reduced thresholds, and expansion of the peripheral receptive fields of spinal cord dorsal horn (SCDH) neurons [6]. While central sensitization has been demonstrated throughout the somatosensory nervous system, its underlying mechanisms have been mainly studied in SCDH neurons, which represent the first central synapse in the relay of nociceptive information transmission from periphery to brain [7]. As a result, identifying changes in SCDH neurons in persistent pain conditions has been at the focus of much research in this field.

One established contributor to injury-induced spinal neuroplasticity is the excitatory amino acid glutamate, which is the most ubiquitous neurotransmitter in the CNS. The activity of glutamate on various receptors in the SCDH is essential for sensory transduction; thus, the binding of glutamate at receptors on nociceptive fibers plays an integral role in nociceptive signalling. In addition to its participation in physiological transmission of nociceptive information, glutamate is also involved in activity-dependent central sensitization following injury [8]. Of the two broad categories of glutamate receptors, ionotropic glutamate receptors, comprising NMDA (N-methyl-D-aspartate), AMPA (α -amino-3-hydroxy-5-methyl-4-isoazolepropionic acid), and kainate receptors, have been more extensively studied and broadly implicated in persistent pain. Activity at both NMDA and AMPA receptors can trigger central sensitization by increasing intracellular calcium levels, activating intracellular pathways and strengthening excitatory synapses [9]. As a result, the blockade of NMDA and AMPA receptors to prevent hyperexcitability of nociceptive neurons was thought to be a promising target for antagonist-based therapeutic strategies.

While iGluR antagonists have been available as analgesics for over 50 years, the ubiquity of their receptor targets and involvement in normal sensory signalling limits the utility of these analgesics due to their detrimental side effects and small therapeutic window [10-12]. Consequently, understanding the role of the second class of glutamate receptors, metabotropic glutamate receptors, in pain transmission and modulation may help the development of alternative therapeutic interventions to reduce chronic pain.

Metabotropic glutamate receptor structure and subtypes

Metabotropic glutamate receptors (mGluRs) were originally described thirty years ago in studies on cultured striatal neurons, wherein glutamate was found to induce the production of inositol trisphosphate through a G protein-coupled receptor (GPCR) [13]. Unlike the cation-gated iGluRs, mGluRs are 7 transmembrane proteins, which upon ligand binding activate second messengers to induce intracellular effects. The mGluRs are also dissimilar from all other classical GPCR groups studied, and are therefore referred to as atypical GPCRs [14, 15]. Currently there are 5 groups of GPCRs and virtually all of them fall under groups A, B, D or E [16]. Metabotropic glutamate receptors are classified as group C, which diverge from the other GPCRs in three ways. First, mGluRs are capable of forming homodimers through disulfide bridges between their cysteine-rich domains [17], and in some cases the dimerization is critical for ligand-dependent activation [18]. Second, unlike most GPCRs that have short extracellular domains, the N-terminal in mGluRs is quite long considering the small size of its ligand [19]. This N-terminal forms a large structure named the Venus fly trap domain, after its unique shape [20]. Interestingly, mGluR mutants containing only the Venus fly trap domain are retained on the cell surface and dimerize with full length receptors, though their specific function is not well understood [20]. Third, while most allosteric modulators of GPCRs bind within the amino acid terminal, many mGluR modulators bind within the transmembrane domain [21].

In addition to the large N-terminal extracellular domain containing the glutamate-binding site of mGluRs, central to their topology is the G protein-interacting intracellular domain [22-25]. G proteins comprise a superfamily that includes several isoforms of their three subunits, α , β , and γ . Activating G proteins is initiated by agonist binding to the receptor, eliciting a conformational change that is transmitted to the G protein, causing the $G\alpha$ subunit to release guanosine diphosphate (GDP) and bind

guanosine triphosphate (GTP). GTP binding alters regions in $G\alpha$ and promotes subunit dissociation from $G\beta\gamma$, and both go on to initiate signalling cascades [26].

Based on sequence homology, signal transduction pathways and pharmacology, the eight mGluR subtypes have been divided into three classes [27]. Group I mGluRs, consisting of mGluR1 and mGluR5, are excitatory receptors primarily located on the post-synaptic membrane, and are coupled to the effector phospholipase C (PLC) through a $G\alpha_q$ -protein-mediated mechanism [24, 25, 27-31]. Conversely, Group II (mGluR2 and mGluR3) and group III (mGluR4 and mGluR6-8, largely autoreceptors) have inhibitory effects following glutamate binding. These receptors are coupled with a G protein that inhibits the enzyme adenylyl cyclase, which in turn reduces cyclic adenosine monophosphate (cAMP) metabolism from adenosine triphosphate (ATP).

Group I mGluR splice variants

Group I mGluR subtypes can be further subdivided into splice variants. The *mGluR1* gene alone produces 5 isoforms (a-e) through alternative splicing [32]. The longest and most well characterized isoform is mGluR1a. Rat mGluR1a is 94% identical to the human homologue [33]. It is also the only splice variant containing the proline-rich motif at the C-terminus, where the scaffolding protein Homer1 may bind [34]. The shortest and least characterized mGluR1 splice variant is mGluR1e which contains only the Venus fly trap domain [32]. mGluR1b-d are similar except for the smaller cytoplasmic domains than mGluR1a. In the mouse dorsal horn, mGluR1a is most abundant, followed by mGluR5d and at much lower levels, mGluR5b [35].

mGluR5 has 2 splice variants, a and b. Like mGluR1a, mGluR5a is the longer isoform by 32 amino acids in the C-terminal tail, though unlike mGluR1, both variants contain the Homer binding domain [34]. The

variants show 100% amino acid sequence identity among rat, mouse and humans [36]; however, little is known about the functional significance of these variants. When transfected into undifferentiated NG108-15 cells, both variants give rise to comparable calcium increases in response to the group I mGluR agonist, DHPG, and the mGluR5 selective agonist, CHPG. Also, glutamate-induced responses are blocked by 2-Methyl-6-(phenylethynyl)-pyridine (MPEP) equally in both variants [36]. Both variants are also expressed on plasma and nuclear membranes, though mGluR5b shows greater concentration on intracellular sites [36]. In the mouse dorsal horn, mGluR5b is more abundant than mGluR5a [35]. One differentiating feature of mGluR5a and b may be their roles in neurite development. mGluR5a severely limits neurite outgrowth, whereas mGluR5b promotes neurite extension and elaboration [36]. One possibility for these separate effects is due to their differential interactions with cytoskeletal components; alternatively, the differences may lie in their downstream signalling cascades [37]. Further investigations are required to both characterize the functional consequences of the various isoforms and identifying the associated underlying mechanisms.

Group I mGluR-linked intracellular messengers

Group I mGluRs are activated by ligand binding at the N-terminal, which produces a conformational change, although constitutive activity in cell lines over-expressing group I mGluRs [38] and in neuronal cultures [39] has also been shown. The activation of group I mGluRs initiates a complex array of interconnected signalling, the subject of which has been the topic of many reviews [14, 30, 40, 41]. Figure 1 depicts a small portion of the downstream signalling cascades that are initiated following mGluR5 activation.

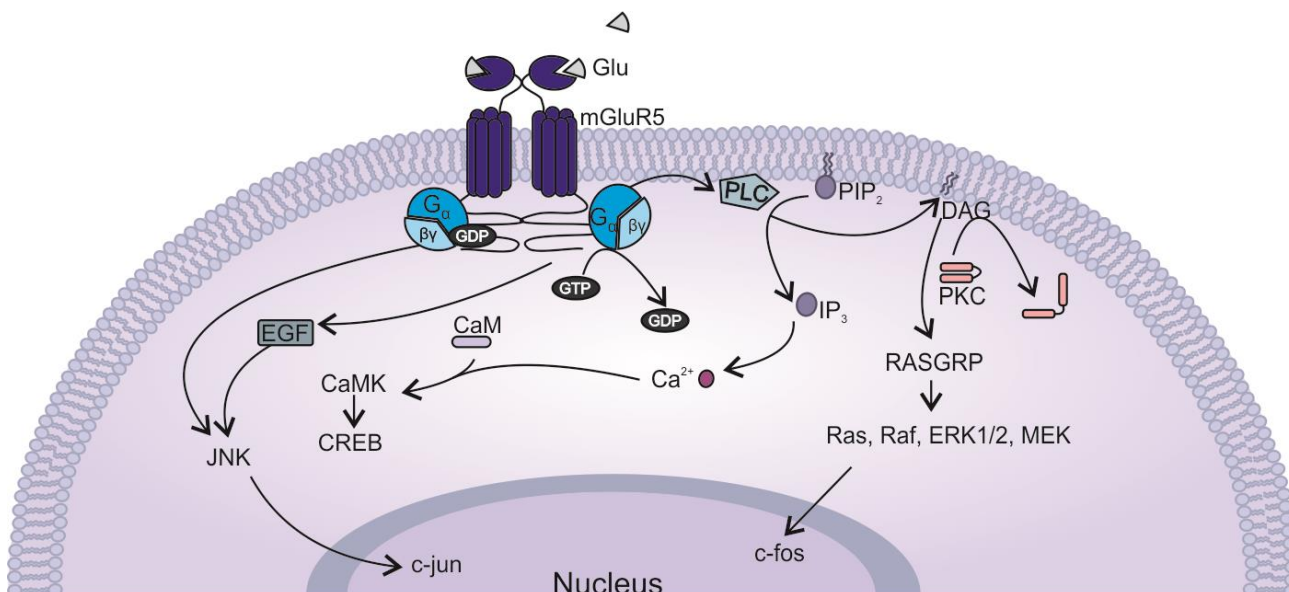


Figure 1. mGluR5 signalling cascade.

Schematic representing an overview of some of the signaling pathways activated following glutamate (Glu) binding to mGluR5 (drawn in dimer form). See text for detailed description on these signalling pathways.

The predominant signalling pathways are initiated following the dissociation of the G $\alpha_{q/11}$ protein subunits from G $\beta\gamma$. Following dissociation, G $\alpha_{q/11}$ triggers the disinhibition of the auto-inhibited membrane-associated enzyme, phospholipase C β 1 (PLC) [42]. PLC catalyzes the hydrolysis reaction of phosphatidylinositol 4,5- biphosphate (PIP₂) into diacylglycerol (DAG) and inositol trisphosphate (IP₃) [13, 43-48]. DAG, a lipid, remains in the plasma membrane, while IP₃ diffuses freely into the cytosol. Each of these two products independently initiates signalling cascades; DAG activates protein kinase C (PKC), while IP₃ leads to Ca²⁺ mobilization [13, 43-48]. The other component of the G protein complex, G $\beta\gamma$, also initiates signalling cascades following dissociation of the heterotrimeric G protein. In addition to the DAG and IP₃ pathways initiated by PLC, as discussed below, group I mGluRs can trigger G protein-mediated PLC-independent signalling, as well as G protein-independent signalling.

DAG-mediated signalling pathway

Production of DAG by the cleavage of PIP₂ is typically a transient process as it is catabolized rapidly by the cell [49]; however its production can be maintained through *de novo* metabolism from phosphatidylcholine in the endoplasmic reticulum (ER). Following its production, DAG activates PKC by directly binding to its C₁ domain [50] [51]. In addition, cytosolic PKC may also be activated by Ca²⁺ binding, and is then recruited to the plasma membrane to interact with DAG [52]. PKC is maintained in its active state by membrane-bound receptors for activated C kinases (RACKs), which also help anchor PKC to the appropriate membrane [53, 54]. The sustained activation of PKC allows for the phosphorylation of its many substrates, which are known to be involved in synaptic potentiation [50].

While the most prominent intracellular target of DAG is PKC, it is now known that there are at least 5 other DAG receptors containing the C₁ binding domain that perform functional roles in DAG signalling: RAS guanyl-releasing protein 1 (RASGRP), Munc13s, chimaerins, protein kinase D, and DAG kinase gamma [55]. Of particular interest is the RASGRP pathway as it has implications for long term potentiation. RASGRP activates Ras through the exchange of bound GDP for GTP, initiating the sequential activation of Raf, mitogen-activated kinase (MAPK) and MAPK kinase (MEK) [56]. Once active, Ras transmits its signal to the enzyme Raf-1 through phosphorylation, at which point activated Raf-1 phosphorylates MEK1/2, which in turn phosphorylates and activates MAPKs [57]. The MAPKs activated following mGluR stimulation are the extracellular signal-regulated kinases 1 and 2 (ERK1/2) [58], which phosphorylate and potentiate the activity of TCF/Elk-1, and thereby induce *c-fos* [59]. The *c-fos* protein, Fos, is an immediate early gene product located in the nucleus that, due to its fast upregulation following stimulation, often serves as a marker of neuronal activity, though more specifically, a marker of ERK signal duration [60]. Fos forms a heterodimer with the protein product, Jun, of the related immediate

early gene, *c-jun*, to form activator protein 1 (AP-1), a transcription factor that regulates gene expression [61], differentiation, proliferation and apoptosis [62].

IP₃-mediated signalling pathway

IP₃ acts on its receptor, IP₃R, a Ca²⁺ channel distributed along the endoplasmic reticulum, which results in further cytosolic increases in cytosolic Ca²⁺. Intracellular Ca²⁺ is involved in initiating several signalling pathways, including contributing to PKC activation and its downstream pathways described above. In addition, Ca²⁺ binds and activates calmodulin (CaM), the main second messenger that transduces Ca²⁺-related signals [63]. Four Ca²⁺/CaM complexes bind and activate Ca²⁺/CaM-dependent kinases (CaMK), which have several downstream targets, one of which is the cyclic AMP-responsive element binding protein (CREB) [64]. CREB is a crucial transcription factor that regulates a wide range of biological processes required for cell growth and differentiation, the details of which are beyond the scope of this thesis.

JNK pathway

In addition to stimulating traditional PLC/IP₃/DAG-dependent pathways, activation of mGluR5 with DHPG has been found to result in phosphorylation of Jun N-terminal kinase (JNK) in cultured cells in the absence of Ca²⁺ release [65]. One mechanism proposed was through transactivation by G proteins of the epidermal growth factor (EGF) receptor tyrosine kinase associated with the C-terminus of mGluR5. Active EGF receptors in turn have been shown to activate JNK [65]. Alternatively, JNK activity may also be linked to the signalling initiated following Gβγ dissociation from the heterotrimeric G protein complex. While research on the downstream pathways following heterotrimeric G protein uncoupling has largely focused on the Gα_q subunit, Gβγ subunits are also known to initiate signalling cascades relevant to neuronal excitability. For instance, Gβγ overexpression in cells is capable of inducing

activated p38 MAPK [66] and JNK activity [67] *in vitro*. In hippocampal slices, DHPG was shown to activate p38 MAPK through the G $\beta\gamma$ -mediated activation of Rap1 [68]. The importance of this pathway is the role that active JNK plays in regulating gene expression. mGluR5 agonist-induced JNK phosphorylation correlates with increased expression of the immediate early gene *c-jun* [65]. As described above, Jun forms heterodimers with Fos to form the AP-1 transcription factor, demonstrating how products from the distinct pathways converge to generate longer lasting changes affecting synaptic plasticity. The Fos/Jun complex is of particular interest to pain researchers as it is implicated in nociceptive signal transduction [69].

G protein-mediated calcium oscillations

In addition to G α_q , it has also been proposed that group I mGluRs may activate other G proteins, including G α_s and G $\alpha_{i/o}$, thereby leading to diverse downstream signalling [70, 71]. For instance, it was found that mGluR1, when transfected into Chinese hamster ovary cells, stimulated cAMP formation and arachidonic acid release [71], but the same was not found for mGluR5 [72]. Thus, despite being described as highly homologous, due to the similarity of their primary structure, functional differences between mGluR1 and mGluR5 do exist. Most notably, mGluR1 and mGluR5, when transfected into cells, produce different kinds of calcium oscillations. While glutamate induces a single-peaked intracellular calcium mobilization in mGluR1a-transfected cells, rapid oscillatory calcium patterns arise in mGluR5a-transfected cells [73]. Peptide mapping analyses pointed to a threonine residue at position 840 of mGluR5a to be responsible for generating oscillations in intracellular calcium signalling [73]. Originally, it was posited that this oscillation required PKC feedback phosphorylation at this residue; however, later it was concluded that both mGluR1a and mGluR5a activation results in repetitive coupling to PLC resulting in DAG formation and the oscillation of IP₃ formation independent of PKC-mediated feedback

[74]. It is instead the transition of mGluRs to a G protein-uncoupled conformation that results in distinct calcium oscillation frequencies between mGluR1 and mGluR5 [74]. The slower uncoupling-recoupling cycle of mGluR1a produces low frequency calcium peaks, whereas specific residues in mGluR5a support rapid mGluR-stimulated oscillations. The differential calcium oscillation frequencies of mGluR1 and mGluR5 may hold significance for synaptic strength and long-term potentiation [75].

G protein-independent signalling

In addition to using a second messenger signaling system to promote increased intracellular Ca^{2+} levels, mGluR signaling can lead to Ca^{2+} influx through direct opening of ion channels. As discussed above, it has been shown that group I mGluRs can activate intracellular signals independent of G proteins [76]. This phenomenon was first described in Aplysia neurons using whole cell patch clamp techniques [76]. The mGluR5-selective agonist, quisqualate, elicited potassium responses that were maintained even after G protein activation was inhibited using non-hydrolyzable GTP or GDP analogues. The same was later observed in CA3 hippocampal slices [77]. The mechanism by which mGluRs activate intracellular signalling without G proteins is still not clear, though it is possibly through Sarcoma (Src) family protein tyrosine kinase [78]. One study posits that Src-family tyrosine kinase associates with the receptor either directly or through an adapter protein, such as Homer, which then interacts with potassium channels [78]. In molecular layer interneuron preparations, mGluR1-mediated currents were not completely blocked by the presence of a nonhydrolyzable G protein inactivator nor a PLC inhibitor, indicating the presence of G protein- and PLC-independent signalling [79]. In the presence of G protein inactivators, residual mGluR1-mediated currents were blocked by inhibiting Src tyrosine kinase and MEK [79]. The researchers suggested that mGluR1 may initiate two pathways: a G protein-PLC-DAG pathway and a Src-MEK-ERK1/2 pathway [79].

Group I mGluR scaffolding interactions

Scaffolding proteins, as depicted in Figure 2, are crucial in regulating signalling pathways by tethering various components into complexes. These complexes have also been found to link group I mGluRs to NMDA and IP₃ receptors, and involve several scaffolding proteins including Preso1, Homer1, Shank, GKAP, and PSD-95 [80]. Homer1 is an alternatively spliced scaffolding protein, with constitutively active long-forms (b & c) containing an EVH1 domain and a coiled-coil region [81, 82]. The EVH1 domain binds to various signalling molecules, including mGluR1a, mGluR5, IP₃ receptors and Shank, while the coiled coil interacts with other long-form Homer proteins [83]. Shank is a common binding partner of Homer and together they form a mesh-like matrix structure in the postsynaptic density [84]. Shank binds with the protein GKAP via its PDZ domain [85]. GKAP is itself associated with PSD-95, the most abundant member of the membrane-associated guanylate kinases (MAGUK) proteins, known to associate directly with NMDA receptors in the postsynaptic density [85].

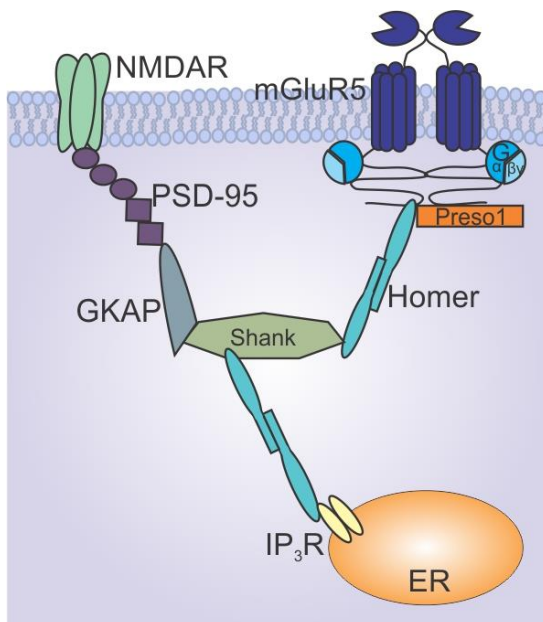


Figure 2. Scaffolding proteins interacting with mGluR5.

mGluR5 is tethered to NMDA receptors (NMDAR) and IP₃ receptors (IP₃R) via various scaffolding proteins including Preso1, Homer, Shank, GKAP and PSD-95.

The interactions between NMDA receptors and group I mGluRs are bi-directional. Activation of group I mGluRs has been shown to potentiate NMDA responses in CA1 pyramidal neurons [86, 87], striatal neurons [88], subthalamic nucleus cells [89], cortical neurons [90], and in the SCDH [91, 92]. Interestingly, in the hippocampus [93] and subthalamic nucleus [89] the NMDA-evoked currents are potentiated by mGluR5 but not mGluR1, whereas in cortical neurons potentiation is mediated exclusively by mGluR1 [90]. Meanwhile, activation of NMDA receptors can enhance group I-mediated increases in PIP hydrolysis in the neonatal rat cortical slices [94], and potentiates group I mGluR agonist-induced inward potassium currents in hippocampal cells [95]. NMDA-induced potentiation of group I mGluR responses is thought to be mediated by reversal of PKC-induced mGluR desensitization *via* activation of calcineurin, a calcium and calmodulin dependent serine/threonine protein phosphatase [96]. It is also important to note that while there is a bidirectional regulatory relationship between group I mGluRs and NMDA, long term potentiation can occur independently of NMDA activity. Specifically, it was shown that T-type calcium currents involved in inducing long term potentiation in hippocampal neurons can be induced by DHPG, while inhibiting NMDA function [97]. While these experiments have yet to be replicated in spinal neurons, T-type calcium channels have been shown to be contributors in acute pain [98], diabetic neuropathy [99], and in rat models of irritable bowel syndrome [100]. Determining if group I mGluRs also modulate T-type calcium channels in these conditions, and whether it involves NMDA interactions, will be an important step in understanding the mechanisms underlying pain-induced spinal plasticity.

Role of group I mGluRs in nociception

The precise role and contribution of each mGluR subtype on pain modulation has been investigated in a number of studies. Overall, it is generally agreed that while group I mGluRs mediate hyperalgesia,

group II and III mGluRs attenuate hyperalgesia in animal models of inflammatory and neuropathic pain [101]. This thesis will focus on the contribution of the excitatory and pro-nociceptive group I mGluRs, and in particular the role of mGluR5.

Group I mGluR agonists

In support of the role of group I mGluRs in nociception, many studies have been conducted on the effects of receptor activation in both naïve animals and animals with injuries that induce persistent pain. Unfortunately, to date there are relatively few selective agonists available for use. The first selective orthosteric agonist at group I mGluRs discovered was 3,5-dihydroxyphenylglycine (DHPG) [102]. DHPG shows similar potencies at mGluR1 and mGluR5, and remains the most selective group I mGluR agonist. In both naïve and inflamed animals, DHPG has potent algescic properties. Intrathecal (i.t.) injection of DHPG produces sustained nociceptive behaviors, such as licking and flinching [35, 103-107], and induces thermal hyperalgesia and mechanical allodynia in naïve animals [108, 109]. In addition, i.t. administration of DHPG potentiates formalin-induced nociceptive responses [110], and potentiates responses to innocuous and noxious stimuli following capsaicin injections [111]. The contribution of both mGluR1 and mGluR5 in driving DHPG-nocifensive responses is supported by findings illustrating that both the mGluR5 antagonist MPEP and the mGluR1 antagonist CPCCOEt are effective at attenuating DHPG-induced pain behaviors [35].

A related compound to DHPG is (RS)-2-chloro-5-hydroxyphenylglycine (CHPG), a phenylglycine derivative which was designed to be a selective orthosteric agonist of mGluR5 [112]. The use of CHPG is limited, however, due to its weak potency, penetrance, and efficacy [113]. Despite this, i.t. CHPG was found to induce thermal hyperalgesia [114-116] and cold allodynia [116] in naïve rats, and potentiates

nociception following carrageenan-induced inflammation [117] or mustard oil injection into the hind limb [118]. Interestingly, one study found the opposite effect in spinothalamic tract cells; thus, following capsaicin-induced central sensitization, CHPG diminished responses to graded mechanical stimuli [111]. However, more recently the selectivity of CHPG for mGluR5 over mGluR1 has come into question, as it does appear to produce weak biased agonist effects at mGluR1, favouring $G_{i/o}$ signaling over the more common $G_{q/11}$ [113]. Given the apparent non-selectivity of CHPG, the opposing effects of DHPG and CHPG in their model are surprising and warrant further investigation. Another study found that chronic administration of CHPG into spinal T11 following spinal cord injury reduced microglia-associated inflammation in rats [119]. The same group later found that intracerebroventricular CHPG was effective in limiting neuroinflammation after traumatic brain injury [120, 121]. Thus, the involvement of group I mGluRs in inflammation appears to depend on where the inflammatory insult occurs. In peripheral inflammatory conditions that result in spinal sensitization, i.t. CHPG exacerbates pain, whereas in contrast neuroinflammation following spinal cord injury and traumatic brain injury benefit from CHPG administration.

Another potent group I mGluR agonist is quisqualate [122]. I.t. injections of quisqualate produce spontaneous licking and scratching behaviors in naïve animals [123-128]. Another group found that spinal injection of quisqualate resulted in reduced mechanical and thermal thresholds, but had no effect when administered into skeletal muscles [129]. Repeated spinal administration of quisqualate produces inflammatory responses in the spinal cord, and is used as a model of spinal cord injury [130-132]. However, the above findings cannot be solely ascribed to group I mGluR activation, as quisqualate is also one of the most potent AMPA and NMDA receptor agonists [133]. Indeed, many of the quisqualate-induced licking and biting behaviors can be abolished by administering an NMDA antagonist [124]. It may

also be its effect on ionotropic glutamate receptors that makes high doses of quisqualate neurotoxic [134], limiting its use as a group I mGluR agonist.

Physiological studies also demonstrate that activation at group I mGluRs has excitatory effects. Thus, the non-selective mGluR agonist 1S,3R-ACPD induces a potentiation of polysynaptic EPSPs in SCDH neurons [135]. Activation of group I mGluRs with DHPG induces slow EPSPs [136, 137] and increased Ca^{2+} release in SCDH neurons [138]. Some studies have reported long-lasting potentiation of EPSPs by mGluR5 activation in neurons within the superficial lamina of the SCDH [135], while little effect was observed in lamina II-V dorsal horn neurons [139], and no effects were found in spinothalamic tract cells [111]. DHPG-evoked neuronal activation in the spinal cord is attenuated by application of the mGluR1 selective antagonists, cyclothiazide (CTZ) [139] or AIDA [111], and following antisense oligonucleotide knockdown of mGluR1 [140]. In contrast, in cultured mouse DRG neurons, DHPG-induced calcium transients were attenuated by application of the mGluR5 antagonist, MPEP, but not by the mGluR1a antagonist, LY367385 [141].

The association of spinal group I mGluRs and nociceptive plasticity quickly drove research towards elucidating the downstream mGluR effectors relevant in persistent pain. Early studies on the downstream targets following group I mGluR activation in inflammatory conditions found that intrathecal application of DHPG produces a dose-dependent increase in spinal pERK1/2 [35]. This increased ERK phosphorylation parallels the dose-dependent increases in DHPG-induced nocifensive behaviors in mice [35]. Further supporting an association between group I mGluRs and ERK was the finding that following i.t. DHPG or i.pl. formalin, a subset of ERK-positive SCDH neurons also express mGluR5 [35], making ERK a plausible downstream target following mGluR5 activation. Prior to these studies, increased ERK phosphorylation had been described in the superficial lamina following either i.pl.

capsaicin or C or A δ -fiber (but not A β -fiber) electric stimulation [142], establishing ERK as a mediator for nociceptor hypersensitivity. Later studies established that ERK phosphorylates the A-type K⁺ channel subunit, Kv4.2, modulating the activity of A-type currents, which are critically involved in neuronal excitability, in cultured spinal cord neurons [143]. It has now been established that mGluR5 through pERK can lead to the phosphorylation of the Kv4.2 subunit, inhibiting A-type currents, affecting neuronal excitability [144]. The majority of the Kv4.2-expressing neurons in the SCDH are located on excitatory, glutamatergic neurons in lamina III [144]. Thus, one pathway by which mGluR5 modulates synaptic plasticity and contributes to central sensitization following injury is through coupling to Kv4.2.

mGluR5 antagonists and inverse agonists

In response to research demonstrating the pronociceptive properties of mGluR5, selective antagonists for mGluR5 have been probed for analgesic potential. While assessing these compounds, it is important to consider both the structure-activity relationship of antagonists, as well as the potential for treating pain disorders. One consideration is whether the antagonists bind at orthosteric sites, and function as competitive antagonists, or bind at allosteric sites as non-competitive antagonists. Unlike competitive antagonists, non-competitive antagonists do not change the affinity of glutamate binding. The first antagonists developed to target mGluR5 were found to bind at the orthosteric site; however, due to a lack of subtype selectivity of these agents, researchers began searching for allosteric compounds [145]. Some of the first developed mGluR5-selective antagonists were 6-methyl-2-(phenylazo)-3-pyridinol (SIB-1757) and (E)-2-methyl-6-(2-phenylethenyl)-pyridine (SIB-1893) [146]. SIB-1757 and SIB-1893 act at the allosteric site, and are non-competitive antagonists that block glutamate-induced calcium responses in cell lines expressing the human mGluR5a [146]. When given i.t. or subcutaneously (s.c.) to

rats following spinal nerve ligation (SNL), SIB-1757 produces a partial reversal of tactile allodynia and full reversal of thermal hyperalgesia [147].

Studies of calcium responses generated from group I mGluRs led to the hypothesis that these receptors oscillate between at least two conformational states, an inactive and an active one [148]. Agonists stabilize the receptor in the active state. Antagonists can be divided into two categories: neutral antagonists and inverse agonists. Neutral antagonists have the same affinity to both the inactive and active conformational states, whereas inverse agonists stabilize the inactive state and therefore inhibit constitutive activity. MPEP has been described as a potent, selective non-competitive mGluR5 antagonist [149]. MPEP was also found to inhibit basal constitutive activity of rat mGluR5a, and thus it is also an inverse agonist that interacts with amino acid residues within the transmembrane domain [150]. It has also been shown to produce antinociceptive effects in various pain models. When administered systemically, MPEP reduces nociception induced by formalin [151], as well as acetic acid-induced writhing [152]. Intrathecal injection of MPEP also attenuates the second phase of the formalin response in mice [35]. Intraperitoneal (i.p.) injections of MPEP produce a dose-dependent reversal of thermal and mechanical hyperalgesia in CFA- and carrageenan-injected animals [152]. In addition, administration of MPEP attenuates the development of tolerance to morphine [153, 154].

While MPEP has consistently demonstrated antinociceptive effects in inflammatory and visceral models, results in neuropathic animals are inconsistent. Application of MPEP to the spinal cord was found to attenuate thermal hyperalgesia, but not mechanical allodynia, following spinal cord injury [155]. Similarly, oral administration of MPEP had no effect on mechanical allodynia, but produced a reduction of thermal hyperalgesia in SNL animals [156]. Conversely, i.p. injection of MPEP dose-dependently reduced mechanical allodynia in rats with SNL [151]. Also, i.t. injection of MPEP attenuated

mechanical allodynia, but had no effect on cold hypersensitivity in rats with chronic constriction injury (CCI) of the sciatic nerve [109, 157]. In contrast, i.t. MPEP administration did not affect mechanical or thermal hyperalgesia after partial sciatic nerve ligation (pSNL), spared nerve injury (SNI), or hind paw carrageenan injection [156, 158]. Finally, one study found that spinal injections of MPEP only partially attenuated mechanical allodynia after SNL, CCI and chemotherapy-induced nerve injury [152]. The inconsistency within neuropathic pain models make interpretation of the effects of MPEP difficult. The MPEP data are further complicated by findings which call into question the selectivity of the compound; MPEP maintains its neuroprotective effects [159] and analgesic efficacy [160] in mGluR5 knock-out mice, when administered at high doses.

Another widely used non-competitive, inverse agonist of mGluR5 is 3-((2-methyl-1,3-thiazol-4-yl) ethynyl) pyridine hydrochloride (MTEP), which shows similar potency at the mGluR5 receptor as MPEP, but has greater selectivity [161]. I.t. application of MTEP inhibits sustained nociceptive behaviors in mice with bone cancer-induced pain [115] and reduces visceromotor responses, as well as mechanical sensitivity, in a colorectal distension model of visceral pain [162]. In rats with SNL, spinal injections of MTEP dose-dependently increase withdrawal thresholds [151]. Finally, i.t. MTEP injections reduce CFA-induced thermal hyperalgesia [151, 152], and decrease nociceptive behavior in the early and late phases of the formalin test [151, 163].

In addition to studies on behavioral outcomes of mGluR5 inhibition, studies on the physiological effects of these antagonists also provide support for their role in nociceptive transmission. Thus, the group I mGluR antagonist, AIDA [164], as well as MPEP and MTEP, have been shown to reduce glutamate release following spinal cord injury [165, 166]. However, AIDA does not block cellular responses to acute, noxious stimulation [167], suggesting these receptors may be more specifically involved in persistent

pain. Selective group I mGluR antagonists have also been shown to reduce dorsal horn hyperactivity after hind paw inflammation [168] or spinal administration of DHPG [111, 139, 168, 169]. Furthermore, superfusion of MPEP into hemisectioned spinal cords inhibits wind-up responses in thalamic neurons evoked by repetitive stimulation [167], and attenuates evoked activity of dorsal root [169] and lamina II dorsal horn neurons [170] in nerve-injured rats.

While MPEP and MTEP are the most widely utilized mGluR5 antagonists in pain studies, several other mGluR5-specific antagonists have also demonstrated antinociceptive effects. In particular, the clinically-validated compound fenobam [171] has been identified as a potent and selective allosteric antagonist of mGluR5 with inverse agonist activity [172]. It inhibits quisqualate-evoked intracellular calcium responses mediated by mGluR5, and blocks 66% of mGluR5 basal activity in cell lines over-expressing mGluR5 [172]. While originally prescribed for anxiety [171], fenobam is now being investigated as a treatment for pain [173]. I.p. injection of fenobam, which shows greater selectivity than MPEP, reduces formalin-induced pain behaviors [160], attenuates inflammation-induced hypersensitivity [160, 174], and has analgesic effects in mice infected with a uropathogenic strain of *E. coli*, a model of painful bladder syndrome [175]. Importantly, unlike MPEP, the analgesic effects of fenobam appropriately disappear in mGluR5 knockout mice [160]. Further, systemic injections of fenobam in both male and female SNI mice, but not in sham mice, produces analgesic conditioned place preference [176]. Dispersion of fenobam in plasma and brain tissue reveals that fenobam is readily detectable in plasma and brain within 5 minutes following i.p. injection and cleared within one hour [160]. Importantly, unlike opioid treatments, chronic administration of fenobam does not produce tolerance in animals with neuropathic pain [174]. Overall, its robust analgesic activity in preclinical models of pain lend further

support for the role of mGluR5 in chronic pain conditions, while its good safety profile and previous use in human clinical trials show promise for its utility as an analgesic.

Localization of mGluRs in the SCDH

With the exception of mGluR6, which is exclusively expressed within the retina [177, 178], all the mGluRs are expressed within the pain pathway, with some selectivity for different subtypes in specific lamina of the SCDH [179]. In the SCDH, mGluR5 [180-182] is found predominantly in the superficial laminae (lamina I and II), which are known to receive input primarily from nociceptive unmyelinated C and thin myelinated A δ fibers. It is also observed at lower levels in the deeper layers of the dorsal horn and near the central canal in lamina X [180]. mGluR5 staining is not detectable in motor neurons or fibre tracts [183, 184]. mGluR1 is also found in the superficial lamina [118, 185-187], but is more densely observed in the deeper regions in lamina V [180, 183, 184, 186]. Showing further support for their role in nociceptive neurotransmission, group I mGluRs have also been described on C-fiber terminals [188]. Electron microscope imaging techniques have identified group I mGluRs mostly on postsynaptic membranes [182, 186, 187], both extrasynaptically and perisynaptically [180, 182], but also at low levels on presynaptic axon terminals [183, 186-188]. In addition, the splice variant, mGluR1a, has been found in dendritic and somatic membranes of neurons in lamina II-V of the SCDH [180], and mGluR5 has been observed in perikarya [186], dendrites [182, 186, 187], vesicle-containing profiles, Golgi and ER membranes in SCDH [186]. Nonspecific antibodies for mGluR2/3 show staining of Group II mGluRs in the dorsal root ganglion (DRG) soma [189] and presynaptically in the SCDH [180, 190]. These receptors are expressed in lamina II-V [169, 187, 191, 192] on axon terminals [190], where they function as autoreceptors, and extrasynaptically [193] on cell bodies and dendrites. mGluR4 is also expressed predominantly in presynaptic terminals [194] in lamina I-II and interneurons [195] in the rat SCDH [196-

198], while mGluR8 is found in most small, medium and large diameter DRG cells [189], but has not been described in SCDH neurons [195, 199].

Expression and regulation of mGluR5 following injury

Several studies have examined SCDH mGluR5 regulation in neuropathic and inflammatory pain models, and the conclusions have been mixed. mGluR5 mRNA expression shows an early increase in large neurons of the lumbar dorsal horn following spinal cord injury [165, 200], and continues to increase up to at least day 30 [201]. In rats with diabetic neuropathy, there is increased expression of mGluR5 in the DRG, but not the SCDH [170]. Upregulation of mGluR5 was observed in A-fibers two weeks after SNL or complete sciatic nerve section; however, no changes were observed after pSNL [156]. mGluR5 is increased in spinal lamina I and II following inflammatory or post-operative pain in sheep [202, 203], and bone cancer-induced pain in mice [115]. Finally, there is increased mGluR5 expression in superficial dorsal horn in mice with persistent ethanol-induced pain [204].

It is important to keep in mind that quantitative evaluation of overall mGluR5 levels is by itself an incomplete story. Absent from these accounts is information on whether the receptor functionality and location on the plasma membrane is maintained or altered by the process. Responsiveness of GPCRs can be attenuated by a family of proteins referred to as regulators of G protein signaling (RGS), which recognize G protein α subunits and accelerate the GTP hydrolysis required for receptor inactivation [205]. Two isoforms, RGS2 and RGS4, interact with $G\alpha_{q/11}$ G proteins and have been shown to block the effects of group I mGluR activation [206, 207]. Receptor responsiveness is also regulated by desensitization which occurs shortly after exposure to agonists. After prolonged stimulation, group I mGluRs undergo both agonist-dependent (homologous) and agonist-independent (heterologous)

desensitization. In neuronal and glial preparations, PKC has been shown to be involved in mGluR1 and mGluR5 desensitization by phosphorylating a residue in the G protein-coupling domain, causing the uncoupling of the receptor from $G\alpha_q$ [208]. In canonical GPCR desensitization, GPCR kinase (GRK) phosphorylation promotes the binding of β -arrestin in response to agonist stimulation [209]. Then, through a β -arrestin1-mediated process, mGluRs are redistributed to endosomes, a process known as internalization [209]. However, internalization also occurs independently of agonist stimulation via clathrin-coated vesicles [209]. Following internalization, several outcomes are possible. The receptor is either dephosphorylated and rapidly recycled back to the cell surface, targeted to lysosomes, or retained in the endosomal compartment [210, 211]. Overall, several mechanisms are in place to either desensitize or relocate mGluRs away from the plasma membrane.

Given that the location of mGluR5 on and within the cell is dynamic, it is a significant drawback that the earlier studies do not address whether the changes in overall expression are specific to the plasma membrane or intracellular locations, where >80% of mGluR5 is located [212]. Recently, the distinction between intracellular and plasma membrane-associated group I mGluRs was studied in rats with persistent inflammation induced by hind paw injections of complete Freund's adjuvant (CFA). The study found that CFA-treated rats have an increased number of plasma membrane-bound mGluR5s in lamina I and II neurons, and that plasma membrane-associated mGluR1s in lamina V were closer to the synapse, indicating that peripheral inflammation induces group I mGluR trafficking in SCDH neurons [213]. Additionally, trafficking occurs in parallel with CFA-induced thermal hyperalgesia, suggesting that mGluR trafficking is associated with persistent nociception [213]. Further, immunolabelling of mGluR5 in the spinal cord reveals that >30% of the receptor is found on nuclear membranes, and this percentage increases significantly following nerve injury [214].

Intracellular GPCRs

The existence of intracellular GPCRs is not an entirely novel concept. In fact, GPCRs have long been found inside cells, including in the ER [215], lysosomes [216, 217], Golgi apparatus [218], endosomes [219], and nuclei [220]. Historically, all intracellular GPCRs were thought to be non-functional, with receptors either in formation, being degraded/recycled, or in transit to the plasma membrane. However, it has more recently become clear that GPCRs can also signal from some intracellular locations. One of the earliest findings of functional intracellular GPCRs comes from studies demonstrating that β -adrenergic receptor endocytosis following desensitization subsequently leads to signalling from the endosome [221, 222]. These studies introduced the concept of intracellular GPCR-signalling and kick-started the search for other functional intracellular GPCRs.

Since then, data documenting G protein-dependent signalling from several intracellular GPCRs has emerged. In particular, a number of GPCRs have been found to be located at nuclear membranes [220, 223]. These nuclear GPCRs are found in a number of tissues including the brain [224], corneal epithelial cells [225], cerebellum [226], hypothalamus [226], myocytes [227], colon tissue [228], liver [229], DRG [230], and pituitary cells [231]. In addition to cell lines and murine models, nuclear GPCRs have also been confirmed in human tissues, including apelin receptors [226], cysteinyl leukotriene type 1 receptors [228], CXC chemokine receptors [224], vasoactive intestinal peptide receptor [232], prostaglandin type E receptors [224], β -adrenergic receptors [233, 234], and endothelin receptors [235, 236]. The apparent ubiquity of nuclear GPCRs highlights the importance of determining their contribution to cellular processes.

As GPCR signaling relies on the various downstream pathways it initiates, the first concern is whether nuclear GPCRs initiate a similar cascade of events following ligand binding as do cell surface receptors. If nuclear GPCRs maintain the topology with which they are organized in the ER, GPCRs on the outer nuclear membrane would be oriented such that their intracellular domains are in the cytoplasm and as such have access to the downstream signalling molecules in the cytoplasm. On the other hand, GPCRs located on the inner nuclear membrane require that the signaling machinery be within the nucleus. In fact, several studies have confirmed the presence of these molecules within the nucleus or on the nuclear membranes, including heterotrimeric G proteins [237, 238], adenylyl cyclase [239], phospholipase C [240], and GPCR kinases [241]. Moreover, nuclear preparations expressing β -adrenergic receptors were found to display the downstream signalling partners Gs, Gi and adenylyl cyclases, and stimulated transcription in the absence of plasma membrane receptors [233]. These findings provide evidence of the potential for nuclear GPCR signalling.

Determining how and from where GPCRs are relocated to the nuclear membrane is a question about which little has been found to date. Given that these receptors are generally found on the nucleus constitutively, it is likely that their trafficking is triggered in an agonist-independent manner. If this is the case, then it is possible they are trafficked directly from the ER following biosynthesis and assembly. Interestingly, elimination of the N-glycosylation sequence in the prostaglandin E₂ receptor resulted in its accumulation in the perinuclear zone [242], suggesting that post-translational modifications may be involved in nuclear localization of other GPCRs as well. Alternatively, these receptors may be trafficked from the plasma membrane via constitutive or agonist-mediated internalization events.

Nuclear mGluR5

While the synaptic and extrasynaptic plasma membrane location of mGluR5 has been the focus of most investigations, electron microscopy reveals that 50-90% of mGluR5 in the brain is in fact intracellular [212, 243, 244]. Indeed, subcellular localization of mGluR5 on intracellular membranes in the superficial lamina of the SCDH neurons was first described more than 20 years ago [182]. At the time, no explanation was given for their purpose. More recently, the presence of nuclear mGluR5 had been well established in heterologous cells, as well as midbrain and cortical neurons [245]. Receptor location was first identified via immunohistochemistry demonstrating colocalization of anti-mGluR5 with the nuclear membrane marker, lamin B₂, in HEK and cortical cells. These results were then confirmed using electron microscopy in preparations from the rat visual cortex. Immunogold particles labeling mGluR5 were associated with the post synaptic density as well as both the inner and out nuclear membranes and throughout the endoplasmic reticulum [245]. Lastly, subcellular fractionation of P3 forebrain cells into nuclear and plasma membrane-enriched fractions showed the presence of mGluR5 protein in both fractions [245]. The same group has then gone on to demonstrate the presence of these receptors on the nuclei of striatal [246] and hippocampal neuronal cultures [247].

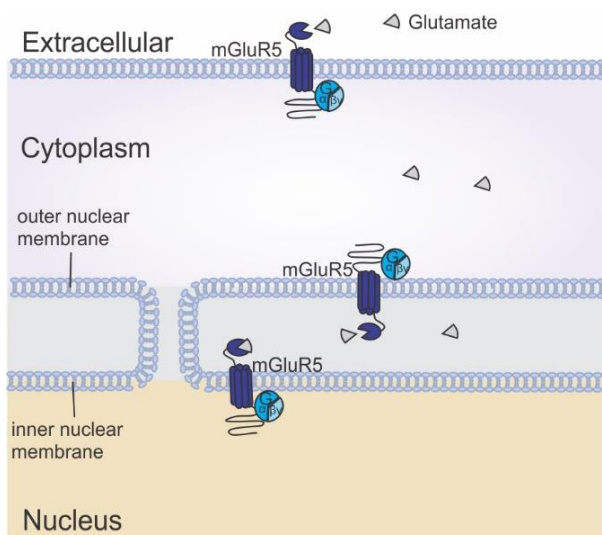


Figure 3. Orientation of mGluR5 on cell surface and nuclear envelope.

Nuclear mGluR5 has its ligand binding domain within the nuclear lumen.

As with other intracellular GPCRs, the orientation of mGluR5 on the nucleus is important for its potential function within these membranes. Antibodies directed against the C- and N- terminal of mGluR5 reveal that the whole receptor is present on the nucleus and that its ligand binding domain is within the lumen of the nuclear envelope [245] (Figure 3). Receptors on the outer nuclear membrane have access to the same cytoplasmic downstream signalling molecules as those located on the plasma membrane, as the G proteins of both are within the cytoplasm. However, receptors located on the inner nuclear membrane would require these components to be found within the nucleus itself. As stated above, much of the machinery for GPCRs has already been observed within the nucleus. The presence of heterotrimeric G proteins, PLC, and PKA, all within the nucleus, support the potential for nuclear mGluR5 signalling.

Importantly, the theory that mGluR5 may signal from the nucleus has been put to test *in vitro*. In both whole cell culture and isolated nuclei, nuclear mGluR5 is capable of binding quisqualate, an mGluR5 agonist, and produce rapid, oscillatory Ca^{2+} elevations in response to glutamate [245]. Additionally, like plasma membrane mGluRs, activation of nuclear mGluR5 receptors has been found to generate nuclear IP_3 which mediates the release of Ca^{2+} , demonstrating that the nucleus can mobilize Ca^{2+} independently from signals originating in the cytoplasm [248]. More recently it was shown that activation of nuclear mGluR5 leads to unique cellular responses that are not initiated via cell surface receptor activation. Specifically, cell surface mGluR5 stimulation leads to phosphorylation of *c-Jun* N-terminal kinase (JNK), calcium/calmodulin-dependent protein kinases (CaMK), and cyclic adenosine monophosphate response element-binding protein (CREB), whereas activation of nuclear mGluR5 leads to phosphorylation of ERK1/2 and the Ets transcription factor, Elk-1, which is essential for activating the immediate early gene (IEG), *c-fos* [248, 249].

Activating nuclear mGluR5

Nuclear receptors are not readily accessible to extracellular molecules unless they can diffuse through the membranes or otherwise be transported across. This particular feature has been exploited in the research on nuclear mGluR5 by using agonists and antagonists that can diffuse through the membranes (permeable), can be transported across the membranes (transportable), or can do neither (non-permeable/non-transportable).

Excitatory amino acid transporters

Glutamate is a charged molecule that does not freely diffuse across lipid membranes; instead, it relies on the presence of various glutamate transporters. One class of transporters are the excitatory amino acid transporters (EAATs) which are important in removing glutamate from the synapse and relocating it within the cell. To date, five EAATs have been cloned (EAAT1-5), with the first two being expressed on astrocytic membranes and the last three on neurons [250]. While EAAT1-3 are widespread in the CNS, including the SCDH, EAAT4 and EAAT5 are limited to Purkinje cells and photoreceptors, respectively [251]. The two glial EAATs, EAAT1 and EAAT2 are also referred to as glutamate/aspartate transporter (GLAST) and glutamate transporter-1 (GLT-1), while EAAT3 is also referred to as excitatory amino acid transporter 1 (EAAC1) [250, 252, 253].

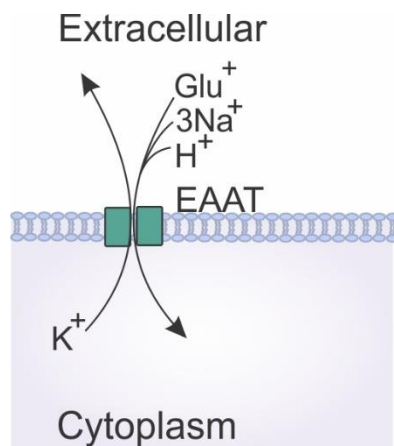


Figure 4. Ion coupling in EAATs.

Glutamate is co-transported with 3 sodium ions and one proton and followed by counter-transport of one potassium ion.

The transport of glutamate by EAATs is thermodynamically driven by an inwardly directed sodium gradient. In this gradient, one glutamate is coupled to the cotransport of three sodium ions, [254] one proton, and the counter-transport of a potassium ion [255] (Figure 4). L-Glutamate and DL-aspartate are both transported with similar affinities, and the majority of glutamate uptake in the CNS is transported through EAAT2 [255]. The primary regulators of extracellular glutamate concentration in the CNS are the astrocytic EAAT1 and EAAT2 [256], which are associated primarily with excitatory synapses [257]. Much like group I mGluRs, neuronal EAAT3 is found perisynaptically on somata and dendrites [258], indicating that it may be involved in scavenging glutamate spillover during high synaptic output. However, unlike the glial EAATs, the majority of EAAT3 is located intracellularly [259]. Stimulating the group I mGluR downstream signalling molecule, PKC, increases EAAT3 transport to the membrane in cell cultures [260], suggesting that EAAT3 enhances glutamate uptake during periods of high glutamate release [251].

As reports on nuclear mGluR5 have shown these receptors to be functional within neuronal populations, glutamate is likely transported intracellularly via EAAT3. Indeed, preventing sodium-dependent uptake in cell cultures using Na⁺ free media or the EAAT antagonist, TBOA, reduces glutamate uptake into hippocampal cells by 80-90% [247]. Another mechanism by which glutamate may enter the cell is through the sodium-independent cystine-glutamate exchangers (X_{CT}). As the name suggests, X_{CT} exchanges glutamate for cystine. Unlike the EAATs, the X_{CT} typically exports glutamate and imports cysteine for the production of glutathione in glia cells [261]; however, the exchange may go in either direction. In cultured striatal and HEK cells, glutamate uptake is also reduced by preventing uptake through X_{CT} [246, 248, 262]; however, X_{CT} does not appear to contribute to glutamate uptake in hippocampal cells [247]. These results suggest that *in vitro*, glutamate transport through the plasma membrane is mediated by EAAT3 and in some cells by X_{CT} as well.

The next question to answer is how cytoplasmic glutamate gains access to the nuclear lumen. Interestingly, the same studies demonstrating the involvement of EAATs and X_{CT} in the uptake of glutamate into the cytoplasm also demonstrated that these transporters prevent uptake of glutamate in isolated nuclei [246]. Specifically, TBOA blocks 30-40% of glutamate uptake into nuclei isolated from striatal neurons, indicating that EAATs contribute to the transport of glutamate across nuclear membranes. In contrast, nuclei isolated from HEK cells showed greater glutamate uptake inhibition by blocking X_{CT} [246]. Both EAAT3 and X_{CT} proteins are present in nuclear fractions in these cells, however the results suggest that the favoured glutamate carrier is cell-type dependent [246].

In vitro glutamate uptake assays on whole cells and isolated nuclei suggest that EAAT3 and X_{CT} are capable of transporting glutamate from outside the cell to within the nuclear lumen. This conclusion is surprising as it suggests that the same transporter which imports glutamate into the cytoplasm also transports it out of the cytoplasm and into the nuclear lumen. One feature of EAAT3 and X_{CT} is that the transport direction may be influenced by changes in electrochemical gradient or glutamate concentration. It is important to acknowledge that in experiments performed on isolated nuclei, the nuclei are not surrounded by a cytoplasmic environment. In addition, as the majority of intracellular glutamate is confined within mitochondria and vesicles [263], isolated nuclei are exposed to free glutamate at concentrations that may never be reached *in vivo*. Under such conditions, it is unclear whether transporters on isolated nuclei function the same way as nuclear transporters within intact cells. And despite the fact that the majority of EAAT3 is intracellular, little is known regarding its function as a glutamate transporter while on intracellular membranes. Thus, while EAAT3 is expressed on both plasma and nuclear membranes *in vivo* and represents a promising candidate for the traffic of glutamate, more

research is needed to study how this transporter functions from inside the cell under normal conditions before conclusions can be made regarding the intracellular transport of glutamate.

Membrane permeability

In contrast to glutamate and quisqualate, which require active transport to pass through cell membranes, small molecules and molecules that are sufficiently lipophilic are capable of diffusing across more freely. Lipophilicity is already an important consideration in pharmacology, as drugs that need to pass through the blood brain barrier face a similar challenge. A useful measure of lipophilicity is the log of the partition coefficient (logP) which uses the ratio of the concentrations of a compound between a nonpolar and a polar solvent. Mathematically, the logP of compound x can be expressed as: $\log P_x = \log \left(\frac{[x]_{non-polar\ phase}}{[x]_{polar\ phase}} \right)$. Greater logP values indicate greater lipophilicity [264]. Conveniently, computational systems have been developed to estimate logP values from molecular structure, making it a useful proxy for estimating membrane permeability, which generally increases with higher logP. However, the permeability-lipophilicity relationship is affected by several factors, including molecular size, pH of the system, and composition of the membrane lipids [265]. One group performed an analysis of parallel artificial membrane permeability assays and determined that there was a linear relationship between molecular weight size and logP on membrane permeability [266]. Compounds with molecule weights less than 300 g/mol have a 50% chance of high permeability with a logP value of 1.7, molecules between 300-350 g/mol need a logP value of 2.2, and molecules between 350-400 g/mol require a log P value of 2.6 or greater to have a 50% chance of being permeable [266]. These values are by no means absolute as they still depend on the calculation used to determine logP, as well as the membrane

composition; however, logP does give an indication as to which compounds are more likely to diffuse through the membrane.

Given that agonists and antagonists that are not actively transported across membranes must diffuse through to act on intracellular mGluR5, knowing which ones are likely to be permeable and which ones are not becomes an important consideration. For instance, the mGluR5 agonist DHPG has a molecular weight of 183.05 g/mol and logP value ~ -2.4 , which makes it very unlikely to diffuse through the plasma membrane. Likewise, the group I mGluR antagonist LY393053 has a molecular weight of 383.462 g/mol and logP value of 0.6 and also does not diffuse passively through membranes. In contrast, the mGluR5 antagonist MPEP which has a molecular weight of 196.24 g/mol and logP value of ~ 3.3 [267], readily diffuses, as does fenobam (MW = 266.68, logP = 2.0). The different effects of permeable and nonpermeable, or transported and non-transported, drug treatment are useful ways of distinguishing activity from intracellular membrane and plasma membrane-bound mGluR5.

Nuclear mGluR5 implications for pain

As of yet, the physiological importance of nuclear mGluRs, and the mechanisms regulating their expression is unknown; however, their role in regulating nuclear Ca^{2+} release, transcription activation, and gene expression suggests an involvement in processes such as synaptic plasticity. Of particular interest to pain researchers is their influence on *c-fos* expression, which is frequently employed as a functional marker to identify activity in spinal neurons in response to noxious stimulation, and is used as a neural correlate of nociception (for review see [268]). Indeed, the membrane permeable mGluR antagonist MPEP has previously been shown to reduce acetic acid-induced Fos expression, a model of visceral pain, in lamina I, II, V, VII and X of the lumbar spinal cord [269]. However, it remains to be seen

whether attenuation of Fos is due to the intracellular or extracellular effects of MPEP *in vivo*. Recent findings have demonstrated that nuclear mGluR5s are found in cultured rat SCDH neurons, and both cytoplasmic and nuclear calcium levels rise in response to application of quisqualate. Importantly, quisqualate-induced calcium responses are only inhibited by the application of the permeable group I mGluR antagonist, fenobam [214]. A calcium fluorophore directed specifically to the nucleus revealed that quisqualate in the presence of the non-permeable antagonist, LY393053, still induces nuclear calcium elevations. Further, quisqualate-induced nuclear calcium release is maintained in isolated nuclei, indicating this process can occur independently from the plasma membrane in spinal cord cells [214].

Hinting at a role in persistent pain processing, it was also discovered that following SNI there was a marked increase in nuclear-bound mGluR5 as measured by quantitative electron microscopy [214]. Consistent with these findings, SNI nuclei had greater binding of glutamate as compared to sham. The greater binding can be attributed to a greater number of receptors, and not a difference in receptor affinity, as both sham and SNI isolated nuclei had equivalent receptor affinity for both the permeable group I mGluR agonist, quisqualate, and non-permeable group I mGluR agonist, DHPG. In these investigations, nuclear mGluR5 was limited to neurons, as glial and endothelial cell nuclei were not labelled. Given the importance of mGluR5 in persistent pain, the discovery of these nuclear receptors in the spinal cord invites researchers to investigate whether they are functionally involved in the pathology of persistent pain.

The *in vitro* studies on nuclear mGluR5 support the idea that these receptors may be stimulated by exogenous glutamate or quisqualate. Antibodies directed against the C- and N- terminal of mGluR5 reveal that the whole receptor is present on the nucleus, and that its ligand binding domain is within the

lumen of the nuclear envelope [245]. Thus, given its orientation, ligands must cross both plasma and nuclear membranes to bind to nuclear mGluR5.

Involvement of EAATs in pain

Indirect evidence for a role of SCDH nuclear mGluR5 in chronic pain is hinted at in studies of EAATs. Following release from the synapse in the SCDH, glutamate is rapidly taken up through EAATs on glia and neuronal membranes to ensure high-fidelity in signal transmission and to prevent excitotoxicity [270]. This uptake is critical as it prevents prolonged activation of glutamate receptors within the SCDH. As mentioned earlier, three EAATs are found in the SCDH: EAAT1-3. While EAAT1 and EAAT2 are expressed in glia and responsible for the majority of synaptic clearance, EAAT3 is expressed in neurons and take up glutamate into spinal cord neurons.

EAAT inhibitors: Development and subtype selectivity

Due to their involvement in regulating synaptic glutamate, the development of EAAT inhibitors has been an important step in elucidating EAAT function in nociceptive signalling. The first generation EAAT inhibitors were competitive inhibitors that did not show subtype selectivity. Compounds such as *threo*- β -hydroxyaspartate (THA) and *L-trans*-2,4-pyrrolidine dicarboxylate (*L-trans*-2,4-PDC), were commonly used as inhibitors of the three EAATs [271], but it was found that competitive, transportable inhibitors caused hetero-exchange leading to efflux of glutamate [272], making them unsuitable for studying the physiological role of EAATs *in vivo*. Later the compound DL- *threo*- β -hydroxyaspartate (TBOA, also referred to as DL- TBOA) was found to work as a potent, non-transportable blocker of all EAAT subtypes, and did not show the same hetero-exchange as its predecessor, THA [273]. TBOA is still a commonly used pan-EAAT inhibitor.

The search for subtype-selective EAAT inhibitors is still underway. One of the earliest subtype-selective inhibitors described is dihydrokainate (DHK), found to be a potent blocker of EAAT2. Early studies revealed that application of DHK to the rat hippocampus increased extracellular concentrations of glutamate, and evoked spontaneous electrical activity [274]. It was later observed that DHK potently inhibits EAAT2 transport in a competitive fashion, whereas it has negligible effects of EAAT1- and EAAT3-mediated transport [271]. Although a competitive EAAT inhibitor, unfortunately, DHK also produces a glutamate efflux [275]; as a result, effects of DHK are a confluence of two factors: inhibition of glutamate uptake via EAAT2 and release of glutamate into the synapse. Further, results using DHK as an “EAAT2-selective” inhibitor must be interpreted with caution, as DHK has also been shown to interact with kainate [276] and AMPA [277] receptors at concentrations that inhibit glutamate transport.

In an effort to improve the selectivity of EAAT2 inhibition, aryl-ether aspartic acid analogs have been recently developed and characterized. These include *N*⁴-[4-(2-bromo-4,5-difluorophenoxy)phenyl]-L-asparagine (WAY-213613), *N*⁴-(2'-methyl-1,1'-biphenyl-4-yl)-L-asparagine (WAY-213394), *N*⁴-[7-(trifluoromethyl)-9*H*-fluoren-2-yl]-L-asparagine (WAY-212922), and 3-[(4'-chloro-2-methyl-1,1'-biphenyl-4-yl)-carbonyl]-amino}-L-alanine (WAY-211686) [278]. Of these, WAY-213613 is the most potent, and, unlike DHK, it has no activity at either iGluRs or mGluRs [278]. Importantly, WAY-213613 has a 50-fold selectivity at EAAT2 over EAAT1 and EAAT3 [278], making it a suitable compound for the study of EAAT2.

Even more recent, was the discovery of the first EAAT1-selective inhibitor, 2-amino-5-oxo-5,6,7,8-tetrahydro-4*H*-chromene-3-carbonitrile (UCPH-101) [279]. Brief exposure to UCPH-101 induces a long-lasting inactive state of EAAT1, while not affecting the pharmacological properties of glutamate, as it modulates EAAT1 through an allosteric site [280]. In rat serum, the half-life of UCPH-101 is 30 minutes,

and it does not penetrate the blood brain barrier as indicated by low bioavailability following oral dosing [281]. In an attempt to improve bioavailability, structural modifications have been produced; however, all modifications result in decreased EAAT1 inhibitory activity, suggesting the binding site is within a lipophilic pocket of EAAT1 [282].

Lastly, a modification of TBOA into L- β -*threo*-benzyl-aspartate (L-TBA) was developed as the first EAAT3-selective inhibitor [283]. Importantly, like UCPH-101, L-TBA is not transported via EAAT3, and does not produce substrate activity at any of the other EAATs [283]. While L-TBA does not show as strong selectivity as other EAAT subtype-specific inhibitors, it still has a 10-fold preference for blocking EAAT3 over EAAT1 and EAAT2 [284], and is highly potent ($IC_{50} = 300$ nM) [285]. Together with WAY-213613 and UCPH-101, subtype-specific effects of EAATs can now be examined.

EAAT inhibitors and nociception

Because subtype-selective inhibitors have only recently been developed, most studies of the role of EAATs in nociception have been performed using the pan-EAAT inhibitor, TBOA. Under normal conditions, spinal administration of TBOA produces sustained nociceptive behaviors in naïve rats [286, 287]. In addition, in naïve animals i.t. TBOA produces thermal and mechanical hypersensitivity, and results in elevated glutamate concentrations [286]. TBOA-induced nociceptive responses are attenuated by glutamate receptor antagonists [286]. Thus, these findings suggest that a decrease in glutamate uptake via EAAT blockers results in accumulation of glutamate at the synapse, which then acts on neuronal glutamate receptors, producing nociceptive behaviors and sensory hypersensitivity.

EAAT expression following injury

Several studies have shown that expression of spinal EAATs is altered under pathological pain conditions. Thus, expression of glial EAATs in the spinal cord has been found to be down-regulated in

rats with chemotherapy-induced neuropathy [288, 289], as well as in models of neck pain [290] and multiple sclerotic-induced neuropathic pain [291]. Similarly, following pSNL, expression of glial EAATs is significantly reduced in the SCDH [292]. EAATs are upregulated up to 5 days after CCI; however, this was followed by a down-regulation 7-14 days postoperatively [293-295]. This biphasic change also occurs in EAAT2 following SNL [296]. Thus, in the chronic phase of pathological pain conditions there is a down-regulation of EAATs, and in particular, glial EAAT1 and 2, which may contribute to nociceptive transmission. In addition to a down-regulation of glial EAATs, there is significant reduction of glutamate uptake by EAATs in the ipsilateral SCDH in rats with CFA-induced inflammation [297], as well as in the CCI model of neuropathic pain [293].

The regulation of EAAT3 in the spinal cord following injury shows mixed results. There was no observed change in EAAT3 expression in the spinal cord of CFA rats [297]. In contrast, there was an increased expression at 4 days followed by a down-regulation at 7 days post-surgery in CCI rats [293, 294]. The downregulation has been observed up to day 14 post-CCI [298]. The expression levels also appear to be dependent on neuropathic pain model, as SNI animals show an increase of EAAT3 expression at 4 days, but return to sham levels by day 14 [298]. Expression of EAAT3 was found to be negatively correlated with severity of injury following whiplash injury in rats [290]. Complicating the factor is that, unlike EAAT1 and EAAT2, a large portion of EAAT3 is kept within the cell [250, 299]; thus, whether the upregulation or downregulation results in different subcellular distributions of EAAT3 is unaccounted for in these data. It is known, however, that the transporter is readily trafficked to and from the plasma membrane following PKC activation [300], making its presence on the membrane more dynamic than glial EAATs.

EAATs inhibitors in animals with persistent pain

Based on findings from EAATs studies, it is reasonable to propose that the mechanistic role of EAATs in nociception is based on their glutamate scavenging function. Thus, the down-regulation of EAAT expression in pathological pain conditions leads to a protracted presence of glutamate at the synapse, which may then act on various glutamate receptors, thereby sustaining nociceptive transmission. However, in contrast to their action in naïve animals, and inconsistent with the above mechanism, spinal administration of EAAT inhibitors have antinociceptive effects in persistent pain conditions. For example, i.t. injection of TBOA blocks prolonged allodynia induced by prostaglandin E₂ [301] and reduces persistent nociceptive behavior in the formalin test [302]. In addition, TBOA alleviates CFA-induced thermal hyperalgesia and Fos expression in CFA rats [303]. Furthermore, the EAAT inhibitor, L-trans-pyrrolidine-2,4-dicarboxylate (L-PDC), reduces EPSP in dorsal horn neurons induced in a model of arthritic pain [304]. The antinociceptive effects of TBOA have been observed in other persistent pain models and is referred to as “paradoxical” [270]. It is important to note, however, that the literature to date focuses largely on non-selectively blocking EAATs in persistent pain conditions. Thus, from these data alone, conclusions cannot be drawn regarding which of the EAATs – or combination of EAATs— contribute to this paradoxical effect.

Interestingly, the selective EAAT2 inhibitor, DHK, shows findings inconsistent with TBOA in animal models of neuropathic and inflammatory pain. For instance, DHK reverses analgesia induced by valproate – an EAAT upregulator – in animals with SNL injury [305]. In addition, spinal DHK application produces reduced paw withdrawal thresholds in the rat model of interstitial cystitis/bladder pain syndrome [306]. The interaction of DHK with iGluRs prevents us from conclusively implicating EAAT2 in these studies; however, these findings are suggestive that EAAT2 inhibition — in the context of

neuropathic pain may indeed be pronociceptive. While conversely, the antinociceptive effects of TBOA are attributable to either the glial EAAT1 or neuronal EAAT3.

Aside from DHK, the pain literature is devoid of subtype-specific EAAT inhibitor data; however, studies altering the expression of different subtypes are available. For instance, amitriptyline increases expression of EAAT1 and EAAT2 following SNI in rats, which attenuates mechanical allodynia [307]. The antibiotic ceftriaxone also increases EAAT2 expression and activity [308]. Systemic treatment with ceftriaxone reduces visceromotor responses and thermal hyperalgesia in mice with colorectal distension, and these effects are blocked by DHK treatment [309]. Similarly, the drug valproate dose-dependently attenuates mechanical allodynia in SNL rats by partially restoring the reduced expression of EAAT1 and EAAT2 in these animals [305]. The antinociceptive effect of valproate is further augmented by application of riluzole, a drug with many actions including increasing EAAT2 activity [305]. The researchers found riluzole to only be effective in conjunction with valproate, and concluded its effects were due to the increased activity of EAAT2. However, the other effects of riluzole, including its blockade of TTX-sensitive channels and inhibition of NMDA and kainate receptors, cannot be discounted. Similarly, riluzole attenuates visceral hypersensitivity and thermal hyperalgesia in rats following maternal separation, a model of stress-induced pain, which also exhibits reduced EAAT1 expression [310]. Again, while the authors attribute the analgesic effects to increased glial EAAT function, the non-specificity of riluzole makes interpretation difficult. Riluzole is currently a treatment for amyotrophic lateral sclerosis, and its potential as a treatment for peripheral neuropathic pain has been assessed in a randomized, placebo-controlled crossover study. Unfortunately, while pain reductions are observed as compared to placebo, the majority of patients report no significant change with riluzole treatment [311].

More compelling arguments come from infusions of adenoviral vectors expressing EAAT2 in the spinal cord. The resulting overexpression of EAAT2 significantly attenuates inflammatory hyperalgesia induced by intraplantar (i.pl.) injection of carrageenan, and prevents the induction of mechanical allodynia following nerve ligation [312]. Moreover, EAAT2 overexpression in astrocytes using a human glial fibrillary acidic protein produces transgenic mice with reduced visceromotor responses to colorectal distention, a model of irritable bowel syndrome [309]. Like the DHK results, these findings suggest that the antinociceptive effects of TBOA are not attributable to EAAT2, and possibly not to EAAT1 either. Instead, as discussed further below, it could be that the antinociceptive effects of pan-EAAT inhibitors observed in animals with persistent pain are driven by actions at the neuronal transporter EAAT3.

Nuclear mGluR hypothesis of persistent pain

In light of the discovery of nuclear mGluR5, the pronociceptive effect of pan-EAAT inhibitors in chronic pain conditions may be explained by the upregulation of nuclear mGluR5 in the spinal cord. Here it is proposed that nuclear mGluR5 is a functional receptor contributing to pain hypersensitivity that characterizes persistent pain conditions. These nuclear envelope-bound receptors have been shown to induce long-term changes at the synapse via calcium modulation [40, 246, 262, 313]; however, activity at these receptors depends on the availability of intracellular ligands, including glutamate. As TBOA-inhibited processes account for 80-90% of EAAT into hippocampal cells [247], EAAT inhibition would significantly reduce nuclear mGluR5 contribution to nociceptive signalling. Thus, under persistent pain conditions, EAAT3 functioning is expected to play a central role in regulating the nociceptive function of intracellular mGluRs.

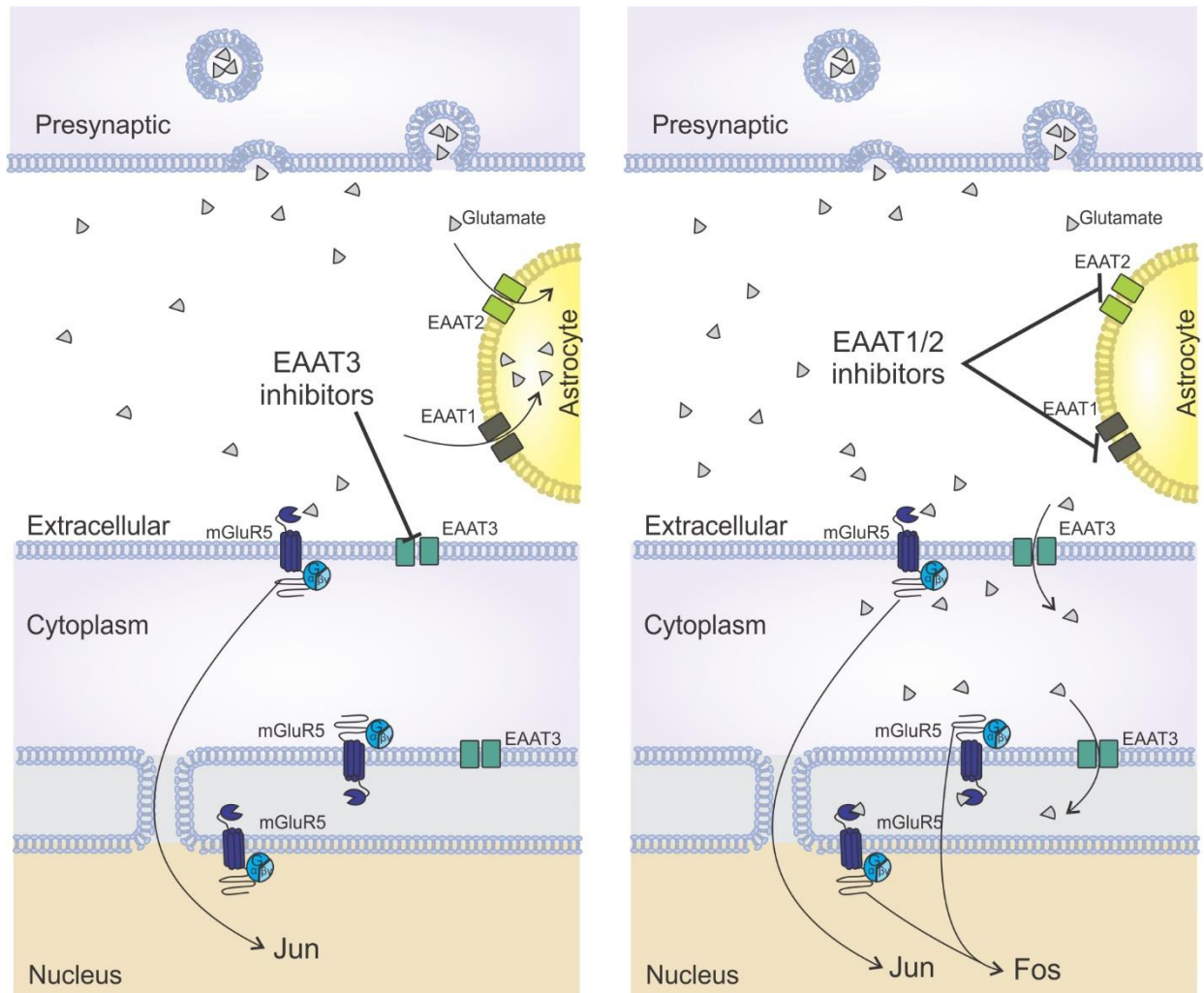


Figure 5: Neuronal versus glial glutamate transporter inhibitors.

Proposed signalling pathways affected following application of neuronal glutamate transporter (EAAT3) inhibitor (left), or glial glutamate transporter (EAAT1/2) inhibitors (right). EAAT1/2 inhibitors prevent glutamate uptake into astrocytes (right panel), while the EAAT3 inhibitor reduces Fos after blocking glutamate uptake into neurons (left panel).

To test the nuclear mGluR5 hypothesis, four lines of experiments were pursued. First, to confirm that there is indeed an increase in nuclear mGluR5 following both inflammatory and neuropathic pain, spinal cords from rats 3 days following injection of CFA, or 7 days following SNI, were extracted and fractionated into plasma membrane, cytoplasmic and nuclear fractions and probed for mGluR5 using

western blot. Next it was assessed whether spinal glutamate produces more nociceptive behaviors in rats with persistent pain due to the higher availability of nuclear mGluR5. It was also determined whether spinal glutamate injection produced an increased SCDH expression of a transcription factor associated with nuclear mGluR5 activation, *c-fos*. These experiments will first confirm that animals with either inflammatory or neuropathic pain do show hypersensitivity to spinal glutamate, and establish a baseline to compare pharmacological manipulations in later experiments. Third, it is predicted there will be differential effects of inhibiting EAAT3, which acts as the gate keeper to the intracellular sites, and EAAT1 and EAAT2, glial transporters which regulate synaptic concentrations of glutamate, on glutamate-induced nociception. Specifically, it is expected that restricting neuronal intracellular glutamate access by selectively inhibiting EAAT3 will be antinociceptive, and will attenuate glutamate-induced Fos expression in persistent pain conditions, whereas selective EAAT1 and EAAT2 inhibition (preventing glial glutamate uptake) will have a pronociceptive effect, similar to that seen in naïve animals (Figure 5). Four, it will be determined whether membrane permeable mGluR5 antagonists, which have access to nuclear receptor sites, have more robust antinociceptive effects in persistent pain conditions than impermeable antagonists, which block only cell surface receptors (Figure 6). In addition, previous reports found that while *c-fos* expression depends on nuclear mGluR5 activation, *c-jun* expression relies on plasma membrane receptors [313]. Thus, both permeable and non-permeable mGluR5 antagonism are expected to reduce glutamate-induced *c-jun* expression, while only permeable mGluR5 antagonists are expected to inhibit glutamate-induced *c-fos* expression.

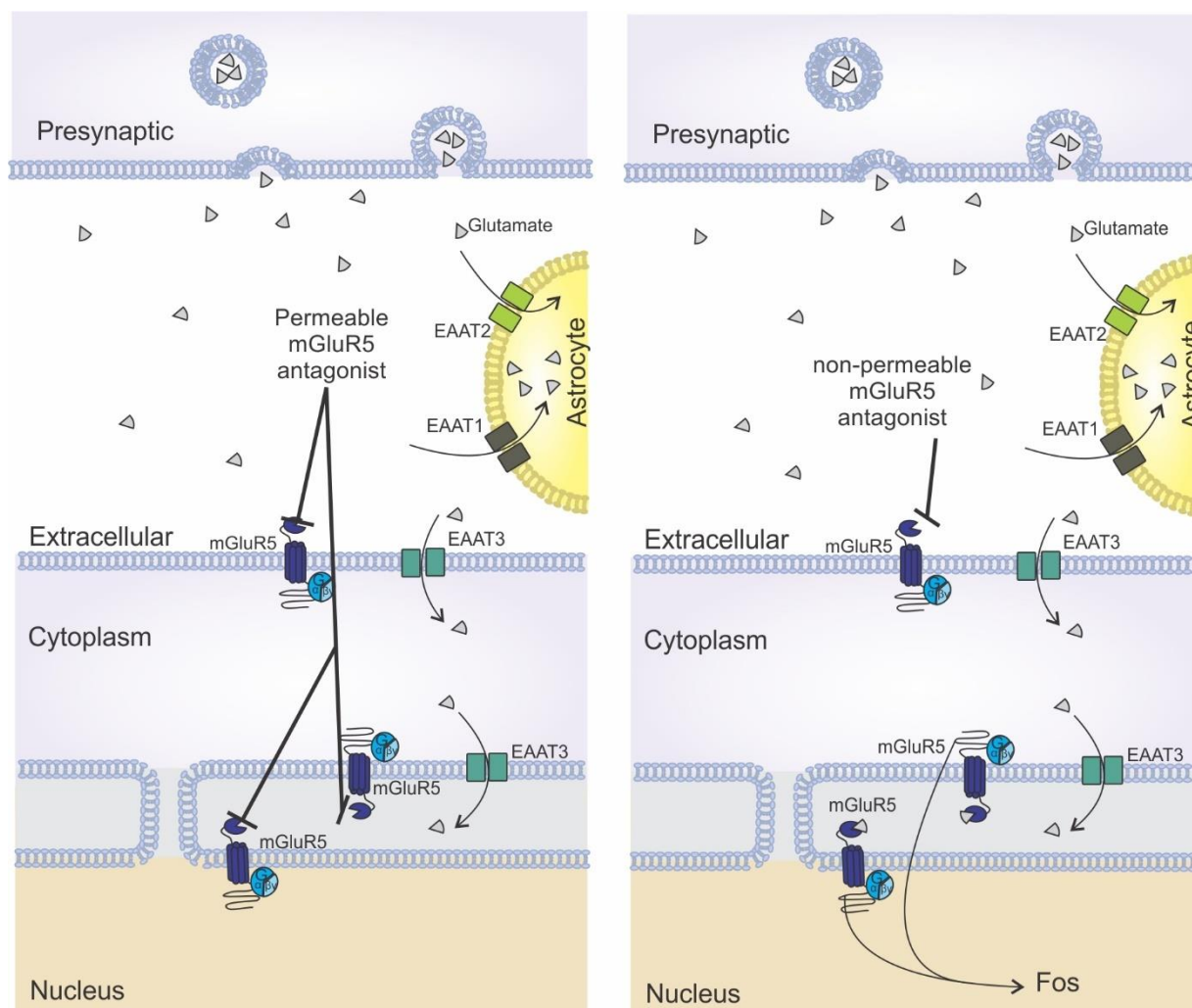


Figure 6. Permeable versus non-permeable mGluR5 antagonists.

Proposed signalling pathways affected following application of permeable mGluR5 antagonists (left), or non-permeable mGluR5 antagonists (right). A permeable mGluR5 antagonist reduces Fos by blocking both cell surface and intracellular mGluR5 (left panel). A non-permeable mGluR5 antagonist does not affect Fos, since it only blocks cell surface mGluR5 (right panel).

Background on methodologies selected

Animal models of neuropathic pain

Neuropathic pain syndromes represent heterogeneous conditions caused by lesions or disease to the somatosensory nervous system, and is estimated to affect 7-8% of adults. In the pursuit of understanding the underlying mechanisms involved in the development and maintenance of neuropathic pain, several

neuropathic pain models have been developed. While there are many causative factors that play a role in neuropathic pain, including metabolic [314], inflammatory [315], and toxic [316], most rodent models rely on mechanical nerve lesions. These models differ in both severity of nerve injury, manipulated by crushing, ligating or transecting nerves, as well as location along the nerve. Each model has its merits and limitations.

The first model developed was the complete transection (CT) of the sciatic nerve, produced by sectioning the sciatic and saphenous nerves resulting in *anesthesia dolorosa*, pain in the absence of touch sensation [317]. While it is no longer a popular model, due to the tendency of animals to severely autotomize the affected limb [318], variations inspired from this model are still employed today. For instance, rather than sectioning the nerve, the chronic constriction injury (CCI) model is produced by placing four loose ligatures of chromic cat-gut around the sciatic nerve [319]. Unlike CT, CCI is a partial nerve injury model, where there exist both intact and injured peripheral axons. CCI results in allodynia, hyperalgesia and spontaneous pain behaviors from 10-14 days post-surgery and involves both inflammatory and neuropathic components [319-321]. The injury develops as a result of constriction of the nerves, thus the severity of the symptoms depends on the tension of the ligature and the degree of damage. While variability in nerve damage may more closely resemble the variability in clinical cases of neuropathic pain, this variability can make it difficult to use in experimental paradigms that require more uniform symptoms. In addition, like the CT model, it can produce autotomizing behaviors, although typically much less [322]. Another model is the Seltzer partial sciatic nerve ligation (pSNL) model where one to two thirds of the sciatic nerve is isolated and ligated. pSNL rodents show evidence of spontaneous pain, mechanical allodynia, and thermal hyperalgesia uniformly across the ipsilateral hind paw, which

occurs within hours of the surgery and lasts several months [323]. As with CCI, pSNL has variability due to potentially different number of nerves being damaged across animals.

Instead of targeting the sciatic nerve, the spinal nerve ligation (SNL) and transection (SNT) models ligate/transect the L5 spinal nerve distal to the dorsal root ganglia [324, 325]. The advantages of these models include preservation of behavioral responses to peripheral stimuli due to the uninjured L4 axons, no autotomizing behaviors, and reduced variability as the same number of nerves are injured across animals [326]. A related model, the L5 ventral root transection (L5 VRT), transects only the ventral root central to the DRG, leaving the dorsal root intact [327]. The VRT is unique in that primary sensory fibers are spared mechanical lesion, but are exposed to the neighbouring degenerated efferent nerves, which is sufficient to produce bilateral mechanical allodynia similar to that of SNT [327]. However, disadvantage common to all three models is that the procedure requires an incision along the spinal column and damage to the paraspinal muscles, which may complicate the pathology.

The neuropathic model selected for the studies presented here is the spared nerve injury (SNI) model. This model is produced by ligating and cutting two branches of the sciatic nerve, the tibial and the common peroneal, while keeping the sural branch intact. The SNI model results in behavioral modifications occurring as early as 24 hours following surgery and lasting beyond 6 months, making it suitable to study early, persistent and chronic phases of neuropathic pain [328]. A unique feature of the SNI model is that the ipsilateral hind paw is not uniformly sensitive. SNI animals develop mechanical hypersensitivity on the medial plantar surface of the paw, which is innervated by the saphenous nerve, but to an even greater extent develop hypersensitivity to the sural nerve plantar skin region [328]. The sural nerve is part of the sciatic nerve plexus, whereas the saphenous nerve is part of the femoral nerve plexus, which enters the spinal cord through distinct DRGs. While both territories show reduced

thresholds, it is important that in the sural nerve there is co-mingling of injured and non-injured cell bodies in the same DRG, which may be important for its greater threshold reduction following SNI. In addition to reduced mechanical thresholds, SNI animals also present with pin-prick hyperalgesia and cold allodynia from 1 day post-surgery to beyond 2 months, and while there is no change to withdrawal latency to a heat stimulus, SNI animals show a greater withdrawal duration to heat [328]. The absence of a reduced heat withdrawal latency response is unique to the SNI model, as it is observed in CCI [329], pSNL [323], SNL [330], and L5 VRT [327] models. Although thermal thresholds are lowered in most animal models, this is not always a feature in clinical neuropathic pain [331]. Tactile, cold, and pin-prick hyperalgesia, which are observed in the SNI model, are associated with central sensitisation in painful neuropathies, whereas thermal hyperalgesia is a symptom more often associated with peripheral sensitization [332].

Animal models of inflammatory pain

The immune system plays an important role in initiating an inflammatory response at the site of tissue injury. A hallmark of this response is the infiltration and activation of immune cells, as well as the production of cytokines and chemokines, which help regulate the amplitude and duration of this response. In the case of persistent pain states, mounting evidence has shown that both neuroinflammation and neuroimmune activation occur following both peripheral and central injury and contribute to chronic pain. In order to understand the mechanisms underlying inflammatory pain processes, several inflammatory models have been developed. Currently there are various agents available to induce a peripheral inflammatory response, including carrageenan, zymosan, capsaicin, bee venom, formalin, mustard oil and complete Freund's adjuvant (CFA), among others. Each of these agents

may be introduced by s.c. injection to produce behavioral sensitivity, tissue swelling and infiltration of immune cells to mimic human inflammatory experience.

Several pro-inflammatory mediators are employed to produce fast-acting and short-lasting inflammatory pain responses including formalin, zymosan, bradykinin and prostaglandin E₂. I.pl. injection of these inflammatory mediators produce spontaneous pain behaviors, including lifting and licking the affected paw, which subside within 45 minutes [333]. Some agents, such as formalin or zymosan produce an early and a late phase pain response, though differ in time course [334, 335]. Interestingly, the two phases can be independently attenuated with different analgesics, suggesting different underlying mechanisms [336]. These models are particularly useful in distinguishing between nociceptive pain (early phase) and persistent pain (late phase) pathways. The disadvantage of these models is that generalization to more chronic painful inflammatory conditions is severely limited due to the short duration of nociception observed therein.

A longer lasting inflammatory mediator is carrageenan, a polysaccharide extract from a species of red algae whose inflammatory properties were originally used to test the efficacy of anti-inflammatory agents [337]. Injection of carrageenan into the hind paw produces edema which is maximal at 5 hours post-injection [338]. Carrageenan-injected rats also exhibit reduced heat withdrawal thresholds from one to 4 hours post-injection, which return to baseline by 8 hours, and exhibit mechanical allodynia measurable up to 24 hours [338]. While this is a good model to observe robust effects on behavioral responses, at higher doses it is immunosuppressive and toxic to the liver and kidneys [339, 340], and though it is longer lasting, its effects are largely gone within a day.

The most widely used mediator for peripheral inflammation is complete Freund's adjuvant (CFA), which consists of a suspension of heat-killed *Mycobacterium butyricum* or *Mycobacterium tuberculosis* in paraffin oil. Without the mycobacteria, the oil mixture serves as the vehicle control, referred to as incomplete Freund's adjuvant (IFA) [341]. Originally, the mycobacterium was used to understand why pathogenic mycobacterium induced lesions [341]. These investigations led to the discovery that animals infected with the mycobacterium exhibited a delayed dermal hypersensitivity and stimulatory effects on immunization, particularly when administered in an oil suspension. The hyperimmunization and delay-type inflammatory effects led to its use as a model for autoimmune diseases, such as arthritis [342]. The use of CFA in these models has become more and more restricted due to the long lasting, painful inflammatory response it produces in inoculated animals [343], incidentally making it a useful tool for the study of inflammatory pain.

The mechanism by which the CFA mycobacterium induces an inflammatory response is still not completely understood. The issue is complicated by the fact that IFA also produces a mild inflammatory response, and may be responsible for early cytokine induction [344]; but data on IFA-induced inflammation is limited. Within four hours, i.pl. CFA upregulates mRNA of the pro-inflammatory cytokines IL-1 β , TNF- α , and IL-6 in the lumbar spinal cord, brainstem and forebrain, which remain elevated at two weeks post-injection [345]. Inflammation of the hind paw also results in significant reduction of paw withdrawal thresholds, which is still significant at 3 weeks [346]. Thus, the advantage that CFA has over other inflammatory models is its protracted behavioral changes allow observation of acute and more chronic inflammatory pain. The CFA model was also chosen in this thesis to observe whether the presence of increased nuclear mGluR5 was a phenomenon restricted to SNI and neuropathic injuries, or whether it is a more common feature of central sensitization occurring in

persistent pain conditions. Also, the only published results, prior to this investigation, on the localization of mGluR5 in persistent pain models was performed using CFA-induced inflammation [213]. While this study did not investigate nuclear mGluR5 specifically, an overall increase in mGluR5 expression was observed with the greatest increase on the plasma membrane and not within the cytoplasm.

Testing methods for assessing pain hypersensitivity

The use of animal models allows for researchers to study, in a controlled manner, aspects of pain that could not ethically be performed on humans, while measuring outcomes that could not be assessed *in vitro*. However, the use of animals introduces the difficult task of inferring and quantifying pain, a sensory percept that reflects a subjective experience. Fortunately, there are many behavioral assays available that have operationalized pain to capture different qualities of the perception. One way to quantify pain is through evoking a withdrawal response by applying a noxious stimulus, such as heat or pressure, to the paw or tail. These 'evoked pain' assays include the Hargreaves or plantar test, von Frey test, tail-flick test and Randall-Selitto test [347]. However, whether these tests are measuring pain or simply reduced thresholds is debateable. Alternatively, sustained pain behaviors, including biting, licking, guarding and flinching can also be measured over a period of time in response to a noxious stimulus. Lastly, pain can be inferred through the use of conditioning methods, which represent a recent addition to the pain field, but have been long in use in the motivation and learning field. The use of any single behavioral assay will be limited by how it operationalizes pain, and therefore 3 different assays were employed in this work: 1) evoked mechanical hypersensitivity assessed using von Frey tests, 2) i.t. glutamate-induced sustained nociceptive behaviors and 3) analgesic conditioned place preference, all of which will be discussed below.

Von Frey thresholds

The most common assay for assessing mechanical hypersensitivity uses von Frey filaments applied to the plantar surface of the hind paw to evoke a withdrawal response [348]. Von Frey thresholds can be assessed in various ways, but a commonly used standard approach is to measure the 50% withdrawal threshold using an up-down procedure [349]. The objective is to determine the stimulus strength required to elicit a withdrawal response in 50% of the trials, referred to as the paw withdrawal threshold (PWT). PWTs have the advantage of being practical and economic to perform, show high inter-rater reliability [348, 350], and reduced mechanical thresholds is a feature observed in human pain studies [351] and in neuropathic pain patients [352]. Another advantage of PWTs is that the source of the stimulus is known – the withdrawal behavior is in response to the von Frey filament. As such, PWTs are said to be measuring evoked pain rather than spontaneous pain. A practical consideration that should be taken into account when analysing PWT data is that mechanical sensation is generally perceived on a logarithmic scale, as per Weber's law. Normally this would be accounted for in the filaments, which provide an approximate logarithmic scale of actual force, thus the output is a linear scale of intensities. However, the Dixon up-down method presumes equal stimuli intervals, despite the fact that the von Frey stimulus strength is recorded on a log-gram scale. This is problematic because it remains common practice to use a linear scale and parametric analyses when assessing PWTs when using the Dixon up-down method [353]. An argument was made that a more rigorous analysis should convert PWT to $\log(\text{PWT})$, as it takes into account Weber's Law and additionally reduces response variability and allows for parametric testing [353]. von Frey testing may also be limited in that it does not capture a major complaint of pain patients: spontaneous pain [352]. Spontaneous pain is the pain that patients typically experience in the affected region in the absence of external stimuli.

Spontaneous and sustained pain

Spontaneous pain in humans can be measured simply by administering questionnaires. In contrast, when using animals, we rely on quantifying various behaviors that correlate with acute painful experiences. These behaviors include licking [354], grooming [328, 355], vocalizations [356], grimaces [357], writhing [358], paw guarding [359], and sleep disturbances [360]. If these behaviors occur after a long-term injury they are typically considered to reflect spontaneous pain; however, when the same behaviors occur after an acute stimulus, they more are accurately described as sustained nociceptive behaviors. Typically, these later assays involve applying a noxious stimulus to the animal and timing, scoring or counting the number of behaviors performed by the animal during a given period. Which assay used depends on the choice of noxious stimulus employed, and the behaviors it elicits. In the studies presented in this paper the length of time spent licking the hind quarters is measured in response to i.t. administration of glutamate. I.t. glutamate has previously been shown to produce licking, biting and scratching of the hind limbs and tail in mice [125, 361]. As discussed above, the advantage of recording behaviors that are generated by the animal is that one is not simply measuring a reduced mechanical threshold, but rather a response to an ongoing painful experience. At the same time, the behavior measured can only be assumed to be the result of pain, as one cannot solicit verbal responses from animals. In particular, many of the behaviors including grooming, licking, and vocalizations can occur in the absence of pain, or correlate with another phenomenon, for example anxiety-induced grooming [362]. For instance, there is a greater licking in response to i.t. glutamate in mice with opioid-abstinence hyperalgesia (OAH) than in naïve mice [361]; however, whether this difference is due to greater pain experienced or to another stressor cannot be ascertained. In addition, the behaviors observed are still evoked by a noxious stimulus, and therefore still do not capture on-going levels of pain produced by a

given injury model. The interpretive difficulty inherent in these behavioral measures emphasizes the importance of using multiple assays.

Conditioned place preference

In hopes of capturing potentially more clinically-relevant measures of ongoing pain and pain relief, Pavlovian conditioning methods have started appearing in the field. Conditioned place preference/avoidance is a preclinical paradigm often used to study the rewarding/aversive effects of drugs. Twenty years ago the argument was put forward that conditioned place preference offers greater clinical relevance than traditional high-intensity, phasic nociceptive stimulation [363], though the pain field has been slow to include this task among the standard pain assessments. The task requires an apparatus with two visually distinct chambers that are separately associated with a drug and its vehicle. The chambers are connected by a third neutral chamber that is not paired with any drug, and allows the animal to pass freely between the two test chambers (Fig. 7). During drug pairing, the animal is restricted to one test chamber immediately after receiving a drug, and at another time is restricted to the other test chamber, after receiving the vehicle treatment. The number of daily pairing sessions varies, but is typically 2-3 pairings sessions [364]. On test day, the animal is placed in the neutral chamber and given access to both test chambers. The time spent in the drug-paired chamber relative to the vehicle-paired chamber is taken to indicate a reinforcing or aversive association with the drug. This paradigm can be used to study the analgesic effects of certain drugs, and at the same time can give an indication of their abuse potential, a new technique referred to as analgesic conditioned place preference. Some analgesics, such as morphine, have strong rewarding effects, whether or not the animal is experiencing pain, and produce a strong conditioned place preference in naïve animals [365] as well as neuropathic [366] and inflamed [363] animals. On the other hand, some compounds only produce a conditioned

place preference in animals currently in pain; for example, neuropathic rats favour chambers paired with gabapentin, while sham animals show no such preference [367]. Likewise, the mGluR5 antagonist fenobam induces conditioned place preference in mice with SNI, but not in sham-treated controls [176].

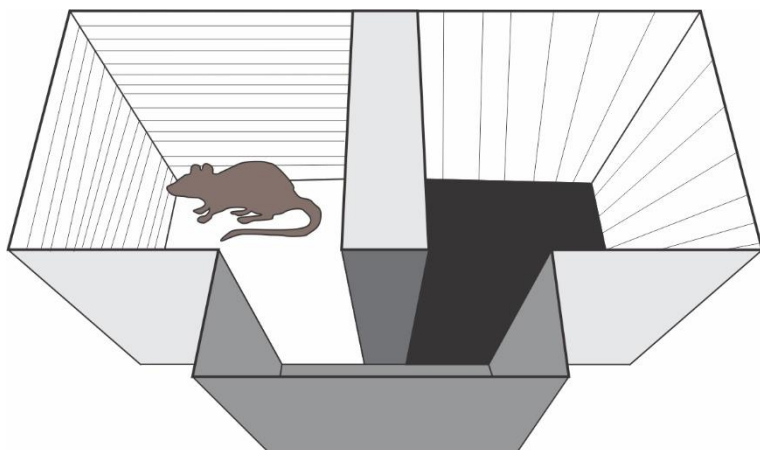


Figure 7. Conditioned place preference apparatus. The apparatus consists of two adjacent, visually distinct chambers connected by doorways to a third neutral chamber (gray). When the doors are open, the animal may move between the two testing chambers via the grey chamber.

Although conditioned place preference is new to the pain field, over the years it has been one of the most popular models to study the motivational effects of drug treatments, and several methodological considerations have been explored [364]. The apparatus itself is challenging since ideal conditioning chambers need to be distinguishable by the animals, without producing a preference at baseline. Unfortunately, many chamber designs have a side which is inherently favoured, and the apparatus is referred to as “biased”. If the experimenters choose to pair the drug with the less favoured side, rather than randomizing the pairing, then the pairing is also called “biased”. Caution should be taken with this approach, as it was found that with a biased apparatus and biased pairing, a conditioned place preference to ethanol [368] or nicotine [369] occurs only when the drug is paired in the less favoured compartment. In the studies presented in this paper, the design of the conditioning apparatus was tested with each rat to ensure there was no significant side preference at baseline, and the side in which animals

received the drug was varied using a randomized block design, so half the rats received the drug in each chamber.

There are several advantages to using and adapting conditioned place preference for analgesic testing. First and foremost is that at the time of testing animals are in a drug-free state. This is particularly useful as it circumvents some difficulties inherent with analgesics that cause sedation or impair motor abilities. It also allows one to assess drugs that produce an aversion. An issue with the von Frey assay in neuropathic animals is the presence of a floor effect. As neuropathic animals often show near the lowest possible von Frey threshold, drugs that exacerbate their condition may go unnoticed. In conditioned place preference, an aversive drug can reveal its effects through place avoidance. In a similar vein, while most pain assays show little or no effect of analgesics in animals without pain, the conditioned place preference paradigm is not limited by the same ceiling effect. As a result, it provides a unique opportunity to assess potential therapeutic agents for analgesic and reward values, without potential floor or ceiling effects.

Methods

Animals

Adult male Long Evans rats (250–300 g) were used in this study. Animals were housed in groups of two to three per cage with sawdust bedding, under a standard 12 h/12 h light/dark cycle (lights on at 08.00 AM), with food and water available *ad libitum*. All experiments were carried out according to protocols approved by the McGill University Animal Care Committee, and followed the guidelines for animal research of the International Association for the Study of Pain (IASP).

Neuropathic model: Spared nerve injury (SNI)

SNI was induced to the left sciatic nerve as previously described [328]. Prior to and throughout the surgery, rats were anesthetized with brief isoflurane (2% in 95% O₂, 5% CO₂) anesthesia. The left sciatic nerve was exposed at the middle inner thigh level using blunt dissection through the biceps femoris and the adhering tissue for an approximately a 10 mm section of the nerve. Two ligatures (6.0 Silk suture thread) 1-2 mm apart were tied around the common peroneal nerve, and the same on the tibial nerve, distal to the sciatic nerve trifurcation (Fig. 8). The two ligated nerves were then cut, leaving the sural nerve intact. Wounds were closed with one or two sutures to the muscle, followed by sutures to the skin (3.0 silk suture thread), and treatment with Furacin topical antibacterial ointment (0.2% nitrofurazone). Sham rats received the same surgery except the sciatic nerve was only exposed, and not further manipulated. The SNI surgery produces a protracted painful condition in the hind paw that can be observed within 24 hours and lasts as long as 6 months [328]. SNI rats were tested between 7-17 days when neuropathic allodynia has fully developed, and sham-operated animals have enough time to completely recover from the incisions.

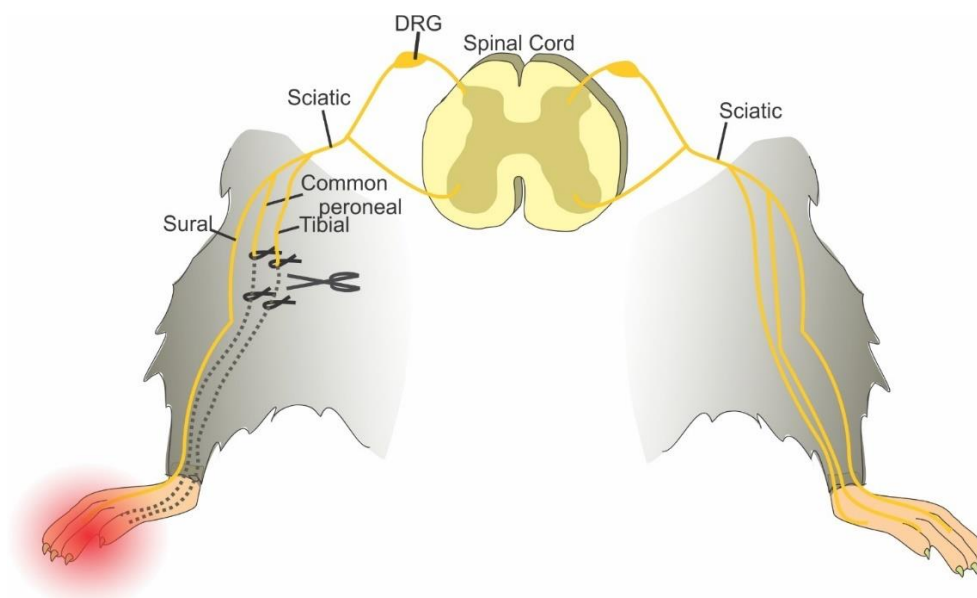


Figure 8. Spared Nerve Injury Model

Two ligatures are placed around the left tibial and common peroneal nerves prior to cutting the nerves. A small section of the nerve is removed to prevent nerve regrowth. The sural nerve is left intact. The right nerves are not manipulated.

Inflammatory model: Complete Freund's adjuvant (CFA)

Persistent inflammation was induced by injecting 50 μ L of complete Freund's adjuvant (CFA) (heat-killed and dried *Mycobacterium tuberculosis*, 0.5mg/mL, suspended in 85% paraffin oil and 15% mannide monoleate; Sigma, Oakville, ON, Canada) s.c. to the dorsal surface of the left hind paw, while the rats were briefly anesthetized with isoflurane (2% in 95% O₂, 5% CO₂). Control rats received a 50 μ L injection of the CFA vehicle – incomplete Freund's adjuvant (IFA). The CFA model of inflammatory pain produces hind paw allodynia within 6 hours and behavioral changes that last up to 2 weeks [345, 370], with evidence of spinal cord central sensitization peaking at 3 days [371], which was chosen as the time point for testing here.

Materials

Glutamate, L- β -threo-benzyl-aspartate (L-TBA), DL-threo- β -benzyloxyaspartate (TBOA), N-[4-(2-Bromo-4,5-difluorophenoxy) phenyl]-L-asparagine (WAY 213613), 2-Amino-5,6,7,8-tetrahydro-4-(4-met-hoxyphenyl)-7-(naphthalen-1-yl)-5-oxo-4H-chromene-3-carbonitrile (UCPH-101), 7-(Hydroxy imino)-cyclopropa[b]chrome-n-1a-carboxylate ethyl ester (CPCCOEt), and N-(3-Chlorophenyl)-N'-(4,5-dihydro-1--methyl-4-oxo-1H-imidazol-2-yl)urea (fenobam) were purchased from Tocris Bioscience (Ellisville, MO). 2-Amino-2-(3-cis/trans-carboxycyclobutyl)-3-(9H-thioxanthen-9-yl) propionic acid (LY393053) was generously gifted from Dr. O'Malley at Washington University, who obtained it from Lilly Research Laboratories, Eli Lilly and Company (Indianapolis, IN).

Drug administration

All drugs (except morphine) were administered by i.t. injection between the L2-L5 spinal vertebrae, while the rat was under isoflurane anesthesia. Drugs were dissolved either in distilled water (glutamate or morphine) or either 5% DMSO + 0.1M cyclodextrin or 25% DMSO in distilled water (all other drugs). Except for morphine, which was given s.c. in a volume of 1 mg/ml, all drugs were prepared to make an injectable volume of 20 μ L for spinal injection and were titrated to have a final pH of 7.40. The prepared drugs were then sonicated for 45 minutes to generate a clear solution or a micro-suspension. All drugs were prepared fresh on the day of treatment. With the exception of the microdialysis experiments, which used a cannula to administer the drug spinally, all other i.t. injections were through intervertebral lumbar punctures. The drug dosages for later experiments were based on the dose-response curves derived from the glutamate-induced pain behavior experiments. In the neuropathic experiments, drugs were administered 7 days post-SNI or sham surgery, and in the inflammatory experiments drugs were administered 3 days post-CFA/IFA injection. The exception to this was in conditioned place preference

experiments, where the drugs were administered 8-11 days post-SNI/sham surgery or 1-2 days post-CFA/IFA injection, and mechanical allodynia testing, which was performed 7-17 post SNI/sham injury.

Nociceptive testing

Glutamate-induced pain behaviors

One week post-SNI or sham surgery, rats were habituated to an observation chamber (30 × 30 × 30 cm) fitted with an acrylic floor, under which was placed a mirror to allow an unobstructed view of the animal's paws for 30 minutes. Following habituation, rats were given two i.t. injections 10 minutes apart: the first was an injection of either a pretreatment drug or vehicle and the second was an injection of 80-800 µg of glutamate. The rats were then returned to the chamber and allowed to move freely. Pain behaviors were measured as the time spent licking the hind paws, lower legs and tail over a thirty minute period. The behaviors were recorded starting from when the rats awoke from anesthesia and made their first coordinated movements. N = 6 for all groups.

Mechanical allodynia testing

Rats were tested for mechanical allodynia between 7 and 17 days after sham or SNI surgery, following each of the 5 drug treatments (L-TBA, WAY+UCPH, fenobam, LY393053 or vehicle). Only one drug was tested per day, with one day in between drug testing, and drug order was counterbalanced using a Latin square design. Prior to each testing session, each rat was habituated to a testing box (27×16×21 cm) with a wire-mesh grid floor, for a 1 h period. Prior to drug administration, a baseline was established using von Frey hairs applied through the grid floor to the ventral surface of the hind paw. Each hair was applied for a 7 second period or until the animal withdrew the hind paw without ambulating. During each testing trial, the series of hairs were presented following a validated up-down procedure [348], and the 50%

paw-withdrawal-threshold (PWT) was calculated for each rat. After a baseline score was established, rats were given either the drug or vehicle via i.t. injection and returned to the testing box. PWTs were collected 30, 60, 120 and 180 minutes following the injection. PWTs were then converted into $\log[\text{PWT}]$ for analysis. $N = 8$ for all groups.

Conditioned place preference – SNI

Conditioned place preference procedures began on day 7 following the sham or SNI surgery. The conditioned place preference apparatus consisted of two pairing chambers connected by a third neutral chamber, with removable doors between the chambers. On the habituation and test sessions (day 7 and 12 post-surgery) all doors were open allowing the rats to freely explore all three chambers. The pairing chambers contained distinctive visual cues (horizontal versus vertical black and white lines) on the walls of the two pairing chambers and differing tactile cues (acrylic versus plywood surface) on the floors of the two pairing chambers. During the habituation session when the rats were allowed to explore all chambers for 30 minutes, an initial measurement of baseline place preference was taken by measuring the time spent in each chamber over 15 minutes. Rats spending more than 75% of the time in one chamber during baseline place preference measurement were removed from the experiment. The next day, using a randomized block design, rats were assigned a chamber-drug pairing. Either the drug or the vehicle was administered i.t. (except morphine and its vehicle, which were given s.c.), and the rats were restricted to one of the two pairing chambers for a period of 60 minutes. The following day, the rats received the other drug/vehicle in the opposite chamber. On the conditioned place preference test day, the rats were placed in the conditioned place preference chamber with all doors open for 15 minutes, and the time spent in the drug- or vehicle-paired or neutral chamber was again measured. The conditioned place preference index (CPP-I) was defined as the time spent in the drug-paired chamber,

divided by the time spent in both the drug- and vehicle-paired chambers, multiplied by 100; a CPP-I greater than 50% indicates a preference for the drug-paired chamber, while a CPP-I less than 50% indicates an aversion to the drug-paired chamber. N = 8 for all groups, except for the morphine study where N = 9 per group.

Conditioned place preference – CFA

The protocol for conditioned place preference in CFA rats was adapted from one previously validated in CFA animals [372]. Habituation occurred prior to any pain manipulation. During the habituation session in which the rats were allowed to explore all chambers for 30 minutes, an initial measurement of baseline place preference (BPP) was taken by measuring the time spent in each chamber over 20 minutes. Rats spending more than 75% of the time in one chamber at habituation were removed from the experiment. Following habituation, rats in the CFA condition were injected with 100 μ l CFA into the left dorsal hind paw. The control group received no injection (naïve). The next morning (18 hours post-CFA), rats were given an i.t. or i.p. vehicle injection and isolated to one room for one hour. The vehicle was saline for the L-TBA and morphine condition, and 5% DMSO + 0.1M cyclodextrin in all other drug conditions. Four hours later each rat received an i.t. injection of the drug (except morphine which was given i.p.) and was isolated to the other room. The following day (48 hours post-CFA) was the conditioned place preference test day. The rats were placed in the chamber with the all doors open for 20 minutes, and the time spent in the drug- or vehicle-paired or neutral chamber was again measured. The CPP-I again was defined as the time spent in the drug-paired chamber divided by the time spent in both the drug- and vehicle-paired chambers multiplied by 100; a CPP-I greater than 50% indicates a preference for the drug-paired chamber, while a CPP-I less than 50% indicates an aversion to the drug-paired

chamber. N = 11 for all groups, except for the morphine study, where N = 8 per group. To avoid a latent drug effect, the drug was always paired second in the afternoon. To test whether there was a specific effect of afternoon testing, one experiment used saline injections in both the morning and afternoon, and the CPP-I of the saline-saline paradigm was measured.

Immunohistochemistry

Tissue preparation

Thirty minutes following i.t. injection of glutamate or vehicle, animals were deeply anesthetized with Equithesin (6.5 mg chloral hydrate and 3 mg sodium pentobarbital in a volume of 0.3 mL per 100 g body weight, i.p.), and then were perfused through the left cardiac ventricle with 100 mL of phosphate buffered saline (PBS), followed by 500 mL of 4% paraformaldehyde (PFA) in 0.1 M phosphate-buffer (PB), pH 7.4, at room temperature for 30 minutes. Subsequently, the spinal cord was extracted and post-fixed in the same fixative for 2 hours at 4°C. The tissue was cryoprotected in 30% sucrose in PB overnight at 4°C. The next day, 20 µM thick cross-sections of L4-L6 spinal cord were cut using a cryostat (Leica, Wetzlar, Germany) and collected on poly-L-lysine coated superfrost plus slides (Fisher Scientific, PA, USA). The slides were stored at -80°C until staining.

Staining protocol

The tissue sections were incubated for 1 hour at room temperature in 10% normal donkey serum in PBS with 0.1% Triton-x (PBS-Tx) to block unspecific labeling. The slides were then stained for either Fos or Jun. The sections were incubated at 4°C for 24 hours using sheep polyclonal antibody to Fos (Abcam, MA, USA, diluted 1:500), and rabbit polyclonal to Jun (Abcam, MA, USA, diluted 1:1000) in PBS-Tx. As controls, some sections were processed omitting the primary antibody, for which no specific staining

was observed. After three rinses in PBS-Tx, the sections were incubated for 4 hours at room temperature with donkey polyclonal anti-rabbit IgG conjugated to Rhodamine Red (Jackson ImmunoResearch Laboratories, Lot # 90396, diluted 1:500). Finally, the sections were washed and cover-slipped with an anti-fading mounting medium (Aqua PolyMount, Polysciences Inc., Warrington, Pa.). The slides were stored at 4°C until examined using fluorescent microscopy. To maintain consistent conditions during microscopy, one no primary slide and one glutamate-treated animal slide was used as negative and positive control, respectively, prior to visualizing slides from each drug condition.

Cell counting

The number of Fos- and Jun-labelled cells were estimated using ImageJ (NIH freeware). Images were first converted into 8-bit format. The *Threshold* command was used to segment the image into labelled cells and background. Particles that were too small (< 100 pixels) or too large (> 1000 pixels) were excluded with the size function. Circularity ($4\pi \times \frac{[Area]}{[perimeter]^2}$) parameters were set up such that particles with size circularity greater than 0.95 were considered artifacts and were excluded. The *Show/Outline* function, which displays the contour of the counted cells, was employed to ensure the selection criteria were appropriate. The average number of Fos- and Jun-labelled cells per animal was used as a single data point, with 10-12 sections averaged per animal (biological replicates). Thus, for immunohistochemical analysis, the sample size is 6 animals, where each point represents the average over all sections for that animal.

Subcellular fractionation and western blot analysis

Tissue collection

Tissue from adult male rat spinal cords was collected at 7 days post-SNI/sham surgery or 3 days post-CFA/IFA injection. Rats were anesthetized with sodium pentobarbital (3 mg/Kg) and decapitated. Spinal cords were removed and a 1 cm section from the lumbar spinal cord was isolated and the dorsal hemisection was collected. Subcellular fractionation was performed using a subcellular protein fractionation kit (ThermoFisher Scientific, #87790). Approximately 50 mg of tissue was washed with ice-cold PBS and excess liquid removed. All the following incubations and centrifugations were performed at 4°C. Tissue was cut into pieces and placed in a pre-chilled homogenization tube where ice-cold cytoplasmic extraction buffer (500 µl) and 1% Halt protease inhibitor cocktail, 100X, was added. Tissue was homogenized with Dounce tissue homogenizer and incubated for 60 minutes. The homogenate was centrifuged at 1,000 g for 60 minutes. The supernatant (cytosolic extract, containing soluble cytoplasmic proteins) was transferred to a pre-chilled tube on ice. Ice-cold membrane extraction buffer (325 µl) and 1% Halt protease inhibitor cocktail, 100X, was added to the pellet and vortexed for 5 seconds then incubated for 60 minutes, with mixing followed by centrifugation at 3,000 g for 5 minutes. The supernatant (membrane extract, containing plasma membrane-bound proteins) was transferred to a pre-chilled tube. Ice-cold nuclear extraction buffer (110 µl) and 1% Halt protease inhibitor cocktail, 100X, was added to the pellet, vortexed for 5 seconds and incubated for 30 minutes, with mixing followed by centrifugation at 5,000 g for 5 minutes. The supernatant (soluble nuclear extract, containing proteins on and within the nucleus) was transferred to a pre-chilled tube, and all fractions were analysed using a Bradford assay and stored at -80 °C.

Western blot

In addition to probing for mGluR5, to confirm appropriate subfractionation, western blots of separate fractions were assessed for: N-Cadherin, a plasma membrane marker; HDAC-1, a nuclear marker; and GAPDH, a cytoplasmic marker. A 10% separating gel was prepared the day prior to running the western blots using 5 ml of 30% acrylamide, 0.8% bisacrylamide, 3.75 ml 4x tris-Cl/SDS (pH 8.8), 6.25 ml MilliQ H₂O, 50 µl of 10% ammonium persulfate and 10 µl TEMED. The stacking gel was prepared using 0.65 ml 30% acrylamide/0.8% bisacrylamide, 1.25 ml 4x tris Cl/SDS (pH 6.8), 3.05 ml MilliQ H₂O, 25 µl 10% ammonium persulfate and 5 µl TEMED. An equal volume of loading buffer with 7% β-mercaptoethanol was added to each tissue sample and heated for 8 minutes. Gels were run and transferred onto PVDF membranes (Bio-Rad) overnight. Membranes were washed 3x10 minutes in 1% PBS-Tx, and then blocked with 10% normal donkey serum (Sigma-Aldrich, D9663) in 1% PBS-Tx for 1 hour at room temperature. Membranes containing the cytoplasmic fraction were cut and the top half probed for mGluR5 and the bottom for GAPDH. For plasma membrane and nuclear membrane blots, the PVDF membranes were probed with mGluR5 first and stripped and reprobed for HDAC-1 or N-Cadherin. Primary antibodies used were monoclonal rabbit anti-mGluR5 (Abcam, ab27190, 1/1,000), polyclonal rabbit anti-N-Cadherin (Abcam, ab18203, 1/2,500), polyclonal rabbit anti-HDAC-1 (Abcam, ab109411, 1/2,500), or polyclonal rabbit anti-GAPDH (Abcam, ab8227, 1/1,000) and incubated overnight at 4°C. Membranes were washed 3x10 minutes in PBS-Tx followed by 1/15,000 anti-rabbit IgG horseradish peroxidase (Abcam, ab6721) for chemiluminescent detection followed by 3 x 10 times washing in 1% PBS-Tx. Detection was performed using Pierce ECL western blotting substrate (ThermoFisher Scientific, cat #32106) and film developed. Densitometric analyses of proteins were performed using ImageJ software (NIH freeware) using the *Gel* analysis tool. The generated histograms were checked for Poisson distribution to ensure

blots were not over-saturated. Quantification was performed by normalizing the mGluR5 bands to the relevant fraction-specific loading control. Loading controls were also compared between groups to ensure there were no condition-specific changes to the loading control proteins.

Microdialysis Sampling

Microdialysis fibres and an i.t. injection catheter were implanted into rats as described previously [373]. 48 hours after 50 μ l i.pl. CFA in the left hind paw or 7 days after SNI surgery, rats were placed in a Ratern interactive system chamber (Bioanalytic Systems, Inc, West Lafayette, IN, USA) with a tethering system, which allowed tubing from the microdialysis catheter to be connected to a syringe pump on one end and to a refrigerated fraction collector on the other. Dialysate samples were collected every 5 minutes at 2 μ l/min flow rate of artificial CSF (154.7 mM Na⁺, 2.9 mM K⁺, 1.1 mM Ca²⁺, 0.82 mM Mg²⁺, 132.49 mM Cl⁻, bubbled with 95% oxygen and 5% CO₂). Six baseline samples were collected after 1 hour equilibrium time (3 samples normalized to 100%). Two samples were collected after i.t. injection of 20 nM UCPH-101 or vehicle.

Statistical analysis

In selecting animals for experimental conditions, cages housing 3 animals each were randomly assigned to a pain condition. Thus, SNI animals were housed with other SNI animals, and CFA animals were housed with other CFA animals. Within each pain condition, animals were randomly assigned to experimental conditions. The exception for this was the conditioned place preference experiments where a randomized block design was used to assign animals to a chamber side. In these experiments, randomization was performed after baseline place preference measurement, such that the baseline place preference for all groups was ~50%. In all experiments, measurements were performed with the

experimenter blind to the experimental drug or dose conditions, but not the pain condition, as SNI and CFA produce visible differences in gait and hind paw swelling, respectively.

All values in graphs are expressed as mean \pm SEM. All statistical tests were performed using GraphPad Prism version 5 for Windows (GraphPad Software, La Jolla, CA). In the studies using i.t. injections of glutamate, no repeated measures were used to avoid any long-term effects of spinal glutamate application. As a result, the behavioral dose-response curves were analysed using between group two-way ANOVAs (pain condition \times dose), and post-hoc comparisons between drug dose to vehicle condition, unless stated otherwise, were performed using two-tailed Dunnett's t-tests. In experiments of mechanical allodynia, each animal experienced each drug condition and the experimenter performing the von Frey assay was not the same as the experimenter performing the drug injections. Paw withdrawal thresholds were analyzed by mixed factor two-way ANOVA, where time post-injection was the repeated factor and drug was the between factor. Dunnett's t-test was used to determine which time points were significantly different from baseline. While it has been argued that paw withdrawal thresholds should be transformed to a logarithmic scale [353], both untransformed and transformed data showed the same statistical significance, so the untransformed data is presented here for clarity of interpretation.

For the conditioned place preference experiments, CPP-I was analyzed in two ways. First, to identify which drug treatments produced a significant conditioned place preference, a one sample t-test was performed. A one-sample t-test compares a sample to a theoretical mean. The null hypothesis for a conditioned place preference test is that animals will spend 50% of their time in the treatment room. Thus, to determine if a drug produces a significant preference or avoidance behavior, a one sample t-test comparing the CPP-I of that group to the theoretical mean of 50% is performed. If the CPP-I of a

drug is significantly greater than 50%, a conditioned place preference is said to have occurred, if the CPP-I of the drug is significantly less than 50%, a conditioned place aversion is said to have occurred. Second, a between measures two factor ANOVA was also performed to determine whether the CPP-I of various drugs differed from each other. This test was to compare whether the time spent in a drug-paired room differed between the conditions, regardless of whether a significant conditioned place preference/aversion was observed.

Immunohistochemical data comparing different pre-treatments were analysed using two-way ANOVAs. Bonferroni post-hoc test was used to determine which drug conditions were significantly different from vehicle pre-treatment, which was first normalized to zero.

Results

mGluR5 is increased in nuclear-enriched SCDH fractions of rats with neuropathic pain

SNI rats were used to test whether nuclear mGluR5 is altered in neuropathic pain. Previously, electron microscopy results from our lab have shown that there is a marked increase in immunogold-labelled mGluR5 on the nuclear envelope in the spinal cord dorsal horn of SNI rats [214]. These data allowed for the quantification of immunogold-labelled mGluR5 associated with the plasma membrane, the nuclear envelope and the cytoplasm. However, absent from this quantification was any indication of whether the tagged receptors were full length or found as monomers and dimers. Importantly, incomplete receptors or a change from dimeric to monomeric forms may influence quantification of electron microscopy results which only identify a portion of the mGluR5 sequence. To determine whether there are changes in full length mGluR5 in both monomeric and dimeric forms on the various membranes, sections from the L4-L6 spinal cord dorsal horn (SCDH) of sham operated and SNI rats were collected and fractionated into cytoplasmic soluble, plasma membrane and nuclear membrane enriched fractions and compared using western blots (Figure 9).

In nuclear-enriched fractions, mGluR5 monomers and dimers were observed in samples from both sham and SNI animals (Figure 9A). A band for HDAC-1, a nuclear loading control, was also observed in each fraction and used to standardize mGluR5 levels of each sample in the densitometric analysis (Figure 9B). Two-way mixed factor ANOVA revealed a significant main effect of pain condition ($F(1,6)=14.72$, $p=0.0086$), with neuropathic animals showing greater overall mGluR5 intensity. Simple main effects showed significant increases in both the monomeric ($t(6)=3.663$, $p=0.0105$) and dimeric ($t(6)=3.996$, $p=0.0010$) forms. There was also a significant main effect of receptor size ($F(1,6)=95.11$, $p<0.0001$). Thus, in the nuclear fraction, there were significantly more monomeric forms of mGluR5 than dimeric forms.

These results agree with the observed increase in mGluR5 on the nuclear envelope as measured by electron microscopy [214]. In addition, the monomeric band of mGluR5 within SNI animals appeared wider than that in controls. This shift may represent post-translational modifications to the protein under neuropathic pain conditions.

Next, plasma membrane-enriched fractions from day 7 sham and SNI animals were analyzed for mGluR5 protein (9C). Blots were stripped and reprobed for N-Cadherin, a loading control for the plasma membrane, to standardize mGluR5 bands in the densitometric quantification (9 C,D). A two-way mixed factor ANOVA revealed a main effect of pain condition ($F(10)=3.826$, $p=0.0067$), with significantly more mGluR5 protein being present in sham animals. Simple main effects revealed no difference in monomeric forms of mGluR5 between the two conditions; however, there was significantly less dimeric mGluR5 in SNI plasma membrane fractions as compared to controls ($t(5)=4.492$, $p=0.0064$). A modest decrease in plasma membrane-bound mGluR5 was also observed in the previous electron microscopy report [214], which agrees with the main effect observed in the westerns.

Lastly, the cytoplasmic-enriched fractions containing cytoplasmic-soluble contents from sham and SNI lumbar SCDHs were assessed for mGluR5 protein by western blot (Figure 9E). The loading control for cytoplasmic fractions, GAPDH, was used to standardize mGluR5 band intensity for densitometric quantification (Figure 9F). As seen in the blot and quantification, there were no observable changes between sham and SNI fractions (Figure 9E-F); however, monomeric forms of mGluR5 were far more predominant than dimeric forms ($F(1,12)=32.02$, $p<0.0001$) within the cytoplasm.

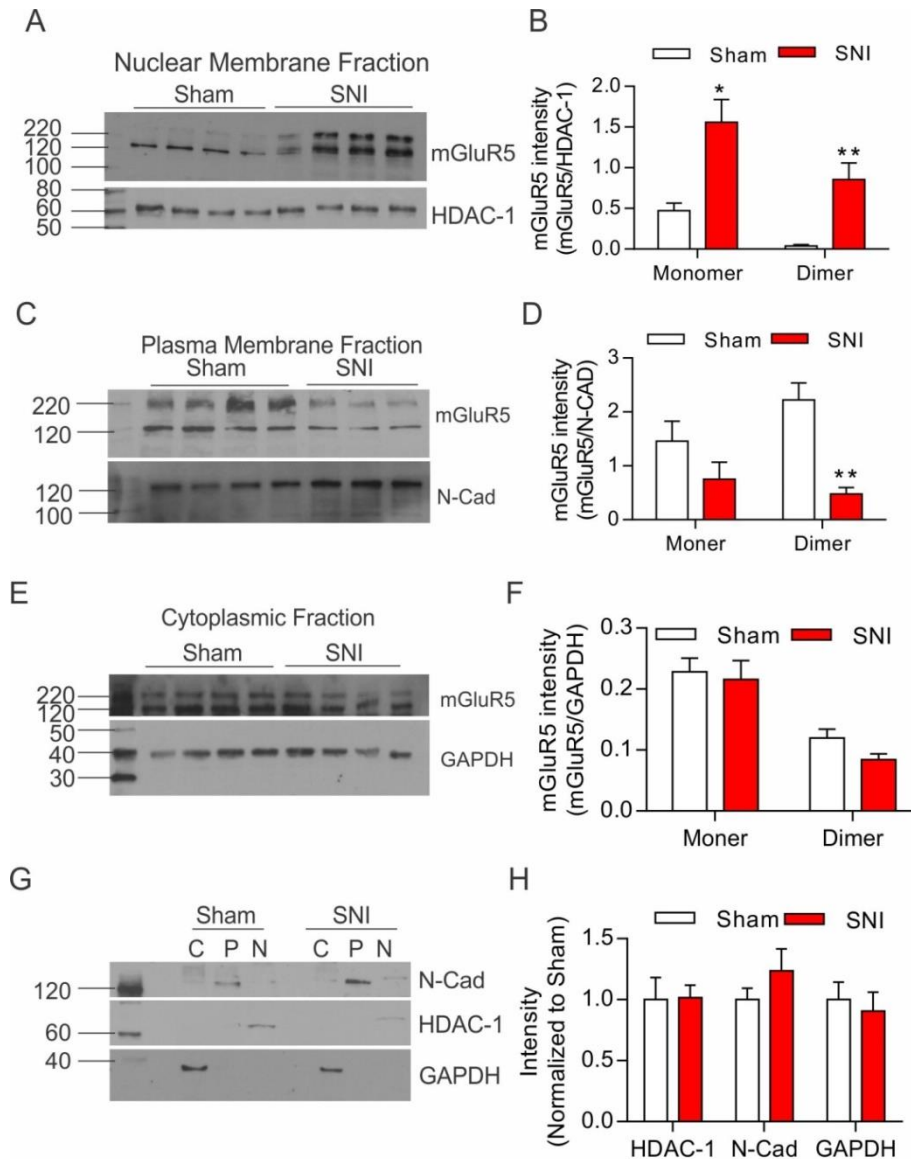


Figure 9. mGluR5 is increased in nuclear fractions in SNI animals.

(A) Western blot of nuclear membrane-enriched fractions from four day 7 sham/SNI rats probed for mGluR5 and with the nuclear marker, HDAC-1 used as a loading control. A protein ladder is on the left. (B) Densitometric quantification of mGluR5 monomer and dimer levels in A normalized to HDAC-1. (C) Western blot of plasma membrane-enriched fractions from sham and SNI samples probed for mGluR5 (top) and plasma membrane loading control, N-cadherin (bottom). A rprotein ladder is on the left. (D) Densitometric quantification of mGluR5 monomer and dimer levels in C normalized to N-cadherin. (E) Western blot of cytoplasmic-enriched fractions from sham and SNI samples probed for mGluR5 (top) and cytoplasmic loading control, GAPDH (bottom). A protein ladder is on the left. (F) Densitometric quantification of mGluR5 monomer and dimer levels in E normalized to GAPDH. (G) Representative western blot of cytoplasmic (c), plasma membrane (p), and nuclear membrane (n) enriched fractions of a 7 -day post-sham and SNI animal probed for each of the 3 loading controls. Ladder is on the left. (H) Densitometric quantification of loading controls taken from blots in A, C and E, normalized to sham levels. N-Cad = N-cadherin. * $p < 0.05$, ** $p < 0.01$.

A sample of cytoplasmic, plasma membrane and nuclear-enriched fractions from sham and SNI animals was also run within a single blot to confirm fraction-enrichment (Figure 9G). N-cadherin was most strongly associated with the plasma membrane-enriched fraction, HDAC-1 was most strongly associated with the nuclear membrane-enriched fraction, and GAPDH was most strongly associated with the cytoplasmic fraction. These results indicate that fraction enrichment was successful. There were also no significant differences in the intensity of any loading control protein used between sham and SNI samples (Figure 9H), indicating that changes in normalized mGluR5 levels are indicative of changes in mGluR5 protein content rather than an artifact of changes in loading control protein.

It is important to note that unlike in the nuclear fraction, the cytoplasmic and plasma membrane fractions do not have the same mobility shift observed in the monomeric band. Thus, the nuclear mGluR5 in SNI animals appear to have unique post-translational modifications in monomeric mGluR5.

mGluR5 is increased in nuclear-enriched SCDH fractions of rats with inflammatory pain

Three days following CFA injection to the hind paw male rats were used to test whether nuclear mGluR5 is altered in inflammatory pain. As with neuropathic animals, L4-L6 segments from the SCDH were removed from CFA and IFA animals and fractionated into plasma membrane, nuclear membrane and cytoplasmic-enriched fractions and analyzed through western blot. mGluR5 bands show up in both monomeric and dimeric forms in all fractions (Figure 10A-F). These bands were normalized to each fraction-specific loading control for quantification.

Western blot of nuclear-enriched fractions from CFA samples showed an apparent increase in mGluR5 band intensity compared to IFA samples (Figure 10A). The nuclear loading control, HDAC-1, was observed in all samples and was used to normalize the mGluR5 monomeric and dimeric bands for the

densitometric quantification (Figure 10B). Two-way mixed factor ANOVA of the results indicated a significant main effect of pain condition ($F(1,6)=10.87$, $p=0.0165$), with CFA samples having greater mGluR5 levels than IFA samples. Bonferroni's multiple comparison test revealed significantly greater normalized monomeric mGluR5 band intensities in CFA samples ($t(6)=3.179$, $p<0.0191$). Interestingly, there was no significant difference in the dimeric band intensity between the two groups. Thus, while there was an overall increase in mGluR5 protein level following CFA-induced inflammation, this difference was largely accounted for by an increase in monomeric mGluR5 levels. Across conditions, there was more protein observed in the monomeric band in nuclear-enriched fractions ($F(1,6)=46.07$, $p<0.0005$). Similar to neuropathic nuclear samples, mGluR5 predominantly appeared as monomers in westerns in the nuclear-enriched fraction of inflamed and control animal SCDHs.

Next, the plasma membrane-enriched fractions from CFA and IFA animals were probed for mGluR5 protein and the plasma membrane loading control, N-cadherin (Figure 10C). Normalizing the dimer and monomer bands of mGluR5 to N-cadherin revealed no detectable difference in plasma membrane mGluR5 levels between CFA and IFA animals as measured by densitometry (Figure 10D). However, in plasma membrane-enriched fractions the dimer mGluR5 band showed greater protein levels than the monomer band ($F(1,6)=91.23$, $p<0.0001$). Thus, in contrast to the nuclear fraction where the mGluR5 protein appears to be mainly present in monomeric form, plasma membrane mGluR5 was more often observed as dimers.

Lastly, the cytoplasmic fraction from inflamed and control animal SCDHs were probed for mGluR5 protein and the cytoplasm loading control, GAPDH, in a western blot (Figure 10E). Monomer and dimer bands were quantified through densitometry and normalized to GAPDH (Figure 10F). Quantification reveals that there was no significant difference in mGluR5 protein levels between CFA and IFA samples.

However, in this fraction, the majority of mGluR5 appeared in the monomeric band ($F(1,6)=32.74$, $p<0.0012$).

A western blot containing a sample from each fraction of an IFA and CFA animal was also probed for each loading control protein to confirm fraction separation (Figure 10G). N-cadherin (top) appeared most strongly in the plasma membrane fraction, HDAC-1 (middle) appears predominantly in the nuclear-enriched fraction and GAPDH (bottom) appeared largely in the cytoplasmic fraction. Thus, fractions were considered to be well separated for the purpose of the above analyses. In addition, the loading control protein in Figure 10A,C and E were all normalized to the sham band to test for changes in loading control proteins between fractions (Figure 10H). No significant differences in loading control proteins were observed between CFA and IFA samples. From this it was concluded that any differences observed in the densitometric quantification were not due to the normalization process, but to changes in mGluR5 protein levels.

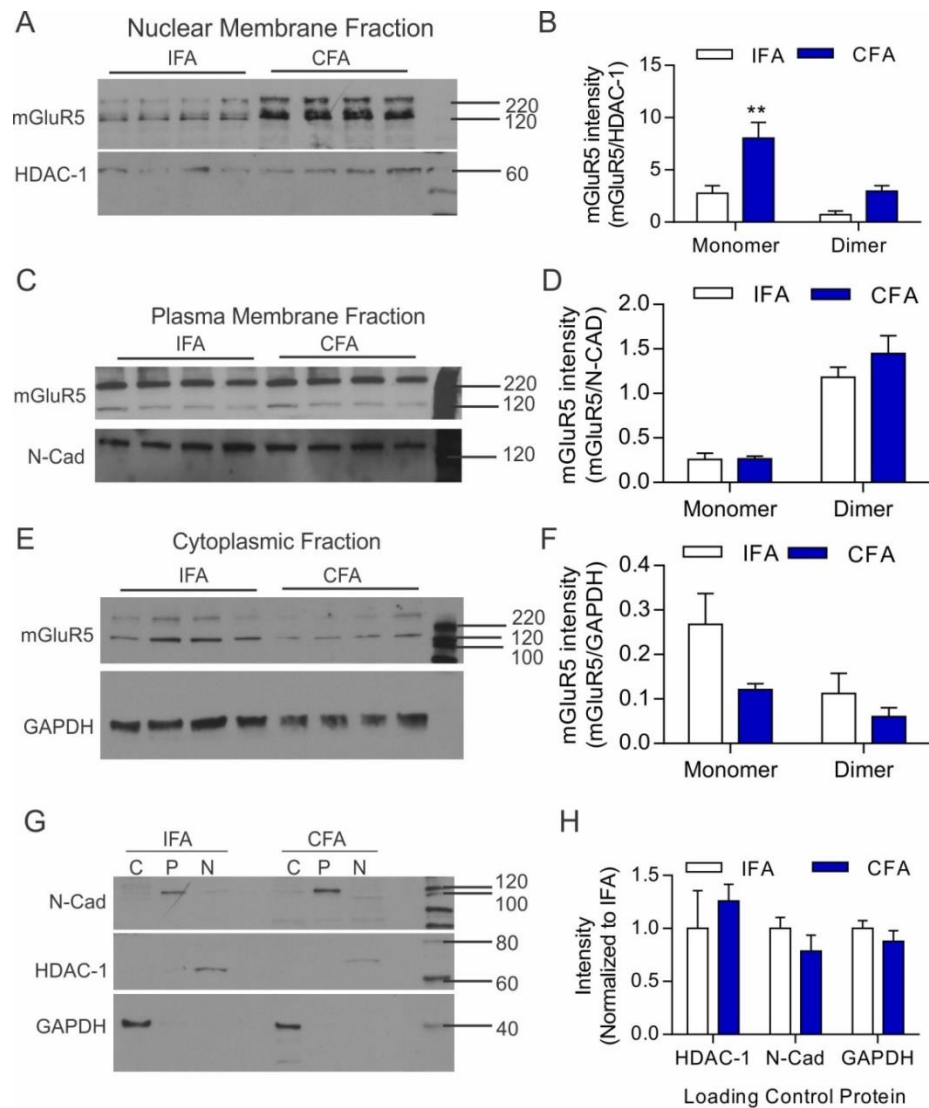


Figure 10. mGluR5 is increased in nuclear fractions in CFA animals

(A) Western blot of nuclear membrane-enriched fractions from four day 3 CFA/IFA rats probed for mGluR5 and with the nuclear marker, HDAC-1 used as a loading control. A protein ladder is on the right. (B) Densitometric quantification of mGluR5 monomer and dimer levels in A normalized to HDAC-1. (C) Western blot of plasma membrane-enriched fractions from IFA and CFA samples probed for mGluR5 (top) and plasma membrane loading control, N-cadherin (bottom). A protein ladder is on the right. (D) Densitometric quantification of mGluR5 monomer and dimer levels in C normalized to N-cadherin. (E) Western blot of cytoplasmic-enriched fractions from IFA and CFA samples probed for mGluR5 (top) and cytoplasmic loading control, GAPDH (bottom). A protein ladder is on the right. (F) Densitometric quantification of mGluR5 monomer and dimer levels in E normalized to GAPDH. (G) Representative western blot of cytoplasmic (C), plasma membrane (P), and nuclear membrane (N) enriched fractions of a 3 day post-IFA and CFA animal probed for each of the 3 loading controls. Ladder is on the right. (H) Densitometric quantification of loading controls taken from blots in A, C and E, normalized to IFA levels. N-Cad = N-cadherin. ** $p < 0.01$.

Nuclear mGluR5 increased by one day following SNI surgery

In the SNI model of neuropathic pain, changes in mechanical allodynia are observed clearly 24 hours following the surgery and persists for at least 9 weeks [328]. To determine when changes in nuclear mGluR5 levels are observed in SNI animals, L4-L6 segments of the spinal cord were collected 24 hours, 3 days, 5 days and 7 days following nerve injury. Subcellular fractionation into plasma membrane, nuclear membrane and cytoplasmic soluble fractions were collected from each time point and compared to naïve animals of the same age. In addition to observing when the mGluR5 appears on the nuclear fraction, we were interested in knowing whether an increase in nuclear mGluR5 was associated with a decrease in mGluR5 within other fractions. This could be suggestive of a migration of mGluR5 between fractions. Alternatively, increases in nuclear mGluR5 presence in the absence of comparable decreases within plasma membrane or cytoplasmic fractions may suggest new receptor formation.

Nuclear fractions collected from naïve and 1, 3, 5 and 7 days post-SNI cords showed mGluR5 monomeric and dimeric bands in the western blot (Figure 11A). The nuclear loading control, HDAC-1, appeared as two bands in this western, and only the lower band appearing around 60 kda was used to normalize the mGluR5. A two-way ANOVA with one within-group measure (monomeric and dimeric bands) and one between group measure (days post-SNI) revealed a significant main effect of both factors ($F_{\text{within}}(1,14)=83.94$, $p<0.0001$, $F_{\text{between}}(4,14)=6.300$, $p<0.0041$). Thus, there was a significant main effect of time-post SNI on nuclear mGluR5 level. To determine which time points showed significant changes compared to naïve animals, Dunnett's post-hoc test for multiple comparisons was performed (Figure 11B). A significant increase in mGluR5 dimer band intensity normalized by HDAC-1 was observed one day following SNI ($t(9)=4.545$, $p<0.0046$) and again at 7 days ($t(9)=3.840$, $p<0.0128$).

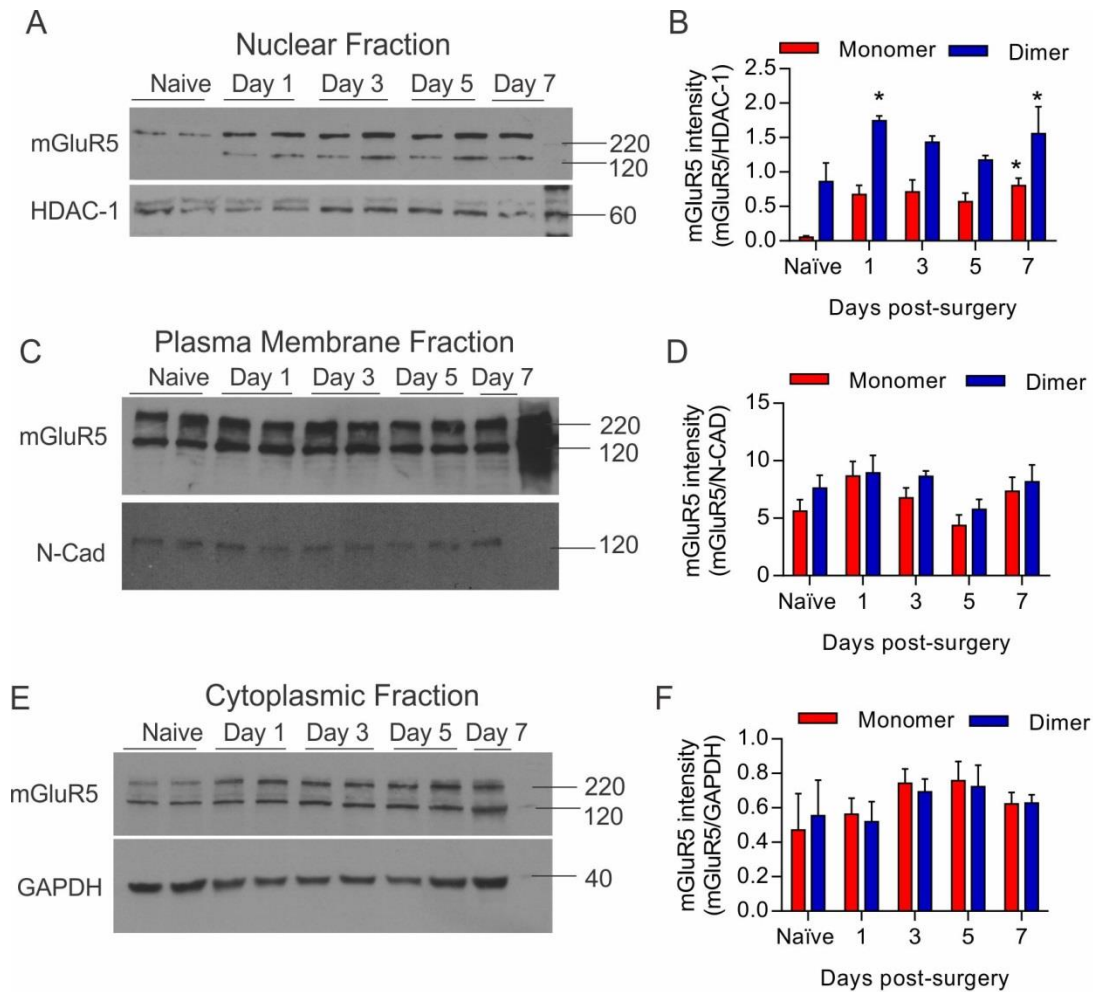


Figure 11. Time course of the changes in subcellular localization of mGluR5 following SNI

(A) Representative western of SCDH nuclear-enriched fractions from naïve rats and SNI rats at day 1, 3, 5 and 7 after surgery. Blots were probed for mGluR5 and nuclear loading control, HDAC-1. A protein ladder is on the right. (B) Densitometric quantification of mGluR5 monomeric and dimeric bands normalized by HDAC-1 in A. (* $p < 0.05$, $N = 4$ animals per group). (C) Representative western of SCDH plasma membrane-enriched fractions from the same group of animals in A. Blots probed with mGluR5 and the plasma membrane loading control, N-Cadherin (N-Cad). A protein ladder is shown on the right. (D) Densitometric quantification of mGluR5 monomeric and dimeric bands normalized using N-cadherin from C. (E) Representative western blot of SCDH cytoplasmic-enriched fractions from the same group of animals in A. Blots probed with mGluR5 and the cytoplasm loading control, GAPDH. A protein ladder is on the right. (F) Densitometric quantification of monomeric and dimeric mGluR5 bands normalized to GAPDH from westerns in E.

In contrast, only at 7 days following SNI was the monomeric band significantly different from naïve animals ($t(9)=3.947$, $p<0.0109$). Thus, starting as early as one day following SNI surgery, there was an increase in mGluR5 protein within the nuclear fraction. However, this significant difference was not maintained at each time point.

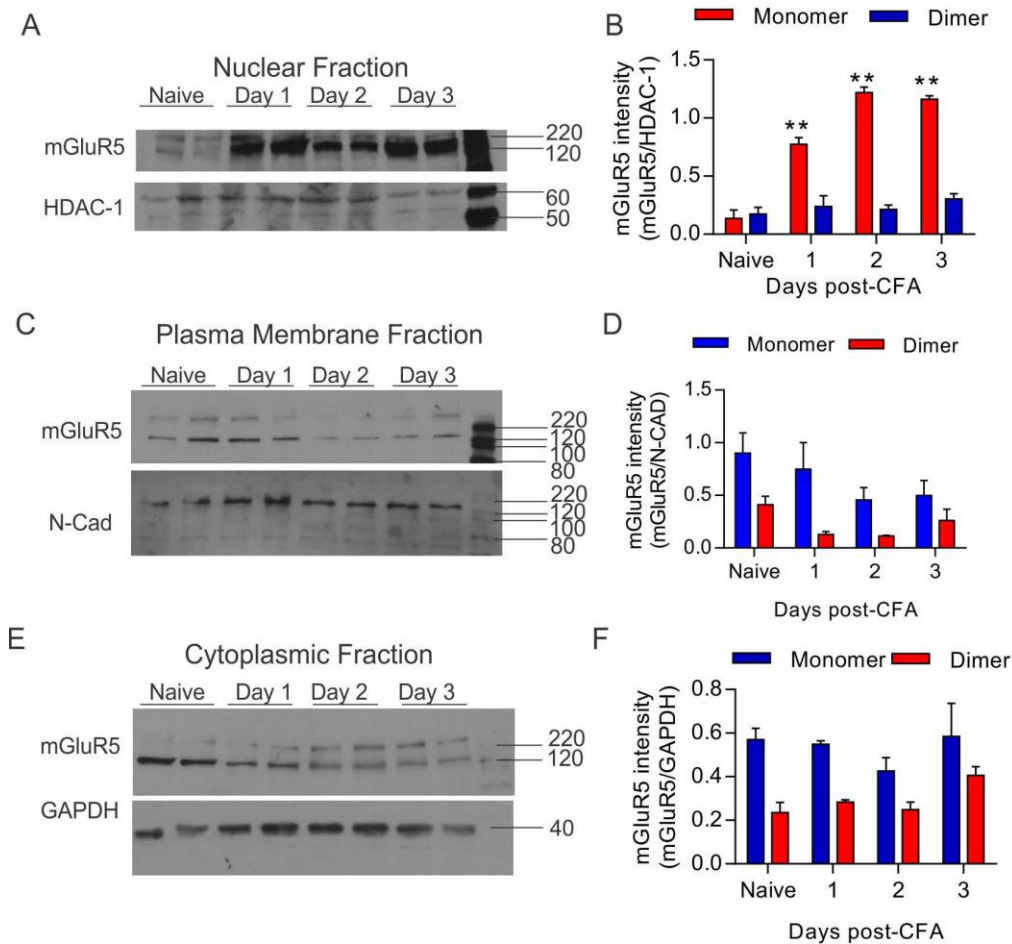
A time course of the plasma membrane-enriched fraction was next assessed through western blot for changes in mGluR5 protein levels (Figure 11C). The blot was also stripped and reprobed for the plasma membrane loading control, N-cadherin, which was used to normalize mGluR5 in the quantification (Figure 11D). Analysis of variance of mGluR5 levels across the course of SNI development showed no significant changes at any time point measured. Similarly, no changes were observed in mGluR5 protein level within the cytoplasmic-soluble fraction (Figure 11E-F) at any time point. Both monomeric and dimeric bands were observed throughout the time course and were normalized to the cytoplasmic loading control, GAPDH. These results do not support the hypothesis that nuclear mGluR5 increases following nerve injury are associated with a reduction in plasma membrane or cytoplasmic mGluR5. Instead, nuclear receptors appeared to be increased early following injury and may represent newly formed receptors.

Nuclear mGluR5 increased by one day following CFA injection

A time course of western blotting for mGluR5 at 1, 2 and 3 days following CFA injection was conducted to identify the changes in mGluR5 protein levels in nuclear membrane, plasma membrane and cytoplasmic-enriched fractions. Samples from each fraction were compared to those in naïve animals. Western blot of nuclear-enriched fractions from L4-L6 SCDH sections revealed a change in mGluR5 band intensity 24 hours after CFA injections (Figure 12A). Quantification of mGluR5 bands revealed a significant increase in the monomeric band starting one day ($t(8)=8.281$, $p<0.0001$) following CFA

injection and persisted to day 3 (Figure 12B). No change was observed in the higher molecular weight band. Pain behaviors are known to arise as soon as 6 hours following CFA injection and persist for days [370], and the early rise in nuclear mGluR5 reflected this rapid onset of spinal hypersensitivity.

Plasma membrane expression levels of mGluR5 were unchanged throughout the duration of the time course (Figure 12C-D). Likewise, one-way ANOVA showed that cytoplasmic mGluR5 (Figure 4E-F) was not significantly different from naïve animals over the 3 days of CFA treatment ($F(3,12) = 1.294$, $p = 0.3212$). Interestingly, previous electron microscopy results on day 3 CFA animals revealed a reduction in cytoplasmic mGluR5 and increase in plasma membrane mGluR5 [213]. No significant reductions were observed in day 3 cytoplasmic fractions, and no increases in plasma membrane fractions were observed in this assay. One possibility for this inconsistency is that the assay employed here uses protein from the entire dorsal horn, whereas electron microscopy results were specific for cells within lamina I and II. Nevertheless, when taken as a whole, the only observable changes in mGluR5 protein levels in the spinal cord dorsal horn were from the nuclear fraction.



Spinal glutamate induces pain behaviors in rats

A dose-response curve of the effects of i.t. glutamate on pain behaviors was performed to assess the differential effects of exogenous spinal glutamate in rats with persistent pain as compared to control rats. At baseline, or with only a vehicle i.t. injection, there were very limited licking behaviors performed by rats in any condition (Figure 13A-D). Figure 13A demonstrates that i.t. glutamate produced robust, dose-dependent nociceptive effects in both sham and SNI rats. Both the main effect of glutamate ($F(5, 50) = 44.89, p < 0.0001$) and main effect of pain condition ($F(1, 50) = 11.87, p < 0.0012$) were significant, indicating that i.t. glutamate produced licking behaviors in a dose-dependent manner regardless of pain condition, but also that neuropathic animals exhibited more pain behaviors than shams. A similar relationship was observed in the inflammatory condition (Figure 13C). CFA rats spent more time licking their hind paw and tail in response to i.t. glutamate than vehicle-treated controls. This difference was confirmed by a significant main effect of group (CFA vs IFA) determined by ANOVA ($F(1,49) = 21.01, p < 0.0001$). In addition, IFA and CFA rats showed a dose-dependent effect of i.t. glutamate on nociceptive behaviors. Specifically, there was a main effect of glutamate dose on the time spent licking ($F(5,49) = 38.49, p < 0.0001$). Overall, these results demonstrate that i.t. glutamate generally produced dose-dependent pain behaviors in rats, and the effect was greater in rats with inflammatory and neuropathic pain.

A dose of i.t. glutamate that (1) showed a significant increase in pain behaviors relative to baseline in all groups, and (2) produced significantly greater pain behaviors in rats with persistent pain relative to the control groups was selected for use in the remaining studies. As shown in figure 13B and D, and confirmed using a two-way mixed-factor ANOVA, 400 μg of i.t. glutamate met these criteria. Assessing criteria (1), there was a significant increase in pain behaviors in SNI ($t(8) = 8.302, p < 0.0001$) and sham-

operated ($t(8) = 3.648$, $p = 0.0130$) rats following i.t. glutamate treatment compared to their baseline values, as determined by the simple main effect of glutamate in each condition using Bonferroni post-hoc tests (Figure 13B). There was also a significant increase in pain behaviors in CFA ($t(8) = 8.3296$, $p < 0.0001$) and IFA-injected ($t(8) = 3.921$, $p = 0.0088$) rats following i.t. glutamate treatment compared to their baseline values (Figure 13D). For criteria (2), it was shown that i.t. glutamate differentially influenced the nociceptive behaviors in the injury and control groups, as confirmed by a significant interaction between group condition and glutamate treatment in the neuropathic ($F(1,16) = 9.173$, $p = 0.0080$) and inflammatory ($F(1,16) = 12.52$, $p = 0.0027$) conditions. Bonferroni post-hoc tests for the interaction confirm that i.t. glutamate produced a significantly greater increase in nociceptive behaviors in SNI compared to sham-operated rats (Figure 13B) ($t(16) = 4.354$, $p < 0.0029$), as well as in CFA compared to IFA-injected rats (Figure 13D) ($t(16) = 6.014$, $p = 0.0001$). Thus, neuropathic and inflamed animals showed greater pain responses to 400 μg of i.t. glutamate than controls.

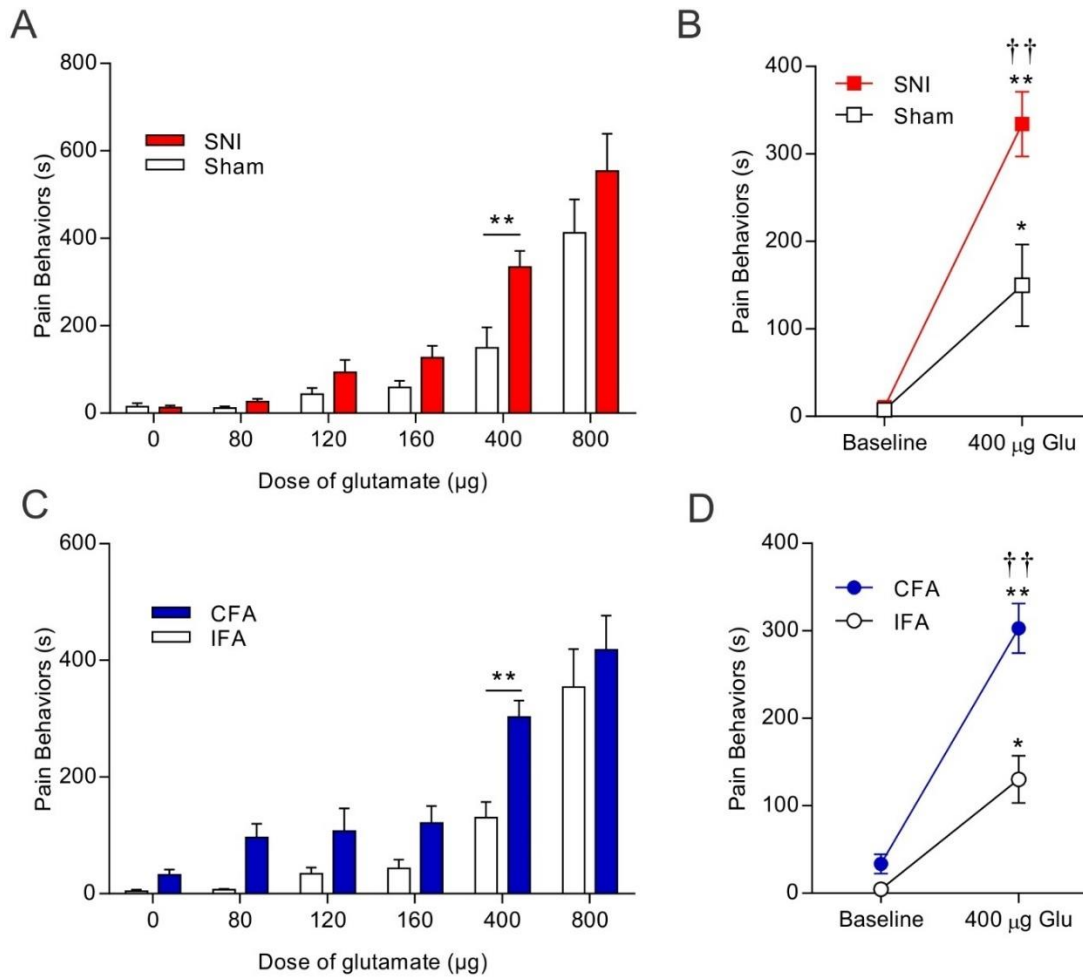


Figure 13. Dose Response curve of glutamate on nociceptive behaviors in SNI and CFA animals.

(A) Dose-response curve of nociceptive responses to i.t. injection of glutamate in SNI and sham rats 7 days post-surgery, as measured by the time in seconds spent licking hind limb and tail. Nociceptive behaviors increased with higher glutamate doses in both SNI and sham rats, and SNI rats exhibited significantly more nociceptive behaviors than shams at the 400 µg dose (** $p < 0.01$ SNI vs. sham, $N = 6$ animals per dose). (B) Comparison between nociceptive responses of SNI and sham rats following i.t. injection of either vehicle or 400 µg of glutamate (Glu). (* $p < 0.05$, ** $p < 0.01$, baseline vs 400 µg glutamate; †† $p < 0.01$ sham vs SNI, $N = 6$ per group). (C) Dose-response curve of nociceptive responses to i.t. injection of glutamate in CFA and IFA control rats 3 days after injection, as measured by the time in seconds spent licking hind limb and tail. Nociceptive behaviors increased with higher glutamate doses in both CFA and IFA rats, and CFA rats exhibited significantly more nociceptive behaviors than IFA rats at the 400 µg dose (** $p < 0.01$ CFA vs. IFA, $N = 6$ animals per dose). (D) Comparison between nociceptive responses of CFA and IFA rats following i.t. injection of either vehicle or 400 µg of glutamate (Glu). (* $p < 0.05$, ** $p < 0.01$, baseline vs 400 µg glutamate; †† $p < 0.01$ IFA vs CFA, $N = 6$ per group).

Glutamate induces greater Fos expression in the SCDH of rats with persistent pain

Although spinal administration of glutamate induces an mGluR5-dependent expression of the transcription factor *c-fos* in SCDH neurons [361, 374], it is unknown if i.t. glutamate-induced expression of these transcription factors is increased after persistent pain. Thus, the expression of Fos was measured in the SCDH 45 minutes following i.t. injection of 400 μ g glutamate in neuropathic, inflammatory and control rats (Figure 14). As shown in Figure 14A, and quantified in 14B, relative to a vehicle injection, glutamate produced a 4.6-fold increase in Fos in sham animals ($t(5) = 11.0$, $p = 0.0001$), a 13-fold increase in SNI animals ($t(5)=7.014$, $p=0.0009$). Similarly, a 5-fold increase in IFA animals ($t(5) = 4.489$, $p = 0.0046$), and a 10.5-fold increase in CFA animals ($t(5) = 5.774$, $p = 0.0022$) was observed following glutamate (Figure 14 C-D). Importantly, glutamate increased Fos more in SNI compared to sham (Figure 14A and B, $t(20) = 6.501$, $p = 0.0009$), and in CFA compared to IFA (Figure 14C and D, $t(20) = 4.146$, $p = 0.0380$). Thus, in both inflammatory and neuropathic pain conditions, hyperalgesic responses to glutamate coincided with greater levels of Fos expression.

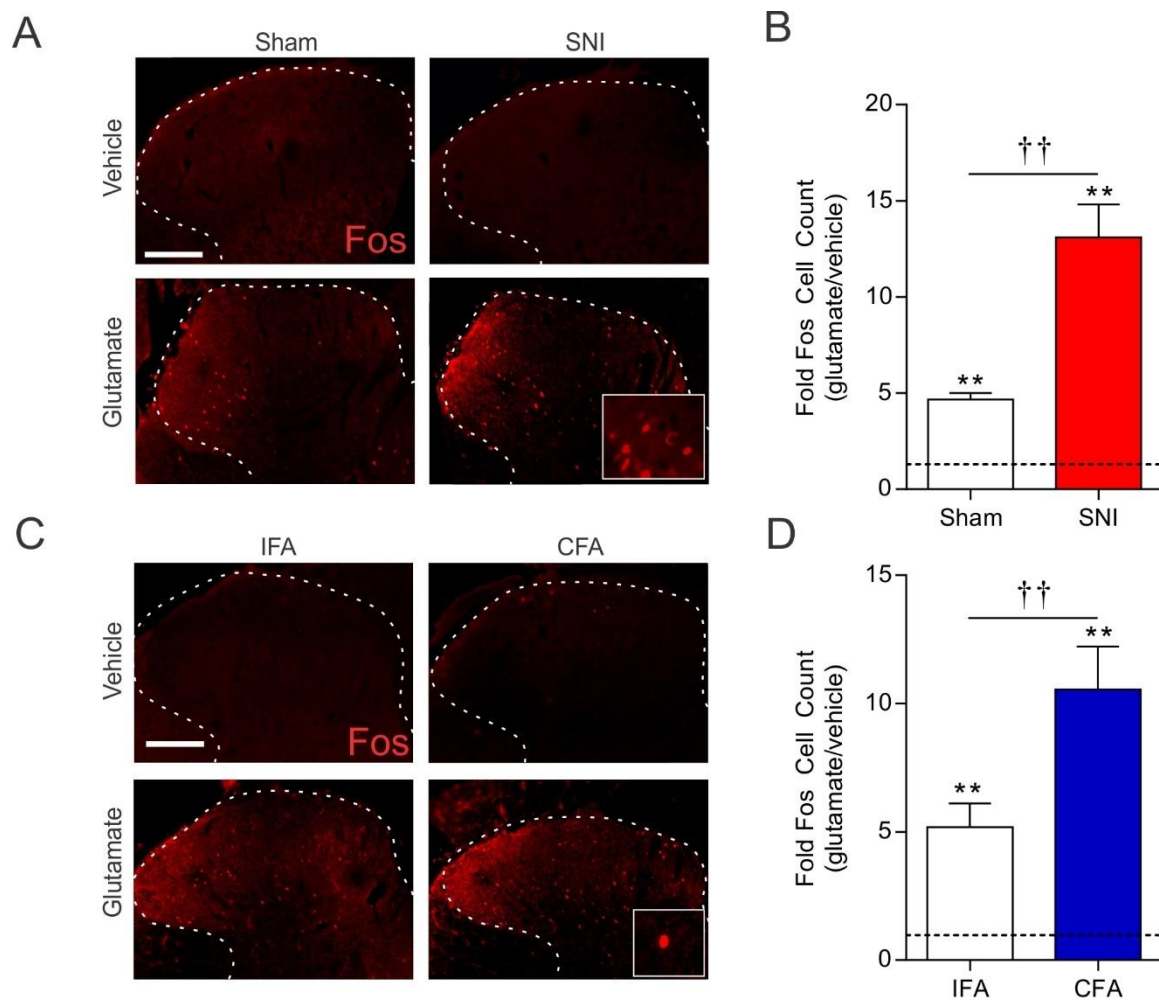


Figure 14. Glutamate-induced Fos expression in SNI and CFA SCDH.

(A) Representative Fos immunofluorescence of ipsilateral SCDH (outlined with dashed lines) of sham and SNI animals 7 days following surgery and 45 minutes following either i.t. vehicle or 400 μg glutamate imaged with 20x objective. Scale bar = 100 μm of main image, inset is 40x objective. (B) Quantification of Fos expression in SNI and sham SCDH measured as the fold increase following glutamate compared to vehicle levels of Fos expression (dotted-line = mean Fos expression in vehicle condition set to 1). A significant increase in Fos was observed following glutamate in both sham and SNI animals, and SNI rats exhibited significantly more Fos than Shams (**p < 0.01 glutamate vs. vehicle, ††p < 0.01 sham vs. SNI). (C) Representative Fos immunofluorescence of ipsilateral SCDH (outlined with dashed lines) of IFA control and CFA animals three days post inflammatory insult and 45 minutes following either i.t. vehicle or 400 μg glutamate imaged with 20x objective. Scale bar = 100 μm of main image, inset is 40x objective. (D) Quantification of Fos expression in CFA and IFA SCDH measured as the fold increase following glutamate compared to vehicle levels of Fos expression (dotted-line = mean Fos expression in vehicle condition set to 1). A significant increase in Fos was observed following glutamate in both IFA and CFA animals, and CFA rats exhibited significantly more Fos than IFA rats (**p < 0.01 glutamate vs. vehicle, ††p < 0.01 IFA vs. CFA; N = 6 per group). Mean ± SEM shown in B and D.

Glutamate induces greater Jun expression in the SCDH of rats with persistent pain

Related to the Fos protein is Jun, the protein product of the immediate early gene *c-jun*. This gene is transcribed following mGluR5-induced phosphorylation of c-Jun-N-terminal kinase (JNK). However, unlike Fos, JNK and Jun are expressed in cell cultures in response to non-permeable mGluR5 agonists [313], indicating they are not reliant on nuclear mGluR5 activation. To determine whether animals with persistent pain show altered Jun expression following noxious stimulation, Jun expression was measured in the SCDH 45 minutes following i.t. glutamate (400 μ g) in neuropathic, inflammatory and control animals (Figure 13). As with Fos, glutamate also increased expression of Jun across all conditions. Relative to a vehicle injection, glutamate produced a 2.6-fold increase in Jun in sham animals ($t(5) = 2.667$, $p = 0.0037$), an 8-fold increase in SNI animals ($t(5) = 18.95$, $p < 0.0001$) (Figure 15 A-B). However, glutamate produced significantly more Jun in neuropathic animals than sham ($t(10) = 11.11$, $p < 0.0001$) (Figure 15B). A similar pattern was also observed in IFA and CFA rats. Following glutamate there was a 2.7-fold Jun increase in IFA animals ($t(5) = 3.180$, $p = 0.0246$), and a 5-fold increase in CFA animals ($t(5) = 20.16$, $p < 0.0001$) (Figure 15 C-D). There was also significantly greater Jun expression in CFA versus IFA animals ($t(10) = 3.642$, $p = 0.0045$) (Figure 15D). Overall, Jun results closely paralleled the effects of glutamate on pain behaviors. Taken together, increases in both glutamate-induced pain behaviors and transcription factor expression in SNI and CFA rats suggest that increased glutamate sensitivity developed in neuropathic and inflammatory conditions.

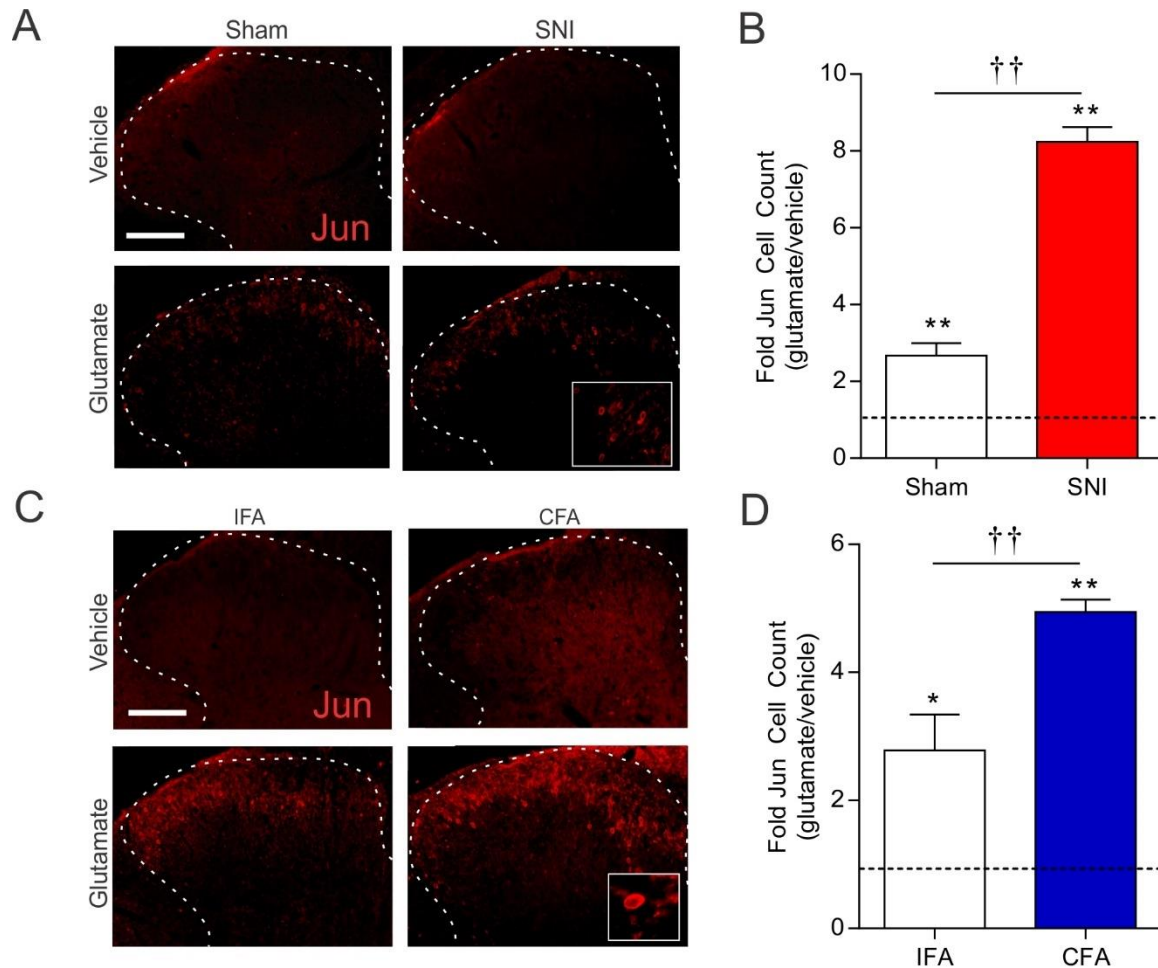


Figure 15. Glutamate-induced Jun Expression in SNI and CFA SCDH.

(A) Representative Jun immunofluorescence of ipsilateral SCDH (outlined with dashed lines) of sham and SNI animals 7 days after surgery and 45 minutes following either i.t. vehicle or 400 μ g glutamate. Scale bar = 100 μ m of main image (20 x objective), inset is 40x objective. (B) Quantification of Jun expression in SNI and sham SCDH measured as the fold increase following glutamate compared to vehicle levels of Jun expression in sham and SNI animals (dotted line = mean Jun expression in vehicle condition set to 1). A significant increase in Jun was observed across groups following i.t. glutamate (** $p < 0.01$, vehicle vs glutamate), and SNI rats exhibited significantly more Jun than sham rats ($\dagger\dagger p < 0.01$ SNI vs sham) (C) Representative Jun immunofluorescence of ipsilateral SCDH (outlined with dashed lines) of IFA control and CFA animals three days after inflammatory insult and 45 minutes following either i.t. vehicle or 400 μ g glutamate. Scale bar = 100 μ m of main image (20 x objective), inset is 40x objective. (D) Quantification of Jun expression in CFA and IFA SCDH measured as the fold increase following glutamate compared to vehicle levels of Jun expression in IFA and CFA animals (dotted line = mean Jun expression in vehicle condition set to 1). A significant increase in Jun was observed across groups following i.t. glutamate (* $p < 0.05$, ** $p < 0.01$ vehicle vs glutamate), and CFA rats exhibited significantly more Jun than IFA rats ($\dagger\dagger p < 0.01$ CFA vs IFA). N = 6 animals per group. Mean \pm SEM shown in B and D.

Blocking neuronal glutamate uptake is antinociceptive in animals with neuropathic pain

To determine whether glutamate's pronociceptive effects were occurring intracellularly or at the synapse, inhibitors targeted to the three spinal excitatory amino acid transporters (EAATs) were applied to the spinal cord. Consistent with previous reports, pretreatment with the pan-EAAT inhibitor, TBOA (10 nmol), had differential effects on control and injured animals, as evidenced by a significant interaction effect ($F(1,20) = 12.71$, $p = 0.0019$) in the one-way ANOVA (Figure 16A). Post-hoc analysis with Bonferroni correction revealed that pretreating rats with 10 μg i.t. TBOA enhanced glutamate-induced pain behaviors only in sham ($t(20) = 2.861$, $p = 0.0193$) animals. In contrast, there was a decrease in glutamate-induced pain behaviors in neuropathic animals pretreated with TBOA ($t(20)=2.637$, $p=0.0317$) (Figure 16A). Thus, while EAAT inhibition was pronociceptive under control conditions, it was antinociceptive in animals with neuropathic pain.

To directly assess the relative contribution of neuronal (EAAT3) and glial (EAAT1 and EAAT2) glutamate transport, inhibitors selective for each were assessed. The selective EAAT3 inhibitor, L-TBA (0.01-100 nmol), was applied spinally 10 minutes before 400 μg i.t. glutamate and pain behaviors, as measured by the time spent licking the hind limb and tail over a 30 minute period, were recorded. In animals with neuropathic pain, L-TBA attenuates glutamate-induced pain behaviors up to a dose of 1 nmol (Figure 16B). Dunnett's post-hoc t-test revealed that L-TBA was maximally effective at 1 nmol in SNI animals ($t(60) = 3.672$, $p = 0.0024$), reducing time spent performing pain behaviors by 53%. In contrast, a 1 nmol dose of L-TBA in sham animals was not significantly different from vehicle ($t(60) = 0.9424$, $p = 0.8107$). At the effective doses of i.t. L-TBA used, SNI and sham animals were indistinguishable based on glutamate-induced pain behaviors. Thus, while inhibiting neuronal uptake of glutamate did not

eliminate the effects of glutamate, it did reduce the enhanced nociceptive responses to glutamate observed in neuropathic animals.

Next, pain behaviors were measured following administration of EAAT1 and EAAT2-selective inhibitors prior to i.t. glutamate. In contrast to L-TBA, blocking glial EAATs with WAY213613 and UCPH-101 dose-dependently potentiated pain behaviors produced by 200 μ g i.t. glutamate ($F(3,36) = 16.645$, $p < 0.0011$) (Figure 16C). Dunnett's post-hoc t-test confirmed that 50 nmol of WAY213613 in conjunction with 50 nmol of UCPH-101 (100 nmol total dose) produced significant increases in glutamate-induced pain behaviors in SNI ($t(36) = 3.403$, $p = 0.0046$), and sham ($t(36) = 2.567$, $p = 0.0384$) animals. Thus, glial EAAT inhibitors, unlike neuronal inhibitors, were pronociceptive in neuropathic animals.

To determine whether the glial EAAT inhibitors prevent the reuptake of glutamate in neuropathic rats, as they normally do (as opposed to functioning in reverse), extracellular spinal glutamate was collected using *in vivo* microdialysis before and after application of either vehicle or the combination of WAY213613 + UCPH-101 in SNI animals (Figure 16D). In these experiments, no exogenous glutamate was used. Neuropathic animals showed significant increases in spinal glutamate concentration during a 5-minute collection period immediately following spinal application of WAY213613 + UCPH-101, as confirmed by post-hoc testing ($t(24) = 3.045$, $p = 0.0112$). No significant effect of vehicle injection was observed ($t(24) = 1.455$, $p = 0.3171$). Thus, the blockade of EAAT1 and EAAT2 through WAY213613 + UCPH-101 produced expected elevated concentrations of spinal glutamate in neuropathic animals and suggests that glial EAATs were functioning in their predicted direction.

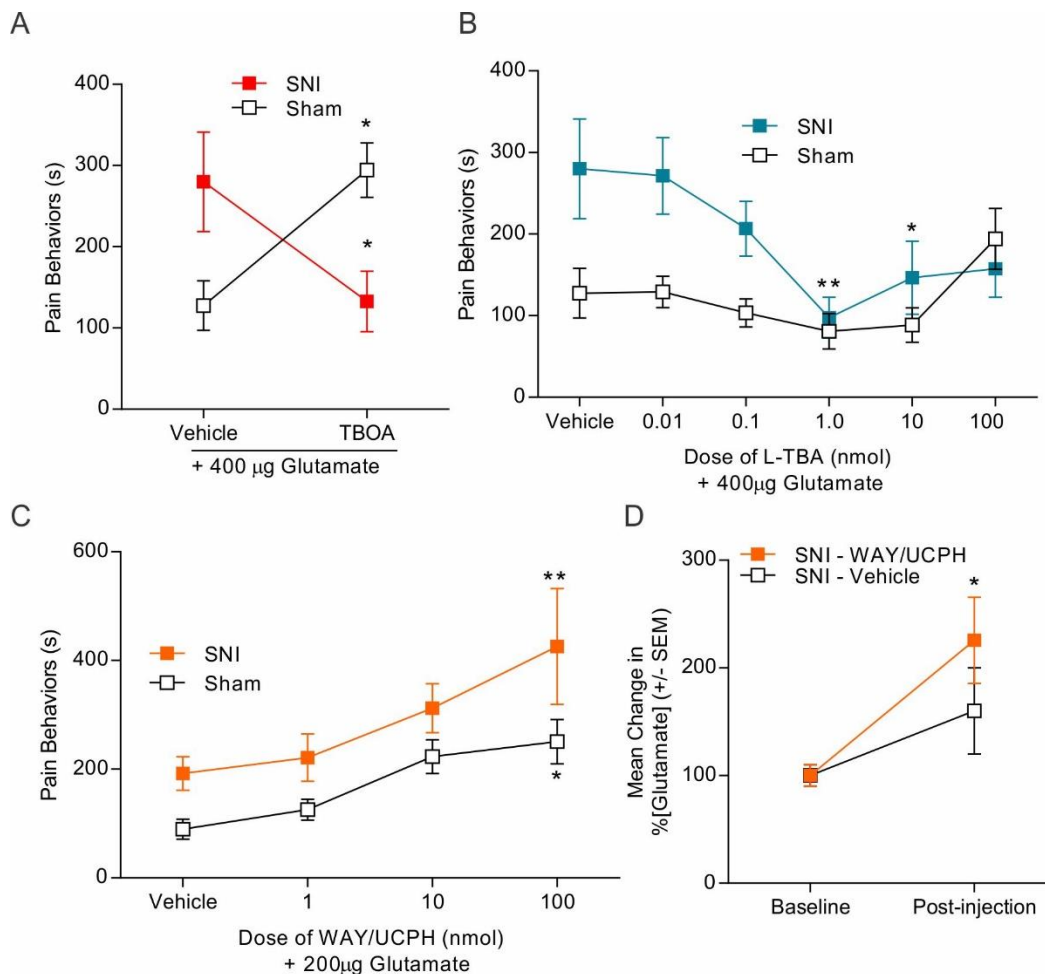


Figure 16. EAAT3-specific inhibitors are analgesic in SNI animals.

(A) Pretreatment with the pan-EAAT inhibitor, TBOA (10 nmol i.t.), attenuated pain behaviors, as measured by the time spent licking hind limb and tail in seconds, induced by 400 µg i.t. glutamate in SNI rats 7 days after surgery, and significantly *potentiated* pain behaviors in sham rats (* $p < 0.05$ SNI vs sham; $N = 6$ per dose). (B) The EAAT3 inhibitor, L-TBA, dose-dependently attenuated pain behaviors induced by 400 µg i.t. glutamate in SNI rats, and was maximally effective at the 1 nmol dose (** $p < 0.01$, * $p < 0.05$ SNI compared to vehicle; $N = 6$ per dose). (C) 50 nmol each of the EAAT1 inhibitor, WAY213613, and the EAAT2 inhibitor, UCPH-101, (WAY/UCPH) dose-dependently *increased* pain behaviors induced by 200 µg i.t. glutamate in SNI rats (* $p < 0.05$ Sham vs vehicle; ** $p < 0.01$ SNI vs vehicle; $N = 6$ per dose). (D) Microdialysis of spinal cords collected in SNI rats showed a significant increase in spinal glutamate following i.t. WAY/UCPH administration. Dialysates collected in two 5 minute time bins measured as percent change from the baseline collection (* $p < 0.05$ SNI WAY/UCPH vs baseline; $N=7$). Mean \pm SEM shown in all graphs.

Blocking neuronal glutamate uptake is antinociceptive in animals with inflammatory pain

The effects of a non-selective EAAT inhibitor TBOA were also examined on i.t. glutamate-induced pain behaviors in IFA and CFA animals. ANOVA revealed a significant interaction effect (Figure 17A) ($F(1,20) = 14.03$, $p = 0.0013$), and post-hoc tests showed a significant increase in pain behaviors in TBOA-treated IFA animals ($t(20) = 2.911$, $p = 0.0172$). In contrast, TBOA did not have a significant effect on glutamate-induced pain behaviors in CFA animals ($t(20) = 2.387$, $p = 0.0532$). Overall, these results demonstrate that EAAT blockade produces differential effects on glutamate-induced pain in control and inflamed animals.

As with the neuropathic animals, the effects of pretreatment with selective neuronal (L-TBA) or glial EAAT inhibitors (WAY213613 + UCPH-101) were examined in inflamed animals. L-TBA produced a significant reduction in i.t. glutamate-induced pain behaviors in CFA animals (Figure 17B), which was significant at the 1 ($t(48) = 3.751$, $p = 0.0024$) and 10 ($t(48) = 3.253$, $p = 0.0105$) nmol doses. Conversely, pretreatment with the EAAT1 and EAAT2 inhibitors, WAY213613 + UCPH-101 significantly increased pain behaviors in both CFA and IFA animals (Figure 17C). Simple main effects revealed that 100 nmol i.t. WAY/UCPH, which corresponds to 50 nmol of WAY-213613 and 50 nmol of UCPH-101, produced significant increases in glutamate-induced pain behaviors in both IFA ($t(40) = 3.666$, $p = 0.0020$) and CFA ($t(40) = 2.890$, $p = 0.0169$) animals. These results suggest that the antinociceptive effect of TBOA was driven by preventing glutamate from being transported into neurons via EAAT3.

To determine whether the glial EAAT inhibitors prevent the reuptake of glutamate in inflamed rats, as they normally do (as opposed to functioning in reverse), extracellular spinal glutamate was collected using *in vivo* microdialysis before and after application of either vehicle or UCPH-101 in CFA animals (Figure 17D). Following spinal administration of UCPH-101, there was an increase in spinal glutamate

concentration above baseline in CFA animals ($t(5) = 3.411, p = 0.0190$). Thus, inhibiting EAAT1 uptake increased spinal glutamate concentration in inflamed animals, which is also associated with increased pain behaviors.

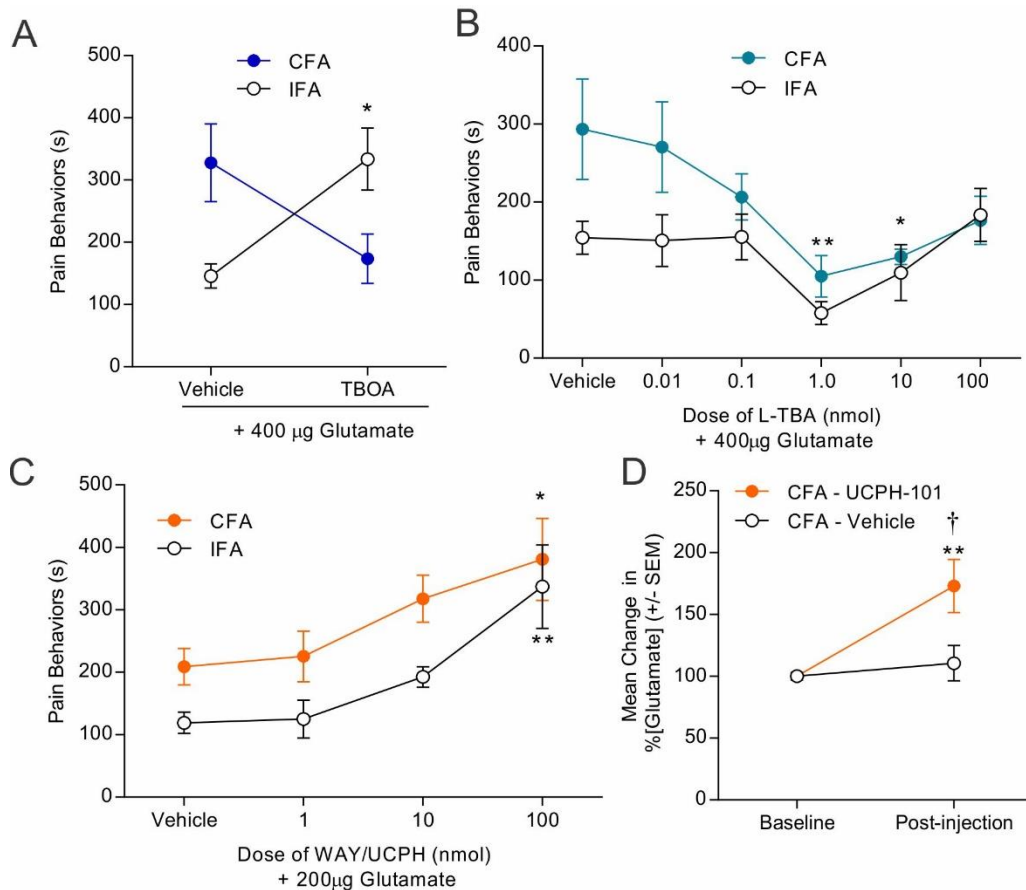


Figure 17. EAAT3-specific inhibitors are analgesic in CFA animals.

(A) Pretreatment with the pan-EAAT inhibitor, TBOA (10 nmol i.t.) significantly *potentiated* pain behaviors in IFA rats (* $p < 0.05$ IFA TBOA vs vehicle; $N = 6$ per dose). (B) The EAAT3 inhibitor, L-TBA, attenuated pain behaviors induced by 400 μg i.t. glutamate in CFA rats, and was maximally effective at the 1 nmol dose (* $p < 0.05$, ** $p < 0.01$ L-TBA compared to vehicle in CFA rats; $N = 6$ per dose). (C) 50 nmol each of the EAAT1 inhibitor, WAY213613, and the EAAT2 inhibitor, UCPH-101, (WAY/UCPH) dose-dependently *increased* pain behaviors induced by 200 μg i.t. glutamate in CFA and IFA controls (** $p < 0.01$, * $p < 0.05$ WAY/UCPH vs vehicle; $N = 6$ per dose). (D) Microdialysis of spinal cords collected in CFA rats showed a significant increase in spinal glutamate following i.t. UCPH-101 administration. Dialysates collected in two 5 minute time bins measured as percent change from the baseline collection. (** $p < 0.01$ WAY/UCPH vs baseline, † $p < 0.05$ UCPH-101 vs vehicle; $N = 7$). Mean \pm SEM shown for all graphs.

Neuronal EAAT inhibitors attenuate mechanical allodynia in neuropathic animals

The EAAT inhibitors were also assessed for their impact on mechanical allodynia in neuropathic and control animals in the absence of i.t. glutamate. Sham animals showed normal paw withdrawal thresholds (PWTs), which were unaffected by i.t. vehicle or L-TBA application (Figure 18A). However, 50 nmol of WAY213613 in conjunction with 50 nmol of UCPH-101 produced significant reductions in PWTs for up to 2 hours in sham animals, as revealed by the mixed factor ANOVA. This was observed as a significant main effect of WAY213613 + UCPH-101 compared to both L-TBA ($t(27) = 7.858$, $p < 0.0001$) and vehicle ($t(27) = 7.212$, $p < 0.0001$), as well as simple effects within the repeated factor at 30 ($t(9) = 8.482$, $p < 0.0001$), 60 ($t(9) = 6.283$, $p = 0.0005$) and 180 ($t(9) = 3.870$, $p = 0.0122$) minutes following glial EAAT inhibitors. In contrast to shams, SNI rats showed ipsilateral mechanical allodynia in the form of very low PWTs one-week post-surgery (Figure 18B). A mixed factor ANOVA revealed that i.t. injection of 1 nmol L-TBA has a significant simple main effect on PWT, significantly increasing thresholds compared to either vehicle ($t(21) = 5.081$, $p = 0.0047$) or WAY213613 + UCPH-101 ($t(21) = 6.053$, $p = 0.0009$) (Figure 18B). Within the repeated measure, L-TBA produced significant increases in PWT compared to baseline at 30 ($t(7) = 4.573$, $p = 0.0081$) and 60 ($t(7) = 3.142$, $p = 0.0487$) minutes post-injection (Figure 18B). Thus, while neuronal EAAT inhibitors alleviated mechanical allodynia experienced by neuropathic animals, glial EAAT inhibitors produced mechanical allodynia in sham animals.

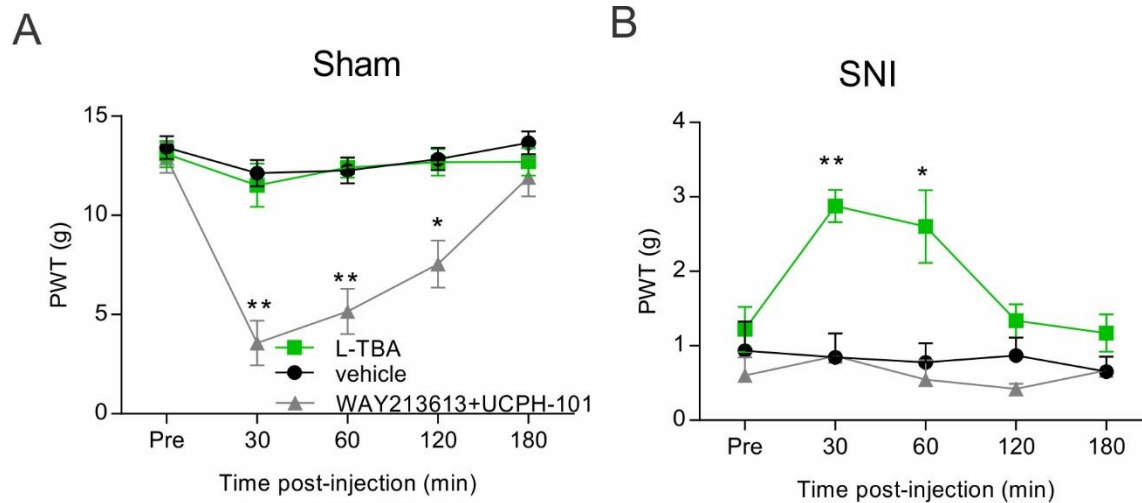


Figure 18. Neuronal EAAT inhibitors reduced mechanical allodynia in SNI rats and glial EAAT inhibitors produce mechanical allodynia in sham rats

(A) The paw withdrawal thresholds (PWT) in the ipsilateral hind paw of sham rats 7 days post-surgery taken before and after i.t. injection of either 1 nmol i.t. L-TBA or 50 nmol each of WAY213613 and UCPH-101 (WAY/UCPH). WAY/UCPH significantly reduced PWTs (i.e., increased mechanical allodynia) up to two hours post-i.t. injection (* $p < 0.05$, ** $p < 0.01$ WAY/UCPH vs vehicle, $N = 8$). No change was observed following either 1 nmol L-TBA or vehicle injection. (B) The paw withdrawal thresholds (PWT) in the ipsilateral hind paw of SNI rats 7 days post-surgery taken before and after i.t. injection of either 1 nmol i.t. L-TBA or 50 nmol each of WAY213613 and UCPH-101 (WAY/UCPH). L-TBA attenuated mechanical allodynia up to one hour post-injection (* $p < 0.05$ L-TBA vs vehicle, $N = 8$). Mean \pm SEM shown in all graphs.

Neuronal EAAT inhibitors produce conditioned place preference in SNI and CFA animals, but not naïves.

Data from the paw withdrawal threshold and glutamate-induced pain studies suggest there are significant differences in neuronal and glial EAAT inhibitors on mechanical allodynia. However, as mentioned before, glutamate-induced pain requires exogenous application of glutamate to show drug effects. Further, paw withdrawal thresholds, while free from the effects of exogenous glutamate, are subject to other limitations. An important limitation of paw withdrawal thresholds is the floor effect in animals with neuropathic pain and the ceiling effect in sham animals. To circumvent these limitations,

a conditioned place preference paradigm was used to assess whether neuronal or glial EAAT inhibitors produce approach or avoidance behaviors following a series of pairing sessions in neuropathic, inflamed and naïve animals. In addition, unlike the other behavioral tests, neuropathic and inflamed animals were compared to naïve animals rather than sham or IFA controls to ensure the control group represent a truly pain-free experimental condition.

Naïve animals and animals 7 days following SNI were placed in the conditioning chamber to evaluate baseline preference for either chamber. At this time point, no group showed an inherent place preference for the chamber they would be later conditioned to with the drug (Figure 19 A). After four daily pairing sessions (two each with drug or vehicle), the time spent in either half of the chamber, or a neutral intervening compartment, was measured for both naïve and SNI rats. To first confirm that the chambers were distinguishable from one another, naïve and SNI rats were conditioned with 10 mg/Kg of i.p. morphine. For these experiments, the null hypothesis states that a drug will fail to produce a preference and thus the group mean will be 50%. To test the presence of a place preference, a single sample t-test comparing the group mean to the theoretic mean of 50% was first performed. As expected, both naïve (mean = 67.6%, $t(8) = 3.122$, $p = 0.0144$) and SNI (mean = 63.9%, $t(8) = 2.601$, $p = 0.0316$) rats exhibited a preference for a compartment previously paired with morphine (Figure 19 B), consistent with the well-established analgesic and rewarding effects of morphine [363]. Spinal injection of 1 nmol L-TBA showed a conditioned place preference effect in SNI rats (mean = 64.0%, $t(8) = 3.366$, $p = 0.0099$), comparable to that of i.p. morphine, whereas no conditioned place preference for L-TBA occurred in naïve animals (mean = 55.5%, $t(7) = 0.6609$, $p = 0.5298$). Conversely, 50 nmol of WAY213613 and 50 nmol of UCPH-101 showed no conditioned place preference in SNI rats (mean = 43.2%, $t(10) = 1.273$, $p=0.2317$), but showed a conditioned place *aversion* (mean = 36.1%, $t(6) = 3.000$, $p = 0.0240$) in naïve

animals (Figure 19B). Thus, while morphine produces a preference in both neuropathic and naïve animals, EAAT3 inhibitors only produce a preference in animals with neuropathic pain. At the same time, EAAT1/2 inhibitors are not analgesic in either condition and in fact are aversive to naïve animals.

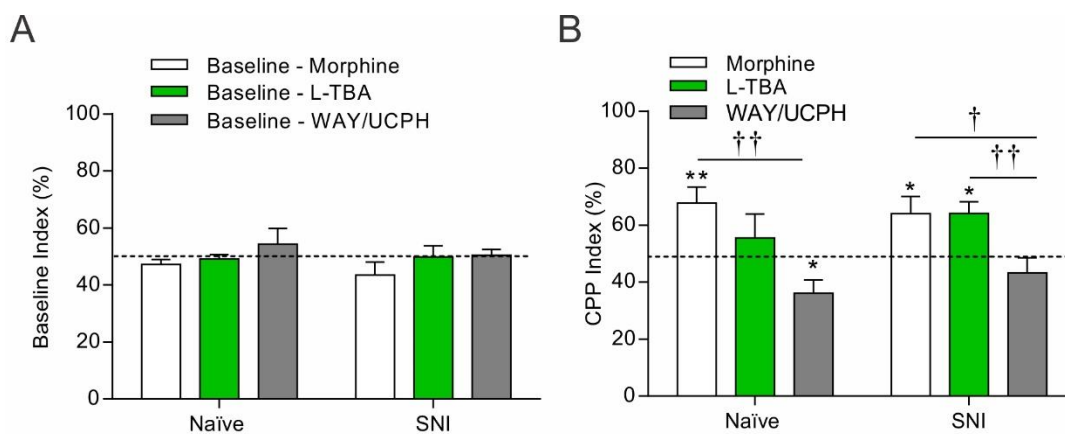


Figure 19. Conditioned place preference of neuronal and glial EAAT inhibitors on SNI and naïve animals

(A) Baseline place preference as measured by percent time spent in chamber selected for drug pairing (prior to drug exposure), for naïve and day 7 SNI rats that later received morphine, L-TBA or WAY/UCPH. There was no inherent place preference in either naïve or SNI animals in any of the groups. (B) Conditioned place preference (CPP-I) for naïve and SNI rats conditioned with 10 mg/Kg of i.p. morphine, 1 nmol of i.t. L-TBA or 50 nmol each i.t. WAY213613 and UCPH-101 (WAY/UCPH). Morphine produced a significant conditioned place preference (CPP) in both naïve and SNI animals. L-TBA produced a CPP comparable to that of morphine in SNI animals, but not in shams, and WAY/UCPH produced a significant conditioned place *aversion* (CPP-I <50%) in shams, but not SNI animals. Morphine had a significantly larger CPP-I than WAY213613 + UCPH-101 in both sham and SNI rats, and L-TBA had a significantly greater CPP effect than WAY213613 + UCPH-101 in SNI animals (* $p < 0.05$, ** $p < 0.01$ compared to 50%; † $p < 0.05$, †† $p < 0.01$ compared to WAY/UCPH, N = 7-11 per group). Dashed line indicates 50%.

While WAY213613 and UCPH-101 also did not show any effect on mechanical allodynia, this was thought to be due to a floor effect since neuropathic animals begin at the lowest threshold. However, this drug combination also failed to produce a significant conditioned place aversion in animals with neuropathic pain in the conditioned place preference paradigm. An important point to note, however, is that while it was not significantly avoided, animals show significantly less preference when conditioned with glial EAATs than those conditioned with the neuronal EAAT inhibitor ($t(47) = 2.675$, $p = 0.0307$) or morphine ($t(47) = 2.668$, $p = 0.0313$).

In a modified conditioned place preference paradigm to accommodate the shorter duration of CFA, naïve and CFA animals had a single pairing of vehicle to one room in the morning and a single pairing of the drug (4 hours later in the afternoon) to the opposite room, and were assessed for conditioned place preference the next day. Unlike in SNI conditioned place preference, in this experiment the baseline measures were taken prior to the onset of the pain condition, that is, prior to injection of CFA. At baseline, animals showed no preference for either room (Figure 20A). To avoid any carry-over effects of the drugs, the vehicle was always paired in the morning and the drug in the afternoon. To ensure that there were no order effects, a group was tested in which saline was paired to the two rooms in both the morning and the afternoon. No preference was shown towards the afternoon-paired room when saline was administered at both time points in either CFA or naïve rats (Figure 20B), indicating that there is no preference associated simply with morning or afternoon pairing. Next, we showed that following a single pairing of morphine (10 mg/kg, i.p.) a conditioned place preference is observed in both CFA (mean = 63.9%, $t(6) = 3.472$, $p = 0.0133$) and naïve (59.7%, $t(6) = 3.970$, $p = 0.0074$) rats. Like in the SNI experiment, 1 nmol of L-TBA produced a conditioned place preference in CFA rats (61.1%, $t(10) = 2.302$, $p = 0.0441$), but not in naïve animals (51.0%, $t(10) = 0.3648$, $p = 0.7229$). There was no significant impact

of WAY2136 + UCPH-101 in either naïve (mean = 45.4%, $t(10) = 1.891$, $p = 0.0879$) or SNI (43.6%, $t(10) = 1.455$, $p = 0.1763$) animals (Figure 20B). However, like in the SNI experiment, CFA animals spent significantly more time in the L-TBA and morphine rooms compared to the WAY213613 + UCPH-101-paired room ($t(52) = 3.524$, $p = 0.0027$). Together, the conditioned place preference results indicate that L-TBA produced a significant rewarding effect in animals with persistent pain, while WAY/UCPH do not. Further, it confirms our previous findings that neuronal EAAT inhibitors were analgesic under persistent pain conditions, while glial EAAT inhibitors are not.

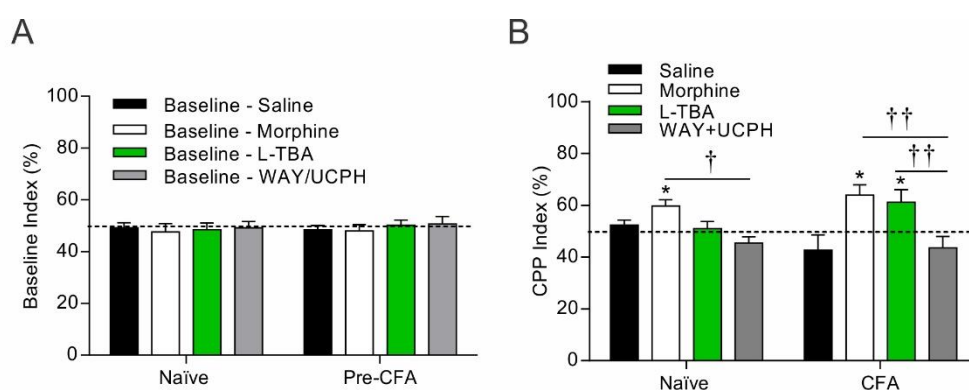


Figure 20. Conditioned place preference of neuronal and glial EAAT inhibitors in naïve and CFA animals

(A) Baseline place preference for naïve and day 3 CFA rats that later received saline, morphine, L-TBA and WAY/UCPH. Pre-CFA = naïve animals selected to receive CFA injection following baseline. There was no inherent place preference in animals in either naïve or CFA animals. **(B)** Conditioned place preference (CPP-I) for naïve and CFA rats conditioned with saline, 10 mg/Kg of i.p. morphine, 1 nmol of i.t. L-TBA or 50 nmol each i.t. WAY213613 and UCPH-101 (WAY/UCPH). A single pairing of saline in the morning and afternoon did not result in a CPP in naïve or CFA animals (48 hours following CFA injection), but a single pairing of morphine produced a significant CPP in both naïve and CFA animals. L-TBA produced a CPP comparable to that of morphine in CFA, but not in naïve, animals. WAY/UCPH did not produce a CPP in any condition. More time was spent in morphine and L-TBA-paired rooms than WAY/UCPH-paired rooms in CFA animals. (* $p < 0.05$ vs 50%; † $p < 0.05$, †† $p < 0.01$ vs WAY/UCPH, $N = 11$ for L-TBA and WAY/UCPH, $N = 8$ for saline and morphine). Mean \pm SEM are presented in all graphs.

EAAT3 inhibitors attenuate glutamate-induced Fos expression

To test whether blocking glutamate's access to nuclear mGluR5 would affect downstream signaling pathways associated with pain behaviors, rats were pretreated with either 1 nmol L-TBA, or 50 nmol each of WAY213613 + UCPH-101 prior to measuring spinal Fos expression induced by 400 μ g spinal glutamate (Figure 21A-D) in SNI, sham, CFA and IFA rats. As discussed earlier, Fos expression has been previously demonstrated to depend on nuclear mGluR5 activation, thus inhibiting glutamate's transport into the neuron was predicted to attenuate Fos expression. Pretreatment with 1 nmol EAAT3 inhibitor, L-TBA, reduced glutamate-induced Fos expression compared to a vehicle pretreatment in both shams and SNI rats (Figure 21A-B). Dunnett's post-hoc t-tests reveal that there is a significant 72% reduction in Fos expression in shams ($t(30) = 4.109$, $p = 0.0006$) and an 84% reduction in SNI rats ($t(30) = 4.810$, $p < 0.0001$). In contrast, pretreatment with the EAAT1 and EAAT2 inhibitors, WAY213613 + UCPH-101 (50 nmol each), failed to reduce Fos expression in SNI animals, but nearly doubled Fos expression compared to a vehicle pre-treatment in shams ($t(30) = 4.934$, $p = 0.0003$) (Figure 21A-B).

There was a similar reduction in glutamate-induced Fos expression in L-TBA pretreated IFA ($t(30) = 3.016$, $p = 0.0098$) and CFA ($t(30) = 3.745$, $p = 0.0013$) animals (Figure 21C-D). As with sham animals, WAY213613 + UCPH-101 also increased Fos expression in IFA controls ($t(30) = 3.787$, $p = 0.0013$). The failure of WAY213613 + UCPH-101 to further increase Fos expression in neuropathic and inflamed animals may have been due to the ceiling effect, as these groups already expressed more than double the Fos in response to glutamate that control animals did (Figure 14). Thus as predicted, preventing glutamate from entering the neuron via EAAT3 attenuated glutamate-induced Fos expression, whereas glial EAAT inhibitors, which allow uptake into neurons, did not. These findings support the notion that intracellular mGluR5 is required for Fos expression.

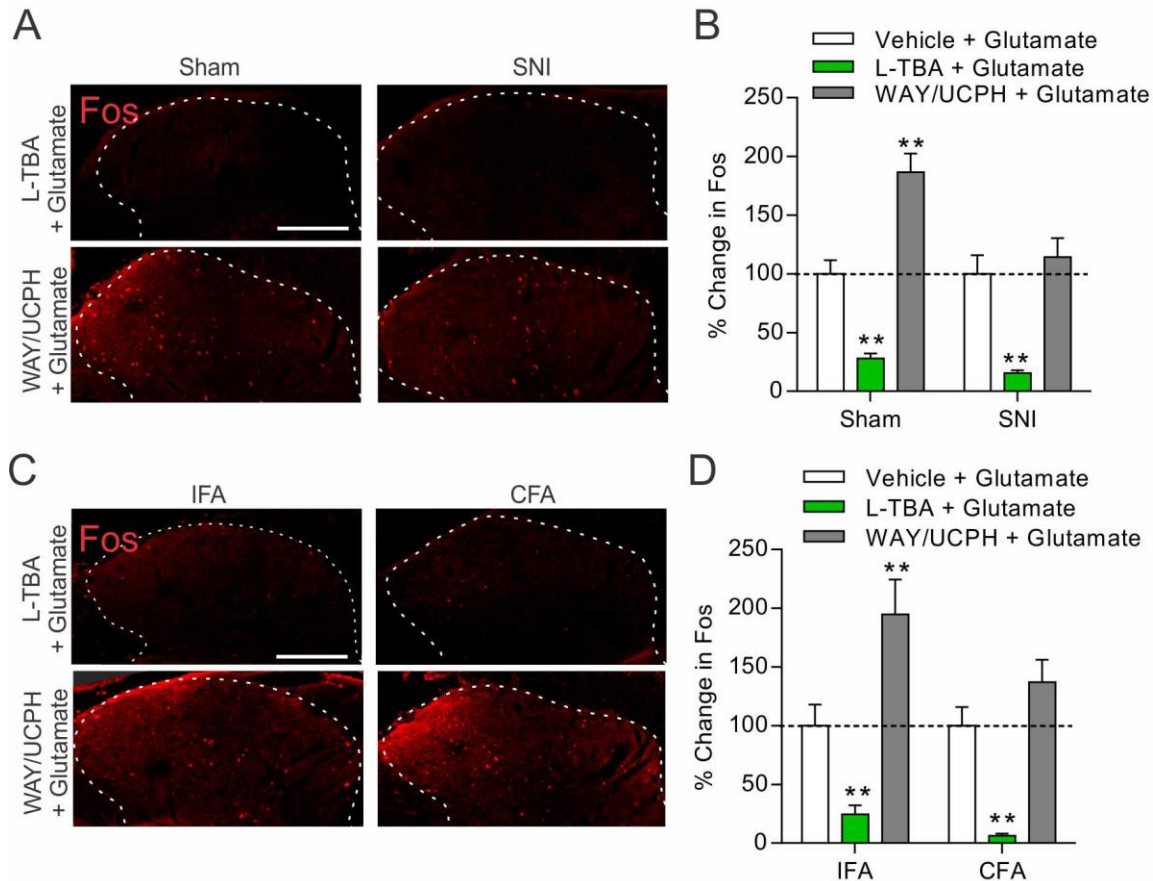


Figure 21. Neuronal, but not glial, EAAT inhibitor attenuates glutamate-induced Fos expression.

(A) Representative immunofluorescence of glutamate-induced Fos expression in the ipsilateral SCDH (outlined with dotted line) of sham and SNI animals 7 days following surgery and 45 minutes following i.t. pretreatment with 1 nmol of L-TBA or 50 nmol of each WAY213613 and UCPH-10 (WAY/UCPH). Scale bars = 100 μ m. (B) Quantification of SCDH Fos expression, where % change in Fos is the percentage change in glutamate-induced Fos expression after drug treatment relative to a group of rats that received glutamate after vehicle (not shown in A). L-TBA significantly attenuated glutamate-induced Fos expression in all conditions, while WAY/UCPH potentiated glutamate-induced Fos expression in sham animals. (** $p < 0.01$ vs vehicle + glutamate, $N = 6$ rats per group). (C) Representative immunofluorescence of glutamate-induced Fos expression in the ipsilateral SCDH (outlined with dotted line) of CFA and IFA animals 45 minutes following i.t. pretreatment with either 1 nmol L-TBA or 50 nmol each WAY212613+UCPH-101. (D) Quantification of SCDH Fos expression, where % change in Fos is the percentage change in glutamate-induced Fos expression after drug treatment relative to a group of rats that received glutamate after vehicle (not shown in C). L-TBA significantly attenuated glutamate-induced Fos expression in all conditions, while WAY/UCPH potentiated glutamate-induced Fos expression in IFA control animals. (** $p < 0.01$ vs vehicle + glutamate, $N = 6$ rats per group). Mean \pm SEM shown in B and D.

EAAT1 and 2 inhibitors potentiate glutamate-induced Jun expression in inflamed and control animals

Previously, mGluR5-induced Jun expression was shown to not depend on intracellular receptors, but rather plasma membrane-bound receptors [313]. As EAAT3 inhibition should not alter the availability of glutamate to activate plasma-membrane bound mGluR5, it was hypothesized that unlike Fos, Jun would be unaffected by L-TBA pretreatment. A 1 nmol dose of i.t. L-TBA, followed by 400 µg glutamate did not significantly alter Jun expression in the SCDH of neuropathic or control animals (Figure 22A-B). This is in contrast to WAY213613 + UCPH-101 pretreatment, which did produce significant increases in Jun expression in sham animals (Figure 22A-B) ($t(30) = 3.087$, $p = 0.0082$). Interestingly, WAY213613 + UCPH-101 did not increase glutamate-induced Jun expression in neuropathic animals (Figure 22B). Again, SNI animals showed the greatest Jun response to glutamate compared with any other group (Figure 15), which may explain the failure to produce further increases with glial EAAT inhibitors. L-TBA also had no effect on glutamate-induced Jun expression in CFA or IFA animals (Figure 22 C-D). However, pretreatment with WAY213613 + UCPH-101 increased glutamate-induced Jun expression relative to a vehicle pretreatment by 64% in IFA ($t(30) = 2.668$, $p = 0.0185$) and by 56% in CFA animals ($t(30) = 2.328$, $p = 0.0432$). Taken together, these results suggest that intraneuronal glutamate differentially impacts downstream signalling pathways; thus, while glutamate within the neuron contributes to Fos expression, it does not affect Jun expression.

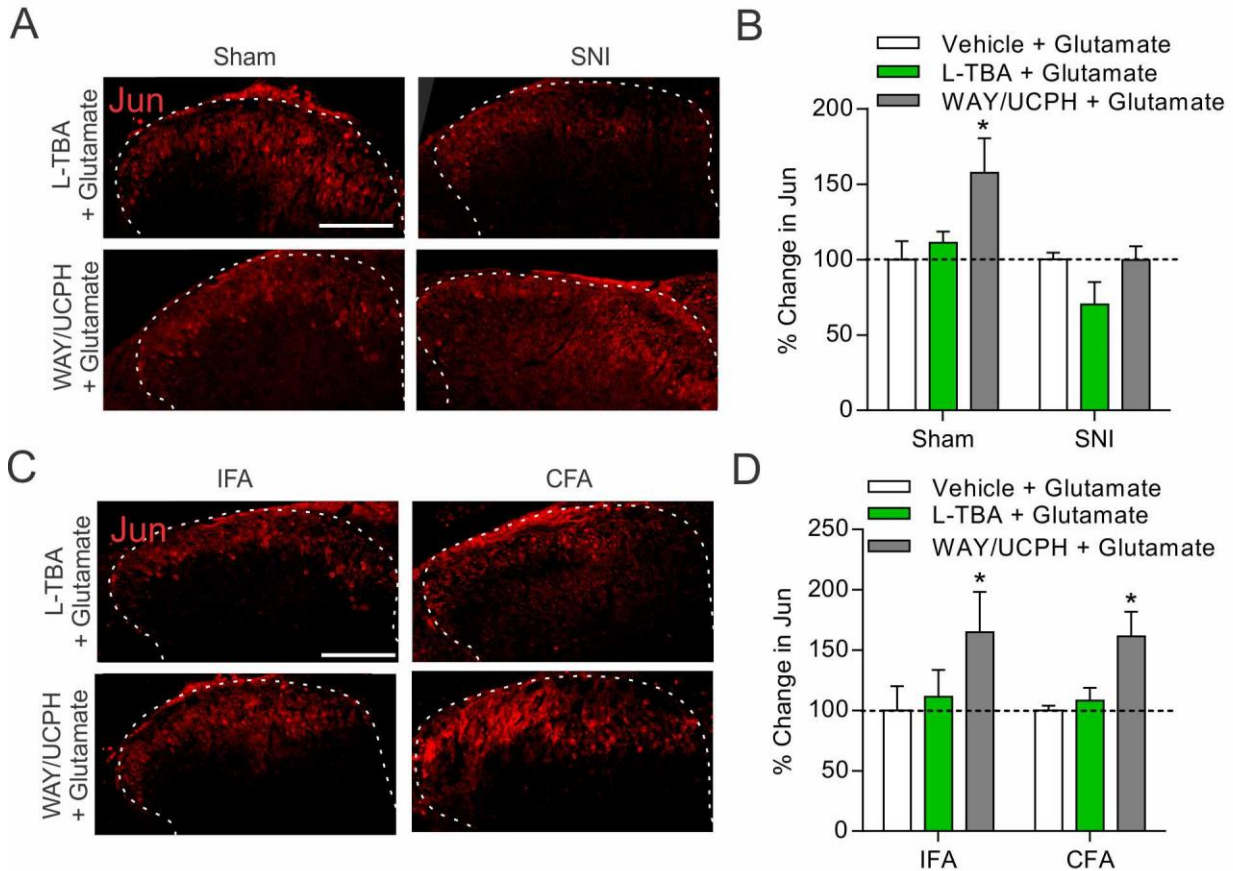


Figure 22. Glial EAAT inhibitor potentiates glutamate-induced Jun expression in control and inflamed rats.

(A) Representative immunofluorescence of glutamate-induced Jun expression in the ipsilateral SCDH (outlined with dotted line) of SNI and sham rats 45 minutes following i.t. pre-treatment with either 1 nmol L-TBA or 50 nmol each WAY213613+UCPH-101 (WAY/UCPH). Scale bar = 100 μ m. (B) Quantification of SCDH Jun expression, where % change in Jun is the percentage change in glutamate-induced Jun expression after drug treatment relative to a group of rats that received glutamate after vehicle (not shown in A). L-TBA had no effect on glutamate-induced Jun expression. WAY/UCPH significantly increased glutamate-induced Jun expression in Shams. (* $p < 0.01$ vs vehicle + glutamate, $N = 6$ rats per groups). (C) Representative immunofluorescence of glutamate-induced Jun expression in the ipsilateral SCDH (outlined with dotted line) of CFA and IFA rats 45 minutes following i.t. pretreatment of 1 nmol L-TBA or 50 nmol each WAY213613 and UCPH-101 pretreatment. Scale bar = 100 μ m. (D) Quantification of SCDH Jun expression, where % change in Jun is the percentage change in glutamate-induced Jun expression after drug treatment relative to a group of rats that received glutamate after vehicle (not shown in C). L-TBA pretreatment did not influence glutamate-induced Jun expression in any condition. Pretreatment with WAY/UCPH significantly increased glutamate-induced Jun in both IFA control and CFA rats. (* $p < 0.05$ vs vehicle + glutamate, $N = 6$ rats per group). Mean \pm SEM shown in B and D.

Permeable mGluR5 antagonists are effective at attenuating glutamate-induced pain in neuropathic animals

While the EAAT inhibitor experiments suggest persistent pain conditions are particularly sensitive to intracellular glutamate, it does not inform which receptor glutamate is targeting to produce the effect. To test the contribution of plasma membrane versus nuclear mGluR5 contributions *in vivo*, the effect of permeable and non-permeable group I mGluR antagonists on pain behaviors were compared. To avoid any long term effects of spinal glutamate, no repeated measures were used for these experiments and so each dose represents a unique sample.

In sham animals both non-permeable and permeable antagonists reduced glutamate-induced pain behaviors (Figure 23 A). The two-way ANOVA revealed no significant main effect of drug condition, indicating the permeable antagonists confer no additional benefit in reducing glutamate-induced pain ($F(1,40) = 0.9827$, $p = 0.3275$); however, there was a significant main effect of drug dose ($F(3, 40) = 7.996$, $p = 0.0004$). Dunnett's post-hoc test determined that LY393053 significantly attenuated pain behaviors at 100 nmol ($t(25) = 3.511$, $p = 0.0061$) and 1 μmol ($t(25) = 2.917$, $p = 0.0251$) doses in sham animals. In addition, fenobam attenuated glutamate-induced pain behaviors significantly at 10 nmol ($t(20) = 3.754$, $p = 0.0034$) and 100 nmol ($t(20) = 4.980$, $p = 0.0002$) doses in shams (Figure 23 A). Thus, blocking extracellular mGluRs or both intracellular and extracellular mGluRs attenuated glutamate-induced pain behaviors in sham animals.

In SNI animals the effects of either fenobam or LY393053 pretreatment on glutamate-induced pain behaviors was also assessed (Figure 23 B). A two-way ANOVA revealed a significant main effect of drug condition ($F(1,30) = 6.942$, $p = 0.0132$), indicating that grouping across doses, fenobam reduces

glutamate-induced pain behaviors to a greater extent than LY393053. Simple effects within each drug condition revealed that LY393053 did not significantly attenuate glutamate-induced pain behaviors at any dose given (Figure 23 B). In contrast, fenobam significantly attenuated glutamate-induced pain at 10 nmol ($t(20) = 4.174$, $p = 0.0013$) and 100 nmol ($t(20) = 2.967$, $p = 0.0202$) doses.

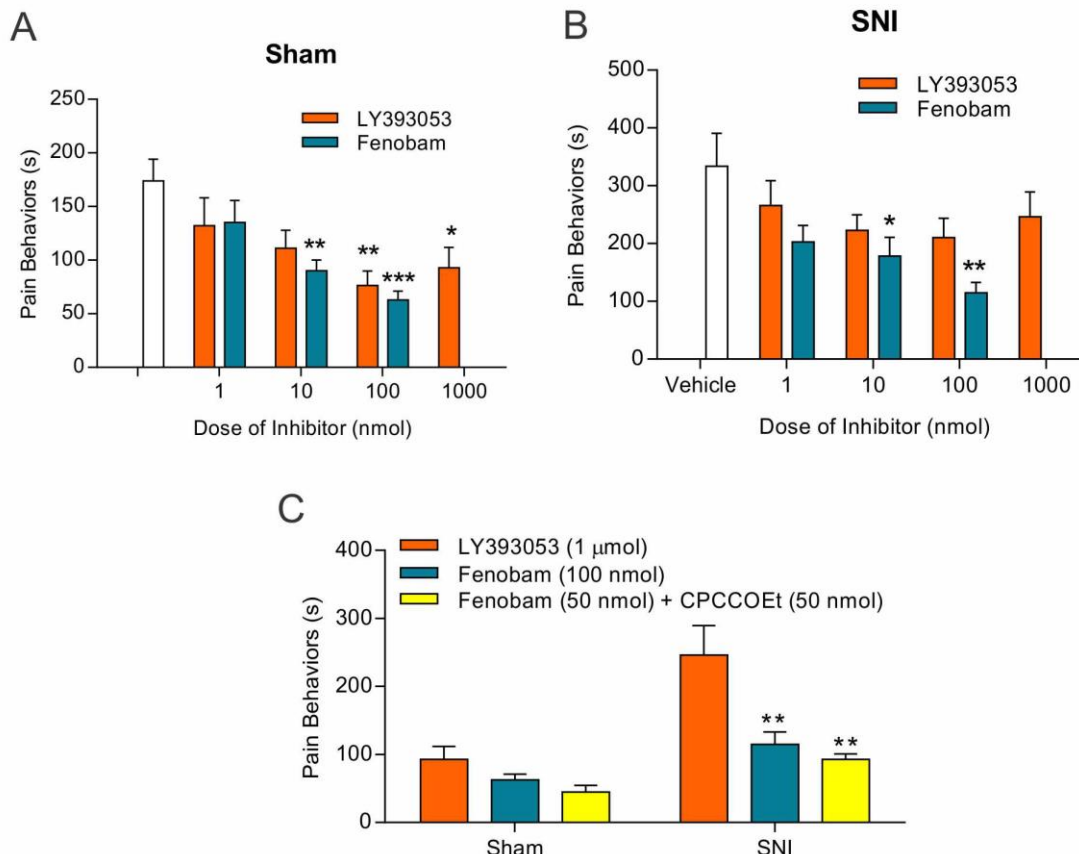


Figure 23. Permeable mGluR5 antagonists attenuate glutamate-induced pain behaviors in neuropathic animals more effectively than non-permeable mGluR5 antagonists.

A) Dose-response curve to i.t. treatment with the non-permeable group I mGluR antagonist, LY393053, and the permeable mGluR5 antagonist, fenobam, against pain behaviors induced by 400 μ g of i.t. glutamate in sham rats. **(B)** Dose-response curve to i.t. treatment with the non-permeable group I mGluR antagonist, LY393053, and the permeable mGluR5 antagonist, fenobam, against pain behaviors induced by 400 μ g of i.t. glutamate in SNI rats. (* $p < 0.05$, ** $p < 0.01$ vs vehicle, $N = 6$). **(C)** Comparison of 1 μ mol of LY393053 to 100 nmol of fenobam alone or 50 nmol each fenobam + CPCCOEt pretreatment on glutamate-induced pain behaviors in SNI and sham animals. Fenobam alone or in conjunction with CPCCOEt was significantly more effective at attenuating glutamate-induced pain behaviors than LY393053 in SNI animals, but not in sham animals. (** $p < 0.01$, $N = 6$). Mean \pm SEM shown in all graphs.

As LY393053 is an antagonist of both mGluR1 and mGluR5, while fenobam is selective only for mGluR5, a single dose of fenobam in conjunction with the permeable mGluR1 antagonist CPPCOEt was also assessed (Figure 23 C). The rationale behind this condition was to ensure that the blockade of mGluR1 was not producing an unanticipated adverse effect in the LY393053 condition. A direct head to head comparison between the highest doses of LY393053 (1 μ mol), fenobam (100 nmol) and the combination of fenobam + CPPCOEt (50 nmol each) revealed that fenobam alone ($t(30) = 4.311$, $p = 0.003$) or in conjunction with CPPCOEt ($t(30) = 5.027$, $p < 0.0001$) reduced glutamate-induced pain behaviors in SNI animals more than LY393053 (Figure 23 C). These results are consistent with the hypothesis that intracellular mGluR5 receptors are selectively involved in pain under neuropathic pain conditions.

Permeable mGluR5 antagonists are effective at attenuating glutamate-induced pain in inflammatory animals

The relative contribution of intracellular mGluRs was also assessed in animals with inflammation. The permeable mGluR5 antagonist, fenobam, and the non-permeable group I mGluR antagonist were assessed for their ability to reduced glutamate-induced pain behaviors in IFA animals (Figure 24 A). The two-way ANOVA revealed no significant main effect of drug condition, indicating that permeable antagonists conferred no additional benefit in reducing glutamate-induced pain ($F(1,40) = 2.605$, $p = 0.1144$); however, there was a significant main effect of drug dose ($F(3, 40) = 6.488$, $p = 0.0011$). Dunnett's post-hoc test determined that fenobam attenuated glutamate-induced pain behaviors significantly at 10 nmol ($t(20) = 2.980$, $p = 0.0197$) and 100 nmol ($t(20) = 3.357$, $p = 0.0085$) doses in IFA rats (Figure 22 A). LY393053 was not significant at any dose given.

In CFA animals the effects of either fenobam or LY303053 pretreatment on glutamate-induced pain behaviors was also assessed (Figure 24 B). Simple effects within each drug condition revealed that LY393053 did not significantly attenuate glutamate-induced pain behaviors at any dose given (Figure 24 B). Fenobam significantly attenuated glutamate-induced pain at 10 nmol ($t(20) = 3.22$, $p = 0.0116$) and 100 nmol ($t(20) = 4.343$, $p = 0.0009$) doses.

A direct head to head comparison between the highest doses of LY393053 (100nmol), fenobam (100 nmol) and the combination of fenobam + CPPCOEt (50 nmol each) revealed that fenobam alone ($t(30) = 3.456$, $p = 0.0032$) or in conjunction with CPCCOEt ($t(30) = 4.793$, $p < 0.0001$) reduced glutamate-induced pain behaviors in CFA animals more than LY393053 (Figure 24 C). These results are consistent with the hypothesis that intracellular mGluR5 receptors are selectively involved in CFA-induced pain.

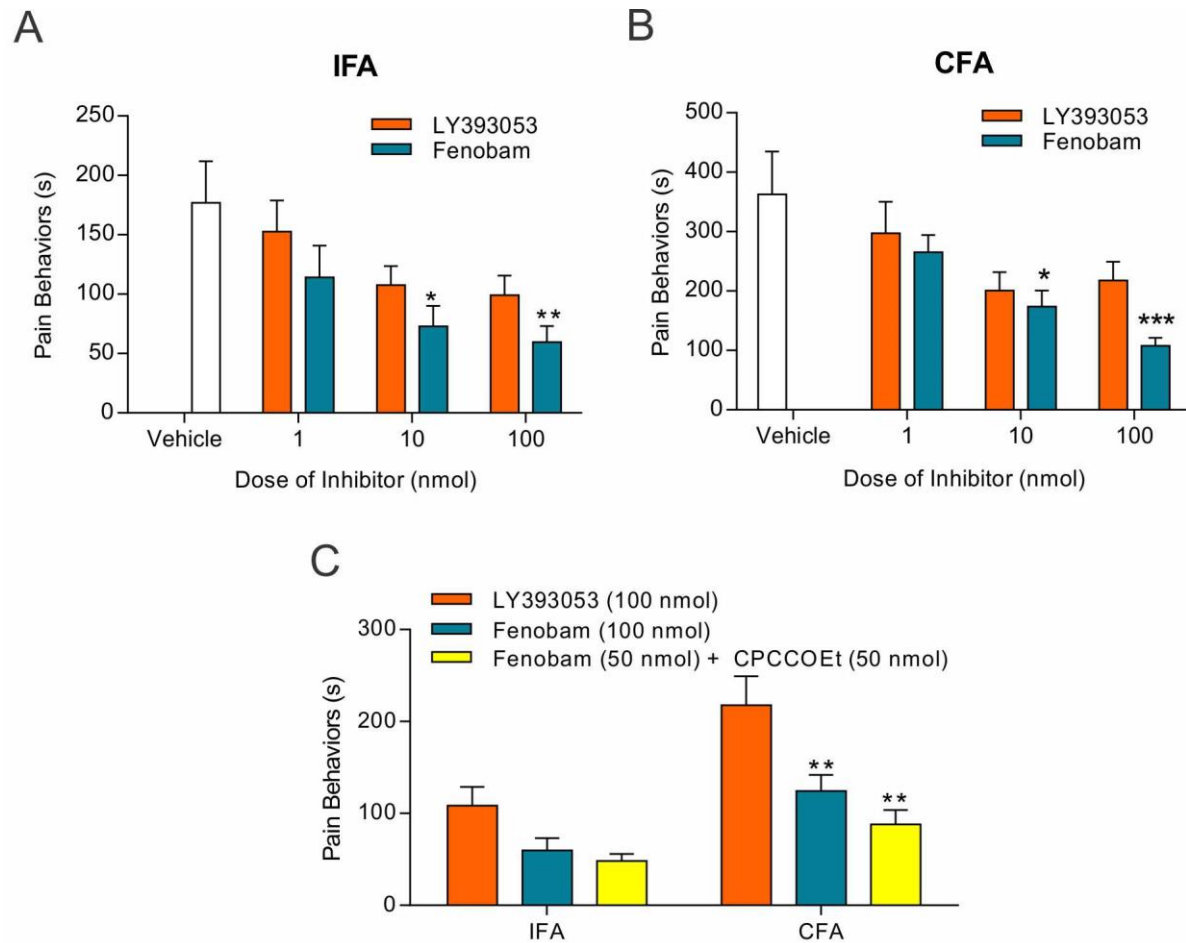


Figure 24. Permeable mGluR5 antagonists attenuate glutamate-induced pain behaviors in inflamed animals.

(A) Dose-response curve to i.t. treatment with the non-permeable group I mGluR antagonist, LY393053, and the permeable mGluR5 antagonist, fenobam, against pain behaviors induced by 400 μ g of i.t. glutamate in IFA rats. (B) Dose-response curve to i.t. treatment with the non-permeable group I mGluR antagonist, LY393053, and the permeable mGluR5 antagonist, fenobam, against pain behaviors induced by 400 μ g of i.t. glutamate in CFA rats (* $p < 0.05$, ** $p < 0.01$ vs vehicle, $N = 6$). (C) Comparison of 100 nmol of LY393053 to 100 nmol of fenobam alone or 50 nmol each fenobam + CPCCOEt pretreatment on glutamate-induced pain behaviors in CFA and IFA animals. Fenobam alone or in conjunction with CPCCOEt was significantly more effective at attenuating glutamate-induced pain behaviors than LY393053 in CFA animals, but not in IFA animals. (** $p < 0.01$, $N = 6$). Mean \pm SEM shown in all graphs.

Permeable mGluR5 antagonists reduce mechanical allodynia in neuropathic animals more effectively than non-permeable mGluR antagonists

Next, we assessed these antagonists on mechanical allodynia in the absence of exogenous glutamate. As sham animals do not present with mechanical allodynia, neither LY393053 nor fenobam had an effect on the PWT of sham animals (Figure 25A). However, in the mixed factor ANOVA, a significant main effect of fenobam as compared to LY393053 was observed on PWT in SNI rats ($t(21) = 2.738$, $p = 0.0370$). Dunnett's post-hoc t-tests revealed spinal injection of 100 nmol fenobam significantly elevated PWTs in SNI animals compared to baseline at 30 minutes ($t(7) = 6.918$, $p = 0.0007$), and 60 minutes ($t(7) = 6.107$, $p = 0.0016$) post-injection (Figure 25B). Further, PWT were significantly greater following fenobam than LY393053 at 30 ($t(14) = 8.041$, $p < 0.0001$) and 60 minutes ($t(14) = 5.615$, $p < 0.0001$). Surprisingly, LY393053 had no effect on PWT in SNI animals at any time point.

While fenobam did produce a significant change from baseline PWT in SNI animals, it should be noted that thresholds remained far below that of sham animals. Thus, fenobam does not rescue mechanical allodynia in nerve injured animals, but does attenuate the severity. At the same time, it directly outperforms a nonpermeable group I mGluR antagonist in this assay, suggesting that the contribution of mGluR5 to mechanical allodynia in nerve injury may be through intracellular receptor pools.

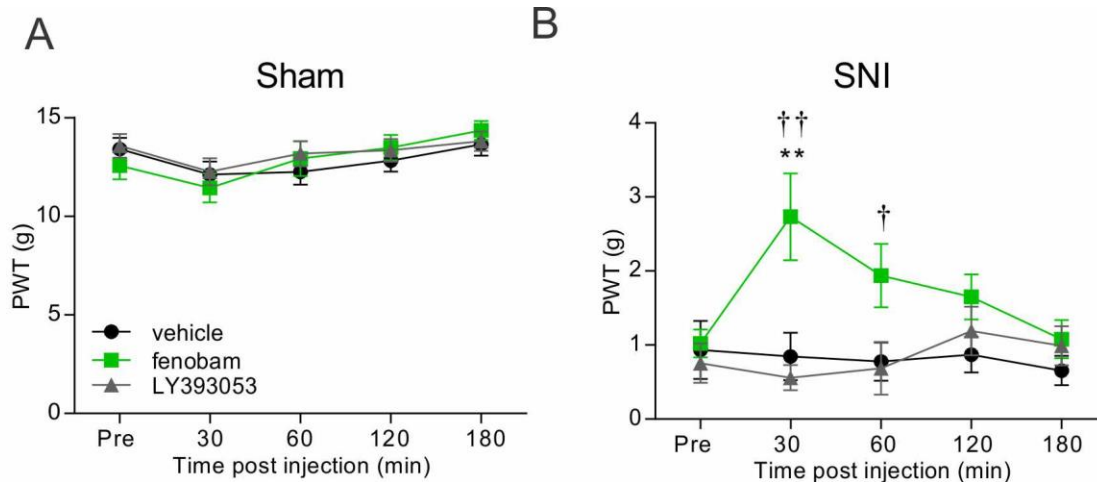


Figure 25. Permeable mGluR5 antagonists attenuate mechanical allodynia in neuropathic animals more effectively than non-permeable group I mGluR antagonists.

(A) Ipsilateral paw withdrawal thresholds (PWT) in day 7 sham rats taken before and after injection of either 100 nmol i.t. fenobam or 100 nmol LY395053. No change in PWT was observed at any time point. (N = 11 per condition). (B) Ipsilateral paw withdrawal thresholds in day 7 SNI rats taken before and after i.t. injection of either fenobam or LY395053. Fenobam, but not LY395053, significantly attenuated mechanical allodynia in SNI animals (**p < 0.01 vs vehicle; †p < 0.05, ††p < 0.01 vs LY395053; N = 6 rats per condition). Mean ± SEM shown for all graphs.

Permeable mGluR5 antagonists produce conditioned place preference in neuropathic and inflamed animals

To avoid ceiling and floor effects endemic to von Frey experiments, and to consider ongoing rather than evoked pain, conditioned place preference was determined for both permeable and non-permeable antagonists in SNI and naïve rats (Figure 26). Neither SNI nor naïve animals showed a place preference prior to conditioning (Figure 26A). Following two pairings of 200 nmol fenobam, however, animals with neuropathic pain showed a strong preference for the fenobam-paired chamber on test day (CPP-I = 62.51%, $t(7) = 2.505$, $p = 0.0099$) (Figure 26B). No such place preference for fenobam was observed for

naïve animals (CPP-I = 52.6%). These experiments demonstrated that i.t. fenobam pro-(1 µmol) did not produce conditioned place preference in either SNI or naïves (Figure 26B).

Animals used for the CFA conditioned place preference experiments also revealed no initial place preference (Figure 24C). Following a single pairing, CFA animals showed a significant conditioned place preference to 200 nmol fenobam (CPP-I = 60.24%, $t(10) = 2.338$, $p=0.0415$, $n=11$), but not to 1 µmol LY393053 (Figure 24D). Naive animals did not show a preference for either drug (Figure 24D). These results show that nuclear mGluR5 receptors contribute differentially to pain signalling in neuropathic and inflammatory conditions. In addition, it suggests that fenobam, like L-TBA, is rewarding only under pain conditions.

An important distinction to be made for these data is that while the effect of fenobam was significant and LY393053 was not, the two conditions were not significantly different from each other. Thus, while fenobam crossed the threshold to be considered a conditioned place preference, LY393053 did not cross the same threshold, but its effects were ultimately indistinguishable from fenobam. This distinction is important as it suggests fenobam cannot be considered more effective in this assay than LY393053.

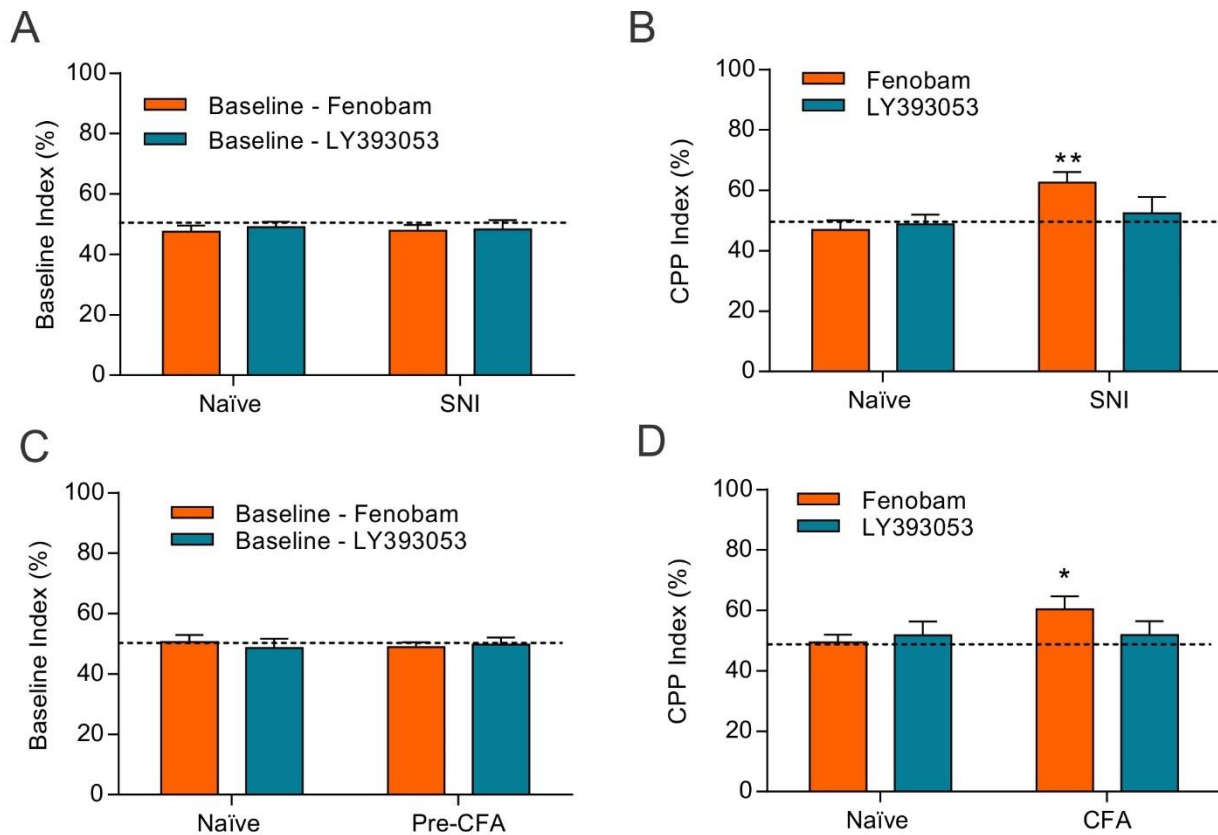


Figure 26. Permeable, but not non-permeable, mGluR5 antagonists produce conditioned place preference in neuropathic and inflamed animals.

(A) Baseline place preference as measured by percent time spent in chamber selected for drug pairing (prior to drug exposure), for naïve and day 7 SNI rats that later received i.t. fenobam or LY393053. Prior to conditioning, naïve rats and SNI rats showed no room preference. (B) Conditioned place preference (CPP-I) for naïve and SNI rats conditioned with 200 nmol fenobam or 1 μ mol LY393053. Following conditioning SNI animals conditioned with fenobam spent significantly more time in the fenobam-paired chamber (** $p < 0.01$ vs 50%). No preference developed in SNI rats following conditioning with LY393053. No CPP was established in naïve animals following a single pairing of either LY393053 or fenobam (N = 9 rats per group). (C) Baseline place preference as measured by percent time spent in chamber selected for drug pairing (prior to drug exposure), for naïve and CFA rats that later received i.t. fenobam or LY393053. Prior to conditioning, rats showed no preference for either chamber. Pre-CFA = naïve animals selected for CFA injection following baseline. (D) Conditioned place preference (CPP-I) for naïve and CFA rats conditioned with 200 nmol fenobam or 1 μ mol LY393053. 48 hours post-CFA rats spent more time in the fenobam paired chamber (* $p < 0.05$ vs 50%) following a single pairing. CFA and naïve rats showed no preference for a chamber paired with LY393053. No CPP was established in naïve animals following a single pairing of either LY393053 or fenobam. (N = 11 rats per group). Mean \pm SEM shown for all graphs. Fenobam produced a significant conditioned place preference specifically in neuropathic rats. In contrast, LY393053

Permeable mGluR5 antagonists attenuate glutamate-induced Fos expression

To test whether permeable and nonpermeable mGluR5 antagonists would differentially affect downstream signaling pathways associated with pain behaviors, SNI or sham rats were pretreated with either 100 nmol fenobam or LY393053 prior to measuring spinal Fos expression induced by 400 μ g spinal glutamate (Figure 27A-B). Two-way ANOVA revealed a significant drug effect, and a main effect of fenobam on Fos expression (fenobam vs vehicle $t(30) = 4.689$, $p = 0.0039$; fenobam vs LY393053 $t(30) = 6.441$, $p = 0.0022$). Fenobam's effect on reducing glutamate-induced Fos expression was significant in both sham ($t(30) = 2.430$, $p = 0.0393$) and SNI animals ($t(30) = 2.359$, $p = 0.0498$). In contrast, LY393053 which does not cross the plasma membrane, did not have an effect on glutamate-induced Fos expression in either SNI or sham animals (Figure 27B).

Pretreatment with 100 nmol fenobam also reduced glutamate-induced Fos expression compared to a vehicle pretreatment in CFA and IFA animals (Figure 27C-D). Dunnett's post-hoc t-tests revealed that fenobam produced a significant 65% reduction in Fos in IFA rats ($t(30) = 2.500$, $p = 0.0112$) and a 70% reduction in Fos in CFA rats ($t(30) = 3.121$, $p = 0.0155$). In contrast, pretreatment with LY393053 failed to attenuate glutamate-induced Fos expression in either IFA or CFA rats (Figure 27D). These findings illustrate the importance of membrane permeability of the mGluR5 antagonist for reducing Fos expression in both control and persistent pain conditions.

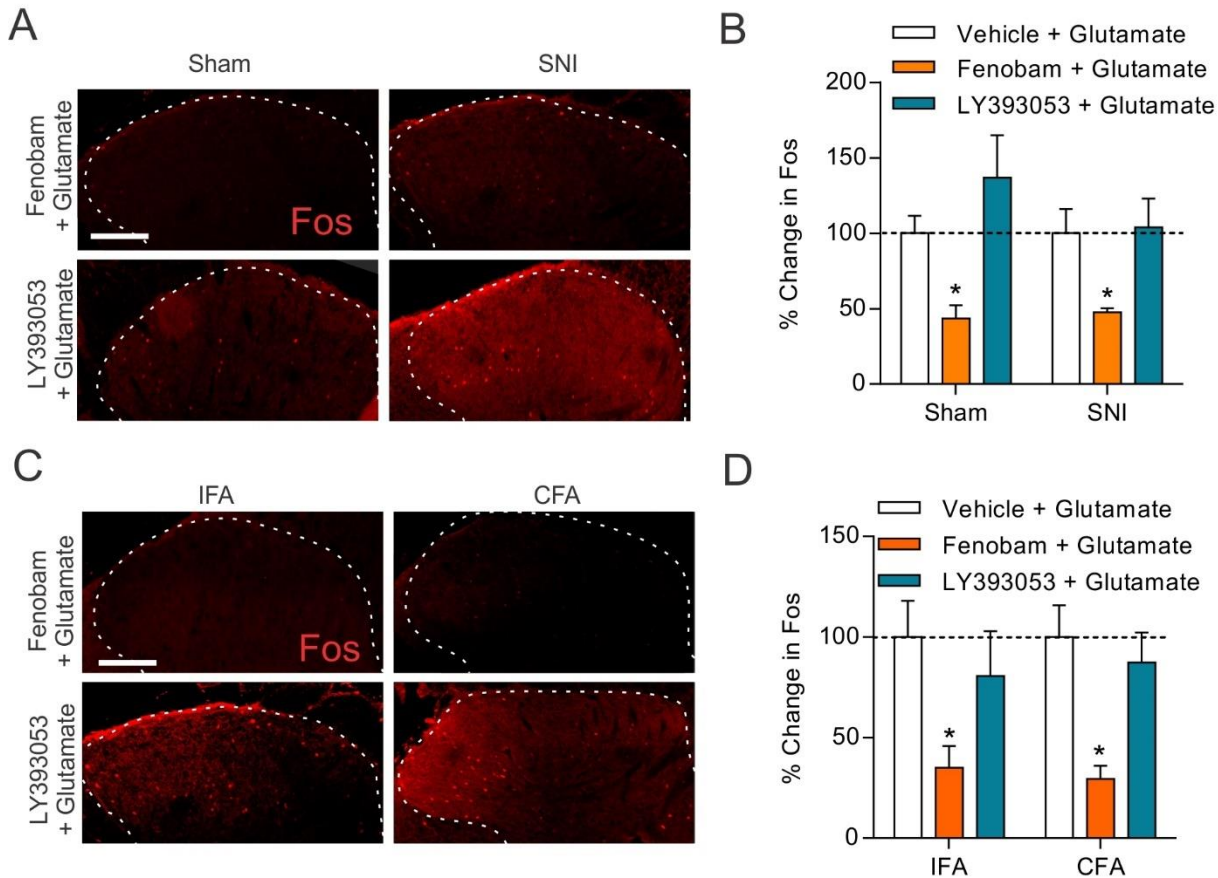


Figure 27. Permeable, but not non-permeable, mGluR5 antagonists attenuate glutamate-induced Fos in the SCDH.

(A) Representative immunofluorescence of glutamate-induced Fos expression in ipsilateral SCDH (outlined in dotted line) following 100 nmol i.t. fenobam or 100 nmol i.t. LY395053 pretreatment in 7 day sham and SNI animals. (B) Quantification of Fos expression, where % change in Fos is the percent change in glutamate-induced Fos expression after drug treatment relative to a group of rats that received glutamate after vehicle (not shown in A) (vehicle + glutamate group set to 100%). Fenobam significantly attenuated glutamate-induced SCDH Fos expression in both SNI and sham animals (* $p < 0.05$ vs vehicle + glutamate). LY393053 failed to reduce glutamate-induced Fos expression in any group. (N = 5 rats per condition). (C) Representative immunofluorescence of glutamate-induced Fos expression in ipsilateral SCDH (outlined in dotted line) following 100 nmol i.t. fenobam or 100 nmol i.t. LY395053 pretreatment in day 3 IFA and CFA animals. (D) Quantification of Fos expression, where % change in Fos is the percent change in glutamate-induced Fos expression after drug treatment relative to a group of rats that received glutamate after vehicle (not shown in C). (vehicle + glutamate group set to 100%). Fenobam significantly attenuated glutamate-induced Fos expression in both CFA and IFA animals (* $p < 0.05$ vs vehicle + glutamate). LY393053 failed to reduce glutamate-induced Fos expression in any group. (N = 5 rats per condition). Mean \pm SEM shown for all graphs.

Permeable and non-permeable mGluR antagonists attenuate glutamate-induced Jun expression

The effects of fenobam and LY393053 were also assessed on spinal glutamate-induced Jun expression in SNI, sham, CFA and IFA rats. Both fenobam and LY393053 were effective at attenuating glutamate-induced Jun expression across all conditions, and the two antagonists did not produce effects that were significantly different from each other (Figure 28A-D). Unlike Fos, the expression of Jun is not known to depend on intracellular mGluRs. Instead, previous findings report that permeable and non-permeable antagonists alike prevent mGluR5-dependent phosphorylation of JNK, which leads to expression of Jun [313]. Consistent findings were shown here, wherein both SNI and sham rats (Figure 28A-B), as well as CFA and IFA rats (Figure 28C-D), either antagonist was equally effective at reducing glutamate-induced Jun expression. Importantly, this finding suggests that plasma membrane mGluRs are still functional in animals with neuropathic pain and continue to activate downstream signalling targets. However, as the behavioral evidence showed, targeting only plasma membrane receptors was not sufficient to attenuate pain or Fos in animals with persistent pain. These data suggest that attenuating Jun expression alone is not sufficient to produce behavioral changes associated with pain reduction.

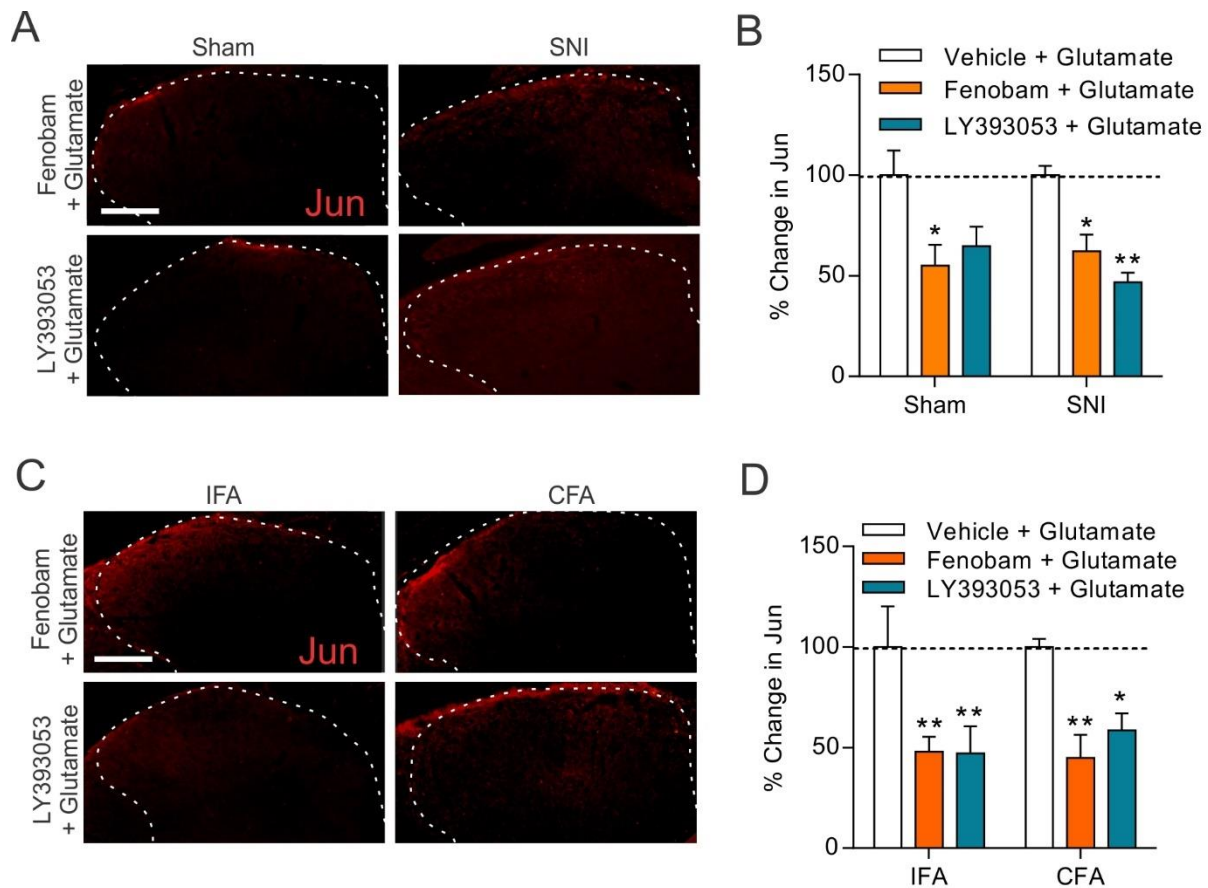


Figure 28. Permeable and nonpermeable mGluR antagonists attenuate glutamate-induced Jun in the SCDH.

(A) Representative immunofluorescence of glutamate-induced Jun expression in the ipsilateral SCDH (outlined in dotted line) following 100 nmol i.t. fenobam or 100 nmol i.t. LY395053 pretreatment in sham and SNI animals. (B) Quantification of Jun expression, where % change in Jun is the percent change in glutamate-induced Jun expression after drug treatment relative to a group of rats that received glutamate after vehicle (not shown in A). (vehicle + glutamate group set to 100%). Both fenobam and LY393053 were effective at attenuating glutamate-induced Jun expression (* $p < 0.05$, ** $p < 0.01$ vs vehicle + glutamate; $N = 6$ per condition). (C) Representative immunofluorescence of glutamate-induced Jun expression in the ipsilateral SCDH (outlined in dotted line) following 100 nmol i.t. fenobam or 100 nmol i.t. LY395053 pretreatment in IFA and CFA animals. (D) Quantification of Jun expression, where % change in Jun is the percent change in glutamate-induced Jun expression after drug treatment relative to a group of rats that received glutamate after vehicle (not shown in C). Both fenobam and LY393053 were effective at attenuating glutamate-induced Jun expression (* $p < 0.05$, ** $p < 0.01$ vs vehicle + glutamate; $N = 6$ per condition). Mean \pm SEM are shown for all graphs.

Discussion

Signal transduction from G protein-coupled receptors (GPCRs) has been long thought to originate only from the plasma membrane, where extracellular molecules interact with ligand binding domains to activate local signalling complexes. The idea that GPCRs are exclusively functional at the cell surface has come under direct challenge in the past decade with the discovery of both receptor and signalling complex components on intracellular membranes. Not only do these receptors represent a unique pool for which ligand may bind, but some have been shown to produce signalling cascades unique from their plasma membrane counterparts, hinting that they may serve a different function intracellularly. One discovered intracellular GPCR, mGluR5, is of particular interest to the pain field due to its known role in nociceptive signal transduction within the SCDH, and involvement in the transition to a pathological, chronic pain state. The body of work presented here provides an account of the upregulation of intracellular mGluR5 in models of inflammatory and neuropathic pain, and provides a description of the behavioral and histological consequences of impairing or facilitating its function.

Five lines of converging evidence are presented here in support of an active role for intracellular mGluR5 in persistent pain: (1) mGluR5 is increased exclusively on nuclear-enriched fractions of the SCDH in rats as early as one day following inflammatory or neuropathic injury, and is maintained throughout the period of testing; (2) inflamed and neuropathic rats experience enhanced i.t. glutamate-induced nociception that is associated with increased expression of immediate early genes, *c-fos* and *c-jun*; (3) inhibiting intracellular receptor access by blocking neuronal EAAT, EAAT3, produces conditioned place preference and attenuates mechanical allodynia, i.t. glutamate-induced nociceptive behaviors, and *c-fos* expression in rats with persistent pain; (4) specific inhibition of glial EAATs, EAAT1 and EAAT2, is pronociceptive in both persistent pain and control conditions, is associated with increased spinal

glutamate concentrations, and fails to attenuate *c-fos* or *c-jun* expression; and (5) in persistent pain conditions, permeable mGluR5 antagonists produce conditioned place preferences and appear more effective at attenuating pain behavior, mechanical allodynia and *c-fos* expression than impermeable group I mGluR antagonists.

Selective upregulation of nuclear mGluR5 following persistent pain

Quantifying changes in mGluR5 expression following inflammation and nerve injury has yielded conflicting and mixed results in the literature. In a study using both experimentally-induced and naturally occurring unilateral digit inflammation in sheep, mGluR5 mRNA and protein were upregulated in the SCDH in early (3 hours) and chronic phases (>2 weeks) of inflammation [202]. However, *in situ* hybridization and rtPCR analysis of spinal mGluR5 following a model of post-surgical pain in sheep revealed only a transient increase in mGluR5 mRNA, observed between 5 and 24 hours following procedure, which subsequently returned to pre-surgical levels [203]. This discrepancy, it should be noted, could be explained by the different models used. Indeed, in a later study the authors found that their model of post-surgical pain persisted only 48 hours, indicating that increased mGluR5 expression lasted only for the duration of the pain [375]. However, even within the same pain model conflicting results have emerged. One group observed that after spinal cord injury (SCI), mGluR5 protein was unchanged from baseline at both early (1 day) and late stages (60 days) of the injury [376]. Another group found the exact opposite result in SCI rats; mGluR5 expression was significantly increased in large dorsal horn neurons in early (7 day), late (14 days) and chronic (30 days) stages [201]. In this case, differences may in part be due to methods in spinal cord measurement. As mGluR5-positive neurons involved in nociceptive transmission are predominantly located in lamina I and II, measurements that take into account all layers of the spinal cord (as in the case of [376]) may fail to observe changes in

mGluR5 expression, whereas those that measure expression levels in the superficial lamina exclusively (as in [201, 202]) should capture more subtle changes.

While differences in duration of pain or protein measurements may account for some distinctions, still others have observed discrepancies between the pain models that were used. For example, there were increases in mGluR5 immunoreactivity in lamina II of the ipsilateral spinal cord after either SNL or L5 SNL; however, the same group found there was no change in mGluR5 expression after pSNL [156]. In all three models, there was significant thermal and mechanical hyperalgesia, but only SNL-induced hyperalgesia was rescued with the permeable mGluR5 antagonist, MPEP, while hyperalgesia after pSNL ligation was not [156]. The ineffectiveness of MPEP as an analgesic in pSNL is particularly interesting as it suggests that pain in this model is mediated through mGluR5-independent means. The reason for the inter-model differences is still unclear, though it may involve the presence of both intact and damaged nerve populations in the same ganglia, which occurs after pSNL, but not SNL.

A shortcoming of all these investigations is that they lack information regarding the subcellular distribution of mGluR5. Here we report a specific increase in nuclear mGluR5 following inflammation and nerve injury. These reports are consistent with electron microscopy data showing an increase in nuclear membrane-bound mGluR5 in the superficial layers of the SCDH in SNI rats [214]. No significant changes were observed in the plasma membrane or cytoplasmic levels from western blots, even though electron microscopy data found a small, but significant decrease in plasma-membrane bound and cytoplasmic mGluR5 [214]. The discrepancy between subcellular fractionation data and electron microscopy data may be because western blot is less sensitive to smaller changes, particularly as the entire lumbar dorsal horn was used rather than just the superficial layers. However, it should be noted that electron microscopy only samples a small fraction of the total number of neurons within the area

of interest. Furthermore, the magnitude of change for nuclear mGluR5 is consistent between electron microscopy results and the western blot data presented here. These data give a new perspective on previous mGluR5 expression results.

As mGluR5 is traditionally believed to be exclusively functional on the cell surface, reports of increased mGluR5 protein has largely assumed that this is indicative of increased plasma membrane expression. This assumption is particularly tenuous in the case of mGluR5, as it has been well-established that the presence of mGluR5 on the cell surface is highly plastic and represents only a fraction of total mGluR5 [212, 243, 244]. The data presented here suggest that instead there is a measurable increased mGluR5 protein on intracellular membranes, specifically at the nucleus. Further, we have previously shown that there is minimal colocalization of mGluR5 with astrocytes in either sham or SNI rats, and electron microscopy data revealed no mGluR5 labelling on the nuclei of glial or endothelial cells [214]. These data strongly suggest that the increased expression of nuclear mGluR5 observed in the western blots is neuronal.

More difficult to reconcile are the previous electron microscopy data indicating an increase in plasma membrane-bound mGluR5 grains in CFA rats [213]. This study was conducted prior to knowledge of nuclear mGluR5, and no quantification of nuclear membrane-bound mGluR5 was performed, thus no conclusion regarding changes on the nucleus in CFA animals could be drawn. However, western blot data here did not reveal any significant change in plasma membrane-bound mGluR5 in CFA rats at any time point, which is inconsistent with the reported increase from electron microscopy data. Again, electron microscopy results were specific to lamina I and II, whereas western results are from the entire dorsal horn. While mGluR5-directed antibodies stain predominantly in lamina I and II, mGluR5 is still observed in lower quantities in the deeper lamina [181]. If there are no changes in plasma membrane-

bound mGluR5 in deeper lamina, small differences localized in the superficial lamina, as was previously reported using electron microscopy [213] could potentially be missed through western quantification. A limitation to these data is the small sample size used and the lamina non-specificity of the assay. Small sample sizes result in underpowered studies which produces a greater number of false negatives. Future studies should be performed to replicate these findings and confer greater confidence in the reliability of the results.

Overall, data from western blots provide an indication regarding the presence of mGluR5 on the nuclear envelope; however, there are limitations to this methodology. First, as mentioned earlier, tissue collection for western blot requires separating the dorsal portion of the cord from the ventral. The precise location of this sectioning would impact which lamina are included within the lysate. However, even though there was consistency in how much tissue was collected per sample, the entire dorsal horn rather than the superficial lamina was collected. This also limits how specific the results are as changes in the subcellular distribution of mGluR5 may not be equal in all lamina. In addition, blots needed to be stripped and reprobed for different antigens, and how even the blots are stripped will impact results. A standardized method for stripping and reprobing each blot was performed, however, stripping was performed in an incubator without a shaker, so uneven stripping is possible. To mitigate the influence of this method, mGluR5 was always probed first and the loading controls second. The absence of significant changes in the loading controls was used to confirm that this process did not differentially impact the pain conditions; however, small sample sizes may render small changes improbable to reach significance. Ultimately, however, the westerns represent a confirmation of the electron microscopy results, which also demonstrated an overall increase in nuclear mGluR5. Lastly, the increased nuclear mGluR5 within the nuclear fraction was also in line with the quantification from westerns presented in [214], where an

independent lab fractionated and analyzed tissue from spinal samples from our lab. Replication of this portion of the results bolsters confidence in these findings, suggesting they represent a true increase in protein content in the nucleus.

Functionality of nuclear mGluR5

An argument could be made that although there is an increase in mGluR5 on the nuclear membrane following SNI and CFA injury, nuclear mGluR5 is not necessarily folded properly or capable of binding glutamate. However, there is strong reason to believe that these receptors are in fact fully functional. Indeed, a research group in Washington University, led by O'Malley, has generated data over fifteen years demonstrating the functionality of nuclear-bound mGluR5. The group studied human embryonic kidney (HEK) cells transfected with cDNA for mGluR5, and found that the entire receptor was present on the nuclear membrane, with the N-terminus within the nuclear lumen [245]. Further data showed that, like plasma membrane mGluR5, nuclear receptors bind both [³H]glutamate and [³H]quisqualate [245]. The group then isolated the nuclei and confirmed that, in the absence of a plasma membrane and its receptors, glutamate produces calcium oscillations in the nucleus. Importantly, passively increasing intracellular calcium levels with caged calcium did not induce the same calcium oscillations, indicating that it is not intracellular calcium causing the activation of mGluR5, but rather activation of mGluR5 that induces calcium oscillations [245]. Later the group replicated many of these findings in striatal neurons, demonstrating that the permeable agonist, quisqualate, induces prolonged calcium oscillations that are blocked by the permeable mGluR5 antagonist, MPEP, but not by non-permeable antagonists LY393053 or LY367366 [246]. In contrast, the non-permeable agonist, DHPG, elicits a transient calcium peak that is blocked by non-permeable antagonists [246]. Further, mobilization of nuclear calcium was prevented by expressing in HEK cells an mGluR5 mutant which blocks G_{q/11} coupling, indicating that mGluR5 couples

to G proteins on the nucleus [248]. Nuclear mGluR5-mediated calcium responses were also blocked by a PLC inhibitor [248]. In addition, a PIP₂/IP₃ biosensor revealed that IP₃ is generated in the nucleus following nuclear mGluR5 stimulation [248]. Taken together, their data provide a strong proof of principle that mGluR5 is capable of coupling to its G_{q/11} protein, which stimulates PLC and IP₃ formation from its location on the nuclear membrane.

To more directly assess the function of nuclear mGluR5 within the context of persistent pain, it has also been shown that isolated nuclei from SCDH of SNI animals bind more glutamate than nuclei isolated from sham animals, suggesting more binding sites and therefore more nuclear receptors [214]. Importantly, glutamate binding assays show no difference in receptor affinity for the mGluR5 agonists DHPG and quisqualate using either plasma membrane or nuclear fractions derived from either SNI or sham rat tissues. This indicates that the increased quantity of bound glutamate in SNI nuclei is not an artifact of increased receptor affinity, but is rather due to increased receptor quantity [214]. Further, the nucleus in SNI and sham SCDH express EAAT3, providing a potential mechanism for intracellular glutamate to access the lumen, which is where the ligand binding domain resides [214]. Importantly, it was also shown that 80% of [³H]glutamate uptake is prevented by inhibiting sodium-dependent transporters, suggesting that EAAT3 contributes to the majority of neuronal glutamate uptake into the SCDH. It is still unclear how glutamate passes the outer nuclear envelope to gain access to the mGluR5 binding site within the nuclear lumen. However, isolated SCDH nuclei produce calcium oscillations in response to the transportable agonist quisqualate, but not the non-transported agonist DHPG [214]. This result, while not indicating the source of the transport, does confirm that mGluR5 agonists are transported prior to activating nuclear mGluR5. This is in line with the receptors being positioned on the nucleus such that the glutamate-binding domain is within the nuclear lumen.

A number of findings from studies on heterologous cells were also replicated in SCDH neurons transfected with a nuclear-targeted red fluorescent, genetically encoded calcium indicator [214]. In these cells, quisqualate produced sustained, elevated nuclear calcium responses which were terminated with fenobam, but not by LY393053. In addition, there was no nucleus-derived calcium response to DHPG application. Thus, as with other cell types, SCDH intracellular mGluR5 is capable of producing nuclear calcium signaling in response to transportable ligands.

Inflammatory and neuropathic pain is associated with glutamate hyperalgesia

Results from the glutamate experiments in this thesis demonstrate that spinally administered glutamate produces sustained nociceptive responses in a dose-dependent manner. Glutamate is endogenously released from presynaptic terminals in response to painful stimuli, and its activity at both ionotropic and metabotropic glutamate receptors is central to the transmission of painful signals in the SCDH. Due to its toxicity, the release and reuptake of glutamate at the synapse is tightly regulated. Under normal physiologic conditions, the spinal cord maintains extracellular concentrations around 5-22 μM in the absence of exogenous stimulation [377-380]. Dropping a 10 g weight on exposed spinal cord, a model of spinal cord injury, briefly increases glutamate concentrations to 530-550 μM [377, 378]. The severity of injury also positively correlates with the concentration of spinal glutamate [381]. Sharp increases in glutamate concentration are also observed following hind paw inflammation, which lasts up to 8 hours post-carrageenan injection [382]. In a chronic constriction injury model of neuropathic pain, spinal concentrations of glutamate were elevated in the spinal cord at day 8 post-operatively [383].

Rather than desensitizing the neurons, the greater concentration of spinal glutamate in inflammatory and neuropathic animals appears to have a sensitizing effect on neurons, since application of i.t.

glutamate produces greater nociceptive responses in these groups. These results are unsurprising as persistent pain induces neuroplasticity in the SCDH leading to changes in the glutamatergic system, including decreased EAAT expression [292, 293, 296], and the upregulation [156, 201] and migration [213] of glutamate receptors in neuropathic and inflammatory animals. As a result, the hyperalgesic response to glutamate is likely due to a confluence of factors, including poorer glutamate clearance mechanisms from glial EAATs, increased resting levels of spinal glutamate, and increased nuclear mGluR5.

In addition to increased behavioral responses to glutamate, SNI and CFA rats show greater Fos and Jun expression in the SCDH. Both Fos and Jun have a long history as markers of neuronal activity. Fos was first described as a member of the activator protein-1 (AP-1) family of inducible transcription factors 30 years ago [384]. The cellular content of Fos is tightly regulated; in quiescent cells the protein is nearly undetectable, whereas its expression is induced rapidly and transiently following sensory stimulation [384-386]. Fos participates in the formation of heterodimers with other IEGs, mainly Jun. The cellular consequences of Fos and Jun expression, as well as the molecular mechanisms involved in their induction remain unclear; however, in the SCDH their expression is correlated with stimulation of A δ and C fibers [387, 388]. Following noxious stimulation, both Fos and Jun are expressed by 30 minutes and peak at 1 hour [388], though duration of Fos and Jun expression appear to differ. While Fos returns to baseline within 3 hours, Jun may be observed days later [389]. In the studies presented here, both Fos and Jun were measured 45 minutes (± 8 minutes) following i.t. injection of glutamate. An important caveat to discuss regarding the glutamate-induced Fos and Jun expression is the time point used to measure protein levels. As only a single measurement of both immediate early genes was taken into account, these results cannot speak to differential effects at later time points. With this limitation in mind, strong

i.t. glutamate-induced increases in both Fos and Jun in control, inflamed, and neuropathic animals alike is consistent with the nociceptive role of spinal glutamate. As with the pain behaviors, spinal glutamate-induced Fos and Jun expression was more pronounced in animals with persistent pain, suggesting greater neuronal activation in response to glutamate.

The next question to ask is what is responsible for the increased glutamate-induced Fos and Jun expression in the SCDH of animals with persistent pain. Importantly, Fos and Jun are known to be differentially regulated in the SCDH [390]. For instance, Jun may be activated from the phosphorylation of c-jun N-terminal kinases (JNKs), which are activated by the upstream MAPK kinases; in contrast, Fos expression correlates strongly with the presence of ERK [389]. As described in the introduction, both of these pathways are downstream of group I mGluR stimulation. Moreover, the two protein products have recently been shown to be differentially regulated by plasma membrane and nuclear-bound mGluR5 [313]. While plasma membrane mGluR5 activation yields increased expression of phosphorylated JNK (activator of Jun), nuclear mGluR5 was required for Fos expression [313]. Using pharmacological isolation, the group also demonstrated that nuclear, but not plasma membrane, mGluR5 was associated with increases in MEK, phosphorylated ERK1/2 and Elk-1 [313]. In other words, the components of the pathway targeting *c-fos* expression have all shown nuclear mGluR5 dependence *in vitro*. As both protein products Fos and Jun are upregulated in response to glutamate in animals with persistent pain, more than one pool of receptors is likely involved in glutamate hypersensitivity.

Intracellular glutamate is pronociceptive in persistent pain conditions

Pronociceptive effect of glial EAAT inhibitors

The glial EAATs, EAAT1 and EAAT2, regulate spinal glutamate concentrations by scavenging glutamate into astrocytes following presynaptic release, terminating its activity on synaptic glutamate receptors. In this thesis, it was shown that i.t. injection of EAAT1 and EAAT2 inhibitors (WAY-213613 and UCPH-101) potentiates glutamate-induced pain behaviors in both injured and control rats, as well as producing a conditioned place avoidance and mechanical allodynia in control rats. These findings are consistent with a report showing an increase in spontaneous pain behaviors following i.t. injection of dihydrokainate (DHK), another glial EAAT inhibitor, in naïve rats [286]. Unlike DHK, UCPH-101 and WAY213613 do not act as agonists to glutamate receptors [278, 280]. Thus, pain-related behaviors evoked by these glial EAAT inhibitors cannot be explained by direct interaction at glutamate receptors. Instead, the sustained nociceptive behaviors produced by glial EAAT inhibitors are most likely due to elevating extracellular glutamate, resulting from the blockade of glutamate reuptake into astrocytes. Evidence for this mechanism of action comes from the microdialysis results described here in neuropathic and inflamed animals. Following WAY213613 + UCPH-101 administration in SNI animals, or UCPH-101 in CFA animals, there are significant increases in spinal glutamate concentrations. Importantly, WAY213613 and UCPH-101 do not prevent the functioning of the neuronal EAAT3 [278]. It has been demonstrated that glutamate is transported into neurons specifically through EAAT3 [391], and that intracellular uptake through EAAT3 is necessary for activation of intracellular receptors [246]. Thus, the pronociceptive effects observed when blocking glial reuptake of glutamate, while sparing neuronal uptake, is likely due to increased activation at both cell surface receptors and intracellular receptors.

Antinociceptive effect of neuronal EAAT inhibitors

It is important to keep in mind that for synaptic glutamate to activate neuronal nuclear mGluR5 it must be transported across both the plasma and nuclear membranes. The majority of extracellular glutamate is taken up into glia via EAAT1/2; however, the mechanism by which glutamate enters into SCDH neurons is largely (~80%) through EAAT3 [214]. The mechanisms involved in transporting glutamate across nuclear membranes, once it has reached the cytoplasm, is less definitive. EAAT3 is expressed in nuclear fractions within the SCDH making it a promising candidate [214]. Still unknown is what directions nuclear EAAT3 guides glutamate transport *in vivo*. If EAAT3 maintains the same topology on the nuclear membrane as it has on the plasma membrane, the predicted direction would be to transport glutamate from the nuclear lumen and into the cytoplasm. This would therefore prevent any nuclear mGluR5 activation from cytoplasmic sources of glutamate. However, in isolated nuclei from various cell populations, both sodium-dependent and sodium-independent mechanisms facilitate glutamate uptake out of the cytoplasm and into the nuclear lumen, indicating the direction of transport is opposite that of plasma membrane EAATs [246]. If the same holds true for intact cells, then both EAAT3 and X_{CT} are likely involved the second phase of transport into the nuclear lumen; however, direct testing of this hypothesis in intact cells has not yet been performed. With this limitation in mind, the EAAT3 inhibitor experiments performed in this thesis at least prevent glutamate from the first phase of transport – from synapse to the neuronal cytoplasm. Interrupting this phase of transport in animals with persistent pain attenuates nociception, suggesting glutamate has a pronociceptive effect within neurons of the SCDH.

In the dose-response curve, it was noted that i.t. pretreatment with L-TBA attenuated glutamate-induced pain behaviors and was maximally effective at 1 nmol. At high doses, L-TBA became less

effective. The reason for this U-shaped curve is possibly because at higher doses L-TBA becomes less selective and blocks EAAT1/EAAT2 transporters as well [392]. At higher doses, L-TBA blockade of EAAT1 and EAAT2 was found to prolong NMDAR signaling [392], thus for the remainder of the studies a 1 nmol dose of L-TBA was used to reduce these non-selective effects. It is important to note that while glutamate-induced pain behaviors were attenuated by pre-treatment with L-TBA, they were not abolished entirely. In fact, inhibiting EAAT3 resulted in comparable levels of glutamate-induced pain in both persistent pain and control animals. These findings suggest that by blocking neuronal uptake of glutamate, neuropathic and inflamed animals no longer show enhanced glutamate-induced nociception, but rather respond to glutamate to the same degree as controls. Thus, intraneuronal glutamate may be accounting only for the glutamate hypersensitivity in neuropathic and inflamed animals rather than overall glutamate-mediated nociceptive signaling.

Interestingly, L-TBA did not have a significant effect on glutamate-induced pain behaviors in control animals. One interpretation is that intraneuronal glutamate does not contribute significantly to nociceptive signalling in the absence of persistent pain. Instead, it is the effects of glutamate on the plasma membrane receptors which are the primary source of glutamate-induced nociception in normal animals. It should also be noted that while L-TBA did not alleviate pain in control animals, it also did not exacerbate pain behaviors. One possible reason the blockade of EAAT3 was not pronociceptive in control animals is that glutamate clearance was largely unaffected due to the functional EAAT1 and EAAT2. EAAT3 is known to contribute substantially less to glutamate clearance as compared to the glial EAATs. For instance, EAAT3 knock-out mice exhibit normal development [393], whereas knock-outs of EAAT1 and EAAT2 show signs of severe excitotoxic neuronal damage [256]. Thus, it is likely that minimal

accumulation of extracellular glutamate occurs following L-TBA administration, unlike after WAY-213613 and UCPH-101, which may explain the absence of a pro-nociceptive effect of L-TBA in control animals.

While the effects of L-TBA on glutamate-induced pain behaviors provides useful information on the relationship between exogenous glutamate and spinal glutamate transporters, the use of non-physiological levels of glutamate limit the interpretation of the data. A more physiologically relevant assay is the von Frey mechanical allodynia test. Mechanical thresholds were significantly, though only modestly, increased in neuropathic animals treated with L-TBA. As with the glutamate-induced pain behaviors, blocking EAAT3 did not abolish the pain in these animals. Again, these results speak to the fact that intracellular glutamate is not the sole contributor to nociception. Instead, it proposes a system which may be exploited to aid in minimizing allodynia. As control animals do not have reduced thresholds, we did not expect, nor did we see, any effect of L-TBA on mechanical allodynia. However, blocking EAAT1 and EAAT2 are sufficient to induce mechanical allodynia in controls. These results are consistent with glutamate-induced pain assays in control animals. As before, blockade of EAAT3 does not result in sufficient extracellular glutamate build-up to affect mechanical sensitivity, whereas EAAT1 and EAAT2 blockade interferes substantially with synaptic glutamate clearance, thereby reducing thresholds.

In addition to attenuating glutamate-induced pain and mechanical allodynia in animals with persistent pain, L-TBA produces conditioned place preferences in SNI and CFA rats. Thus, animals with persistent pain are motivated to seek a drug that blocks neuronal glutamate uptake. In addition, L-TBA fails to produce conditioned place preferences in rats without pain, suggesting its effects are not sufficiently rewarding in controls to promote a reliable approach behavior. From this we can conclude that L-TBA is analgesic in SNI and CFA rats, but not rewarding in naïve animals. A point to bear in mind,

however, is that the conditioned place preference between the two groups (naïve vs persistent pain) was not significant. Thus, in a conditioned place preference assay the effect of L-TBA in animals in pain and naïve animals are indistinguishable. A great limitation of the conditioned place preference paradigm was the overall small effect sizes observed. Even morphine, which has substantial analgesic efficacy and potency, only increases room preference from 50% to ~60%. In an effort to overcome the poor sensitivity of the assay, larger sample sizes were employed to bolster power.

Also noteworthy is the finding that in CFA and SNI rats, L-TBA produces conditioned place preferences comparable to that of morphine. Unlike glutamate-induced pain behaviors and mechanical allodynia, which rely on the use of an exogenous stimulus to produce a pain response, there is no external noxious stimulus in the conditioned place preference paradigm. Further, there is no drug at the time of testing, making behaviors performed during the test truly free of any pharmacological manipulation. Instead, the behaviors are performed in response to ongoing pain felt due to the SNI or CFA condition. We show that SNI and CFA rats seek out the room associated with L-TBA, and it suggests that L-TBA is involved in reducing the spontaneous, ongoing pain. In other words, L-TBA is negatively reinforcing. Conversely, as naïve animals do not seek out the room associated with L-TBA, it suggests that L-TBA does not provide significant positive reinforcement, unlike morphine.

Lastly, it was shown that L-TBA attenuates glutamate-induced Fos expression, but has no effect on Jun expression. These findings are consistent with previous reports *in vitro* demonstrating that Fos relies on nuclear mGluR5 membrane receptor activation, whereas activation of the Jun pathway depends on plasma membrane stimulation [313]. These results also demonstrate that the analgesic effects of L-TBA do not depend on plasma membrane-bound receptors, as Jun is unaffected by L-TBA pre-treatment.

Instead, it is through L-TBA's blocking of glutamate access to intracellular sites that is sufficient to prevent activation of Fos.

TBOA

The differential effect of the nonspecific EAAT inhibitors, TBOA, on naïve and persistent pain animals is well established in the literature [297, 301, 394]. Furthermore, it is shown here that blocking all EAATs with TBOA potentiates the nociceptive effects of glutamate in control rats, but either attenuates (SNI) or has no effect (CFA) on glutamate-induced nociception in rats with persistent pain. These findings are more interpretable in light of results from the specific EAAT inhibitor studies. Under control conditions, TBOA has a similar effect on glutamate-induced nociception as the glial EAAT inhibitors. In this case, it is expected the pronociceptive effect is mediated through prolonged activation of glutamate at cell surface receptors, since synaptic glutamate is not taken up by astrocytes. Importantly, this effect is not due to intracellular effects of glutamate, as neuronal EAAT inhibitors are likewise inhibited by TBOA. This is also consistent with the nonsignificant effect of L-TBA in control animals, suggesting that acute nociception typically relies largely on plasma membrane-bound receptors. However, in SNI rats, TBOA shows a similar antinociceptive effect as inhibiting EAAT3 alone; suggesting that neuronal intracellular receptors contribute to the nociception in these rats. Further, the antinociceptive effect of TBOA is observed despite prolonged glutamate exposure to plasma membrane receptors, suggesting intracellular glutamate plays a substantial role in pain expression under neuropathic conditions. It has been previously shown that administration of TBOA blocks IL-1 β -induced Fos expression only in CFA rats, but not naïve rats [303]. Here it was shown that Fos is similarly reduced using the selective EAAT3 inhibitor, but not EAAT1 and EAAT2 inhibitors; again, suggesting that the driving force behind the antinociceptive effect of TBOA is its blockade of EAAT3. Additionally, this

emphasizes the importance of intracellular glutamate in potentiating nociceptive signalling in persistent pain conditions.

In summary, the EAAT inhibitor experiments suggest that the pronociceptive effect of glutamate is in part dependent on its location. Under persistent pain conditions intracellular glutamate access is important for nociception, whereas under control conditions glutamate has a greater effect on cell surface receptors. Taken together, these data also explain the paradoxical antinociceptive effects of pan-EAAT inhibitors on persistent pain [270, 286, 297, 302].

Alternative hypotheses for the EAAT inhibitor paradox

The data shown here emphasizes that glutamate not only produces nociceptive responses by activating receptors at the cell surface, but also that in persistent pain states a second intracellular action is involved. However, prior to this proposed mechanism, alternative hypotheses (described below) had been put forward to account for the paradoxical finding that EAAT inhibitors produce analgesia in animals with persistent pain.

Inverse EAAT hypothesis

Prior to this thesis, the leading hypothesis to explain the paradoxical findings with EAAT inhibitors was the proposal that the actions of EAATs are reversed in pathological pain conditions. Thus, it was proposed that EAAT inhibitors reduce enhanced extracellular glutamate concentrations by preventing EAATs from pumping glutamate into the synapse, which occurs in pathological conditions [270]. Reversal of EAATs has been demonstrated in conditions where metabolic functioning is compromised, such as ischemia in cortical neurons [395]. Under these conditions, intracellular concentrations of ATP are insufficient to maintain ion gradients, causing a reversal of EAATs [395]. Indeed, under pathological pain

conditions there is an elevated energy demand in the spinal cord [396-398]. Thus, it could be argued that the enhanced metabolic strain associated with persistent pain causes EAAT reversal that increases glutamate release into the synapse [270]. However, no direct evidence has been reported for spinal EAAT reversal, and the results from EAAT2 studies are inconsistent with this hypothesis. First, the EAAT2 activator, MS-153, has no effect on inflammatory pain behaviors in CFA rats [297], and second, overexpression of EAAT2 on astrocytes in the spinal cord, either through adenovirus gene transfer [312], or treatment with the β -lactam antibiotic ceftriaxone [399], attenuates the induction of inflammatory and neuropathic pain. Under the reverse EAAT function hypothesis, enhanced EAAT2 activation or overexpression of EAAT2 would be expected to have pronociceptive effects. In this thesis, it was shown using selective agents that preferentially block glial EAATs produces the expected pronociceptive effects in both normal animals and those with persistent pain. Further, microdialysis results show that WAY213613 and UCPH-101 do not reduce extracellular glutamate in CFA or SNI animals, but rather enhance spinal glutamate, as would be expected if EAAT function is normal (i.e., not reversed). Other laboratories have also used *in vivo* microdialysis to show that spinal TBOA produces increased extracellular glutamate in CFA animals [286]. If EAATs were expelling glutamate into the synapse, their blockade would lower spinal glutamate, rather than increase it. These findings provide strong evidence against the hypothesis that reversal of EAATs is accounting for the antinociceptive effects of EAAT inhibitors in persistent pain conditions.

Glutamate-induced neurotoxicity hypothesis

Another proposal put forward to explain the EAAT inhibitor-induced analgesia in animals with persistent pain is that blockade of spinal EAAT uptake leads to chronic elevation of spinal extracellular glutamate, possibly leading to excitotoxicity, destroying dorsal horn neurons, and interfering with

nociceptive signaling pathways [270]. Indeed, application of glutamate is known to produce neurotoxicity and cell death [400]. However, TUNEL labeling and cresyl violet histochemical staining of the spinal cord in CFA rats following TBOA revealed no evidence of cell apoptosis, indicating that loss of nociceptive neurons is not likely responsible for the analgesic effects of TBOA [297]. Further, glutamate-induced neurotoxicity does not follow the same time course as TBOA-induced analgesia. Cell death following glutamate-induced neurotoxicity in cell cultures is most apparent several hours following glutamate exposure [400]. In contrast, TBOA produces acute analgesia (within minutes) in neuropathic and inflamed rats. In paw withdrawal studies here, it was observed that the effects of neuronal and glial EAAT inhibitors alike are highest within the first 60 minutes then diminish. If the analgesia induced through L-TBA or TBOA was mediated through neuronal apoptosis, these effects would be long term, not transient.

Presynaptic glutamate hypothesis

Rather than producing neurotoxic effects, excessive glutamate build-up at the synapse could lead to activation of inhibitory presynaptic glutamate receptors, resulting in a negative feedback loop. In hippocampal cultures the EAAT inhibitor L-trans-PDC decreases ESPCs, which is blocked by application of MCPG, a competitive antagonist of group II mGluRs [401]. The authors suggest the elevated glutamate concentrations stimulate presynaptic group II mGluRs, resulting in presynaptic inhibition of excitatory synaptic transmission [401]. And in fact, group II antagonists are effective in attenuating persistent pain in neuropathic rats [402]. While presynaptic mGluRs are involved in regulating release of glutamate, microdialysis results reported here show the relationship between elevated extracellular glutamate and pain behaviors is positive, not negative. Specifically, glial EAAT inhibitors both elevate extracellular glutamate and are pronociceptive, arguing against a simple negative feedback process.

Antagonizing intracellular mGluR5 is antinociceptive in persistent pain

The main conclusion drawn from the EAAT inhibitor experiments is that intracellular glutamate plays a role in nociceptive signaling under neuropathic and inflammatory pain conditions. To discriminate whether glutamate is exerting its effects intraneuronally, permeable and nonpermeable mGluR5 antagonists were used, and suggested a role for intracellular mGluR5 in mediating nociception in rats with persistent pain. The design for these experiments was inspired from *in vitro* studies investigating nuclear mGluR5. In cultured cells, the permeable mGluR5 agonist quisqualate induces nuclear calcium oscillations, which persist even in the presence of the non-transported group I mGluR antagonist, LY393053 [246]. Importantly, the same group also showed that LY393053 potently blocks quisqualate binding on isolated nuclei, but it was not transported into intact cells [246]. This last finding is critical as it makes a strong argument that LY393053 is ineffective due to transportability, not efficacy or potency. In contrast, MPEP, the fully permeable mGluR5 antagonist, blocks quisqualate-induced calcium oscillations in intact cells. Confirming that the differences between MPEP and LY393053 are indeed due to permeability rather than potency differences, it was also shown that both MPEP and LY393053 are equally capable of blocking calcium elevations induced by the non-permeable mGluR5 agonist, DHPG. The comparison between permeable and non-permeable agonists was not performed in this thesis as the non-permeable agonist, DHPG, results in presynaptic release of glutamate (which could then enter the neuron), and thus does not function as a true non-permeable agonist *in vivo* [403].

LY393053 and Fenobam: Permeability

LY393053, or 2-amino-2-(3-cis and trans-carboxycyclobutyl)-3-(9H-thioxanthen-9-yl) propionic acid, is a potent second generation phenylglycine-like antagonist, which is selective for both mGluR5 and mGluR1, but does not show activity on group II or III mGluRs, nor any iGluRs [404]. Importantly, LY393053

has a very low partition-coefficient (logP) value. LogP is a measure of lipophilicity; it describes the ratio of concentrations of a compound in each phase of an immiscible mixture containing a hydrophobic (octanol) and hydrophilic (water) phase, where greater values indicate greater lipophilicity [264]. Various calculations are used to determine logP values based on molecular structure, making it a useful proxy for estimating membrane permeability which generally increases with higher logP; however, the permeability-lipophilicity relationship is affected by several factors, including molecular size, pH of the system, and composition of the membrane lipids [265]. Research performed on artificial membranes provides the following useful guide on the relationship between molecular weight, logP and permeability: compounds with molecular weights less than 300 g/mol have a 50% chance of high permeability with a logP value of 1.7, molecules between 300-350 g/mol need a logP value of 2.2, and molecules between 350-400 g/mol require a log P value of 2.6 or greater to have a 50% chance of being permeable [266]. Thus, while LY393053 (MW = 383.4) has a very low logP value of 0.6, rendering it theoretically impermeable to plasma membranes, the permeability was also validated from *in vitro* studies showing that it is indeed not transported across cell membranes [246]. Unfortunately, there are no specific mGluR5 antagonists that are verifiably cell impermeable, making use of the less specific, group I mGluR antagonist LY393053 necessary.

While previous studies on nuclear mGluR5 have used MPEP [248, 249, 313] as the permeable mGluR5 antagonist, the more selective mGluR5 antagonist fenobam was used here. The concern over MPEP's selectivity arose from a study comparing the analgesic effects of MPEP and fenobam on formalin-induced pain behaviors in mGluR5 knockout mice. While both fenobam and MPEP were effective at attenuating formalin-induced pain behaviors in wild-type mice, MPEP continued to show modest analgesic effects in mGluR5 knock-out mice, whereas fenobam did not [160]. Fenobam (MW = 266.7) is a potent, mGluR5

specific antagonist with a calculated logP value of 1.86-2.0 (depending on calculation used) indicating a >50% chance of high lipophilicity [405]. Fenobam permeability was also assessed *in vitro*, and was found to block quisqualate-induced calcium response in spinal cord cells as effectively as MPEP [214]. Thus, using fenobam and LY393053, pharmacological differentiation of intracellular and cell surface mGluR5 function was achieved.

Behavioral differences between permeable and non-permeable antagonists

In neuropathic and inflamed rats, fenobam has greater antinociceptive effects than the LY393053, as measured by its ability to attenuate mechanical allodynia. In its dose response profile, fenobam had a significant effect in attenuating glutamate-induced pain behaviors in all animals. The dose response profile of LY393053 was more variable. There was no significant main effect of LY393053 in SNI, CFA, or IFA control animals on glutamate-induced pain, but it was significant in attenuating glutamate-induced pain in sham animals. From the dose-response profiles alone, the two drug conditions are comparable; however, fenobam reached significance while LY393053 did not. While the effects of these two agents on spinal glutamate-induced nociception may not reflect dramatic differences, together with their disparate effects on allodynia and CPP (see below), the hypothesis for a role of intracellular mGluR5 in persistent pain states is supported. Furthermore, as the two drugs diverged in their effects against glutamate-induced nociception at higher doses, we performed a head to head comparison of 100 nmol of each drug and found that there was a significant advantage of using fenobam over LY393053 in animals with persistent pain. In contrast, no significant difference between the two antagonists was observed in either control group. These findings suggest that at the highest dose, accessing the intracellular pool of receptors using fenobam produces significantly greater analgesia in animals with persistent pain than LY393053. Because LY393053 is not selective for mGluR5, but antagonizes both

mGluR1 and mGluR5, the permeable mGluR1 antagonist, CPPCOEt was used in conjunction with fenobam to account for mGluR1 activation (i.e., comparing fenobam to LY393053 on a level playing field). As expected, the blockade of mGluR1 did not mitigate the efficacy of fenobam, indicating that the ineffectiveness of LY393053 is not due to an inhibition of mGluR1.

While we expect the differences between LY393053 and fenobam in neuropathic and inflamed animals are likely due to differences in drug permeability, an alternative explanation is differences in drug potency. Indeed, some studies report that fenobam, which has an IC_{50} value of 0.33 μM [406], is more potent than LY393053, which is reported to have an IC_{50} of 1.6 μM at mGluR5 and 1.0 μM at mGluR1 [407], thus a greater dose of LY393053 would be required to achieved the same effect as fenobam. However, the reported IC_{50} values for LY393053 were obtained using quisqualate in the phosphoinositol hydrolysis assays, which we now know activates two pools of receptors, one of which is inaccessible to LY393053. Thus, the lower potency of LY393053 may be due to unchallenged intracellular mGluR5 activation by quisqualate in these studies. In fact, one report that used DHPG, a non-transported mGluR5 agonist, to assess LY393053 activity found that the *in vivo* ED_{50} for LY393053 was 654-955 fmol [404], which would suggest a much lower IC_{50} . It could be argued further that even this value is an overestimation, as DHPG *in vivo* is known to stimulate the release of presynaptic glutamate [403], and therefore may still stimulate intracellular mGluR5.

In addition to relieving glutamate-induced pain, fenobam was effective at attenuating mechanical allodynia in neuropathic animals, while LY393053 was not. Like L-TBA, fenobam shows only a modest increase in paw withdrawal threshold and not a full recovery. While here all animals only received a single i.t. dose of fenobam, others have reported that daily oral dosing of fenobam is effective and does not produce analgesic tolerance in a wide variety of mouse pain models [173]. Surprisingly, LY393053

had no effect on mechanical allodynia in neuropathic animals. Based on these findings, it is suggested that plasma membrane group I mGluRs do not contribute significantly to mechanical allodynia. Interestingly, pretreatment of LY393053 prior to knee joint inflammation with CFA reduced development of thermal hyperalgesia; however, it was ineffective at attenuating established thermal hyperalgesia in the same model [408]. This suggests that plasma membrane group I mGluR stimulation is important to the development of pain, while intracellular mGluR5 becomes critical during the maintenance phase.

Lastly, fenobam produced a conditioned place preference in SNI and CFA animals, but not in naïve rats. To more directly address the potency concerns, in the conditioned place preference paradigm a 1 μ mol i.t. dose of LY393053 failed to produce a conditioned place preference, whereas a 200 nmol dose of fenobam was successful. It is important to note that these results test each drug for the presence of a conditioned place preference effect and do not compare the CPP-I between each drug, nor does it compare between pain conditions. The presence of a conditioned place preference is measured only as spending significantly more than 50% of the time in a drug paired room, but does not compare whether one drug out-performed another, or whether the effect is greater in animals with persistent pain or not. Thus, while fenobam and LY393053 did not differ significantly from each other for conditioned preference on the test day, fenobam's effect reached the threshold of significance difference from 50% while LY393053 did not. This is an important factor to consider when interpreting these results, as LY393053 was indistinguishable from baseline, but also from fenobam. This speaks to the tests sensitivity, and it is likely that the overall effect of each drug given the low number of pairings (1 or 2) is insufficient to distinguish them from one another. However, the results still show a within group effect of fenobam, which was the critical comparison. Another group has previously shown that fenobam produces an analgesic conditioned place preference when administered i.p. in SNI mice [176]. This group

also demonstrated that analgesic conditioned place preference occurs equally well in both male and female mice, but not in shams. Importantly, while studies here and [176] both report strong conditioned place preference to morphine in sham or naïve animals, there is no significant conditioned place preference to fenobam in shams or naïve animals. This being said, there was no between-group differences for persistent pain and naïve conditions. Thus, while naïve animals did not significantly prefer the fenobam or L-TBA paired room, the amount of time spent in these rooms were not different from the SNI or CFA animals. Again, this speaks to the sensitivity of the test and it is difficult to draw definitive conclusions regarding the abuse potential of these drugs given the data.

Fos and Jun expression following permeable and nonpermeable antagonists

In addition to the different behavioral outcomes of fenobam and LY393053, the two antagonists show different effects on glutamate-induced immediate early gene induction. While pretreatment with fenobam attenuates glutamate-induced *c-fos* and *c-jun* expression, LY393053 only attenuates *c-jun*. An important result from these studies is the comparable effect of both antagonists on the Jun expression. This finding is consistent with the *in vitro* data, which shows phosphorylated JNK, the kinase responsible for the transcription of Jun, is increased following treatment with the non-permeable agonist DHPG; in contrast, Fos was only upregulated following application of the transportable agonist quisqualate [313]. Further, while permeable MPEP blocks quisqualate-induced Fos expression, non-permeable LY393053 does not [313]. The comparable effect of LY393053 and fenobam on glutamate-induced Jun is also additional support that differences between the two antagonists are not simply due to diverse potencies and efficacies, if this were the case, fenobam would have a greater effect on both Fos and Jun.

Fenobam-dependent Fos reduction was observed in persistent pain and control conditions alike, suggesting that glutamate-induced Fos expression is at least in part dependent on intracellular mGluR5

stimulation under normal conditions, as well as after inflammatory and neuropathic pain. This finding is important as it suggests that the downstream signaling pathways themselves are not necessarily altered under persistent pain conditions. Instead, it suggests that there are two pools of receptors in the spinal cord, each associated with distinct downstream signaling pathways. Following injury, the pool of receptors involved in the Fos-inducing pathway – i.e. the intracellular mGluR5 pool – increases from basal levels, and amplifies nociceptive signaling. Indeed, cultured cells from sham spinal cords still express nuclear mGluR5 and bind glutamate; however, the contribution towards nociceptive signaling from this intracellular pool is minimal. As a result, there is no significant advantage gained from using permeable mGluR5 antagonists over non-permeable antagonists in acute pain, as was observed in the glutamate-induced pain behaviors in sham and IFA animals.

The results from the antagonist studies have important implications for the use of mGluR5 antagonists in therapeutics. Importantly, results here show that efficacy in attenuating acute nociceptive responses may not translate to chronic pain if the antagonists are non-permeable. Further, these results call for an investigation of the permeability of mGluR antagonists presently used, as well as considering cell permeability during chemical engineering of receptor ligands for mGluR5.

Location-dependent signaling of mGluR5

Because group I mGluRs play important roles in synaptic plasticity, as well as various disorders, their signal transduction pathways have been heavily studied. Through pharmacological manipulations, it is shown here that intracellular mGluR5 contributes more towards Fos expression, whereas plasma membrane mGluR5 is more heavily implicated in Jun expression. These findings provide *in vivo* support for previous *in vitro* studies. It has also been shown that intracellular mGluR5 activation results in phosphorylation of CaMKII and extracellular regulating kinase (pERK) [313]. Importantly, pERK has low

de novo expression in sham animals, but is strongly upregulated in the nucleus of SCDH neurons of SNI animals [214]. A downstream effector of pERK, activity-regulated cytoskeletal-associated protein (Arc/Arg3.1), is also upregulated in SCDH nuclei of SNI rats [214]. Treatment with fenobam reduces pERK1/2 and Arc/Arg3.1 in SNI rats [214], suggesting that these nuclear mGluR5 are persistently active in neuropathic conditions. Another downstream target of pERK, pElk-1, is also increased following quisqualate stimulation, but not DHPG [313]. In addition, chromatin immunoprecipitation studies reveal that pElk-1 binds to *egr1* and *c-fos* promoter following quisqualate stimulation, but not DHPG [313]. Thus, nuclear mGluR5 stimulation is proposed to initiate a pCaMKII/pERK/pElk-1/*egr1*/*c-fos* pathway that is not observed when only cell surface receptors are activated. In contrast, DHPG and quisqualate both initiate the phosphorylation of CaMKIV, CREB and JNK, which is blocked by the non-permeable antagonist LY393053 [313]. While it is apparent that the signaling pathways of mGluR5 are location-dependent, it is still unclear why this would be the case. In cell cultures, it has been shown that the calcium response triggered by mGluR5 is sustained following intracellular receptor stimulation, whereas it is transient following plasma membrane stimulation [263]. Thus, longer lasting calcium elevations may be a prerequisite for initializing this pCaMKII/*c-fos* pathway.

It is also important to emphasize that the pharmacological manipulations used in this thesis do not identify where specifically the intracellular mGluR5 is exerting its effects (i.e., nucleus, ER, etc.). From the subcellular fractionation and previous electron microscopy data, the only location with observed increases in mGluR5 is the nuclear membrane; however, it has also been shown that mGluR5 is present on ER membranes in brain and SCDH neurons [214, 245, 263]. Using 4-Methoxy-7-nitroindolinyI-cage-L-glutamate (MNI-glutamate), a caged compound allowing for glutamate to become functional in localized regions within the cell, recent evidence shows that intracellular glutamate initiates a local calcium

response in dendritic ER membranes [263]. Thus, while the immunological data presented here identify the nucleus as the most likely location for mGluR5-dependent nociceptive signaling, the design of these studies prevent the ruling out of other intracellular membranes, such as the ER, in contributing to pain.

Intracellular glutamate

The presence of mGluR5 on the nucleus and its ability to bind glutamate and produce nuclear calcium oscillations raises the question regarding the contribution of intracellular glutamate action at these receptors. As discussed earlier, extracellular concentrations in the spinal cord are maintained at low levels (5-22 μM) in the absence of exogenous stimulation [377-380]. However, intracellular concentrations of glutamate are estimated to be considerably greater. In cells transfected with EAAT3, a transmembrane concentration gradient exceeding 10^6 -fold greater intracellular glutamate can be maintained under equilibrium conditions [255], and calibrated antibody labelling suggests a concentration of ~ 10 mM can be maintained within neurons [409]. However, most glutamate is not free within the cytoplasm, but rather sequestered into vesicles and within mitochondria [263]. Specific intracellular glutamate transporters exist, carrying little resemblance to the EAATs, which uptake cytoplasmic glutamate into vesicles. Unlike the EAATs, vesicular EAATs (VGLUTs) function independently of sodium and potassium; instead uptake is driven by an ATP-generated H^+ membrane potential [410]. VGLUTs also show low affinity, but high selectivity, for L-glutamate, and can reach vesicular glutamate concentrations of 100 mM [411]. Thus, intracellular glutamate concentrations are sufficiently regulated such that it is expected intracellular mGluR5 is not constantly stimulated. Importantly, much greater concentrations of glutamate are required to stimulate intracellular, as opposed to cell surface, mGluR5; in cell cultures, the half-maximal glutamate concentration required to stimulate cell surface mGluR calcium responses is ~ 2 μM , whereas intracellular mGluR calcium responses require ~ 61 μM [263].

Because mGluR5 is not intrinsically active without external glutamate in these cell cultures, this suggests that free glutamate within the cell cytoplasm falls below this concentration. What is unknown is how quickly following uptake through EAAT3 is glutamate scavenged into intracellular vesicles or the mitochondria, and whether the kinetics of intracellular glutamate scavenging is affected in persistent pain conditions. Answers to these questions would be useful in understanding whether the increased extracellular glutamate in the spinal cord of neuropathic and inflamed animals is transported in quantities sufficient to activate intracellular mGluR5, as the findings presented here suggest. Although, that fact that the stimulation of nuclear mGluR5-linked intracellular messengers is increased in SCDH extracted from neuropathic rats [214] suggest this may be the case.

Origin of nuclear mGluR5

The time course analysis suggests that mGluR5 is quickly increased at the nucleus following injury and persists for the duration studied. Whether these receptors are being moved from the plasma membrane, cytoplasm or are created anew is still unknown. However, as many have reported an increase in mGluR5 mRNA as early as one day following injury, it is possible that more receptors are being created and translocated to the nuclear membrane, rather than being trafficked from plasma membrane locations. Another important question is how long after these receptors appear on the nucleus do they become functionally active in signalling. Whether all the components required for G protein signaling show a comparable time course for induction following injury has yet to be tested. Here we show that nuclear mGluR5 increases within one day following either SNI or CFA manipulation; however, behavioral measures began at much later time points. In both the inflammatory and neuropathic pain models, the onset of pain hypersensitivity has been shown to commence as early as one day following

surgery/injection. As of yet, we cannot infer whether this early phase (within 24 hours of injury) of pain hypersensitivity is associated with the increased presence of mGluR5 on the nucleus.

Alternatively, as electron microscopy results would suggest, some receptors may be trafficked from the plasma membrane and relocated to the nucleus following injury [214]. There are several mechanisms by which mGluR5 trafficking may occur. In heterologous cells and primary neural cultures, group I mGluRs undergo agonist-dependent and -independent endocytosis through second messenger-dependent protein kinases and β -arrestin-mediated pathways (reviewed in [211, 412]). Following injury, spinal glutamate concentrations are increased, which may lead to agonist-dependent endocytosis of mGluR5. While this pathway would lead to mGluR5 internalization, this is typically viewed as a transient stage wherein the receptors are degraded or recycled. The presumption has also been that recycling targets the receptors back to the plasma membrane, which we now know is not its only active location. Thus, not only does the internalization mechanism need to be identified, but also the potential process involved in both targeting and anchoring mGluR5 to the nuclear envelope.

Homer1 proteins as mGluR scaffolds

A possible contributor to mGluR5 mobilization and function are the Homer1 proteins. Homer1 is a neuronal scaffolding protein consisting of two major splice variants. The long forms, Homer 1b and c are constitutively active and are involved in tethering mGluR5 to other receptors such as NMDA, to other scaffolding proteins, and to downstream signalling effectors [413-415]. The short form, Homer1a is produced following neuronal stimulation and so is considered an immediate early gene [82, 416]. All splice variants contain an EVH1 domain, a conserved protein domain that is implicated in both signalling and nuclear transport events. The EVH1 domain interacts with proteins expressing the PPXXF motif [413, 414]. This sequence exists in group I mGluRs, IP3 receptors, Shank and ryanodine receptors. In contrast,

only the long form variants contain a coiled-coil domain which forms dimers, allowing Homer1b and c to form networks connecting proteins with the PPXXF motif [413, 414].

Homer1a acts as a natural dominant negative isoform that blocks interactions between long-forms and their ligands by competing for the EVH1 binding site on the ligand proteins. Thus, Homer1a uncouples mGluRs from their signalling targets and may function as a mechanism for homeostatic plasticity to dampen neuronal glutamate responsiveness [414]. In contrast, the long form Homer1c enables stabilization of synaptic changes during long term potentiation. Of particular interest is the finding that Homer 1b inhibits surface expression of mGluR5 in heterologous and Purkinje cells, causing its retention on ER membranes and perinuclear organelles, whereas expressing mGluR5 alone allowed the receptor to successfully travel to the plasma membrane [417]. In transfected cerebellar granule cells with mGluR5 and Homer 1b/c, depolarization resulted in transient expression of Homer 1a and the targeting of mGluR5 to neurites, which persisted long after Homer1a levels disappeared [418]. These results would suggest that Homer 1b/c may tether mGluR5 following Homer1a-induced mGluR5 trafficking. While Homer1b/c is strongly expressed throughout the spinal cord, naïve rats only express very low levels of Homer1a [419]. Following i.pl. injection of CFA, however, Homer1a is rapidly induced in the spinal cord neurons [419]. Further, the same group found that preventing the upregulation of Homer1a exacerbated inflammatory pain. Homer1a mRNA levels were increased from 4 to 8 hours following painful chronic compression of the dorsal root ganglion, and were returned to baseline after 24 hours, at which time thermal hyperalgesia appears [420]. In a different study, Homer 1b/c antisense reduced spinal CREB phosphorylation and Fos expression, when administered following the onset of inflammation [421].

Interpreting the body of Homer data in light of our findings is challenging as the Homer experiments and conclusions drawn were done so without the knowledge of functional intracellular receptors. Homer 1a appears to be important in dissociating mGluR5 from its scaffolds, Homer 1b and c, which may free up the receptor to be internalized through ligand-dependent or independent mechanisms. Preventing Homer 1a from inactivating the receptors exacerbates the initial injury as the receptors continue to signal from the cell surface. However, when Homer1a expression then drops at 24 hours, Homer1b/c can re-establish connectivity either to the cell surface or potentially also to nuclear membranes, rendering the receptor functional once more. Thus, Homer 1a is only beneficial for as long as it is being expressed and preventing group I mGluR signalling. However, because the receptors are freed from their scaffolds by Homer 1a, it also allows them to traffic. This process in itself is not detrimental provided the receptors remain non-functional. However, the return of Homer 1b/c would stabilize the relocated receptors and potentially allow signalling from the nucleus. It is important to note, however, that the role of Homer b/c is likely critical for both nuclear and plasma membrane signaling, as their disruption reduces spinal CREB phosphorylation, which has been associated with plasma membrane mGluR5, as well as Fos expression, associated with nuclear mGluR5 [313].

Nuclear mGluR5: Involvement in other pathologies?

The aim of this thesis has been to detail the accumulated evidence regarding the role of intracellular mGluR5 in spinal cord central sensitization following nerve injury and inflammation. While this account leaves many questions unanswered about the mechanisms involved in the trafficking, nuclear localization and differential signaling from these receptors, it provides support for a novel signaling location of mGluR5 that has behavioral consequences. Importantly, these results suggest a re-examination of other pathologies that implicate mGluR5 dysregulation may be warranted. Functional

nuclear mGluR5 was originally described in brain tissue, both midbrain and cortical neurons [245], and later in hippocampal CA1 neurons [247], indicating a possible contribution to neurological disorders. Some disorders which implicate mGluR5 include fragile X syndrome [422], amyotrophic lateral sclerosis (ALS) [423], schizophrenia [424], and epilepsy [425].

Disorders which would be promising to study are those that already have been shown to involve downstream signalling components that are now known to be associated with nuclear mGluR5. Fragile X syndrome (FXS), which is the most common inherited cause of mental retardation and autism, is caused by a mutation in the fragile X mental retardation protein gene (*FMR1*) [426]. Importantly, in *FMR1* KO mice, enhanced and altered mGluR5 signaling is observed in the hippocampus and cerebellum; specifically, these mice have increased Arc/Arg3.1 and phosphorylated ERK [427], which are downstream of nuclear mGluR5 activation [249]. In addition, the symptoms and aberrant mGluR5 signaling accompanying *FMR1* deletion are ameliorated by reducing mGluR5 expression [428], use of permeable mGluR5 antagonist MPEP, or simply by deletion of Homer1a [429]. While clinical trials with the permeable mGluR5 antagonist, AFQ056, developed by Novartis ended following negative results [430], exploratory analyses of a smaller clinical trial revealed positive results in patients with a fully methylated *FMR1* promoter [431]. These findings inform research that animal models of FXS may only capture a subset of the clinical population; however, this subset may involve nuclear mGluR5 signaling and benefit from permeable mGluR5 antagonists.

Experiment Limitations

While interpreting the results of experiments presented in this thesis it is important to also consider their limitations. First, quantification of mGluR5 in this thesis relies on western blot data. Western blots

are useful for quantifying relative amounts of protein between samples and can indicate monomeric, dimeric and modified forms of the protein of interest. One of the limitations of westerns is the absence of spatial resolution. As tissue from the entire dorsal portion of the spinal cord was obtained, specific lamina distribution of mGluR5 is unknown. It is important, therefore to consider these results in tandem with the original quantification of mGluR5 in neuropathic animals which was based on images from electron microscopy [214]. It is also important to note that the subcellular distribution of mGluR5 based on western blots will be influenced by the success of subcellular fractionation. Fractionation was considered successful if the markers for nucleus, cytoplasm, plasma membrane were predominantly found within the correct fraction. However, no fraction was completely devoid of any contamination from other fractions. Thus, these data should be considered approximations for protein content within the plasma membrane, cytoplasm, and nuclear membrane. This is particularly important for the cytoplasmic fraction as it should only contain cytoplasmic-soluble proteins. The ubiquitous presence of mGluR5 within the cytoplasmic fraction across all samples suggests that proteins bound on intracellular membranes are also retained in this fraction. From which membranes these proteins are sourced is unknown by this data alone. In the same vein, selecting the correct loading controls is critical for western interpretation. The loading controls selected in this thesis were chosen for their fraction-specificity. In this manner, mGluR5 content is normalized to a protein representative of the fraction rather than of total protein. Thus, mGluR5 increases relative to HDAC-1 levels were interpreted as increases in nuclear mGluR5. As no significant changes in the loading controls were observed between conditions we can conclude that changes in mGluR5 are not an artifact of systematic differences in the loading control. However, if one fraction is contaminated with another fraction then the loading control may not reflect protein content. I do not anticipate fraction contamination to be a major source of variability as all

samples were fractionated at the same time, under the same conditions. Other points of interest are apparent mobility shifts in the mGluR5 protein band particularly within nuclear fractions. The bands in nuclear fractions often show a wider spread, and may point to post-translational modifications. One possibility may be related to an N-linked glycosylation site which has been described in mGluR5a [432]. If this mobility shift represents a true glycosylated state of mGluR5, it raises interesting questions regarding the function of the glycosylated product which cannot be answered by these data.

A significant limitation common to animal studies is small sample sizes, and this limitation presents itself throughout the studies performed here. There are two main problems with small sample sizes. First, the sample tested may not accurately represent its population, and erroneous differences may lead to the incorrect rejection of the null hypothesis. Reports of false positives, or type I error, in published data has received more attention in several fields in the recent years and it raises concern regarding the reproducibility of experiments [433-435]. One way in which the experiments reported here try to overcome this limitation is by using several methods to answer the same question. Multiple pain assays comparing the same compounds were performed for the dual purpose of capturing a better representation of pain and increasing confidence in results with the convergent findings. The other issue with small sample sizes which receives less attention is the inflation of type II error. Even with a properly powered study (power ~ 0.8), there is a 20% chance of a false negative. Type II error becomes a greater concern when the experimenter expects a condition to have no effect, as we allow for a much higher rate of false negatives. Thus, we must also be cautious with how nonsignificant findings are interpreted. Again, the studies presented in this thesis are limited by the sample size which makes smaller effects more difficult to detect. Thus, it is important to avoid conclusions about non-significant results, particularly when sample sizes are limited, until replication studies have been performed.

These studies are also limited in that they rely on pharmacological manipulations of receptor and transporter activity. How well each pharmacological manipulation works depends on the properties of the compound as well as the environment in which it has been administered. While the specificity of fenobam has been well reported, other compounds, in particular L-TBA, is not as selective. One way that future studies can serve to build upon these results would be to make use of transgenic mouse models rather than pharmacological manipulations. While a simple knockout model could result in compensatory mechanisms, a neural tube promoter to drive expression in the spinal cord in conjunction with a tamoxifen inducible knockout of EAAT3 would give temporal and spatial resolution on the role of neuronal glutamate transport in pain conditions. Alternatively, knockdown of EAAT3 following or immediately prior to injury would also provide similar insights. The limitation of either of these methodologies is that they do not prevent the functioning of transporters already in place on the membranes or their relocation. Ultimately, the reliance on pharmacological methodologies is a limiting factor in these studies, and development of more selective compounds will provide future studies more tools to provide more definite answers.

Future directions

While these studies implicate nuclear mGluR5 in inflammatory and neuropathic pain, ultimately, they represent only the first steps to understanding these receptors. These findings inform us that intracellular mGluR5 is worthwhile investigating, and point to several paths that should be pursued. First and foremost, the mechanism through which mGluR5 is upregulated on the nuclear membrane following nerve injury or inflammation is still unknown. Whether the receptors are being created *de novo* following injury or are trafficked from various sources cannot be ascertained from these experiments. Future studies would benefit greatly from determining the process by which these receptors come to be on the

nucleus. Some evidence points towards internalization of cell surface receptors following injury. First, the massive efflux of glutamate into the spinal cord following spinal cord injury [377, 380] or inflammation [382] may drive agonist-dependent endocytosis. In HEK cells, treatment with glutamate is sufficient to cause the redistribution of group I mGluRs to internal membranes by a β -arrestin1-dependent mechanism [209]. Particularly interesting to the researchers of that study, as the possibility of functional intracellular mGluRs was unknown, was that quisqualate-induced IP formation was not hindered by β -arrestin-mediated internalization of mGluRs. It is expected that receptor internalization does not eliminate functioning provided the receptor is trafficked to functional intracellular sites. One way to investigate whether a similar phenomenon is occurring following injury is to collect spinal cords within hours following injury, when endogenous extracellular glutamate levels are at their greatest, and coimmunoprecipitate mGluR5 with β -arrestin1. The binding of β -arrestin1 to mGluR5 following injury would provide a potential mechanism for injury-induced plasticity of mGluR5. Next, as Homer1a is predicted to be a prerequisite for mGluR5 internalization, preventing the induction of Homer1a following injury could prevent β -arrestin-mediated transport, testable again by co-immunoprecipitation. At the same time, preventing Homer1a induction following injury may prevent the accumulation of nuclear mGluR5, testable by subcellular fractionation and western blot.

Very recent findings in cell cultures suggest that nuclear mGluR5s represent a distinct pool of receptors that are recycled off and on the nuclear membrane, and do not interact with the pool of receptors that cycle on and off the plasma membrane [436]. While plasma membrane receptors, constituting ~15% of total receptors, undergo constitutive cycles of endocytosis and recycling, the remaining receptors on the transgolgi network are trafficked back to the ER and undergo lateral diffusion through nuclear pore complexes to reach the inner nuclear membrane [436]. In addition, amino acids

852-876 on the C terminus were shown to be necessary and sufficient for inner nuclear membrane localization of these receptors. In light of these latest findings, it is unlikely that plasma membrane receptors are being relocated to the nucleus, however, they may be relocated to intracellular stores.

It is also possible that mGluR5 nuclear upregulation is the result of newly created receptors. As the increase in mGluR5 in nuclear-enriched fractions did not specifically correlate with a significant decrease in mGluR5 within the plasma membrane or cytoplasmic fraction, the generation of new receptors is a distinct possibility. Supporting this view, increases in mGluR5 mRNA has been observed within hours following inflammation and post-surgical pain [202, 203]. If the newly formed receptors are being retained within the cell, the mechanism responsible for their retention needs to be elucidated. A possible contender is the scaffolding protein Homer1b/c, which has been shown to prevent mGluR5 from being exported to the plasma membrane following its induction [417]. Importantly, although Homer1b/c expression is reduced early (4 hours) following CCI [421], its expression is increased at 7 days post-CCI when hyperalgesia is presented and reduced again at 28 days when hyperalgesia recedes [437]. Future studies will use cell-penetrating peptides with nuclear localization sequences that interfere with mGluR5 and Homer1 interactions at the nucleus. If Homer 1 is responsible for anchoring nuclear mGluR5, interrupting this interaction will attenuate persistent pain. Another approach would be to use an inducible reporter line for mGluR5. A *mGluR5^{eGFP-CRE-ERT2}* mouse line could elucidate the location of newly formed mGluR5 if tamoxifen-induced recombination were performed immediately following injury. Colocalization of GFP-positive mGluR5 with a nuclear marker would indicate that mGluR5 is being actively produced and retained on the nucleus following injury.

In addition, stronger support for nuclear mGluR5 involvement in nociception would be gained through use of agonists that target the nuclear envelope receptor selectively. These studies are performed *in*

vitro using caged ligands which are only activated after they have been transported into the cell [247]. More recently, a light-sensitive caged mGluR5 antagonist, JF-NP-26, has been developed [438]. While inactive in the absence of LED-based illumination, JF-NP-26 converts to an efficacious analgesic in CCI rats following exposure to violet light [438]. Developing this technology such that drug activity can be modulated based on local environment rather than light exposure would allow us to directly assess the analgesic potential of exclusively targeting intracellular mGluR5. In addition to benefiting the scientific community, caged antagonists may prove to be clinically useful. One difficulty with pharmacological therapies for pain management is unwanted side effects. Often, the receptor involved in the detrimental effects of disease also serves important functions in non-pathological states, thus targeting the aberrant dysfunction without influencing the normative function becomes the challenge. Caged antagonists represent a unique opportunity to block the aberrant intracellular mGluR5 functioning without altering the function of plasma membrane receptors.

Lastly, future research should also focus on how extracellular glutamate gains access to the nuclear lumen to activate nuclear mGluR5. A lot of evidence has been put forward demonstrating that EAAT3 transports glutamate from the synapse into the neuron, and here it was shown that blocking this transport was an effective means of reducing pain in animals with inflammatory and neuropathic pain. However, glutamate must not only make it into the cell, but into the nuclear lumen. Studies that use isolated nuclei show that both sodium dependent and sodium-independent processes could be involved in transporting glutamate across the nuclear membrane. The limitation of these studies is their use of isolated nuclei. The direction of glutamate transport is dependent on the environment on either side of the membrane, thus how nuclear transporters work within the cell remains to be assessed. In a similar design to the caged antagonist studies, using an EAAT3 inhibitor or X_{CT} inhibitor activated following

transport into the cell would be useful to determine whether either of these transporters are responsible for the nuclear transport of glutamate in intact cells by inhibiting the second step (cytoplasm to nucleus) without inhibiting the first (extracellular to cytoplasmic) of transport.

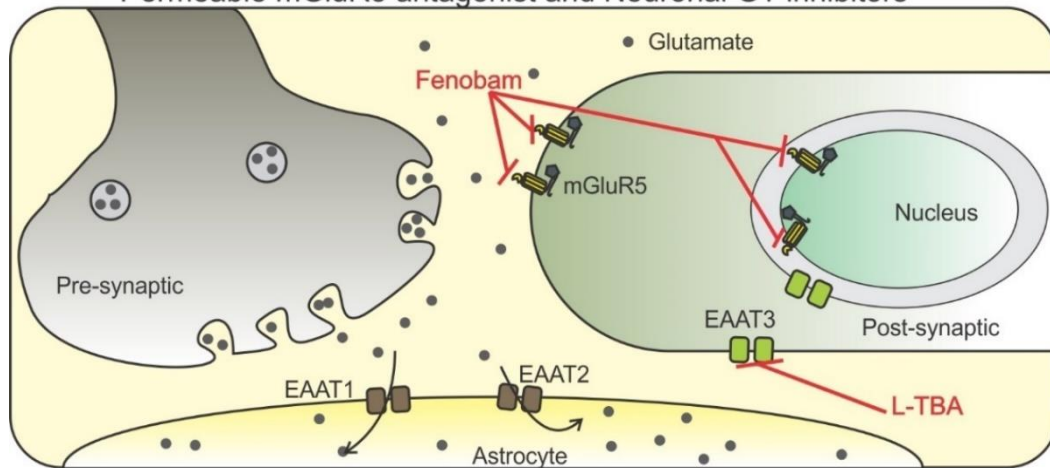
Conclusions

Spinal glutamate receptors play a fundamental role in mediating the central sensitization that accompanies pain conditions. To date, research on these receptors has almost exclusively been performed assuming that the active location of glutamate receptors is on the cytoplasmic membrane. The findings presented here underscore the idea that mGluR5 is upregulated on the nucleus following inflammation and neuropathic injury, and that these intracellular receptors are functional and contribute to nociceptive signal transduction via distinct pathways from cell surface receptors.

Using an array of different pain assays and immunohistological assessments, the proposed model for nuclear mGluR5 involvement is illustrated in Figure 29. In summary, I propose that in inflammatory and neuropathic pain conditions there is an upregulation of mGluR5 on the nuclear membrane in the SCDH. These receptors are functional, but in the absence of persistent pain may not be a significant source of nociceptive signalling. However, following nerve injury or inflammatory insult, either the migration to or generation of new receptors at the nucleus allows these GPCRs to become involved in the hyperexcitability of spinal nociceptive neurons. As illustrated in the top panel, the contribution of nuclear mGluR5 to pain can be attenuated using either permeable mGluR5 antagonists (fenobam) or EAAT3 inhibitors (L-TBA). Both these drugs prevent glutamate from binding to the intracellular mGluR5, thereby silencing their downstream signaling cascades, which include nuclear calcium signalling, ERK1/2 and expression of Fos. These compounds also do not interfere with the clearance of glutamate by EAAT1 or

Nuclear mGluR5 model of Persistent Pain

Permeable mGluR5 antagonist and Neuronal GT inhibitors



Non-Permeable mGluR5 antagonist and Glial GT inhibitors

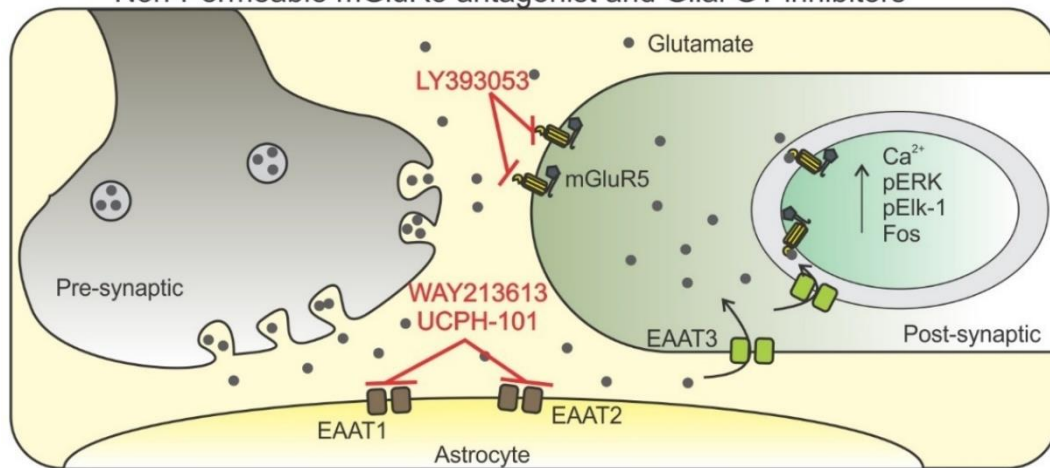


Figure 29. Schematic summary illustrating the effect of targeted mGluR5 treatments on neuropathic and inflammatory pain.

Glutamate is released from the pre-synaptic neuron and binds at cell surface and intracellular mGluR5 receptors in the SCDH. mGluR5 on the nuclear membrane is upregulated in CFA and SNI animals, and is associated with increased intracellular signalling leading to Fos expression. (**Top panel**) Blocking glutamate from binding to intracellular mGluR5 receptors either by using the permeable mGluR5 antagonist fenobam, or preventing its intracellular access with the EAAT3 inhibitor L-TBA, prevents glutamate-induced Fos expression and attenuates pain in neuropathic and inflammatory conditions. (**Bottom panel**) Selectively blocking cell surface mGluR5 receptors using the non-permeable antagonist LY393053, or preventing glutamate reuptake through EAAT1 and EAAT2 with WAY + UCPH, allows excess glutamate to be transported into the neuron via EAAT3 and bind to the functional nuclear mGluR5, which enhances expression of Fos and exacerbates pain.

EAAT2 into surrounding glial cells. In contrast, non-permeable antagonists such as LY393053, and EAAT1

and EAAT2 inhibitors like WAY213613 and UCPH-101, both allow glutamate to be transported into the cell, bind to intracellular mGluR5 and initiate signalling cascades that contribute to pain, which becomes more significant in persistent pain conditions when nuclear mGluR5 is upregulated.

Given the important role of mGluR5 in nociceptive transmission in chronic pain states, understanding the functional consequences of intracellular receptor activation has implications for therapeutic strategies in pain disorders. A difficulty with today's pharmacological therapeutic strategies is that the selected targets often play important functions in non-pathological states as well as in chronic pain, resulting in undesirable side effects. Importantly, as intracellular mGluR5 may become physiologically relevant to nociceptive transmission largely under persistent pain conditions, developing drugs that can selectively target this locus may have fewer adverse effects. While the findings in this thesis ultimately represent only the beginning of our foray into intracellular mGluR5-mediated central sensitization, it provides a basis for which future research can build on to better understand its role in nociceptive synaptic plasticity.

References

1. Staud, R., *Peripheral pain mechanisms in chronic widespread pain*. Best Pract Res Clin Rheumatol, 2011. **25**(2): p. 155-64.
2. Phillips, K. and D.J. Clauw, *Central pain mechanisms in chronic pain states--maybe it is all in their head*. Best Pract Res Clin Rheumatol, 2011. **25**(2): p. 141-54.
3. Koltzenburg, M., H.E. Torebjork, and L.K. Wahren, *Nociceptor modulated central sensitization causes mechanical hyperalgesia in acute chemogenic and chronic neuropathic pain*. Brain, 1994. **117 (Pt 3)**: p. 579-91.
4. Marchettini, P., et al., *Sensitized nociceptors in reflex sympathetic dystrophies*. Funct Neurol, 1989. **4**(2): p. 135-40.
5. Serra, J., et al., *C-nociceptors sensitized to cold in a patient with small-fiber neuropathy and cold allodynia*. Pain, 2009. **147**(1-3): p. 46-53.
- 6.Coderre, T.J., et al., *Contribution of central neuroplasticity to pathological pain: review of clinical and experimental evidence*. Pain, 1993. **52**(3): p. 259-85.
7. Cervero, F. and J.M. Laird, *From acute to chronic pain: mechanisms and hypotheses*. Prog Brain Res, 1996. **110**: p. 3-15.
8. Woolf, C.J., *Evidence for a central component of post-injury pain hypersensitivity*. Nature, 1983. **306**(5944): p. 686-8.
9. Latremoliere, A. and C.J. Woolf, *Central sensitization: a generator of pain hypersensitivity by central neural plasticity*. J Pain, 2009. **10**(9): p. 895-926.
10. Klepstad, P., et al., *Evidence of a role for NMDA receptors in pain perception*. Eur J Pharmacol, 1990. **187**(3): p. 513-8.
11. Persson, J., et al., *Beneficial effects of ketamine in a chronic pain state with allodynia, possibly due to central sensitization*. Pain, 1995. **60**(2): p. 217-22.
12. Nakazato, E., A. Kato, and S. Watanabe, *Brain but not spinal NR2B receptor is responsible for the anti-allodynic effect of an NR2B subunit-selective antagonist CP-101,606 in a rat chronic constriction injury model*. Pharmacology, 2005. **73**(1): p. 8-14.
13. Sladeczek, F., et al., *Glutamate stimulates inositol phosphate formation in striatal neurones*. Nature, 1985. **317**(6039): p. 717-9.
14. Willard, S.S. and S. Koochekpour, *Glutamate, glutamate receptors, and downstream signaling pathways*. Int J Biol Sci, 2013. **9**(9): p. 948-59.
15. Brauner-Osborne, H., P. Wellendorph, and A.A. Jensen, *Structure, pharmacology and therapeutic prospects of family C G-protein coupled receptors*. Curr Drug Targets, 2007. **8**(1): p. 169-84.
16. Kroeze, W.K., D.J. Sheffler, and B.L. Roth, *G-protein-coupled receptors at a glance*. J Cell Sci, 2003. **116**(Pt 24): p. 4867-9.
17. Romano, C., W.L. Yang, and K.L. O'Malley, *Metabotropic glutamate receptor 5 is a disulfide-linked dimer*. J Biol Chem, 1996. **271**(45): p. 28612-6.
18. El Moustaine, D., et al., *Distinct roles of metabotropic glutamate receptor dimerization in agonist activation and G-protein coupling*. Proc Natl Acad Sci U S A, 2012. **109**(40): p. 16342-7.
19. Kniazeff, J., et al., *Dimers and beyond: The functional puzzles of class C GPCRs*. Pharmacol Ther, 2011. **130**(1): p. 9-25.
20. Beqollari, D. and P.J. Kammermeier, *Venus fly trap domain of mGluR1 functions as a dominant negative against group I mGluR signaling*. J Neurophysiol, 2010. **104**(1): p. 439-48.
21. Kubo, Y., T. Miyashita, and Y. Murata, *Structural basis for a Ca²⁺-sensing function of the metabotropic glutamate receptors*. Science, 1998. **279**(5357): p. 1722-5.
22. Okamoto, T., et al., *Expression and purification of the extracellular ligand binding region of metabotropic glutamate receptor subtype 1*. J Biol Chem, 1998. **273**(21): p. 13089-96.

23. O'Hara, P.J., et al., *The ligand-binding domain in metabotropic glutamate receptors is related to bacterial periplasmic binding proteins*. *Neuron*, 1993. **11**(1): p. 41-52.
24. Masu, M., et al., *Sequence and expression of a metabotropic glutamate receptor*. *Nature*, 1991. **349**(6312): p. 760-5.
25. Jingami, H., S. Nakanishi, and K. Morikawa, *Structure of the metabotropic glutamate receptor*. *Curr Opin Neurobiol*, 2003. **13**(3): p. 271-8.
26. Wall, M.A., et al., *The structure of the G protein heterotrimer Gi alpha 1 beta 1 gamma 2*. *Cell*, 1995. **83**(6): p. 1047-58.
27. Pin, J.P. and R. Duvoisin, *The metabotropic glutamate receptors: structure and functions*. *Neuropharmacology*, 1995. **34**(1): p. 1-26.
28. Pin, J.P. and F. Acher, *The metabotropic glutamate receptors: structure, activation mechanism and pharmacology*. *Curr Drug Targets CNS Neurol Disord*, 2002. **1**(3): p. 297-317.
29. Pellicciari, R., et al., *Metabotropic glutamate receptors: structure and new subtype-selective ligands*. *Farmaco*, 2001. **56**(1-2): p. 91-4.
30. Hermans, E. and R.A. Challiss, *Structural, signalling and regulatory properties of the group I metabotropic glutamate receptors: prototypic family C G-protein-coupled receptors*. *Biochem J*, 2001. **359**(Pt 3): p. 465-84.
31. Belenikin, M.S., V.A. Palyulin, and N.S. Zefirov, *The modeling of the structure of the cysteine-rich domain of metabotropic glutamate receptors*. *Dokl Biochem Biophys*, 2004. **394**: p. 21-5.
32. Costantino, G. and R. Pellicciari, *Homology modeling of metabotropic glutamate receptors. (mGluRs) structural motifs affecting binding modes and pharmacological profile of mGluR1 agonists and competitive antagonists*. *J Med Chem*, 1996. **39**(20): p. 3998-4006.
33. Berthele, A., et al., *Differential expression of rat and human type I metabotropic glutamate receptor splice variant messenger RNAs*. *Neuroscience*, 1998. **85**(3): p. 733-49.
34. Shiraishi-Yamaguchi, Y. and T. Furuichi, *The Homer family proteins*. *Genome Biol*, 2007. **8**(2): p. 206.
35. Karim, F., C.C. Wang, and R.W.t. Gereau, *Metabotropic glutamate receptor subtypes 1 and 5 are activators of extracellular signal-regulated kinase signaling required for inflammatory pain in mice*. *J Neurosci*, 2001. **21**(11): p. 3771-9.
36. Mion, S., et al., *Bidirectional regulation of neurite elaboration by alternatively spliced metabotropic glutamate receptor 5 (mGluR5) isoforms*. *Mol Cell Neurosci*, 2001. **17**(6): p. 957-72.
37. Joly, C., et al., *Molecular, functional, and pharmacological characterization of the metabotropic glutamate receptor type 5 splice variants: comparison with mGluR1*. *J Neurosci*, 1995. **15**(5 Pt 2): p. 3970-81.
38. Prezeau, L., et al., *Changes in the carboxyl-terminal domain of metabotropic glutamate receptor 1 by alternative splicing generate receptors with differing agonist-independent activity*. *Mol Pharmacol*, 1996. **49**(3): p. 422-9.
39. Ango, F., et al., *Agonist-independent activation of metabotropic glutamate receptors by the intracellular protein Homer*. *Nature*, 2001. **411**(6840): p. 962-5.
40. Jong, Y.J., et al., *Location-dependent signaling of the group 1 metabotropic glutamate receptor mGlu5*. *Mol Pharmacol*, 2014. **86**(6): p. 774-85.
41. Kalinowska, M. and A. Francesconi, *Group I Metabotropic Glutamate Receptor Interacting Proteins: Fine-Tuning Receptor Functions in Health and Disease*. *Curr Neuropharmacol*, 2016. **14**(5): p. 494-503.
42. Hicks, S.N., et al., *General and versatile autoinhibition of PLC isozymes*. *Mol Cell*, 2008. **31**(3): p. 383-94.
43. Sugiyama, H., I. Ito, and C. Hirono, *A new type of glutamate receptor linked to inositol phospholipid metabolism*. *Nature*, 1987. **325**(6104): p. 531-3.
44. Schoepp, D.D. and B.G. Johnson, *Pharmacology of metabotropic glutamate receptor inhibition of cyclic AMP formation in the adult rat hippocampus*. *Neurochem Int*, 1993. **22**(3): p. 277-83.

45. Schoepp, D.D. and P.J. Conn, *Metabotropic glutamate receptors in brain function and pathology*. Trends Pharmacol Sci, 1993. **14**(1): p. 13-20.
46. Monaghan, D.T., R.J. Bridges, and C.W. Cotman, *The excitatory amino acid receptors: their classes, pharmacology, and distinct properties in the function of the central nervous system*. Annu Rev Pharmacol Toxicol, 1989. **29**: p. 365-402.
47. Henzi, V., et al., *L-proline activates glutamate and glycine receptors in cultured rat dorsal horn neurons*. Mol Pharmacol, 1992. **41**(4): p. 793-801.
48. Farooqui, A.A. and L.A. Horrocks, *Excitatory amino acid receptors, neural membrane phospholipid metabolism and neurological disorders*. Brain Res Brain Res Rev, 1991. **16**(2): p. 171-91.
49. Eichmann, T.O. and A. Lass, *DAG tales: the multiple faces of diacylglycerol--stereochemistry, metabolism, and signaling*. Cell Mol Life Sci, 2015. **72**(20): p. 3931-52.
50. Wierda, K.D., et al., *Interdependence of PKC-dependent and PKC-independent pathways for presynaptic plasticity*. Neuron, 2007. **54**(2): p. 275-90.
51. Zhang, G., et al., *Crystal structure of the cys2 activator-binding domain of protein kinase C delta in complex with phorbol ester*. Cell, 1995. **81**(6): p. 917-24.
52. Haneda, M., D. Koya, and R. Kikkawa, *Cellular mechanisms in the development and progression of diabetic nephropathy: activation of the DAG-PKC-ERK pathway*. Am J Kidney Dis, 2001. **38**(4 Suppl 1): p. S178-81.
53. Mochly-Rosen, D., H. Khaner, and J. Lopez, *Identification of intracellular receptor proteins for activated protein kinase C*. Proc Natl Acad Sci U S A, 1991. **88**(9): p. 3997-4000.
54. Mochly-Rosen, D. and A.S. Gordon, *Anchoring proteins for protein kinase C: a means for isozyme selectivity*. FASEB J, 1998. **12**(1): p. 35-42.
55. Brose, N. and C. Rosenmund, *Move over protein kinase C, you've got company: alternative cellular effectors of diacylglycerol and phorbol esters*. J Cell Sci, 2002. **115**(Pt 23): p. 4399-411.
56. Wang, J.Q., et al., *Glutamate signaling to Ras-MAPK in striatal neurons: mechanisms for inducible gene expression and plasticity*. Mol Neurobiol, 2004. **29**(1): p. 1-14.
57. Jones, D.R., et al., *Expression of a catalytically inactive form of diacylglycerol kinase alpha induces sustained signaling through RasGRP*. FASEB J, 2002. **16**(6): p. 595-7.
58. Calabresi, P., et al., *Activation of metabotropic glutamate receptor subtype 1/protein kinase C/mitogen-activated protein kinase pathway is required for postischemic long-term potentiation in the striatum*. Mol Pharmacol, 2001. **60**(4): p. 808-15.
59. Gille, H., A.D. Sharrocks, and P.E. Shaw, *Phosphorylation of transcription factor p62TCF by MAP kinase stimulates ternary complex formation at c-fos promoter*. Nature, 1992. **358**(6385): p. 414-7.
60. Murphy, L.O., et al., *Molecular interpretation of ERK signal duration by immediate early gene products*. Nat Cell Biol, 2002. **4**(8): p. 556-64.
61. Halazonetis, T.D., et al., *c-Jun dimerizes with itself and with c-Fos, forming complexes of different DNA binding affinities*. Cell, 1988. **55**(5): p. 917-24.
62. Shaulian, E. and M. Karin, *AP-1 in cell proliferation and survival*. Oncogene, 2001. **20**(19): p. 2390-400.
63. Stevens, F.C., *Calmodulin: an introduction*. Can J Biochem Cell Biol, 1983. **61**(8): p. 906-10.
64. Ribeiro, F.M., et al., *Group I metabotropic glutamate receptor signalling and its implication in neurological disease*. CNS Neurol Disord Drug Targets, 2010. **9**(5): p. 574-95.
65. Yang, L., et al., *A signaling mechanism from G alpha q-protein-coupled metabotropic glutamate receptors to gene expression: role of the c-Jun N-terminal kinase pathway*. J Neurosci, 2006. **26**(3): p. 971-80.
66. Yamauchi, J., et al., *Activation of p38 mitogen-activated protein kinase by signaling through G protein-coupled receptors. Involvement of Gbetagamma and Galphaq/11 subunits*. J Biol Chem, 1997. **272**(44): p. 27771-7.

67. Coso, O.A., et al., *Signaling from G protein-coupled receptors to c-Jun kinase involves beta gamma subunits of heterotrimeric G proteins acting on a Ras and Rac1-dependent pathway.* J Biol Chem, 1996. **271**(8): p. 3963-6.
68. Huang, C.C., et al., *Rap1-induced p38 mitogen-activated protein kinase activation facilitates AMPA receptor trafficking via the GDI.Rab5 complex. Potential role in (S)-3,5-dihydroxyphenylglycine-induced long term depression.* J Biol Chem, 2004. **279**(13): p. 12286-92.
69. Naranjo, J.R., et al., *Molecular pathways of pain: Fos/Jun-mediated activation of a noncanonical AP-1 site in the prodynorphin gene.* Neuron, 1991. **6**(4): p. 607-17.
70. Francesconi, A. and R.M. Duvoisin, *Opposing effects of protein kinase C and protein kinase A on metabotropic glutamate receptor signaling: selective desensitization of the inositol trisphosphate/Ca²⁺ pathway by phosphorylation of the receptor-G protein-coupling domain.* Proc Natl Acad Sci U S A, 2000. **97**(11): p. 6185-90.
71. Aramori, I. and S. Nakanishi, *Signal transduction and pharmacological characteristics of a metabotropic glutamate receptor, mGluR1, in transfected CHO cells.* Neuron, 1992. **8**(4): p. 757-65.
72. Abe, T., et al., *Molecular characterization of a novel metabotropic glutamate receptor mGluR5 coupled to inositol phosphate/Ca²⁺ signal transduction.* J Biol Chem, 1992. **267**(19): p. 13361-8.
73. Kawabata, S., et al., *Control of calcium oscillations by phosphorylation of metabotropic glutamate receptors.* Nature, 1996. **383**(6595): p. 89-92.
74. Dale, L.B., et al., *Spatial-temporal patterning of metabotropic glutamate receptor-mediated inositol 1,4,5-triphosphate, calcium, and protein kinase C oscillations: protein kinase C-dependent receptor phosphorylation is not required.* J Biol Chem, 2001. **276**(38): p. 35900-8.
75. Zarnadze, S., et al., *Cell-specific synaptic plasticity induced by network oscillations.* Elife, 2016. **5**.
76. Kehoe, J., *Glutamate activates a K⁺ conductance increase in Aplysia neurons that appears to be independent of G proteins.* Neuron, 1994. **13**(3): p. 691-702.
77. Guerineau, N.C., et al., *Activation of a nonselective cationic conductance by metabotropic glutamatergic and muscarinic agonists in CA3 pyramidal neurons of the rat hippocampus.* J Neurosci, 1995. **15**(6): p. 4395-407.
78. Heuss, C., et al., *G-protein-independent signaling mediated by metabotropic glutamate receptors.* Nat Neurosci, 1999. **2**(12): p. 1070-7.
79. Kubota, H., et al., *mGluR1-mediated excitation of cerebellar GABAergic interneurons requires both G protein-dependent and Src-ERK1/2-dependent signaling pathways.* PLoS One, 2014. **9**(9): p. e106316.
80. Xiao, B., J.C. Tu, and P.F. Worley, *Homer: a link between neural activity and glutamate receptor function.* Curr Opin Neurobiol, 2000. **10**(3): p. 370-4.
81. Hayashi, M.K., H.M. Ames, and Y. Hayashi, *Tetrameric hub structure of postsynaptic scaffolding protein homer.* J Neurosci, 2006. **26**(33): p. 8492-501.
82. Brakeman, P.R., et al., *Homer: a protein that selectively binds metabotropic glutamate receptors.* Nature, 1997. **386**(6622): p. 284-8.
83. Tu, J.C., et al., *Coupling of mGluR/Homer and PSD-95 complexes by the Shank family of postsynaptic density proteins.* Neuron, 1999. **23**(3): p. 583-92.
84. Hayashi, M.K., et al., *The postsynaptic density proteins Homer and Shank form a polymeric network structure.* Cell, 2009. **137**(1): p. 159-71.
85. Naisbitt, S., et al., *Shank, a novel family of postsynaptic density proteins that binds to the NMDA receptor/PSD-95/GKAP complex and cortactin.* Neuron, 1999. **23**(3): p. 569-82.
86. Harvey, J. and G.L. Collingridge, *Signal transduction pathways involved in the acute potentiation of NMDA responses by 1S,3R-ACPD in rat hippocampal slices.* Br J Pharmacol, 1993. **109**(4): p. 1085-90.
87. Aniksztejn, L., P. Bregestovski, and Y. Ben-Ari, *Selective activation of quisqualate metabotropic receptor potentiates NMDA but not AMPA responses.* Eur J Pharmacol, 1991. **205**(3): p. 327-8.

88. Pisani, A., et al., *Enhancement of NMDA responses by group I metabotropic glutamate receptor activation in striatal neurones*. Br J Pharmacol, 1997. **120**(6): p. 1007-14.
89. Awad, H., et al., *Activation of metabotropic glutamate receptor 5 has direct excitatory effects and potentiates NMDA receptor currents in neurons of the subthalamic nucleus*. J Neurosci, 2000. **20**(21): p. 7871-9.
90. Heidinger, V., et al., *Metabotropic glutamate receptor 1-induced upregulation of NMDA receptor current: mediation through the Pyk2/Src-family kinase pathway in cortical neurons*. J Neurosci, 2002. **22**(13): p. 5452-61.
91. Jones, M.W. and P.M. Headley, *Interactions between metabotropic and ionotropic glutamate receptor agonists in the rat spinal cord in vivo*. Neuropharmacology, 1995. **34**(8): p. 1025-31.
92. Bleakman, D., et al., *Metabotropic glutamate receptors potentiate ionotropic glutamate responses in the rat dorsal horn*. Mol Pharmacol, 1992. **42**(2): p. 192-6.
93. Mannaioni, G., et al., *Metabotropic glutamate receptors 1 and 5 differentially regulate CA1 pyramidal cell function*. J Neurosci, 2001. **21**(16): p. 5925-34.
94. Challiss, R.A., et al., *Modulatory effects of NMDA on phosphoinositide responses evoked by the metabotropic glutamate receptor agonist 1S,3R-ACPD in neonatal rat cerebral cortex*. Br J Pharmacol, 1994. **112**(1): p. 231-9.
95. Luthi, A., B.H. Gähwiler, and U. Gerber, *Potentiation of a metabotropic glutamatergic response following NMDA receptor activation in rat hippocampus*. Pflugers Arch, 1994. **427**(1-2): p. 197-202.
96. Alagarsamy, S., et al., *NMDA-induced potentiation of mGluR5 is mediated by activation of protein phosphatase 2B/calcineurin*. Neuropharmacology, 2005. **49 Suppl 1**: p. 135-45.
97. Nicholson, E. and D.M. Kullmann, *T-type calcium channels contribute to NMDA receptor independent synaptic plasticity in hippocampal regular-spiking oriens-alveus interneurons*. J Physiol, 2017. **595**(11): p. 3449-3458.
98. Choi, S., et al., *Attenuated pain responses in mice lacking Ca(V)3.2 T-type channels*. Genes Brain Behav, 2007. **6**(5): p. 425-31.
99. Todorovic, S.M. and V. Jevtovic-Todorovic, *Targeting of CaV3.2 T-type calcium channels in peripheral sensory neurons for the treatment of painful diabetic neuropathy*. Pflugers Arch, 2014. **466**(4): p. 701-6.
100. Marger, F., et al., *T-type calcium channels contribute to colonic hypersensitivity in a rat model of irritable bowel syndrome*. Proc Natl Acad Sci U S A, 2011. **108**(27): p. 11268-73.
101. Neugebauer, V., *Metabotropic glutamate receptors--important modulators of nociception and pain behavior*. Pain, 2002. **98**(1-2): p. 1-8.
102. Ito, I., et al., *3,5-Dihydroxyphenyl-glycine: a potent agonist of metabotropic glutamate receptors*. Neuroreport, 1992. **3**(11): p. 1013-6.
103. Asiedu, M.N., et al., *Spinal protein kinase M zeta underlies the maintenance mechanism of persistent nociceptive sensitization*. J Neurosci, 2011. **31**(18): p. 6646-53.
104. Dolan, S. and A.M. Nolan, *Behavioural evidence supporting a differential role for group I and II metabotropic glutamate receptors in spinal nociceptive transmission*. Neuropharmacology, 2000. **39**(7): p. 1132-8.
105. Fisher, K. and T.J. Coderre, *Comparison of nociceptive effects produced by intrathecal administration of mGluR agonists*. Neuroreport, 1996. **7**(15-17): p. 2743-7.
106. Fundytus, M.E., et al., *In vivo antinociceptive activity of anti-rat mGluR1 and mGluR5 antibodies in rats*. Neuroreport, 1998. **9**(4): p. 731-5.
107. Lorrain, D.S., et al., *Activation of spinal group I metabotropic glutamate receptors in rats evokes local glutamate release and spontaneous nociceptive behaviors: effects of 2-methyl-6-(phenylethynyl)-pyridine pretreatment*. Neurosci Lett, 2002. **327**(3): p. 198-202.
108. Fisher, K. and T.J. Coderre, *Hyperalgesia and allodynia induced by intrathecal (RS)-dihydroxyphenylglycine in rats*. Neuroreport, 1998. **9**(6): p. 1169-72.

109. Hama, A.T., *Acute activation of the spinal cord metabotropic glutamate subtype-5 receptor leads to cold hypersensitivity in the rat.* Neuropharmacology, 2003. **44**(4): p. 423-30.
110. Fisher, K. and T.J. Coderre, *The contribution of metabotropic glutamate receptors (mGluRs) to formalin-induced nociception.* Pain, 1996. **68**(2-3): p. 255-63.
111. Neugebauer, V., P.S. Chen, and W.D. Willis, *Role of metabotropic glutamate receptor subtype mGluR1 in brief nociception and central sensitization of primate STT cells.* J Neurophysiol, 1999. **82**(1): p. 272-82.
112. Doherty, A.J., et al., *(RS)-2-chloro-5-hydroxyphenylglycine (CHPG) activates mGlu5, but no mGlu1, receptors expressed in CHO cells and potentiates NMDA responses in the hippocampus.* Neuropharmacology, 1997. **36**(2): p. 265-7.
113. Kammermeier, P.J., *The orthosteric agonist 2-chloro-5-hydroxyphenylglycine activates mGluR5 and mGluR1 with similar efficacy and potency.* BMC Pharmacol, 2012. **12**: p. 6.
114. Lin, Y.R., et al., *Antinociceptive actions of honokiol and magnolol on glutamatergic and inflammatory pain.* J Biomed Sci, 2009. **16**: p. 94.
115. Ren, B.X., et al., *Intrathecal injection of metabotropic glutamate receptor subtype 3 and 5 agonist/antagonist attenuates bone cancer pain by inhibition of spinal astrocyte activation in a mouse model.* Anesthesiology, 2012. **116**(1): p. 122-32.
116. Urban, M.O., et al., *Role of metabotropic glutamate receptor subtype 5 (mGluR5) in the maintenance of cold hypersensitivity following a peripheral mononeuropathy in the rat.* Neuropharmacology, 2003. **44**(8): p. 983-93.
117. Li, W. and V. Neugebauer, *Differential roles of mGluR1 and mGluR5 in brief and prolonged nociceptive processing in central amygdala neurons.* J Neurophysiol, 2004. **91**(1): p. 13-24.
118. Young, M.R., et al., *The involvement of metabotropic glutamate receptors and their intracellular signalling pathways in sustained nociceptive transmission in rat dorsal horn neurons.* Neuropharmacology, 1995. **34**(8): p. 1033-41.
119. Byrnes, K.R., et al., *Activation of metabotropic glutamate receptor 5 improves recovery after spinal cord injury in rodents.* Ann Neurol, 2009. **66**(1): p. 63-74.
120. Byrnes, K.R., et al., *Delayed mGluR5 activation limits neuroinflammation and neurodegeneration after traumatic brain injury.* J Neuroinflammation, 2012. **9**: p. 43.
121. Loane, D.J., et al., *Activation of mGluR5 and inhibition of NADPH oxidase improves functional recovery after traumatic brain injury.* J Neurotrauma, 2013. **30**(5): p. 403-12.
122. Kuang, D. and D.R. Hampson, *Ion dependence of ligand binding to metabotropic glutamate receptors.* Biochem Biophys Res Commun, 2006. **345**(1): p. 1-6.
123. Maeda, Y., et al., *Inhibitory effects of salmon calcitonin on the tail-biting and scratching behavior induced by substance P and three excitatory amino acids.* J Neural Transm Gen Sect, 1994. **96**(2): p. 125-33.
124. Kolhekar, R. and G.F. Gebhart, *NMDA and quisqualate modulation of visceral nociception in the rat.* Brain Res, 1994. **651**(1-2): p. 215-26.
125. Ferreira, S.H. and B.B. Lorenzetti, *Glutamate spinal retrograde sensitization of primary sensory neurons associated with nociception.* Neuropharmacology, 1994. **33**(11): p. 1479-85.
126. Brewer, K.L., et al., *Dermatomal scratching after intramedullary quisqualate injection: correlation with cutaneous denervation.* J Pain, 2008. **9**(11): p. 999-1005.
127. Aanonsen, L.M. and G.L. Wilcox, *Nociceptive action of excitatory amino acids in the mouse: effects of spinally administered opioids, phencyclidine and sigma agonists.* J Pharmacol Exp Ther, 1987. **243**(1): p. 9-19.
128. Aanonsen, L.M., S. Lei, and G.L. Wilcox, *Excitatory amino acid receptors and nociceptive neurotransmission in rat spinal cord.* Pain, 1990. **41**(3): p. 309-21.
129. Brewer, K.L. and R.P. Yeziarski, *Effects of adrenal medullary transplants on pain-related behaviors following excitotoxic spinal cord injury.* Brain Res, 1998. **798**(1-2): p. 83-92.

130. Yu, C.G. and R.P. Yeziarski, *Activation of the ERK1/2 signaling cascade by excitotoxic spinal cord injury*. Brain Res Mol Brain Res, 2005. **138**(2): p. 244-55.
131. Sun, X.F. and A.A. Larson, *Behavioral sensitization to kainic acid and quisqualic acid in mice: comparison to NMDA and substance P responses*. J Neurosci, 1991. **11**(10): p. 3111-23.
132. Choi, S.S., et al., *Comparison of the spinal neuropathic pain induced by intraspinal injection of N-methyl-D-aspartate and quisqualate in rats*. J Korean Neurosurg Soc, 2011. **50**(5): p. 420-5.
133. Jin, R., et al., *Mechanism of activation and selectivity in a ligand-gated ion channel: structural and functional studies of GluR2 and quisqualate*. Biochemistry, 2002. **41**(52): p. 15635-43.
134. Urca, G. and R. Urca, *Neurotoxic effects of excitatory amino acids in the mouse spinal cord: quisqualate and kainate but not N-methyl-D-aspartate induce permanent neural damage*. Brain Res, 1990. **529**(1-2): p. 7-15.
135. Zhong, J., et al., *Dual modulation of excitatory synaptic transmission by agonists at group I metabotropic glutamate receptors in the rat spinal dorsal horn*. Brain Res, 2000. **887**(2): p. 359-77.
136. Galik, J., et al., *Involvement of group I metabotropic glutamate receptors and glutamate transporters in the slow excitatory synaptic transmission in the spinal cord dorsal horn*. Neuroscience, 2008. **154**(4): p. 1372-87.
137. Park, Y.K., et al., *Activation of presynaptic group I metabotropic glutamate receptors enhances glutamate release in the rat spinal cord substantia gelatinosa*. Neurosci Lett, 2004. **361**(1-3): p. 220-4.
138. Heinke, B. and J. Sandkuhler, *Group I metabotropic glutamate receptor-induced Ca(2+)-gradients in rat superficial spinal dorsal horn neurons*. Neuropharmacology, 2007. **52**(3): p. 1015-23.
139. Young, M.R., et al., *Behavioural and electrophysiological evidence supporting a role for group I metabotropic glutamate receptors in the mediation of nociceptive inputs to the rat spinal cord*. Brain Res, 1997. **777**(1-2): p. 161-9.
140. Young, M.R., et al., *Antisense ablation of type I metabotropic glutamate receptor mGluR1 inhibits spinal nociceptive transmission*. J Neurosci, 1998. **18**(23): p. 10180-8.
141. Hu, H.J., G. Bhave, and R.W.t. Gereau, *Prostaglandin and protein kinase A-dependent modulation of vanilloid receptor function by metabotropic glutamate receptor 5: potential mechanism for thermal hyperalgesia*. J Neurosci, 2002. **22**(17): p. 7444-52.
142. Ji, R.R., et al., *Nociceptive-specific activation of ERK in spinal neurons contributes to pain hypersensitivity*. Nat Neurosci, 1999. **2**(12): p. 1114-9.
143. Hu, H.J., K.S. Glauner, and R.W.t. Gereau, *ERK integrates PKA and PKC signaling in superficial dorsal horn neurons. I. Modulation of A-type K+ currents*. J Neurophysiol, 2003. **90**(3): p. 1671-9.
144. Hu, H.J., et al., *Metabotropic glutamate receptor 5 modulates nociceptive plasticity via extracellular signal-regulated kinase-Kv4.2 signaling in spinal cord dorsal horn neurons*. J Neurosci, 2007. **27**(48): p. 13181-91.
145. Carroll, F.I., *Antagonists at metabotropic glutamate receptor subtype 5: structure activity relationships and therapeutic potential for addiction*. Ann N Y Acad Sci, 2008. **1141**: p. 221-32.
146. Varney, M.A., et al., *SIB-1757 and SIB-1893: selective, noncompetitive antagonists of metabotropic glutamate receptor type 5*. J Pharmacol Exp Ther, 1999. **290**(1): p. 170-81.
147. Dogrul, A., et al., *Peripheral and spinal antihyperalgesic activity of SIB-1757, a metabotropic glutamate receptor (mGLUR(5)) antagonist, in experimental neuropathic pain in rats*. Neurosci Lett, 2000. **292**(2): p. 115-8.
148. Nakahara, K., M. Okada, and S. Nakanishi, *The metabotropic glutamate receptor mGluR5 induces calcium oscillations in cultured astrocytes via protein kinase C phosphorylation*. J Neurochem, 1997. **69**(4): p. 1467-75.
149. Gasparini, F., et al., *2-Methyl-6-(phenylethynyl)-pyridine (MPEP), a potent, selective and systemically active mGlu5 receptor antagonist*. Neuropharmacology, 1999. **38**(10): p. 1493-503.

150. Pagano, A., et al., *The non-competitive antagonists 2-methyl-6-(phenylethynyl)pyridine and 7-hydroxyiminocyclopropan[b]chromen-1a-carboxylic acid ethyl ester interact with overlapping binding pockets in the transmembrane region of group I metabotropic glutamate receptors*. J Biol Chem, 2000. **275**(43): p. 33750-8.
151. Varty, G.B., et al., *The antinociceptive and anxiolytic-like effects of the metabotropic glutamate receptor 5 (mGluR5) antagonists, MPEP and MTEP, and the mGluR1 antagonist, LY456236, in rodents: a comparison of efficacy and side-effect profiles*. Psychopharmacology (Berl), 2005. **179**(1): p. 207-17.
152. Zhu, C.Z., et al., *Assessing the role of metabotropic glutamate receptor 5 in multiple nociceptive modalities*. Eur J Pharmacol, 2004. **506**(2): p. 107-18.
153. Kozela, E., A. Pilc, and P. Popik, *Inhibitory effects of MPEP, an mGluR5 antagonist, and memantine, an N-methyl-D-aspartate receptor antagonist, on morphine antinociceptive tolerance in mice*. Psychopharmacology (Berl), 2003. **165**(3): p. 245-51.
154. Narita, M., et al., *Involvement of spinal metabotropic glutamate receptor 5 in the development of tolerance to morphine-induced antinociception*. J Neurochem, 2005. **94**(5): p. 1297-305.
155. Mills, C.D., K.M. Johnson, and C.E. Hulsebosch, *Group I metabotropic glutamate receptors in spinal cord injury: roles in neuroprotection and the development of chronic central pain*. J Neurotrauma, 2002. **19**(1): p. 23-42.
156. Hudson, L.J., et al., *Metabotropic glutamate receptor 5 upregulation in A-fibers after spinal nerve injury: 2-methyl-6-(phenylethynyl)-pyridine (MPEP) reverses the induced thermal hyperalgesia*. J Neurosci, 2002. **22**(7): p. 2660-8.
157. Fisher, K., C. Lefebvre, and T.J.Coderre, *Antinociceptive effects following intrathecal pretreatment with selective metabotropic glutamate receptor compounds in a rat model of neuropathic pain*. Pharmacol Biochem Behav, 2002. **73**(2): p. 411-8.
158. Walker, K., et al., *Metabotropic glutamate receptor subtype 5 (mGlu5) and nociceptive function. I. Selective blockade of mGlu5 receptors in models of acute, persistent and chronic pain*. Neuropharmacology, 2001. **40**(1): p. 1-9.
159. Lea, P.M.t., V.A. Movsesyan, and A.I. Faden, *Neuroprotective activity of the mGluR5 antagonists MPEP and MTEP against acute excitotoxicity differs and does not reflect actions at mGluR5 receptors*. Br J Pharmacol, 2005. **145**(4): p. 527-34.
160. Montana, M.C., et al., *The metabotropic glutamate receptor subtype 5 antagonist fenobam is analgesic and has improved in vivo selectivity compared with the prototypical antagonist 2-methyl-6-(phenylethynyl)-pyridine*. J Pharmacol Exp Ther, 2009. **330**(3): p. 834-43.
161. Cosford, N.D., et al., *[3H]-methoxymethyl-MTEP and [3H]-methoxy-PEPy: potent and selective radioligands for the metabotropic glutamate subtype 5 (mGlu5) receptor*. Bioorg Med Chem Lett, 2003. **13**(3): p. 351-4.
162. Lindstrom, E., et al., *Involvement of metabotropic glutamate 5 receptor in visceral pain*. Pain, 2008. **137**(2): p. 295-305.
163. Sevostianova, N. and W. Danysz, *Analgesic effects of mGlu1 and mGlu5 receptor antagonists in the rat formalin test*. Neuropharmacology, 2006. **51**(3): p. 623-30.
164. Mills, C.D., et al., *AIDA reduces glutamate release and attenuates mechanical allodynia after spinal cord injury*. Neuroreport, 2000. **11**(14): p. 3067-70.
165. Mills, C.D., et al., *Involvement of metabotropic glutamate receptors in excitatory amino acid and GABA release following spinal cord injury in rat*. J Neurochem, 2001. **79**(4): p. 835-48.
166. Moroni, F., et al., *Presynaptic mGlu1 type receptors potentiate transmitter output in the rat cortex*. Eur J Pharmacol, 1998. **347**(2-3): p. 189-95.
167. Bordi, F. and A. Ugolini, *Involvement of mGluR(5) on acute nociceptive transmission*. Brain Res, 2000. **871**(2): p. 223-33.

168. Boxall, S.J., et al., *Metabotropic glutamate receptor activation contributes to nociceptive reflex activity in the rat spinal cord in vitro*. Neuroscience, 1996. **74**(1): p. 13-20.
169. Boxall, S.J., et al., *mGluR activation reveals a tonic NMDA component in inflammatory hyperalgesia*. Neuroreport, 1998. **9**(6): p. 1201-3.
170. Li, J.Q., et al., *Regulation of increased glutamatergic input to spinal dorsal horn neurons by mGluR5 in diabetic neuropathic pain*. J Neurochem, 2010. **112**(1): p. 162-72.
171. Pecknold, J.C., et al., *Treatment of anxiety using fenobam (a nonbenzodiazepine) in a double-blind standard (diazepam) placebo-controlled study*. J Clin Psychopharmacol, 1982. **2**(2): p. 129-33.
172. Porter, R.H., et al., *Fenobam: a clinically validated nonbenzodiazepine anxiolytic is a potent, selective, and noncompetitive mGlu5 receptor antagonist with inverse agonist activity*. J Pharmacol Exp Ther, 2005. **315**(2): p. 711-21.
173. Gereau, I.R., Cavallone, L., *Preclinical and translational studies of fenobam, an mGlu5 NAM, for the treatment of pain*. Molecular Pain, 2014. **10**(Suppl 1): p. O3.
174. Montana, M.C., et al., *Metabotropic glutamate receptor 5 antagonism with fenobam: examination of analgesic tolerance and side effect profile in mice*. Anesthesiology, 2011. **115**(6): p. 1239-50.
175. Crock, L.W., et al., *Metabotropic glutamate receptor 5 (mGluR5) regulates bladder nociception*. Mol Pain, 2012. **8**(1): p. 20.
176. Lax, N.C., et al., *The mGluR5 antagonist fenobam induces analgesic conditioned place preference in mice with spared nerve injury*. PLoS One, 2014. **9**(7): p. e103524.
177. Vardi, N., et al., *Localization of mGluR6 to dendrites of ON bipolar cells in primate retina*. J Comp Neurol, 2000. **423**(3): p. 402-12.
178. Quraishi, S., et al., *Distribution of group-III metabotropic glutamate receptors in the retina*. J Comp Neurol, 2007. **501**(6): p. 931-43.
179. Ferraguti, F. and R. Shigemoto, *Metabotropic glutamate receptors*. Cell Tissue Res, 2006. **326**(2): p. 483-504.
180. Alvarez, F.J., et al., *Differential distribution of metabotropic glutamate receptors 1a, 1b, and 5 in the rat spinal cord*. J Comp Neurol, 2000. **422**(3): p. 464-87.
181. Berthele, A., et al., *Distribution and developmental changes in metabotropic glutamate receptor messenger RNA expression in the rat lumbar spinal cord*. Brain Res Dev Brain Res, 1999. **112**(1): p. 39-53.
182. Vidnyanszky, Z., et al., *Cellular and subcellular localization of the mGluR5a metabotropic glutamate receptor in rat spinal cord*. Neuroreport, 1994. **6**(1): p. 209-13.
183. Valerio, A., et al., *Metabotropic glutamate receptor mRNA expression in rat spinal cord*. Neuroreport, 1997. **8**(12): p. 2695-9.
184. Valerio, A., et al., *mGluR5 metabotropic glutamate receptor distribution in rat and human spinal cord: a developmental study*. Neurosci Res, 1997. **28**(1): p. 49-57.
185. Fotuhi, M., et al., *Differential localization of phosphoinositide-linked metabotropic glutamate receptor (mGluR1) and the inositol 1,4,5-trisphosphate receptor in rat brain*. J Neurosci, 1993. **13**(5): p. 2001-12.
186. Jia, H., A. Rustioni, and J.G. Valtchanoff, *Metabotropic glutamate receptors in superficial laminae of the rat dorsal horn*. J Comp Neurol, 1999. **410**(4): p. 627-42.
187. Tang, F.R. and M.K. Sim, *Pre- and/or post-synaptic localisation of metabotropic glutamate receptor 1alpha (mGluR1alpha) and 2/3 (mGluR2/3) in the rat spinal cord*. Neurosci Res, 1999. **34**(2): p. 73-8.
188. Romano, C., et al., *Distribution of metabotropic glutamate receptor mGluR5 immunoreactivity in rat brain*. J Comp Neurol, 1995. **355**(3): p. 455-69.
189. Carlton, S.M. and G.L. Hargett, *Colocalization of metabotropic glutamate receptors in rat dorsal root ganglion cells*. J Comp Neurol, 2007. **501**(5): p. 780-9.
190. Carlton, S.M., G.L. Hargett, and R.E. Coggeshall, *Localization of metabotropic glutamate receptors 2/3 on primary afferent axons in the rat*. Neuroscience, 2001. **105**(4): p. 957-69.

191. Ohishi, H., et al., *Distribution of the mRNA for a metabotropic glutamate receptor (mGluR3) in the rat brain: an in situ hybridization study*. J Comp Neurol, 1993. **335**(2): p. 252-66.
192. Petralia, R.S., et al., *The metabotropic glutamate receptors, mGluR2 and mGluR3, show unique postsynaptic, presynaptic and glial localizations*. Neuroscience, 1996. **71**(4): p. 949-76.
193. Azkue, J.J., et al., *The metabotropic glutamate receptor subtype mGluR 2/3 is located at extrasynaptic loci in rat spinal dorsal horn synapses*. Neurosci Lett, 2000. **287**(3): p. 236-8.
194. Azkue, J.J., et al., *Immunoreactivity for the group III metabotropic glutamate receptor subtype mGluR4a in the superficial laminae of the rat spinal dorsal horn*. J Comp Neurol, 2001. **430**(4): p. 448-57.
195. Boxall, S.J., et al., *Enhanced expression of metabotropic glutamate receptor 3 messenger RNA in the rat spinal cord during ultraviolet irradiation induced peripheral inflammation*. Neuroscience, 1998. **82**(2): p. 591-602.
196. Li, H., et al., *Localization of a metabotropic glutamate receptor, mGluR7, in axon terminals of presumed nociceptive, primary afferent fibers in the superficial layers of the spinal dorsal horn: an electron microscope study in the rat*. Neurosci Lett, 1997. **223**(3): p. 153-6.
197. Ohishi, H., et al., *Distributions of the mRNAs for L-2-amino-4-phosphonobutyrate-sensitive metabotropic glutamate receptors, mGluR4 and mGluR7, in the rat brain*. J Comp Neurol, 1995. **360**(4): p. 555-70.
198. Ohishi, H., et al., *Presynaptic localization of a metabotropic glutamate receptor, mGluR7, in the primary afferent neurons: an immunohistochemical study in the rat*. Neurosci Lett, 1995. **202**(1-2): p. 85-8.
199. Nakajima, Y., et al., *Molecular characterization of a novel retinal metabotropic glutamate receptor mGluR6 with a high agonist selectivity for L-2-amino-4-phosphonobutyrate*. J Biol Chem, 1993. **268**(16): p. 11868-73.
200. Yan, H.Y., et al., *[Expression changes of metabotropic glutamate receptor 5 in neuropathic pain]*. Zhongguo Yi Xue Ke Xue Yuan Xue Bao, 2007. **29**(1): p. 111-6.
201. Gwak, Y.S. and C.E. Hulsebosch, *Upregulation of Group I metabotropic glutamate receptors in neurons and astrocytes in the dorsal horn following spinal cord injury*. Exp Neurol, 2005. **195**(1): p. 236-43.
202. Dolan, S., et al., *Up-regulation of metabotropic glutamate receptor subtypes 3 and 5 in spinal cord in a clinical model of persistent inflammation and hyperalgesia*. Pain, 2003. **106**(3): p. 501-12.
203. Dolan, S., et al., *Differential expression of central metabotropic glutamate receptor (mGluR) subtypes in a clinical model of post-surgical pain*. Pain, 2004. **110**(1-2): p. 369-77.
204. Miyoshi, K., M. Narita, and T. Suzuki, *Involvement of mGluR5 in the ethanol-induced neuropathic pain-like state in the rat*. Neurosci Lett, 2006. **410**(2): p. 105-9.
205. Dohlman, H.G. and J. Thorner, *RGS proteins and signaling by heterotrimeric G proteins*. J Biol Chem, 1997. **272**(7): p. 3871-4.
206. Saugstad, J.A., et al., *RGS4 inhibits signaling by group I metabotropic glutamate receptors*. J Neurosci, 1998. **18**(3): p. 905-13.
207. Kammermeier, P.J. and S.R. Ikeda, *Expression of RGS2 alters the coupling of metabotropic glutamate receptor 1a to M-type K⁺ and N-type Ca²⁺ channels*. Neuron, 1999. **22**(4): p. 819-29.
208. Mundell, S.J., et al., *Desensitization and internalization of metabotropic glutamate receptor 1a following activation of heterologous Gq/11-coupled receptors*. Biochemistry, 2004. **43**(23): p. 7541-51.
209. Dale, L.B., et al., *Agonist-stimulated and tonic internalization of metabotropic glutamate receptor 1a in human embryonic kidney 293 cells: agonist-stimulated endocytosis is beta-arrestin1 isoform-specific*. Mol Pharmacol, 2001. **60**(6): p. 1243-53.
210. Nakamura, K., et al., *Signaling and phosphorylation-impaired mutants of the rat follitropin receptor reveal an activation- and phosphorylation-independent but arrestin-dependent pathway for internalization*. J Biol Chem, 1998. **273**(38): p. 24346-54.
211. Dhimi, G.K. and S.S. Ferguson, *Regulation of metabotropic glutamate receptor signaling, desensitization and endocytosis*. Pharmacol Ther, 2006. **111**(1): p. 260-71.

212. Hubert, G.W., M. Paquet, and Y. Smith, *Differential subcellular localization of mGluR1a and mGluR5 in the rat and monkey Substantia nigra*. J Neurosci, 2001. **21**(6): p. 1838-47.
213. Pitcher, M.H., A. Ribeiro-da-Silva, and T.J. Coderre, *Effects of inflammation on the ultrastructural localization of spinal cord dorsal horn group I metabotropic glutamate receptors*. J Comp Neurol, 2007. **505**(4): p. 412-23.
214. Vincent, K., et al., *Intracellular mGluR5 plays a critical role in neuropathic pain*. Nat Commun, 2016. **7**: p. 10604.
215. Meads, M.B. and P.G. Medveczky, *Kaposi's sarcoma-associated herpesvirus-encoded viral interleukin-6 is secreted and modified differently than human interleukin-6: evidence for a unique autocrine signaling mechanism*. J Biol Chem, 2004. **279**(50): p. 51793-803.
216. Shen, B., B. Rosenberg, and S.J. Orlow, *Intracellular distribution and late endosomal effects of the ocular albinism type 1 gene product: consequences of disease-causing mutations and implications for melanosome biogenesis*. Traffic, 2001. **2**(3): p. 202-11.
217. Rozenfeld, R. and L.A. Devi, *Regulation of CB1 cannabinoid receptor trafficking by the adaptor protein AP-3*. FASEB J, 2008. **22**(7): p. 2311-22.
218. Diaz Anel, A.M. and V. Malhotra, *PKC ζ is required for beta1gamma2/beta3gamma2- and PKD-mediated transport to the cell surface and the organization of the Golgi apparatus*. J Cell Biol, 2005. **169**(1): p. 83-91.
219. Irannejad, R. and M. von Zastrow, *GPCR signaling along the endocytic pathway*. Curr Opin Cell Biol, 2014. **27**: p. 109-16.
220. Boivin, B., et al., *G protein-coupled receptors in and on the cell nucleus: a new signaling paradigm?* J Recept Signal Transduct Res, 2008. **28**(1-2): p. 15-28.
221. Tohgo, A., et al., *The stability of the G protein-coupled receptor-beta-arrestin interaction determines the mechanism and functional consequence of ERK activation*. J Biol Chem, 2003. **278**(8): p. 6258-67.
222. Shenoy, S.K. and R.J. Lefkowitz, *Trafficking patterns of beta-arrestin and G protein-coupled receptors determined by the kinetics of beta-arrestin deubiquitination*. J Biol Chem, 2003. **278**(16): p. 14498-506.
223. Gobeil, F., et al., *G-protein-coupled receptors signalling at the cell nucleus: an emerging paradigm*. Can J Physiol Pharmacol, 2006. **84**(3-4): p. 287-97.
224. Gobeil, F., Jr., et al., *Regulation of eNOS expression in brain endothelial cells by perinuclear EP(3) receptors*. Circ Res, 2002. **90**(6): p. 682-9.
225. Lind, G.J. and H.D. Cavanagh, *Nuclear muscarinic acetylcholine receptors in corneal cells from rabbit*. Invest Ophthalmol Vis Sci, 1993. **34**(10): p. 2943-52.
226. Lee, D.K., et al., *Agonist-independent nuclear localization of the Apelin, angiotensin AT1, and bradykinin B2 receptors*. J Biol Chem, 2004. **279**(9): p. 7901-8.
227. Buu, N.T., R. Hui, and P. Falardeau, *Norepinephrine in neonatal rat ventricular myocytes: association with the cell nucleus and binding to nuclear alpha 1- and beta-adrenergic receptors*. J Mol Cell Cardiol, 1993. **25**(9): p. 1037-46.
228. Nielsen, C.K., et al., *A novel localization of the G-protein-coupled CysLT1 receptor in the nucleus of colorectal adenocarcinoma cells*. Cancer Res, 2005. **65**(3): p. 732-42.
229. Hocher, B., et al., *Intracellular distribution of endothelin-1 receptors in rat liver cells*. Biochem Biophys Res Commun, 1992. **184**(1): p. 498-503.
230. Boer, P.A. and J.A. Gontijo, *Nuclear localization of SP, CGRP, and NK1R in a subpopulation of dorsal root ganglia subpopulation cells in rats*. Cell Mol Neurobiol, 2006. **26**(2): p. 191-207.
231. Morel, G., et al., *Synthesis and internalization of atrial natriuretic factor in anterior pituitary cells*. Mol Cell Endocrinol, 1988. **55**(2-3): p. 219-31.
232. Valdehita, A., et al., *Nuclear localization of vasoactive intestinal peptide (VIP) receptors in human breast cancer*. Peptides, 2010. **31**(11): p. 2035-45.

233. Boivin, B., et al., *Functional beta-adrenergic receptor signalling on nuclear membranes in adult rat and mouse ventricular cardiomyocytes*. Cardiovasc Res, 2006. **71**(1): p. 69-78.
234. Vaniotis, G., et al., *Nuclear beta-adrenergic receptors modulate gene expression in adult rat heart*. Cell Signal, 2011. **23**(1): p. 89-98.
235. Bkaily, G., et al., *Presence of functional endothelin-1 receptors in nuclear membranes of human aortic vascular smooth muscle cells*. J Cardiovasc Pharmacol, 2000. **36**(5 Suppl 1): p. S414-7.
236. Jacques, D., et al., *The distribution and density of ET-1 and its receptors are different in human right and left ventricular endocardial endothelial cells*. Peptides, 2005. **26**(8): p. 1427-35.
237. Dupre, D.J. and T.E. Hebert, *Biosynthesis and trafficking of seven transmembrane receptor signalling complexes*. Cell Signal, 2006. **18**(10): p. 1549-59.
238. Dupre, D.J., et al., *The role of Gbetagamma subunits in the organization, assembly, and function of GPCR signaling complexes*. Annu Rev Pharmacol Toxicol, 2009. **49**: p. 31-56.
239. Schulze, W. and I.B. Buchwalow, *Adenylyl cyclase in the heart: an enzymocytochemical and immunocytochemical approach*. Microsc Res Tech, 1998. **40**(6): p. 473-8.
240. Kim, C.G., D. Park, and S.G. Rhee, *The role of carboxyl-terminal basic amino acids in Gqalpha-dependent activation, particulate association, and nuclear localization of phospholipase C-beta1*. J Biol Chem, 1996. **271**(35): p. 21187-92.
241. Johnson, L.R., M.G. Scott, and J.A. Pitcher, *G protein-coupled receptor kinase 5 contains a DNA-binding nuclear localization sequence*. Mol Cell Biol, 2004. **24**(23): p. 10169-79.
242. Boer, U., et al., *Requirement of N-glycosylation of the prostaglandin E2 receptor EP3beta for correct sorting to the plasma membrane but not for correct folding*. Biochem J, 2000. **350 Pt 3**: p. 839-47.
243. Kuwajima, M., et al., *Subcellular and subsynaptic localization of group I metabotropic glutamate receptors in the monkey subthalamic nucleus*. J Comp Neurol, 2004. **474**(4): p. 589-602.
244. Paquet, M. and Y. Smith, *Group I metabotropic glutamate receptors in the monkey striatum: subsynaptic association with glutamatergic and dopaminergic afferents*. J Neurosci, 2003. **23**(20): p. 7659-69.
245. O'Malley, K.L., et al., *Activation of metabotropic glutamate receptor mGlu5 on nuclear membranes mediates intranuclear Ca2+ changes in heterologous cell types and neurons*. J Biol Chem, 2003. **278**(30): p. 28210-9.
246. Jong, Y.J., et al., *Functional metabotropic glutamate receptors on nuclei from brain and primary cultured striatal neurons. Role of transporters in delivering ligand*. J Biol Chem, 2005. **280**(34): p. 30469-80.
247. Purgert, C.A., et al., *Intracellular mGluR5 can mediate synaptic plasticity in the hippocampus*. J Neurosci, 2014. **34**(13): p. 4589-98.
248. Kumar, V., Y.J. Jong, and K.L. O'Malley, *Activated nuclear metabotropic glutamate receptor mGlu5 couples to nuclear Gq/11 proteins to generate inositol 1,4,5-trisphosphate-mediated nuclear Ca2+ release*. J Biol Chem, 2008. **283**(20): p. 14072-83.
249. Kumar, V., et al., *Activation of intracellular metabotropic glutamate receptor 5 in striatal neurons leads to up-regulation of genes associated with sustained synaptic transmission including Arc/Arg3.1 protein*. J Biol Chem, 2012. **287**(8): p. 5412-25.
250. Rothstein, J.D., et al., *Localization of neuronal and glial glutamate transporters*. Neuron, 1994. **13**(3): p. 713-25.
251. Amara, S.G. and A.C. Fontana, *Excitatory amino acid transporters: keeping up with glutamate*. Neurochem Int, 2002. **41**(5): p. 313-8.
252. Domercq, M., et al., *Expression of glutamate transporters in rat optic nerve oligodendrocytes*. Eur J Neurosci, 1999. **11**(7): p. 2226-36.
253. Gras, G., et al., *Regulated expression of sodium-dependent glutamate transporters and synthetase: a neuroprotective role for activated microglia and macrophages in HIV infection?* Brain Pathol, 2003. **13**(2): p. 211-22.

254. Kanai, Y., et al., *Electrogenic properties of the epithelial and neuronal high affinity glutamate transporter*. J Biol Chem, 1995. **270**(28): p. 16561-8.
255. Zerangue, N. and M.P. Kavanaugh, *Flux coupling in a neuronal glutamate transporter*. Nature, 1996. **383**(6601): p. 634-7.
256. Rothstein, J.D., et al., *Knockout of glutamate transporters reveals a major role for astroglial transport in excitotoxicity and clearance of glutamate*. Neuron, 1996. **16**(3): p. 675-86.
257. Chaudhry, F.A., et al., *Glutamate transporters in glial plasma membranes: highly differentiated localizations revealed by quantitative ultrastructural immunocytochemistry*. Neuron, 1995. **15**(3): p. 711-20.
258. Danbolt, N.C., *Glutamate uptake*. Prog Neurobiol, 2001. **65**(1): p. 1-105.
259. Sheldon, A.L., M.I. Gonzalez, and M.B. Robinson, *A carboxyl-terminal determinant of the neuronal glutamate transporter, EAAC1, is required for platelet-derived growth factor-dependent trafficking*. J Biol Chem, 2006. **281**(8): p. 4876-86.
260. Dowd, L.A. and M.B. Robinson, *Rapid stimulation of EAAC1-mediated Na⁺-dependent L-glutamate transport activity in C6 glioma cells by phorbol ester*. J Neurochem, 1996. **67**(2): p. 508-16.
261. Bridges, R.J., N.R. Natale, and S.A. Patel, *System xc(-) cystine/glutamate antiporter: an update on molecular pharmacology and roles within the CNS*. Br J Pharmacol, 2012. **165**(1): p. 20-34.
262. Jong, Y.J., K.E. Schweteye, and K.L. O'Malley, *Nuclear localization of functional metabotropic glutamate receptor mGlu1 in HEK293 cells and cortical neurons: role in nuclear calcium mobilization and development*. J Neurochem, 2007. **101**(2): p. 458-69.
263. Jong, Y.I. and K.L. O'Malley, *Mechanisms Associated with Activation of Intracellular Metabotropic Glutamate Receptor, mGluR5*. Neurochem Res, 2016.
264. Leeson, P.D. and B. Springthorpe, *The influence of drug-like concepts on decision-making in medicinal chemistry*. Nat Rev Drug Discov, 2007. **6**(11): p. 881-90.
265. Camenisch, G., G. Folkers, and H. van de Waterbeemd, *Shapes of membrane permeability-lipophilicity curves: extension of theoretical models with an aqueous pore pathway*. Eur J Pharm Sci, 1998. **6**(4): p. 325-29.
266. Waring, M.J., *Defining optimum lipophilicity and molecular weight ranges for drug candidates-Molecular weight dependent lower logD limits based on permeability*. Bioorg Med Chem Lett, 2009. **19**(10): p. 2844-51.
267. Ametamey, S.M., et al., *Radiosynthesis and preclinical evaluation of 11C-ABP688 as a probe for imaging the metabotropic glutamate receptor subtype 5*. J Nucl Med, 2006. **47**(4): p. 698-705.
268. Harris, J.A., *Using c-fos as a neural marker of pain*. Brain Res Bull, 1998. **45**(1): p. 1-8.
269. Bianchi, R., et al., *mGlu5 receptor antagonist decreases Fos expression in spinal neurons after noxious visceral stimulation*. Brain Res, 2003. **960**(1-2): p. 263-6.
270. Tao, Y.X., J. Gu, and R.L. Stephens, Jr., *Role of spinal cord glutamate transporter during normal sensory transmission and pathological pain states*. Mol Pain, 2005. **1**: p. 30.
271. Arriza, J.L., et al., *Functional comparisons of three glutamate transporter subtypes cloned from human motor cortex*. J Neurosci, 1994. **14**(9): p. 5559-69.
272. Koch, H.P., et al., *Differentiation of substrate and nonsubstrate inhibitors of the high-affinity, sodium-dependent glutamate transporters*. Mol Pharmacol, 1999. **56**(6): p. 1095-104.
273. Shigeri, Y., et al., *Effects of threo-beta-hydroxyaspartate derivatives on excitatory amino acid transporters (EAAT4 and EAAT5)*. J Neurochem, 2001. **79**(2): p. 297-302.
274. Munoz, M.D., et al., *Effects of dihydrokainic acid on extracellular amino acids and neuronal excitability in the in vivo rat hippocampus*. Neuropharmacology, 1987. **26**(1): p. 1-8.
275. Fallgren, A.B. and R.E. Paulsen, *A microdialysis study in rat brain of dihydrokainate, a glutamate uptake inhibitor*. Neurochem Res, 1996. **21**(1): p. 19-25.

276. Bunch, L. and P. Krogsgaard-Larsen, *Subtype selective kainic acid receptor agonists: discovery and approaches to rational design*. Med Res Rev, 2009. **29**(1): p. 3-28.
277. Medrano, M.C., et al., *Functional and morphological characterization of glutamate transporters in the rat locus coeruleus*. Br J Pharmacol, 2013. **169**(8): p. 1781-94.
278. Dunlop, J., et al., *Characterization of novel aryl-ether, biaryl, and fluorene aspartic acid and diaminopropionic acid analogs as potent inhibitors of the high-affinity glutamate transporter EAAT2*. Mol Pharmacol, 2005. **68**(4): p. 974-82.
279. Jensen, A.A., et al., *Discovery of the first selective inhibitor of excitatory amino acid transporter subtype 1*. J Med Chem, 2009. **52**(4): p. 912-5.
280. Abrahamsen, B., et al., *Allosteric modulation of an excitatory amino acid transporter: the subtype-selective inhibitor UCPH-101 exerts sustained inhibition of EAAT1 through an intramonomeric site in the trimerization domain*. J Neurosci, 2013. **33**(3): p. 1068-87.
281. Erichsen, M.N., et al., *Structure-activity relationship study of first selective inhibitor of excitatory amino acid transporter subtype 1: 2-Amino-4-(4-methoxyphenyl)-7-(naphthalen-1-yl)-5-oxo-5,6,7,8-tetrahydro-4H-chromene-3-carbonitrile (UCPH-101)*. J Med Chem, 2010. **53**(19): p. 7180-91.
282. Erichsen, M.N., et al., *Probing for improved potency and in vivo bioavailability of excitatory amino acid transporter subtype 1 inhibitors UCPH-101 and UCPH-102: design, synthesis and pharmacological evaluation of substituted 7-biphenyl analogs*. Neurochem Res, 2014. **39**(10): p. 1964-79.
283. Esslinger, C.S., et al., *The substituted aspartate analogue L-beta-threo-benzyl-aspartate preferentially inhibits the neuronal excitatory amino acid transporter EAAT3*. Neuropharmacology, 2005. **49**(6): p. 850-61.
284. Shimamoto, K., et al., *Syntheses of optically pure beta-hydroxyaspartate derivatives as glutamate transporter blockers*. Bioorg Med Chem Lett, 2000. **10**(21): p. 2407-10.
285. Shimamoto, K., et al., *Characterization of novel L-threo-beta-benzoyloxyaspartate derivatives, potent blockers of the glutamate transporters*. Mol Pharmacol, 2004. **65**(4): p. 1008-15.
286. Liaw, W.J., et al., *Spinal glutamate uptake is critical for maintaining normal sensory transmission in rat spinal cord*. Pain, 2005. **115**(1-2): p. 60-70.
287. Weng, H.R., J.H. Chen, and J.P. Cata, *Inhibition of glutamate uptake in the spinal cord induces hyperalgesia and increased responses of spinal dorsal horn neurons to peripheral afferent stimulation*. Neuroscience, 2006. **138**(4): p. 1351-60.
288. Cata, J.P., et al., *Altered discharges of spinal wide dynamic range neurons and down-regulation of glutamate transporter expression in rats with paclitaxel-induced hyperalgesia*. Neuroscience, 2006. **138**(1): p. 329-38.
289. Weng, H.R., et al., *Spinal glial glutamate transporters downregulate in rats with taxol-induced hyperalgesia*. Neurosci Lett, 2005. **386**(1): p. 18-22.
290. Dong, L. and B.A. Winkelstein, *Simulated whiplash modulates expression of the glutamatergic system in the spinal cord suggesting spinal plasticity is associated with painful dynamic cervical facet loading*. J Neurotrauma, 2010. **27**(1): p. 163-74.
291. Olechowski, C.J., et al., *A diminished response to formalin stimulation reveals a role for the glutamate transporters in the altered pain sensitivity of mice with experimental autoimmune encephalomyelitis (EAE)*. Pain, 2010. **149**(3): p. 565-72.
292. Xin, W.J., H.R. Weng, and P.M. Dougherty, *Plasticity in expression of the glutamate transporters GLT-1 and GLAST in spinal dorsal horn glial cells following partial sciatic nerve ligation*. Mol Pain, 2009. **5**: p. 15.
293. Sung, B., G. Lim, and J. Mao, *Altered expression and uptake activity of spinal glutamate transporters after nerve injury contribute to the pathogenesis of neuropathic pain in rats*. J Neurosci, 2003. **23**(7): p. 2899-910.
294. Wang, S., et al., *Downregulation of spinal glutamate transporter EAAC1 following nerve injury is regulated by central glucocorticoid receptors in rats*. Pain, 2006. **120**(1-2): p. 78-85.

295. Yan, H., et al., *[Effect of spinal glutamate transporter 1 on chronic constriction injury of sciatic nerve and morphine tolerance of rats]*. Yao Xue Xue Bao, 2009. **44**(6): p. 581-5.
296. Wang, W., et al., *Temporal changes of astrocyte activation and glutamate transporter-1 expression in the spinal cord after spinal nerve ligation-induced neuropathic pain*. Anat Rec (Hoboken), 2008. **291**(5): p. 513-8.
297. Yaster, M., et al., *Effect of inhibition of spinal cord glutamate transporters on inflammatory pain induced by formalin and complete Freund's adjuvant*. Anesthesiology, 2011. **114**(2): p. 412-23.
298. Mirzaei, V., et al., *Comparison of changes in mRNA expression of spinal glutamate transporters following induction of two neuropathic pain models*. Spinal Cord, 2010. **48**(11): p. 791-7.
299. Yang, W. and M.S. Kilberg, *Biosynthesis, intracellular targeting, and degradation of the EAAC1 glutamate/aspartate transporter in C6 glioma cells*. J Biol Chem, 2002. **277**(41): p. 38350-7.
300. Trotti, D., et al., *Inhibition of the glutamate transporter EAAC1 expressed in Xenopus oocytes by phorbol esters*. Brain Res, 2001. **914**(1-2): p. 196-203.
301. Minami, T., et al., *Characterization of the glutamatergic system for induction and maintenance of allodynia*. Brain Res, 2001. **895**(1-2): p. 178-85.
302. Niederberger, E., et al., *Modulation of spinal nociceptive processing through the glutamate transporter GLT-1*. Neuroscience, 2003. **116**(1): p. 81-7.
303. Yang, K.Y., et al., *Blockade of spinal glutamate recycling produces paradoxical antinociception in rats with orofacial inflammatory pain*. Prog Neuropsychopharmacol Biol Psychiatry, 2015. **57**: p. 100-9.
304. Asghar, A.U., G.C. Bird, and A.E. King, *Glutamate uptake inhibition modulates dorsal horn neurotransmission: a comparison between normal and arthritic rats*. Neuroreport, 2001. **12**(18): p. 4061-4.
305. Hobo, S., J.C. Eisenach, and K. Hayashida, *Up-regulation of spinal glutamate transporters contributes to anti-hypersensitive effects of valproate in rats after peripheral nerve injury*. Neurosci Lett, 2011. **502**(1): p. 52-5.
306. Ackerman, A.L., et al., *Glt1 glutamate receptor mediates the establishment and perpetuation of chronic visceral pain in an animal model of stress-induced bladder hyperalgesia*. Am J Physiol Renal Physiol, 2015: p. ajprenal 00297 2015.
307. Mao, Q.X. and T.D. Yang, *Amitriptyline upregulates EAAT1 and EAAT2 in neuropathic pain rats*. Brain Res Bull, 2010. **81**(4-5): p. 424-7.
308. Rothstein, J.D., et al., *Beta-lactam antibiotics offer neuroprotection by increasing glutamate transporter expression*. Nature, 2005. **433**(7021): p. 73-7.
309. Lin, Y., et al., *Increased glial glutamate transporter EAAT2 expression reduces visceral nociceptive response in mice*. Am J Physiol Gastrointest Liver Physiol, 2009. **296**(1): p. G129-34.
310. Gosselin, R.D., et al., *Riluzole normalizes early-life stress-induced visceral hypersensitivity in rats: role of spinal glutamate reuptake mechanisms*. Gastroenterology, 2010. **138**(7): p. 2418-25.
311. Galer, B.S., et al., *Lack of efficacy of riluzole in the treatment of peripheral neuropathic pain conditions*. Neurology, 2000. **55**(7): p. 971-5.
312. Maeda, S., et al., *Gene transfer of GLT-1, a glial glutamate transporter, into the spinal cord by recombinant adenovirus attenuates inflammatory and neuropathic pain in rats*. Mol Pain, 2008. **4**: p. 65.
313. Jong, Y.J., V. Kumar, and K.L. O'Malley, *Intracellular metabotropic glutamate receptor 5 (mGluR5) activates signaling cascades distinct from cell surface counterparts*. J Biol Chem, 2009. **284**(51): p. 35827-38.
314. Cameron, N.E., et al., *Vascular factors and metabolic interactions in the pathogenesis of diabetic neuropathy*. Diabetologia, 2001. **44**(11): p. 1973-88.
315. Moalem, G. and D.J. Tracey, *Immune and inflammatory mechanisms in neuropathic pain*. Brain Res Rev, 2006. **51**(2): p. 240-64.

316. Farquhar-Smith, P., *Chemotherapy-induced neuropathic pain*. *Curr Opin Support Palliat Care*, 2011. **5**(1): p. 1-7.
317. Wall, P.D., J.W. Scadding, and M.M. Tomkiewicz, *The production and prevention of experimental anesthesia dolorosa*. *Pain*, 1979. **6**(2): p. 175-82.
318. Wall, P.D., et al., *Autotomy following peripheral nerve lesions: experimental anaesthesia dolorosa*. *Pain*, 1979. **7**(2): p. 103-11.
319. Bennett, G.J. and Y.K. Xie, *A peripheral mononeuropathy in rat that produces disorders of pain sensation like those seen in man*. *Pain*, 1988. **33**(1): p. 87-107.
320. Sugimoto, T., G.J. Bennett, and K.C. Kajander, *Transsynaptic degeneration in the superficial dorsal horn after sciatic nerve injury: effects of a chronic constriction injury, transection, and strychnine*. *Pain*, 1990. **42**(2): p. 205-13.
321. Bridges, D., S.W. Thompson, and A.S. Rice, *Mechanisms of neuropathic pain*. *Br J Anaesth*, 2001. **87**(1): p. 12-26.
322. Ro, L.S., et al., *Effect of NGF and anti-NGF on neuropathic pain in rats following chronic constriction injury of the sciatic nerve*. *Pain*, 1999. **79**(2-3): p. 265-74.
323. Seltzer, Z., R. Dubner, and Y. Shir, *A novel behavioral model of neuropathic pain disorders produced in rats by partial sciatic nerve injury*. *Pain*, 1990. **43**(2): p. 205-18.
324. Kinnman, E. and J.D. Levine, *Sensory and sympathetic contributions to nerve injury-induced sensory abnormalities in the rat*. *Neuroscience*, 1995. **64**(3): p. 751-67.
325. Kim, S.H. and J.M. Chung, *An experimental model for peripheral neuropathy produced by segmental spinal nerve ligation in the rat*. *Pain*, 1992. **50**(3): p. 355-63.
326. Challa, S.R., *Surgical animal models of neuropathic pain: Pros and Cons*. *Int J Neurosci*, 2015. **125**(3): p. 170-4.
327. Li, L., et al., *Effect of lumbar 5 ventral root transection on pain behaviors: a novel rat model for neuropathic pain without axotomy of primary sensory neurons*. *Exp Neurol*, 2002. **175**(1): p. 23-34.
328. Decosterd, I. and C.J. Woolf, *Spared nerve injury: an animal model of persistent peripheral neuropathic pain*. *Pain*, 2000. **87**(2): p. 149-58.
329. Vogel, C., et al., *Absence of thermal hyperalgesia in serotonin transporter-deficient mice*. *J Neurosci*, 2003. **23**(2): p. 708-15.
330. Obata, K., et al., *Role of mitogen-activated protein kinase activation in injured and intact primary afferent neurons for mechanical and heat hypersensitivity after spinal nerve ligation*. *J Neurosci*, 2004. **24**(45): p. 10211-22.
331. Koltzenburg, M., *Painful neuropathies*. *Curr Opin Neurol*, 1998. **11**(5): p. 515-21.
332. Woolf, C.J. and R.J. Mannion, *Neuropathic pain: aetiology, symptoms, mechanisms, and management*. *Lancet*, 1999. **353**(9168): p. 1959-64.
333. Hong, Y. and F.V. Abbott, *Behavioural effects of intraplantar injection of inflammatory mediators in the rat*. *Neuroscience*, 1994. **63**(3): p. 827-36.
334. Damas, J. and J.F. Liegeois, *The inflammatory reaction induced by formalin in the rat paw*. *Naunyn Schmiedebergs Arch Pharmacol*, 1999. **359**(3): p. 220-7.
335. Meller, S.T. and G.F. Gebhart, *Intraplantar zymosan as a reliable, quantifiable model of thermal and mechanical hyperalgesia in the rat*. *Eur J Pain*, 1997. **1**(1): p. 43-52.
336. Hunskaar, S. and K. Hole, *The formalin test in mice: dissociation between inflammatory and non-inflammatory pain*. *Pain*, 1987. **30**(1): p. 103-14.
337. Winter, C.A., E.A. Risley, and G.W. Nuss, *Carrageenin-induced edema in hind paw of the rat as an assay for antiinflammatory drugs*. *Proc Soc Exp Biol Med*, 1962. **111**: p. 544-7.
338. Hargreaves, K., et al., *A new and sensitive method for measuring thermal nociception in cutaneous hyperalgesia*. *Pain*, 1988. **32**(1): p. 77-88.

339. Thomson, A.W. and C.H. Horne, *Toxicity of various carrageenans in the mouse*. Br J Exp Pathol, 1976. **57**(4): p. 455-9.
340. Thomson, A.W. and E.F. Fowler, *Carrageenan: a review of its effects on the immune system*. Agents Actions, 1981. **11**(3): p. 265-73.
341. Freund, J., *The mode of action of immunologic adjuvants*. Bibl Tuberc, 1956(10): p. 130-48.
342. Courtenay, J.S., et al., *Immunisation against heterologous type II collagen induces arthritis in mice*. Nature, 1980. **283**(5748): p. 666-8.
343. Billiau, A. and P. Matthys, *Modes of action of Freund's adjuvants in experimental models of autoimmune diseases*. J Leukoc Biol, 2001. **70**(6): p. 849-60.
344. Lorentzen, J.C., et al., *Protracted, relapsing and demyelinating experimental autoimmune encephalomyelitis in DA rats immunized with syngeneic spinal cord and incomplete Freund's adjuvant*. J Neuroimmunol, 1995. **63**(2): p. 193-205.
345. Raghavendra, V., F.Y. Tanga, and J.A. DeLeo, *Complete Freund's adjuvant-induced peripheral inflammation evokes glial activation and proinflammatory cytokine expression in the CNS*. Eur J Neurosci, 2004. **20**(2): p. 467-73.
346. Ren, K., *An improved method for assessing mechanical allodynia in the rat*. Physiol Behav, 1999. **67**(5): p. 711-6.
347. Whiteside, G.T., A. Adedoyin, and L. Leventhal, *Predictive validity of animal pain models? A comparison of the pharmacokinetic-pharmacodynamic relationship for pain drugs in rats and humans*. Neuropharmacology, 2008. **54**(5): p. 767-75.
348. Chaplan, S.R., et al., *Quantitative assessment of tactile allodynia in the rat paw*. J Neurosci Methods, 1994. **53**(1): p. 55-63.
349. Dixon, W.J., *Efficient analysis of experimental observations*. Annu Rev Pharmacol Toxicol, 1980. **20**: p. 441-62.
350. Bonin, R.P., C. Bories, and Y. De Koninck, *A simplified up-down method (SUDO) for measuring mechanical nociception in rodents using von Frey filaments*. Mol Pain, 2014. **10**: p. 26.
351. Liu, S.S. and P.D. Ware, *Differential sensory block after spinal bupivacaine in volunteers*. Anesth Analg, 1997. **84**(1): p. 115-9.
352. Rolke, R., et al., *Quantitative sensory testing in the German Research Network on Neuropathic Pain (DFNS): standardized protocol and reference values*. Pain, 2006. **123**(3): p. 231-43.
353. Mills, C., et al., *Estimating efficacy and drug ED50's using von Frey thresholds: impact of weber's law and log transformation*. J Pain, 2012. **13**(6): p. 519-23.
354. Chellman, G.J., et al., *Rat paw-lick/muscle irritation model for evaluating parenteral formulations for pain-on-injection and muscle damage*. Fundam Appl Toxicol, 1990. **15**(4): p. 697-709.
355. Vos, B.P., G. Hans, and H. Adriaensen, *Behavioral assessment of facial pain in rats: face grooming patterns after painful and non-painful sensory disturbances in the territory of the rat's infraorbital nerve*. Pain, 1998. **76**(1-2): p. 173-8.
356. Han, J.S., et al., *Computerized analysis of audible and ultrasonic vocalizations of rats as a standardized measure of pain-related behavior*. J Neurosci Methods, 2005. **141**(2): p. 261-9.
357. Langford, D.J., et al., *Coding of facial expressions of pain in the laboratory mouse*. Nat Methods, 2010. **7**(6): p. 447-9.
358. Kokka, N. and A.S. Fairhurst, *Naloxone enhancement of acetic acid-induced writhing in rats*. Life Sci, 1977. **21**(7): p. 975-80.
359. Clatworthy, A.L., et al., *Role of peri-axonal inflammation in the development of thermal hyperalgesia and guarding behavior in a rat model of neuropathic pain*. Neurosci Lett, 1995. **184**(1): p. 5-8.
360. Landis, C.A., J.D. Levine, and C.R. Robinson, *Decreased slow-wave and paradoxical sleep in a rat chronic pain model*. Sleep, 1989. **12**(2): p. 167-77.

361. Li, X. and J.D. Clark, *Hyperalgesia during opioid abstinence: mediation by glutamate and substance p*. *Anesth Analg*, 2002. **95**(4): p. 979-84, table of contents.
362. Kalueff, A.V. and P. Tuohimaa, *The grooming analysis algorithm discriminates between different levels of anxiety in rats: potential utility for neurobehavioural stress research*. *J Neurosci Methods*, 2005. **143**(2): p. 169-77.
363. Sufka, K.J., *Conditioned place preference paradigm: a novel approach for analgesic drug assessment against chronic pain*. *Pain*, 1994. **58**(3): p. 355-66.
364. Tzschentke, T.M., *Measuring reward with the conditioned place preference paradigm: a comprehensive review of drug effects, recent progress and new issues*. *Prog Neurobiol*, 1998. **56**(6): p. 613-72.
365. van der Kooy, D., et al., *Reinforcing effects of brain microinjections of morphine revealed by conditioned place preference*. *Brain Res*, 1982. **243**(1): p. 107-17.
366. Narita, M., et al., *Comparative pharmacological profiles of morphine and oxycodone under a neuropathic pain-like state in mice: evidence for less sensitivity to morphine*. *Neuropsychopharmacology*, 2008. **33**(5): p. 1097-112.
367. Park, H.J., et al., *Persistent hyperalgesia in the cisplatin-treated mouse as defined by threshold measures, the conditioned place preference paradigm, and changes in dorsal root ganglia activated transcription factor 3: the effects of gabapentin, ketorolac, and etanercept*. *Anesth Analg*, 2013. **116**(1): p. 224-31.
368. Cunningham, C.L., N.K. Ferree, and M.A. Howard, *Apparatus bias and place conditioning with ethanol in mice*. *Psychopharmacology (Berl)*, 2003. **170**(4): p. 409-22.
369. Le Foll, B. and S.R. Goldberg, *Nicotine induces conditioned place preferences over a large range of doses in rats*. *Psychopharmacology (Berl)*, 2005. **178**(4): p. 481-92.
370. Djouhri, L., et al., *Time course and nerve growth factor dependence of inflammation-induced alterations in electrophysiological membrane properties in nociceptive primary afferent neurons*. *J Neurosci*, 2001. **21**(22): p. 8722-33.
371. Abbadie, C., et al., *Spinal cord substance P receptor immunoreactivity increases in both inflammatory and nerve injury models of persistent pain*. *Neuroscience*, 1996. **70**(1): p. 201-9.
372. Okun, A., et al., *Transient inflammation-induced ongoing pain is driven by TRPV1 sensitive afferents*. *Mol Pain*, 2011. **7**: p. 4.
373. Kumar, N., et al., *Metabotropic glutamate receptors (mGluRs) regulate noxious stimulus-induced glutamate release in the spinal cord dorsal horn of rats with neuropathic and inflammatory pain*. *J Neurochem*, 2010. **114**(1): p. 281-90.
374. Urca, G. and G. Raigorodsky, *Behavioral classification of excitatory amino acid receptors in mouse spinal cord*. *Eur J Pharmacol*, 1988. **153**(2-3): p. 211-20.
375. Dolan, S. and A.M. Nolan, *Blockade of metabotropic glutamate receptor 5 activation inhibits mechanical hypersensitivity following abdominal surgery*. *Eur J Pain*, 2007. **11**(6): p. 644-51.
376. Mills, C.D., S.D. Fullwood, and C.E. Hulsebosch, *Changes in metabotropic glutamate receptor expression following spinal cord injury*. *Exp Neurol*, 2001. **170**(2): p. 244-57.
377. Xu, G.Y., et al., *Concentrations of glutamate released following spinal cord injury kill oligodendrocytes in the spinal cord*. *Exp Neurol*, 2004. **187**(2): p. 329-36.
378. Vetter, G., G. Geisslinger, and I. Tegeder, *Release of glutamate, nitric oxide and prostaglandin E2 and metabolic activity in the spinal cord of rats following peripheral nociceptive stimulation*. *Pain*, 2001. **92**(1-2): p. 213-8.
379. Skilling, S.R., et al., *Extracellular amino acid concentrations in the dorsal spinal cord of freely moving rats following veratridine and nociceptive stimulation*. *J Neurochem*, 1988. **51**(1): p. 127-32.
380. Dmitrieva, N., et al., *Differential release of neurotransmitters from superficial and deep layers of the dorsal horn in response to acute noxious stimulation and inflammation of the rat paw*. *Eur J Pain*, 2004. **8**(3): p. 245-52.

381. Panter, S.S., S.W. Yum, and A.I. Faden, *Alteration in extracellular amino acids after traumatic spinal cord injury*. *Ann Neurol*, 1990. **27**(1): p. 96-9.
382. Lawand, N.B., T. McNearney, and K.N. Westlund, *Amino acid release into the knee joint: key role in nociception and inflammation*. *Pain*, 2000. **86**(1-2): p. 69-74.
383. Sung, B., et al., *Altered spinal arachidonic acid turnover after peripheral nerve injury regulates regional glutamate concentration and neuropathic pain behaviors in rats*. *Pain*, 2007. **131**(1-2): p. 121-31.
384. Curran, T. and J.I. Morgan, *Memories of fos*. *Bioessays*, 1987. **7**(6): p. 255-8.
385. Hughes, P. and M. Dragunow, *Induction of immediate-early genes and the control of neurotransmitter-regulated gene expression within the nervous system*. *Pharmacol Rev*, 1995. **47**(1): p. 133-78.
386. Anton, F., et al., *c-FOS-like immunoreactivity in rat brainstem neurons following noxious chemical stimulation of the nasal mucosa*. *Neuroscience*, 1991. **41**(2-3): p. 629-41.
387. Herdegen, T., et al., *Sequential expression of JUN B, JUN D and FOS B proteins in rat spinal neurons: cascade of transcriptional operations during nociception*. *Neurosci Lett*, 1991. **129**(2): p. 221-4.
388. Herdegen, T., et al., *Specific temporal and spatial distribution of JUN, FOS, and KROX-24 proteins in spinal neurons following noxious transsynaptic stimulation*. *J Comp Neurol*, 1991. **313**(1): p. 178-91.
389. Watson, L., et al., *JNK and c-Jun but not ERK and c-Fos are associated with sustained neointima-formation after balloon injury*. *Eur J Clin Invest*, 2000. **30**(1): p. 11-7.
390. Herdegen, T., et al., *The transcription factors c-JUN, JUN D and CREB, but not FOS and KROX-24, are differentially regulated in axotomized neurons following transection of rat sciatic nerve*. *Brain Res Mol Brain Res*, 1992. **14**(3): p. 155-65.
391. Dunlop, J., Z. Lou, and H.B. McIlvain, *Properties of excitatory amino acid transport in the human U373 astrocytoma cell line*. *Brain Res*, 1999. **839**(2): p. 235-42.
392. Sun, W., et al., *Specificity and actions of an arylaspartate inhibitor of glutamate transport at the Schaffer collateral-CA1 pyramidal cell synapse*. *PLoS One*, 2011. **6**(8): p. e23765.
393. Peghini, P., J. Janzen, and W. Stoffel, *Glutamate transporter EAAC-1-deficient mice develop dicarboxylic aminoaciduria and behavioral abnormalities but no neurodegeneration*. *EMBO J*, 1997. **16**(13): p. 3822-32.
394. Niederberger, E., et al., *The glutamate transporter GLAST is involved in spinal nociceptive processing*. *Biochem Biophys Res Commun*, 2006. **346**(2): p. 393-9.
395. Rossi, D.J., T. Oshima, and D. Attwell, *Glutamate release in severe brain ischaemia is mainly by reversed uptake*. *Nature*, 2000. **403**(6767): p. 316-21.
396. Benani, A., et al., *Up-regulation of fatty acid metabolizing-enzymes mRNA in rat spinal cord during persistent peripheral local inflammation*. *Eur J Neurosci*, 2003. **18**(7): p. 1904-14.
397. Neto, F.L., et al., *Supraspinal metabolic activity changes in the rat during adjuvant monoarthritis*. *Neuroscience*, 1999. **94**(2): p. 607-21.
398. Schadrack, J., et al., *Metabolic activity changes in the rat spinal cord during adjuvant monoarthritis*. *Neuroscience*, 1999. **94**(2): p. 595-605.
399. Inquimbert, P., et al., *Peripheral nerve injury produces a sustained shift in the balance between glutamate release and uptake in the dorsal horn of the spinal cord*. *Pain*, 2012. **153**(12): p. 2422-31.
400. Choi, D.W., *Ionic dependence of glutamate neurotoxicity*. *J Neurosci*, 1987. **7**(2): p. 369-79.
401. Maki, R., M.B. Robinson, and M.A. Dichter, *The glutamate uptake inhibitor L-trans-pyrrolidine-2,4-dicarboxylate depresses excitatory synaptic transmission via a presynaptic mechanism in cultured hippocampal neurons*. *J Neurosci*, 1994. **14**(11 Pt 1): p. 6754-62.
402. Simmons, R.M., et al., *Group II mGluR receptor agonists are effective in persistent and neuropathic pain models in rats*. *Pharmacol Biochem Behav*, 2002. **73**(2): p. 419-27.
403. Lefebvre, C., et al., *Evidence that DHPG-induced nociception depends on glutamate release from primary afferent C-fibres*. *Neuroreport*, 2000. **11**(8): p. 1631-5.

404. Kingston, A.E., et al., *Inhibition of group I metabotropic glutamate receptor responses in vivo in rats by a new generation of carboxyphenylglycine-like amino acid antagonists*. *Neurosci Lett*, 2002. **330**(2): p. 127-30.
405. Murty, S.B. and R.B. Murty, *Delivery systems for improving oral bioavailability of fenobam, its hydrates, and salts*. 2013, Google Patents.
406. Wallberg, A., et al., *Phenyl ureas of creatinine as mGluR5 antagonists. A structure-activity relationship study of fenobam analogues*. *Bioorg Med Chem Lett*, 2006. **16**(5): p. 1142-5.
407. Chen, Y., et al., *Evaluation of the activity of a novel metabotropic glutamate receptor antagonist (+/-)-2-amino-2-(3-cis and trans-carboxycyclobutyl-3-(9-thioxanthyl)propionic acid) in the in vitro neonatal spinal cord and in an in vivo pain model*. *Neuroscience*, 2000. **95**(3): p. 787-93.
408. Zhang, L., et al., *Group I metabotropic glutamate receptor antagonists block secondary thermal hyperalgesia in rats with knee joint inflammation*. *J Pharmacol Exp Ther*, 2002. **300**(1): p. 149-56.
409. Kanai, Y. and M.A. Hediger, *The glutamate/neutral amino acid transporter family SLC1: molecular, physiological and pharmacological aspects*. *Pflügers Arch*, 2004. **447**(5): p. 469-79.
410. Shigeri, Y., R.P. Seal, and K. Shimamoto, *Molecular pharmacology of glutamate transporters, EAATs and VGLUTs*. *Brain Res Brain Res Rev*, 2004. **45**(3): p. 250-65.
411. Schikorski, T. and C.F. Stevens, *Quantitative ultrastructural analysis of hippocampal excitatory synapses*. *J Neurosci*, 1997. **17**(15): p. 5858-67.
412. Esseltine, J.L. and S.S. Ferguson, *Regulation of G protein-coupled receptor trafficking and signaling by Rab GTPases*. *Small GTPases*, 2013. **4**(2): p. 132-5.
413. Tu, J.C., et al., *Homer binds a novel proline-rich motif and links group 1 metabotropic glutamate receptors with IP3 receptors*. *Neuron*, 1998. **21**(4): p. 717-26.
414. Xiao, B., et al., *Homer regulates the association of group 1 metabotropic glutamate receptors with multivalent complexes of homer-related, synaptic proteins*. *Neuron*, 1998. **21**(4): p. 707-16.
415. Soloviev, M.M., et al., *Mouse brain and muscle tissues constitutively express high levels of Homer proteins*. *Eur J Biochem*, 2000. **267**(3): p. 634-9.
416. Vazdarjanova, A., et al., *Experience-dependent coincident expression of the effector immediate-early genes arc and Homer 1a in hippocampal and neocortical neuronal networks*. *J Neurosci*, 2002. **22**(23): p. 10067-71.
417. Roche, K.W., et al., *Homer 1b regulates the trafficking of group I metabotropic glutamate receptors*. *J Biol Chem*, 1999. **274**(36): p. 25953-7.
418. Ango, F., et al., *Dendritic and axonal targeting of type 5 metabotropic glutamate receptor is regulated by homer1 proteins and neuronal excitation*. *J Neurosci*, 2000. **20**(23): p. 8710-6.
419. Tappe, A., et al., *Synaptic scaffolding protein Homer1a protects against chronic inflammatory pain*. *Nat Med*, 2006. **12**(6): p. 677-81.
420. Ma, Z.L., et al., *Effect of the synaptic scaffolding protein Homer1a on chronic compression of dorsal root ganglion*. *Ann Clin Lab Sci*, 2009. **39**(1): p. 71-5.
421. Miletic, G., et al., *Early changes in Homer1 proteins in the spinal dorsal horn are associated with loose ligation of the rat sciatic nerve*. *Anesth Analg*, 2009. **109**(6): p. 2000-7.
422. Dolen, G. and M.F. Bear, *Role for metabotropic glutamate receptor 5 (mGluR5) in the pathogenesis of fragile X syndrome*. *J Physiol*, 2008. **586**(6): p. 1503-8.
423. Aronica, E., et al., *Immunohistochemical localization of group I and II metabotropic glutamate receptors in control and amyotrophic lateral sclerosis human spinal cord: upregulation in reactive astrocytes*. *Neuroscience*, 2001. **105**(2): p. 509-20.
424. Matosin, N. and K.A. Newell, *Metabotropic glutamate receptor 5 in the pathology and treatment of schizophrenia*. *Neurosci Biobehav Rev*, 2013. **37**(3): p. 256-68.
425. Kandratavicius, L., et al., *Distinct increased metabotropic glutamate receptor type 5 (mGluR5) in temporal lobe epilepsy with and without hippocampal sclerosis*. *Hippocampus*, 2013. **23**(12): p. 1212-30.

426. O'Donnell, W.T. and S.T. Warren, *A decade of molecular studies of fragile X syndrome*. Annu Rev Neurosci, 2002. **25**: p. 315-38.
427. Park, S., et al., *Elongation factor 2 and fragile X mental retardation protein control the dynamic translation of Arc/Arg3.1 essential for mGluR-LTD*. Neuron, 2008. **59**(1): p. 70-83.
428. Dolen, G., et al., *Correction of fragile X syndrome in mice*. Neuron, 2007. **56**(6): p. 955-62.
429. Ronesi, J.A., et al., *Disrupted Homer scaffolds mediate abnormal mGluR5 function in a mouse model of fragile X syndrome*. Nat Neurosci, 2012. **15**(3): p. 431-40, S1.
430. FRAXA, *Novartis Discontinues Development of mavuglurant (AFQ056) for Fragile X Syndrome*. 2014.
431. Jacquemont, S., et al., *Epigenetic modification of the FMR1 gene in fragile X syndrome is associated with differential response to the mGluR5 antagonist AFQ056*. Sci Transl Med, 2011. **3**(64): p. 64ra1.
432. Bhave, G., et al., *Membrane topology of a metabotropic glutamate receptor*. J Biol Chem, 2003. **278**(32): p. 30294-301.
433. Ioannidis, J.P., *Why most published research findings are false*. PLoS Med, 2005. **2**(8): p. e124.
434. Open Science, C., *PSYCHOLOGY. Estimating the reproducibility of psychological science*. Science, 2015. **349**(6251): p. aac4716.
435. Prinz, F., T. Schlange, and K. Asadullah, *Believe it or not: how much can we rely on published data on potential drug targets?* Nat Rev Drug Discov, 2011. **10**(9): p. 712.
436. Sergin, I., et al., *Sequences within the C Terminus of the Metabotropic Glutamate Receptor 5 (mGluR5) Are Responsible for Inner Nuclear Membrane Localization*. J Biol Chem, 2017. **292**(9): p. 3637-3655.
437. Miletic, G., et al., *Increased levels of Homer1b/c and Shank1a in the post-synaptic density of spinal dorsal horn neurons are associated with neuropathic pain in rats*. Neurosci Lett, 2005. **386**(3): p. 189-93.
438. Font, J., et al., *Optical control of pain in vivo with a photoactive mGlu5 receptor negative allosteric modulator*. Elife, 2017. **6**.

Appendix I: Vincent et al. 2016

*Provided with permission from the authors

ARTICLE

Received 19 Sep 2015 | Accepted 4 Jan 2016 | Published 3 Feb 2016

DOI: 10.1038/ncomms10604

OPEN

Intracellular mGluR5 plays a critical role in neuropathic pain

Kathleen Vincent^{1,2,*}, Virginia M. Cornea^{1,2,*}, Yuh-Jiin I. Jong³, André Laferrière^{1,2}, Naresh Kumar^{1,2}, Aiste Mickeviciute^{1,2}, Jollee S.T. Fung^{1,2}, Pouya Bandegi^{1,2}, Alfredo Ribeiro-da-Silva^{1,4}, Karen L. O'Malley³ & Terence J. Coderre^{1,2}

Spinal mGluR5 is a key mediator of neuroplasticity underlying persistent pain. Although brain mGluR5 is localized on cell surface and intracellular membranes, neither the presence nor physiological role of spinal intracellular mGluR5 is established. Here we show that in spinal dorsal horn neurons >80% of mGluR5 is intracellular, of which ~60% is located on nuclear membranes, where activation leads to sustained Ca²⁺ responses. Nerve injury inducing nociceptive hypersensitivity also increases the expression of nuclear mGluR5 and receptor-mediated phosphorylated-ERK1/2, Arc/Arg3.1 and c-fos. Spinal blockade of intracellular mGluR5 reduces neuropathic pain behaviours and signalling molecules, whereas blockade of cell-surface mGluR5 has little effect. Decreasing intracellular glutamate via blocking EAAT-3, mimics the effects of intracellular mGluR5 antagonism. These findings show a direct link between an intracellular GPCR and behavioural expression *in vivo*. Blockade of intracellular mGluR5 represents a new strategy for the development of effective therapies for persistent pain.

¹ Alan Edwards Centre for Research on Pain, McGill University, 3655 Promenade Sir William Osler, Montreal, Quebec, Canada H3G 1Y6. ² Department of Anesthesia, McGill University, 3655 Promenade Sir William Osler, Montreal, Quebec, Canada H3G 1Y6. ³ Department of Anatomy & Neurobiology, Washington University School of Medicine, 660 South Euclid Avenue, St Louis, Missouri 63110, USA. ⁴ Department of Pharmacology & Therapeutics, McGill University, 3655 Promenade Sir William Osler, Montreal, Quebec, Canada H3G 1Y6. * These authors contributed equally to this work. Correspondence and requests for materials should be addressed to K.L.O. (email: omalleyk@wustl.edu) or to T.J.C. (email: terence.coderre@mcgill.ca).

Many G-protein-coupled receptors (GPCRs) are not only expressed at the cell surface but also on various intracellular membranes including the nucleus^{1–12}. Although intracellular GPCRs have been shown to play critical roles in gene transcription, ionic homeostasis, cell proliferation, neural circuit remodelling and synaptic plasticity^{2,5–7,12}, the physiological relevance of intracellular receptors in intact organisms remains unknown^{1–12}. Metabotropic glutamate 5 receptor (mGluR5) is a GPCR associated with both cell surface and intracellular membranes in striatum, hippocampus and visual cortex, where it couples with $G_{q/11}$ /PLC/IP₃ to release cytoplasmic and nucleoplasmic calcium (Ca^{2+})^{7–11}. Intracellular mGluR5 is activated following glutamate transport into the cell via excitatory amino-acid transporters (EAATs), or cysteine–glutamate exchangers (xCT), located on cell surface and endoplasmic reticular (ER) membranes⁸. Selective activation of intracellular versus cell-surface mGluR5 triggers unique Ca^{2+} patterns and downstream signalling cascades associated with each receptor pool^{7–10,12}.

mGluR5 is abundantly expressed in neurons of the spinal cord dorsal horn (SCDH)^{13,14}, which serves as the first CNS relay in the transmission of nociceptive information¹⁵. SCDH mGluR5 plays a key role in glutamate-induced plasticity of pain-related processes, including nociceptive hypersensitivity after nerve injury^{16–18}. Specifically, spinal mGluR5 activation induces nociception in normal animals^{19,20}, while its blockade produces analgesia^{16–18}. Despite spinal mGluR5's key role in neuropathic pain^{16–18}, it remains unknown whether its effects are due to cell surface or intracellular signalling.

Here we show that mGluR5 and associated effector molecules are increased on SCDH nuclear membranes following spared-nerve injury (SNI), a model of neuropathic pain²¹. Nuclear receptor-associated generation of downstream messengers are also increased. Blockade of spinal intracellular mGluR5 inhibits pain behaviours and mGluR5-linked signalling molecules in nerve-injured rats, whereas blockade of cell surface mGluR5 has little effect. Finally, inhibition of spinal EAAT3 mimics the effects of intracellular mGluR5 antagonism by preventing intracellular uptake of ligand. Our results demonstrate a selective involvement of spinal intracellular mGluR5 in pain processing and provide *in vivo* evidence for a pathophysiological function of a GPCR associated with intracellular membranes.

Results

SCDH nuclear mGluR5 activates nuclear Ca^{2+} responses. We used immunocytochemistry in neonatal SCDH cultures, as well as sections and cellular fractions of adult lumbar (L4–L6) tissue to assess the subcellular distribution of mGluR5. We found SCDH cultures expressed mGluR5 on the cell surface, dendrites and on intracellular membranes including the nucleus where mGluR5 colocalized with lamin-B₂, a nuclear envelope marker (Fig. 1a; upper panels). Detectable mGluR5 staining was seen only on neurons, identified with the neuronal nuclear antigen, NeuN (Fig. 1a; lower panels). Depending on the tissue preparation, mGluR5-positive neurons constituted ~30% of the cells plated. Electron microscopy was used to assess mGluR5 subcellular localization in adult rat SCDH with pre-embedding, silver-intensified immunogold labelling. mGluR5 was detected on the plasma membrane and intracellularly especially on nuclear membranes (Fig. 1b,c). Nuclear mGluR5 was only detected on SCDH neurons; glial and endothelial cell nuclei were not labelled (Fig. 1b; Supplementary Fig. 1a,b). No mGluR5 labelling occurred in the absence of primary antibody (Supplementary Fig. 1c), and mGluR5 labelling was prevented by preincubation of primary antibody with a specific mGluR5 blocking peptide

(Supplementary Fig. 1d). Subfractionation studies showed mGluR5 in both nuclear and plasma membrane fractions, indicated by membrane-specific markers, lamin-B₂ and pan-cadherin (Pan-Cad), respectively (Fig. 1d). The neuronal sodium-dependent EAAT3 was also found on nuclear and plasma membranes (Fig. 1d). The ratio of nuclear to plasma membrane protein was higher for mGluR5 than for EAAT3 (Fig. 1e). Thus, mGluR5 is highly expressed on intracellular and especially nuclear membranes of SCDH neurons.

Striatal and hippocampal intracellular mGluR5 can be activated by agonist uptake via glutamate transporters/exchangers^{7–10}. Alternatively, intracellular receptors can be modulated by permeable ligands. Permeability can be gauged using published lipophilicity values (LogP) where values > 2 are considered membrane permeable²². LogP values indicate that glutamate (– 2.7) and the Group 1, mGluR agonists, quisqualate (LogP, – 3.9) and DHPG (– 2.4) are membrane impermeable, as is the Group 1 antagonist, LY393053 (0.6). In contrast, the mGluR5 antagonist 2-methyl-6-(phenylethynyl)-pyridine (MPEP; 3.3) is membrane permeable^{7–10}. To directly test whether sodium- or chloride-dependent processes were involved in glutamate, quisqualate, DHPG or LY393053 uptake in SCDH neurons, cultures were treated with radiolabelled ligand in the presence and absence of transport or exchange inhibitors. Sodium-dependent transporter activity accounted for ~80% of glutamate, but only ~25% of quisqualate uptake, whereas chloride-dependent uptake, likely via xCT transport, blocked only ~20% of glutamate uptake, but ~50% of quisqualate uptake (Fig. 1f). Sodium- and chloride-free conditions reduced quisqualate and glutamate uptake by > 80% (Fig. 1f). DHPG and LY393053 did not compete with glutamate uptake, confirming their designation as impermeable, non-transported ligands (Fig. 1f). Two potent inhibitors of all EAAT subtypes, three-β-benzyloxyaspartate (TBOA) and three-β-OH-aspartic acid (THA) blocked about 60% of glutamate uptake, whereas L-cystine, a blocker of the xCT exchanger, had no significant effect (Fig. 1f). Thus, sodium-dependent, EAAT-mediated activity primarily accounts for intracellular glutamate uptake.

Since mGluR5 couples to $G_{q/11}$ and PLC to generate IP₃-mediated release of Ca^{2+} , we used Ca^{2+} imaging to test whether activation of intracellular SCDH mGluR5 is functionally active. SCDH cultures grown on glass coverslips were loaded with the Ca^{2+} indicator, Oregon Green BAPTA-AM, and subsequently treated with agonists and/or antagonists with variable intracellular access. Bath application of the impermeable, non-transported DHPG (100 μM) led to a rapid, transient Ca^{2+} rise (Fig. 1g). In contrast, the impermeable, transported agonist, quisqualate (10 μM), produced a long, sustained rise in Ca^{2+} in both the cytoplasm and the nucleus, which was terminated by addition of the permeable mGluR5 antagonist, MPEP (10 μM; Fig. 1h). Although the impermeable antagonist LY393053 blocked DHPG-mediated Ca^{2+} responses (Fig. 1i), it did not affect those induced by quisqualate (Fig. 1j). These data indicate that functional activity is generated by two separate pools of mGluR5—on the cell surface and on intracellular membranes.

Although surface receptors always contribute to the time course of the Ca^{2+} response, their appearance of doing so varies depending on the scan speed at which images are collected. Because SCDH mGluR5-positive neurons are not as abundant as in striatal or hippocampal cultures, a scan speed of 5.36 s per scan was used here to capture a larger area with more neurons. Thus, compiled data in Fig. 1k reflect group differences in which the contribution of the surface receptor is obscured due to the slow scan speed.

Results from multiple experiments assessing drug-induced changes of both the amplitude of the initial Ca^{2+} peak and the

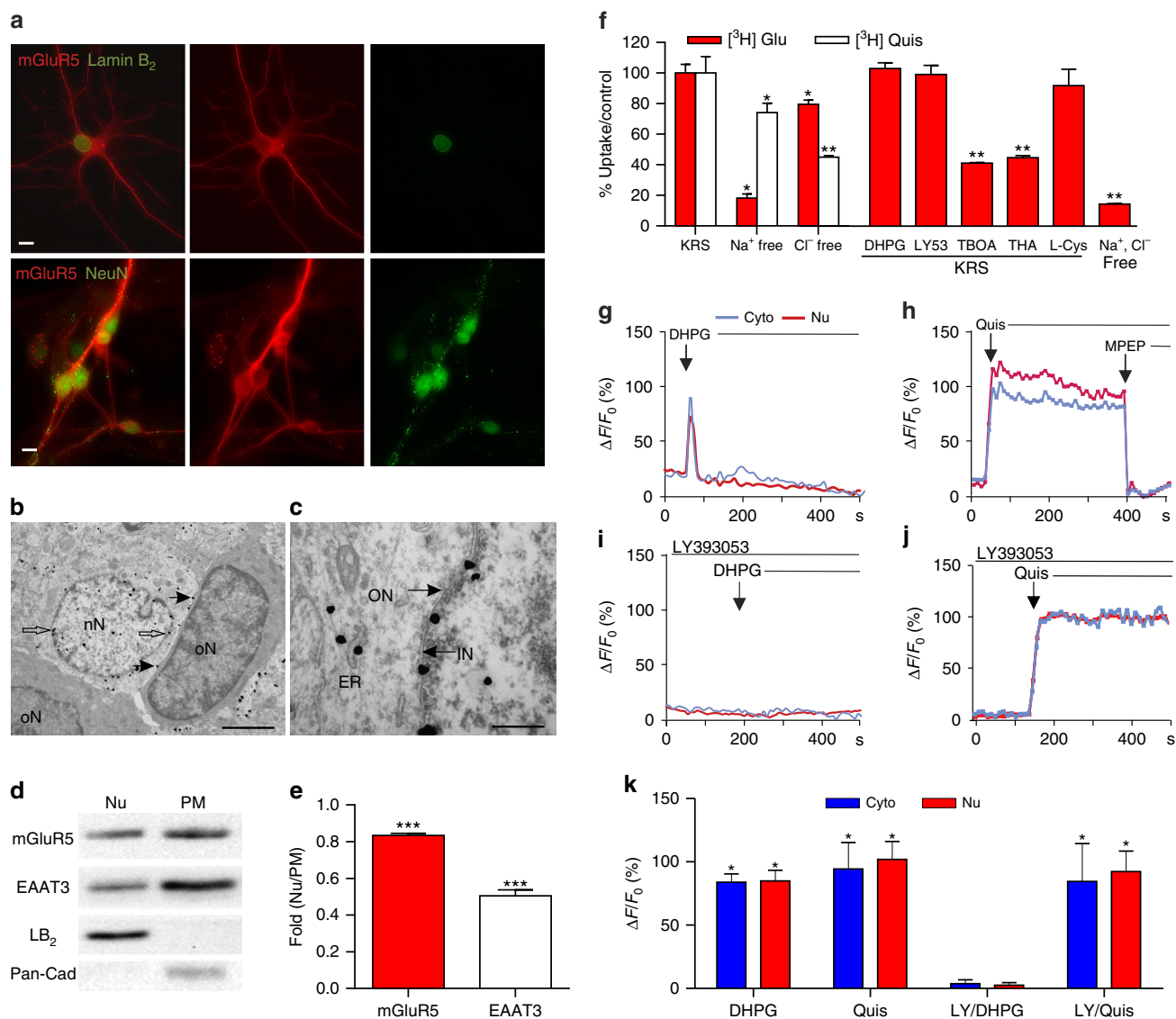


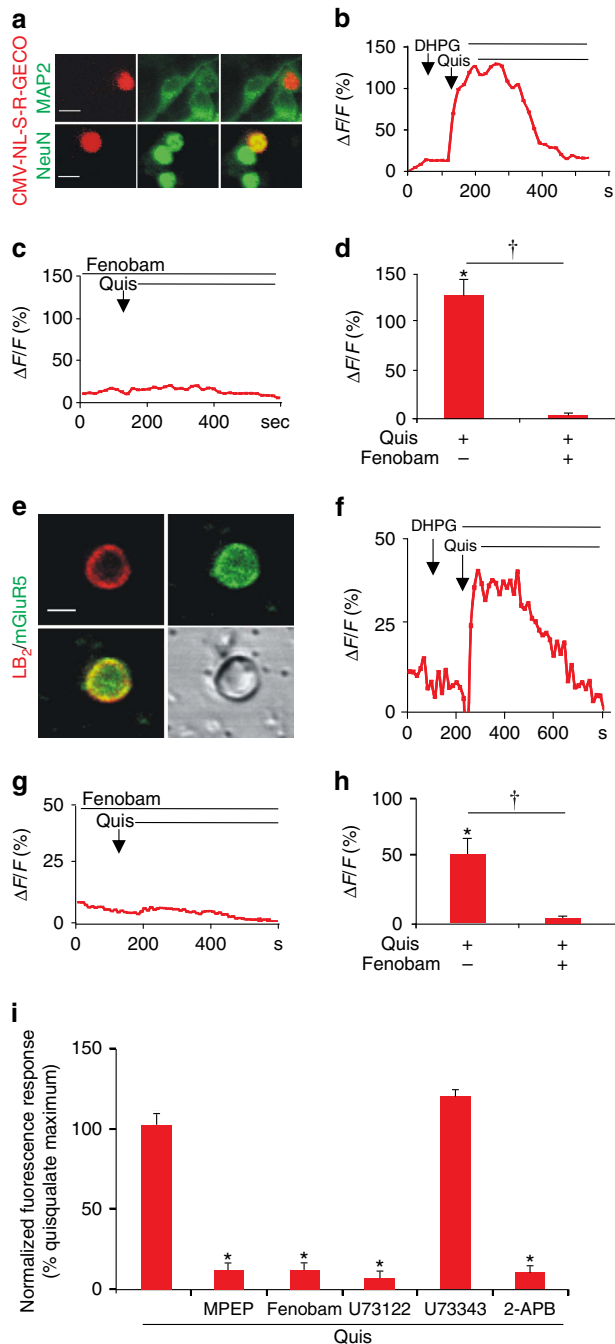
Figure 1 | Functional nuclear mGluR5 in SCDH neurons. Fluorescence-microscopy showing (a) mGluR5 (red), Lamin-B₂ (green-upper) or NeuN-IR (green-lower) in cultured rat SCDH neurons. Scale bar, 10 μm. (b,c) Electron-micrographs showing mGluR5-immunogold in L4-L6 SCDH. Scale bar, (b) 2 μm, (c) 0.5 μm. mGluR5 is detected in cytoplasm and neuronal nuclei (nN), and on nuclear (white arrows) and plasma (black arrows) membranes, but not glial nuclei (oN, oligodendrocyte nucleus) (b). mGluR5 is on inner (IN), and outer (ON), nuclear membranes (black arrows) and on endoplasmic reticular (ER) membranes (c). (d) Western blots of mGluR5, EAAT3, Lamin-B₂ (LB₂), and Pan-cadherin (Pan-Cad) in nuclear (Nu), or plasma membrane (PM) fractions of rat SCDH (L4-L6), quantified in e. Data shown represent the mean of three experiments, Student's *t*-test ****P* < 0.001. (f) [³H]-glutamate (Glu) or [³H]-Quis uptake in cultured rat SCDH neurons with buffer modified as indicated. DHPG (100 μM), LY393053 (LY53: 20 μM), or L-cystine (400 μM) did not block [³H]-Glu uptake, whereas TBOA or THA (100 μM) inhibited it ~60%. Data shown represent the mean of three experiments done in triplicate, Student's *t*-test **P* < 0.05, ***P* < 0.01 compared to KRS. (g-j) Representative traces of cytoplasmic (cyto, blue) or nuclear (red) Ca²⁺ responses to DHPG (100 μM g,i), quisqualate (Quis, 10 μM, h,j), MPEP (10 μM, h) and/or LY393053 (20 μM, i,j) in cultured rat SCDH neurons. (k) Compiled data from maximum response ($\Delta F/F_0$, %) from *N* = 12 identified neurons (g); *N* = 32 identified neurons (h); *N* = 25 identified neurons (i); *N* = 23 identified neurons (j); **P* < 0.05 compared with baseline. All values in figure are expressed as mean ± s.e.m. KRS, Krebs-Ringer solution.

magnitude of the overall Ca²⁺ response revealed that DHPG peak amplitudes (for example, Fig. 1g) were $61.2 \pm 3.56\%$ of the LY393053 + quisqualate peak amplitudes (Fig. 1j) and that at most the DHPG response constituted ~10% ($9.79 \pm 2.27\%$) of the overall quisqualate response (~4 min). Thus, during periods of high activity and/or sustained presynaptic glutamate release, intracellular uptake of glutamate can lead to a Ca²⁺ response that is not only spatially and temporally unique, but also approximately nine times larger than a surface response.

Since Oregon Green Bapta AM is a global Ca²⁺ indicator dye, the specific contribution of nuclear mGluR5 to intracellular Ca²⁺

changes is equivocal. To address this we performed two experiments. First, SCDH neurons were transiently transfected with a genetically encoded Ca²⁺ indicator (pCMV-NL-S-R-GECO) that is restricted to the cell nucleus (Fig. 2a). Once correct targeting to the nucleus was verified, receptor-mediated Ca²⁺ responses were determined as before. Consistent with the previous data, bath application of the impermeable, non-transported agonist, DHPG, did not induce changes in the nuclear-restricted Ca²⁺ indicator, whereas quisqualate did (Fig. 2b). Pretreatment with the cell permeant mGluR5 antagonist fenobam blocked all quisqualate responses (Fig. 2c,d). To more

directly assess nuclear mGluR5 function, isolated nuclei were prepared from P30 L4–6 SCDH. Nuclei were resuspended in intracellular medium, and Oregon Green BAPTA-AM was allowed to accumulate while nuclei were attaching to coated coverslips (Fig. 2e). Although heterogeneous, ~5 to 10% of isolated nuclei were mGluR5 positive (Fig. 2e). Quisqualate, but not DHPG, induced a sustained Ca^{2+} rise (Fig. 2f) that could be blocked by fenobam (Fig. 2g,h). To confirm the presence of mGluR5 on responding nuclei, coverslips were fixed and processed for mGluR5 immunoreactivity combined with lamin B₂ staining and then field-relocated immediately following imaging (Fig. 2e). Responsive nuclei were always mGluR5 positive, although not all mGluR5-positive nuclei responded, possibly due to damage in the course of nuclear preparation. Taken together, these data unequivocally establish that nuclear mGluR5 is functionally active.



To test whether activated intracellular SCDH mGluR5 coupled to PLC to generate IP_3 -mediated release of Ca^{2+} , we used a fluorescence-based Ca^{2+} imaging plate-reader assay. Cells were preincubated with various inhibitors (10 μM MPEP, 10 μM fenobam, 5 μM U73122 (a PLC inhibitor), 5 μM U73343 (an inactive analog of U73122) or 100 μM 2-APB (an IP_3 R inhibitor) and loaded with Fura-2 AM before Ca^{2+} flux measurement. Results showed that besides being blocked by MPEP and fenobam, mGluR5-mediated Ca^{2+} responses can also be blocked by the PLC inhibitor, U73122 and the IP_3 R inhibitor 2-APB, but not the PLC inactive analogue, U73343 (Fig. 2i). These data show that >90% of SCDH mGluR5 couples to PLC to induce release of Ca^{2+} from intracellular stores associated with IP_3 Rs. Collectively, these data show that intracellular, including nuclear, SCDH mGluR5 can function independently of signals originating at the cell surface and thus plays a dynamic role in mobilizing Ca^{2+} in a specific, localized manner.

Nerve injury increases nuclear mGluR5 in SCDH neurons.

To test whether intracellular mGluR5 contributes to the known role of this receptor in neuropathic pain we used the rodent SNI model which mimics various aspects of human neuropathic pain, inducing spontaneous pain, allodynia and hyperalgesia (Supplementary Fig. 2a–d)²¹. Ultrastructural analysis showed that the percentage of mGluR5 associated with the nuclear membrane increased in SCDH neurons from SNI versus control rats (Fig. 3a–c). Conversely, plasma membrane and intracellular mGluR5 decreased in SNI rats, whereas the percentage of intranuclear mGluR5 remained unchanged (Fig. 3a–c). Western blotting of subcellular fractions from L4–L6 SCDH supported the electron microscopy data showing increased levels of mGluR5 in SNI versus sham nuclear fractions (Fig. 3d,e). In contrast, there was no change in EAAT3 levels across membrane fractions or

Figure 2 | mGluR5-mediated nuclear Ca^{2+} changes in SCDH neurons or isolated nuclei.

Cultured rat SCDH neurons were transfected with the nuclear-targeted red fluorescent, genetically encoded Ca^{2+} indicator, CMV-NL-S-R-GECO, on DIV6 and then immunostained or imaged in real time on DIV9. (a) Images of SCDH neurons transfected with CMV-NL-S-R-GECO (red) expressed in neuronal cells (as indicated by MAP2 staining; green in the upper panel) and colocalized with the neuronal nuclear marker, NeuN (green in the lower panel) Scale bar, 10 μm . (b) Representative trace of nuclear Ca^{2+} responses to agonist stimulation. DHPG application (100 μM) did not induce Ca^{2+} changes whereas quisqualate (Quis, 10 μM) application resulted in sustained nuclear Ca^{2+} rises. (c) Fenobam (10 μM) blocked Quis-induced nuclear Ca^{2+} responses. (d) Compiled data from peak $\Delta F/F_0$ (%) with $N=22$ identified nuclei (b) and $N=50$ nuclei (c) Student's t -test, $*P<0.05$, compared with baseline; $^\dagger P<0.05$, Quis alone compared to Quis + fenobam. (e) Image of purified nucleus from L4–L6 SCDH stained with lamin B₂ (red) and mGluR5 (green). Scale bar, 5 μm . (f) Isolated SCDH nuclei were loaded with Oregon Green BAPTA and imaged to acquire baseline Ca^{2+} changes before agonist application in the presence of AMPA and mGluR1 receptor antagonists. Representative trace of nuclear Ca^{2+} responses to agonist stimulation. DHPG application (100 μM) did not induce Ca^{2+} changes, while quisqualate (Quis, 10 μM) application resulted in sustained nuclear Ca^{2+} rises. (g) Fenobam (10 μM) blocked the nuclear Ca^{2+} response induced by Quis. (h) Compiled data from peak $\Delta F/F_0$ (%) with $N=5$ identified nuclei (f) and $N=15$ identified nuclei (g) Student's t -test, $*P<0.05$, compared with baseline $^\dagger P<0.05$, Quis alone compared to Quis + fenobam. (i) SCDH cultures (35,000 cells per well) were preincubated with indicated inhibitors (10 μM MPEP, 10 μM Fenobam, 5 μM U73122, 5 μM U73343, 100 μM 2-APB), loaded with Fura-2 AM before EC₈₀ quisqualate (5.2 μM) addition and Ca^{2+} flux measurement. Three separate experiments were done in triplicate, Student's t -test, $*P<0.05$, compared to quisqualate alone. All values in figure are expressed as mean \pm s.e.m.

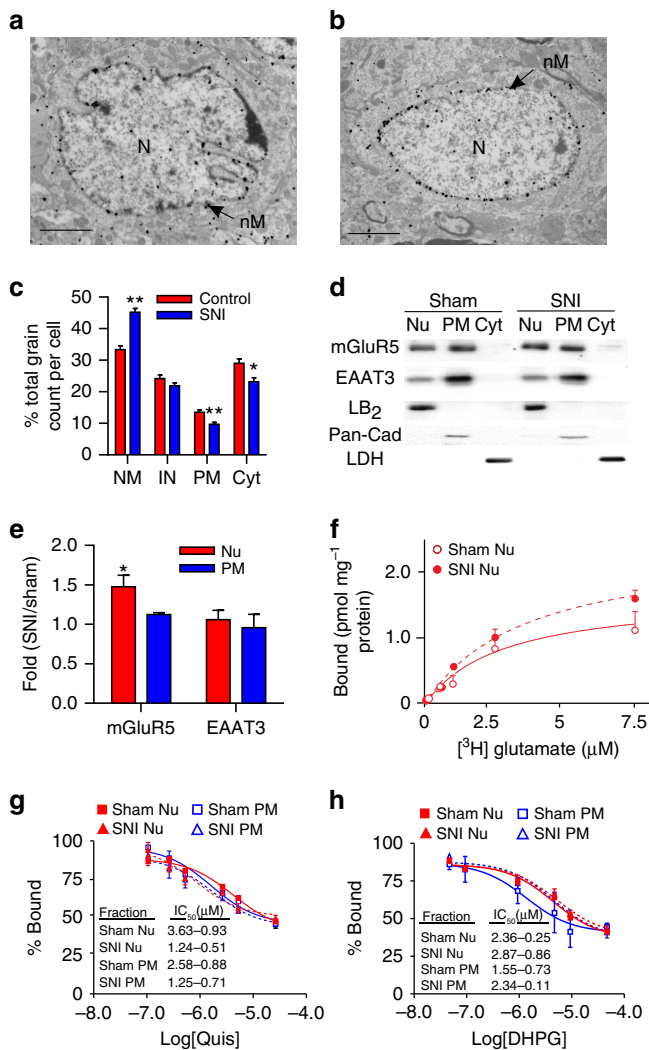


Figure 3 | Nerve injury increases SCDH nuclear mGluR5.

Electron-micrographs showing increased nuclear mGluR5 in a SCDH neuron of spared-nerve injury (SNI) versus sham rat (**a**). (N, nucleus; nM, nuclear membrane). Scale bar, (**a,b**) 2 μ m. (**c**) Percentage of mGluR5-labelled grains on plasma (PM) or nuclear (NM) membranes, or within cytoplasm (Cyt) or the intranuclear (IN) compartment in SNI and control rats (103 somata were counted from three SNI rats and 86 somata were counted from two control rats, ANOVA $*P < 0.01$; $**P < 0.001$). (**d**) Western blot of nuclear (Nu), cytoplasmic (Cyt) and plasma membrane (PM) fractions from sham and SNI lumbar SCDH. mGluR5 is increased in nuclear (Lamin-B₂ (LB₂)) but not PM (Pan-cadherin (Pan-Cad)) or Cyt (lactate dehydrogenase (LDH)) fractions from SCDH of SNI rats, quantified in (**e**). (**e**) Data shown represent the mean of three experiments, Student's *t*-test $P < 0.05$. (**f**) There are significantly more ³H-glutamate sites in SNI nuclear preparations (dashed line) with respect to sham nuclei (solid line) (SNI B_{max} = 2.87 ± 0.15 pmol mg⁻¹, sham B_{max} = 1.96 ± 0.21 pmol mg⁻¹, $*P < 0.05$) (**g,h**) percentage binding and IC₅₀ values of Quis (**g**) or DHPG (**h**) on nuclear or PM are comparable in sham and SNI animals. Data shown represent the mean of three experiments, comparisons with Student's *t*-test. All values in figure are expressed as mean \pm s.e.m.

treatment conditions (Fig. 3d,e). Although reactive astrogliosis is observed after SNI, there was very little colocalization of mGluR5 and the astrocyte marker GFAP in SCDH of either sham or SNI rats (Supplementary Fig. 2e).

Consistent with the above results, increased numbers of mGluR5 binding sites were found in SNI, but not sham SCDH

nuclear membranes (B_{max} of 2.87 ± 0.15 pmol mg⁻¹ versus 1.96 ± 0.21 pmol mg⁻¹; Fig. 3f). However, glutamate binding assays showed no significant differences in receptor affinity for DHPG or quisqualate using plasma membrane or nuclear membrane fractions derived from either sham or SNI rat tissues (Fig. 3g,h). These results suggest that nuclear mGluR5 has the same affinity for binding ligands as plasma membrane receptors. One caveat to these assays is that DHPG and quisqualate only displaced $\sim 50\%$ of glutamate. This is surprising since the conditions used here were identical to protocols used previously to determine half-maximal inhibitory concentrations (IC₅₀s) for DHPG and quisqualate in hippocampal and striatal preparations^{7–10}. In those experiments radiolabelled glutamate displacement was between 75 and 80%, and the derived IC₅₀ values were essentially the same for DHPG and quisqualate using nuclear and plasma membrane (PM) fractions in striatal and hippocampal preparations^{7,9}, as shown here for SCDH. Although we have blocked other glutamate binding sites (NMDA, AMPA, kainate and mGluRs), there may be other sites we have not accounted for. Nonetheless, the derived values are similar to those published by ourselves^{7,9} and others²³. Taken together, these results demonstrate increased levels of nuclear mGluR5 in SCDH neurons of neuropathic animals, implicating a pathophysiological role of intracellular mGluR5 in neuropathic pain.

Nerve injury increases nuclear signalling. mGluR5 activation leads to phosphorylation of ERK1/2 in SCDH^{20,24} and increased activity-regulated cytoskeletal-associated protein (Arc/Arg3.1) in striatum¹². However, it is unknown if these effectors are activated by intracellular mGluR5 in SCDH. Using subcellular fractionation followed by western blotting of tissue derived from L4–L6 SCDH, we found increases in phosphorylated-ERK1 (pERK1, 4.4-fold increase) and pERK2 (8.7-fold increase) in nuclear fractions from SNI rats as compared with sham rats after normalization with total ERK1/2 (Fig. 4a,b). Both pERK1 and 2 were very low in cytoplasmic fractions, and along with total ERK1/2 showed no difference between groups (Fig. 4a). Arc/Arg3.1 levels in the SCDH nuclear fractions of SNI rats were also increased compared with sham rats (6.5-fold increase; Fig. 4a,b). These results indicate that there is a concomitant increase in mGluR5 (Fig. 3a,b) and enhanced activation of downstream signalling proteins, pERK1, pERK2 and Arc/Arg3.1 in the nuclear compartment in SCDH of SNI rats versus shams (Fig. 4a,b). Importantly, these effects were mGluR5-specific since SNI-induced mGluR5 levels, pERK1, pERK2 and Arc were all significantly reduced by fenobam (Fig. 4a,b).

In addition to triggering pain behaviours^{25,26} (Supplementary Fig. 2b,c), spinal administration of glutamate induces a mGluR5-dependent expression of transcription factors such as *c-fos* in SCDH neurons^{26,27}. However, the relative contributions of intracellular versus plasma membrane mGluR5 to spinal transcription factor expression are unknown. Here we found that Fos and Jun were both increased in the SCDH ipsilateral (Fig. 4c–f) and contralateral (Supplementary Fig. 3a–d) to the nerve surgery 45 min after intrathecal injection of 400 μ g glutamate in sham and SNI rats. Importantly, both gene products were significantly higher in the ipsilateral SCDH of SNI versus sham animals (Fig. 4c–f), paralleling increased glutamate-induced pain behaviours in SNI rats (Supplementary Fig. 2c,d). Taken together, increases in both glutamate-induced pain behaviours and transcription factor expression in SNI rats suggest that enhanced responses to spinal glutamate contributes to neuropathic pain. We next ask whether increased levels of intracellular mGluR5 observed in neuropathic animals are responsible for these effects.

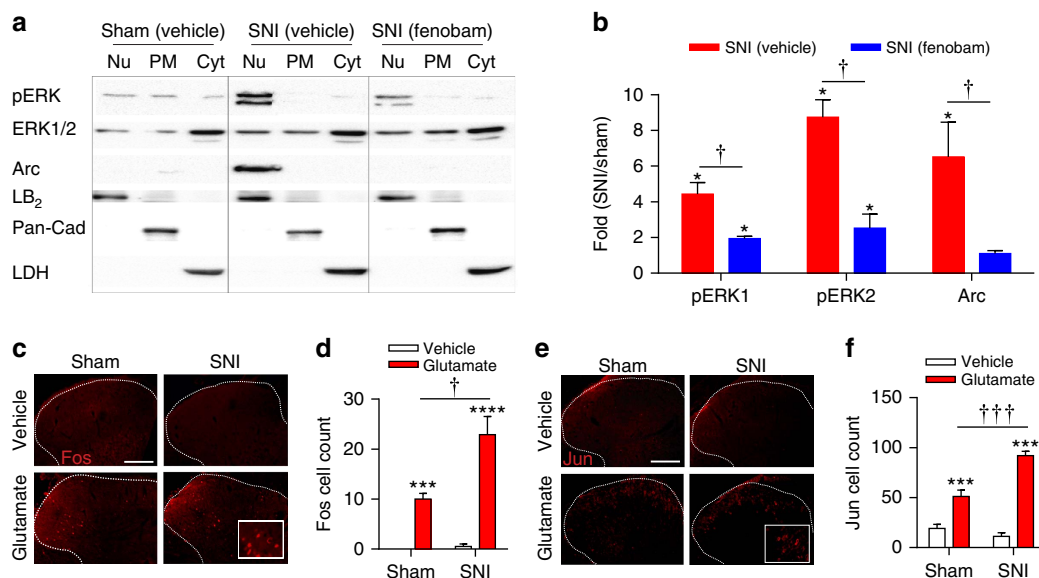


Figure 4 | Nerve injury increases SCDH nuclear signalling molecules. (a) Western blot analysis of pERK1/2 and Arc/Arg3.1 expression in nuclear (Nu), plasma membrane (PM) and cytosolic (Cyt) fractions of SCDH from sham, spared-nerve injury (SNI), and SNI + fenobam rats. (b) Quantification reveals increased pERK1, pERK2 and Arc/Arg3.1 in nuclear fractions of SNI rats compared with sham rats ($*P < 0.05$). Fenobam (100 nmol, i.t.) treatment significantly reduced these responses ($\dagger P < 0.05$). Data shown represent the mean of three experiments, Student's *t*-test. (c, e) Representative Fos/Jun in ipsilateral SCDH (outlined with dashed lines) of sham and SNI animals following spinal injection of vehicle or glutamate (400 μ g), with higher power insets. Scale bar, 100 μ m. (d, f) Fos and Jun are increased in the ipsilateral SCDH of sham rats and further increased in SNI rats (ANOVA $***P < 0.001$, with respect to vehicle; $\dagger P < 0.05$, $\dagger\dagger P < 0.001$ with respect to sham). 6–12 sections were averaged for each animal, with $N = 6$ animals per group. All values in figure are expressed as mean \pm s.e.m.

Intracellular mGluR5 blockade reduces pain and *c-fos*. To investigate the role of intracellular versus cell surface mGluR5 in neuropathic pain, we tested the *in vivo* effects of permeable and impermeable antagonists on pain behaviours induced by 400 μ g of spinal glutamate in sham and SNI rats. Spinal pretreatment with the permeable mGluR5 antagonist fenobam (1–100 nmol) produced a highly significant, dose-dependent reduction of glutamate-induced pain behaviours in SNI rats, whereas pretreatment with the impermeable antagonist LY393053 (1–1,000 nmol; Fig. 5a,b) was less effective. As LY393053 antagonizes both mGluR1 and mGluR5, we also tested a 50:50 mixture of CPCCOEt, a permeable mGluR1 antagonist, with fenobam. Contrary to canonical models, fenobam alone (~66%), or combined with CPCCOEt (~70%), produced significantly greater analgesia than LY393053 (~23%) in SNI rats (Fig. 5c).

To mimic physiological conditions (with no exogenous glutamate added), mechanical sensitivity was assessed in both sham and SNI rats by determining paw withdrawal thresholds (PWTs) to plantar hind paw stimulation with von Frey filaments. SNI rats exhibited allodynia (Fig. 5d), as their PWTs were lower than shams (Fig. 5e). PWTs were evaluated in SNI rats following spinal injection of LY393053, fenobam or vehicle. Treatment with either vehicle or LY393053 did not elevate PWTs in SNI rats (Fig. 5d), whereas fenobam significantly elevated PWTs (reflecting relief of allodynia) for one hour post injection (Fig. 5d). As expected, neither antagonist had a significant effect on PWTs in sham animals (Fig. 5e).

Spontaneous pain was also assessed using a conditioned place preference (CPP) paradigm in which a drug or its vehicle were first paired (in counterbalanced order) with opposite sides of a conditioning chamber with differing visual cues. After four daily pairing sessions (two each with drug or vehicle), the time spent in either chamber, or a neutral connecting compartment, was measured for both naive and SNI rats. We first showed that both groups of rats exhibited a preference for a compartment

previously paired with morphine (10 mg kg⁻¹; Supplementary Fig. 4a), consistent with its well-established analgesic and rewarding effects²⁸. Further CPP experiments demonstrated that fenobam produced a place preference effect (CPP Index significantly above 50%) in SNI, but not in naive, rats (Fig. 5f). However, no such place preference was observed in response to spinal treatment with the impermeable mGluR5 antagonist LY393053 (Fig. 5f), establishing that analgesia was produced by fenobam only. Importantly, SNI rats treated with either fenobam or LY393053 showed no baseline place preference (BPP) before drug pairings (Supplementary Fig. 4b). Collectively, multiple pain behaviour experiments show that intracellular mGluR5 is critical for expression of spontaneous pain and mechanical allodynia in neuropathic rats. These results show for the first time that an intracellular GPCR modulates a behavioural phenotype, and that intracellular availability of a given ligand is an important determinant of its therapeutic efficacy.

To test whether blocking cell surface or intracellular mGluR5 would affect downstream signalling pathways associated with pain behaviours, rats were pretreated with either LY393053 or fenobam before measuring spinal glutamate-induced Fos and Jun expression. Consistent with the pain behaviour results, LY393053 did not attenuate spinal glutamate-induced Fos in ipsilateral dorsal horn of SNI rats, whereas pretreatment with fenobam did (Fig. 5g,h). However, neither LY393053 nor fenobam reduced Fos in the ipsilateral dorsal horn of sham rats (Fig. 5g,h), or the contralateral dorsal horn of sham or SNI rats (Supplementary Fig. 4c,d). Both LY393053 and fenobam were equally effective in attenuating glutamate-induced Jun in the ipsilateral (Fig. 5i,j) and contralateral (Supplementary Fig. 4e,f) SCDH of SNI and sham rats. These results suggest that in neuropathic animals *c-fos* is largely dependent on intracellular mGluR5, whereas *c-jun* is not.

EAAT3 inhibition reduces pain and *c-fos*. As intracellular mGluR5 appears essential for the expression of neuropathic pain,

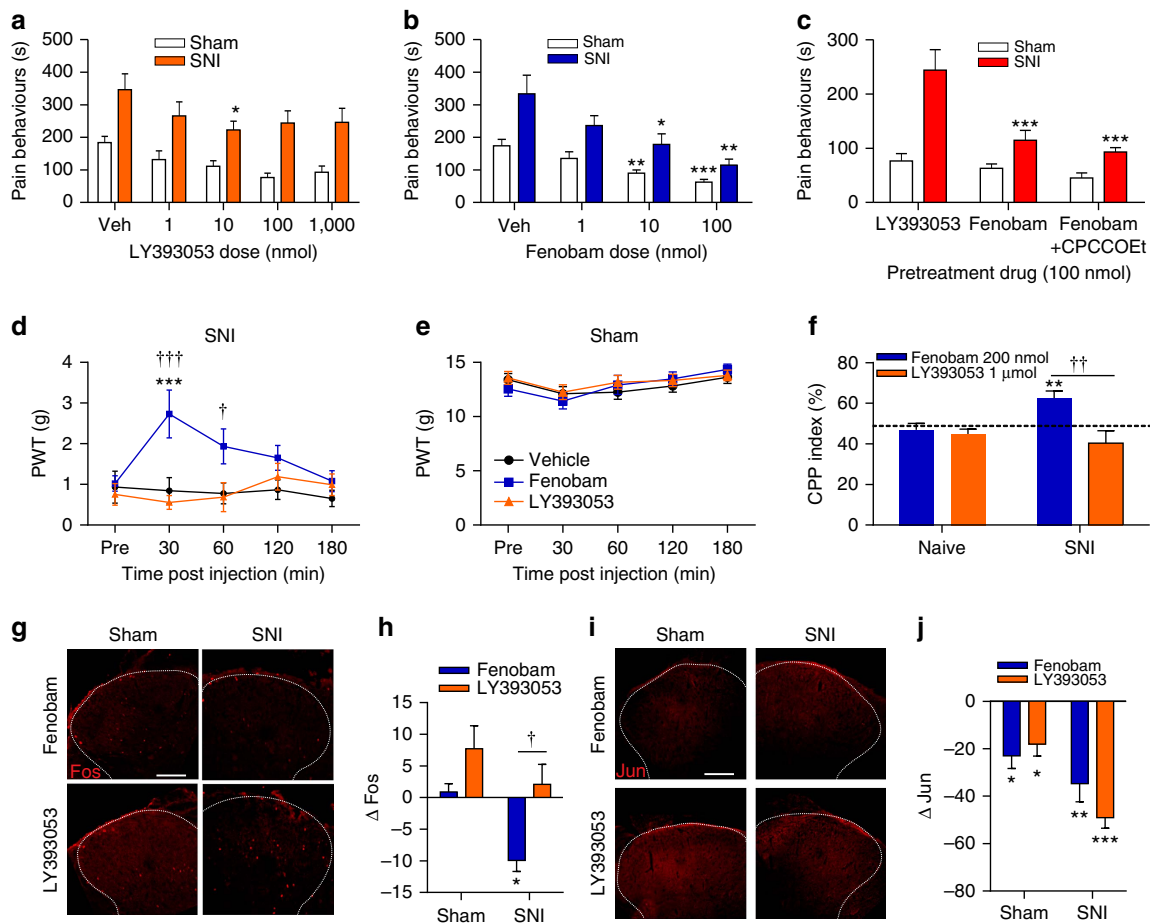


Figure 5 | Membrane permeable mGluR5 antagonist reduces pain and Fos. (a) LY393053 (1–1,000 nmol) weakly attenuates glutamate-induced pain behaviours in SNI rats (at the 10 nmol dose only, $P = 0.0362$), but not sham rats (vehicle, veh). $N = 6$ rats per group. (b) Fenobam (1–100 nmol) dose-dependently attenuates glutamate-induced pain behaviours in both sham and SNI rats (ANOVA $*P < 0.05$, $**P < 0.01$, $***P < 0.001$). $N = 6$ rats per group. (c) Fenobam (100 nmol) or fenobam + CPCCOEt (100 nmol) reduce glutamate-induced pain behaviours significantly more than LY393053 (100 nmol) in SNI rats. (ANOVA $***P < 0.001$ with respect to LY393053). Conversely, drug effects are equivalent in sham rats. $N = 6$ rats/group. Fenobam/LY393053 (100 nmol) data repeated from a and b. (d) Paw withdrawal thresholds (PWTs) of SNI rats are increased by fenobam, but not LY393053 (each 100 nmol), (ANOVA 30-min $P < 0.001$; 60-min $P = 0.0156$) $***P < 0.001$ versus vehicle, $^{\dagger}P < 0.05$, $^{\dagger\dagger}P < 0.001$ with respect to LY393053 (legend as in e) $N = 8$ rats per group. (e) Neither fenobam nor LY393053 affect PWTs of sham rats. $N = 8$ rats per group (f) SNI, but not naive, rats show conditioned place preference (CPP) to fenobam (200 nmol), (ANOVA CPP index = 62.51%, $P = 0.0099$; $**P < 0.01$), but not LY393053 (1 μ mol). Consequently, fenobam exhibits significantly greater CPP than LY393053 ($^{\dagger\dagger}P < 0.01$ fenobam versus LY393053). $N = 8$ rats/group. (g) Representative glutamate-induced Fos in ipsilateral SCDH (outlined with dashed lines) of sham and SNI animals after spinal pretreatment with fenobam or LY393053. Scale bar, 100 μ m. (h) Glutamate-induced Fos in ipsilateral SCDH of SNI rats is reduced by fenobam (ANOVA $P = 0.0024$ versus glutamate), but not LY393053 ($***P < 0.01$ with respect to vehicle). Consequently, fenobam-treated rats exhibited significantly lower Fos than LY393053-treated rats (ANOVA $P = 0.0258$ versus LY393053, $^{\dagger}P < 0.05$ with respect to the LY393053). Fos expression was unaffected by either fenobam or LY393053 in sham rats. Six to 12 sections were averaged per animal, with $N = 6$ animals/group. (i) Representative glutamate-induced Jun in ipsilateral-SCDH (outlined with dashed lines) of sham and SNI animals following pretreatment with fenobam or LY393053 (100 nmol each). Scale bar, 100 μ m. (j) Jun is reduced by either fenobam or LY393053 in both sham and SNI rats (ANOVA sham $P = 0.0074$; SNI $P = 0.0060$) or LY393053 (sham $P = 0.0154$; SNI $P < 0.0001$). ($*P < 0.05$; $***P < 0.001$). Six to 12 sections were averaged for each animal, with $N = 6$ animals per group. All values in figure are expressed as mean \pm s.e.m.

we hypothesized that blocking ligand entry into SCDH neurons would also alleviate pain behaviours. In SCDH glutamate is primarily taken up by sodium-dependent transporters including the neuronal EAAT3 (EAAC1; Slc1a1), glial EAAT1 (GLAST, Slc1a3) and glial EAAT2 (GLT-1; Slc1a2)²⁹. Previously, spinal administration of the pan-EAAT inhibitor, TBOA, was shown to be pronociceptive in naive animals³⁰, but antinociceptive in animals with persistent pain^{31–33}. We show here that TBOA had similar paradoxical effects on spinal glutamate-induced pain behaviours in sham versus SNI rats (Supplementary Fig. 5a). Improved EAAT ligand specificity allowed us to selectively test the contributions of either neuronal or glial transporters in sham and neuropathic rats.

The EAAT3 specific inhibitor L- β -threo-benzyl-aspartate (L-TBA, 0.01–1 nmol) was used to block neuronal uptake of glutamate, whereas WAY213613 and UCPH-101 (WAY + UCPH; 1–100 nmol) were used to block EAAT1 and 2, respectively. Pain behaviours induced by 400 μ g of spinal glutamate were recorded 10 min following administration of neuronal or glial EAAT inhibitors. After intrathecal L-TBA, a dose-dependent decrease in glutamate-induced pain behaviours was observed in SNI rats, but not sham animals (Fig. 6a). In contrast, intrathecal treatment with a 50:50 mixture of glial EAAT1,2 inhibitors, produced a dose-dependent increase in pain behaviours in SNI rats (Fig. 6b). These results are consistent with the hypothesis that the accessibility of glutamate to intracellular mGluR5 is

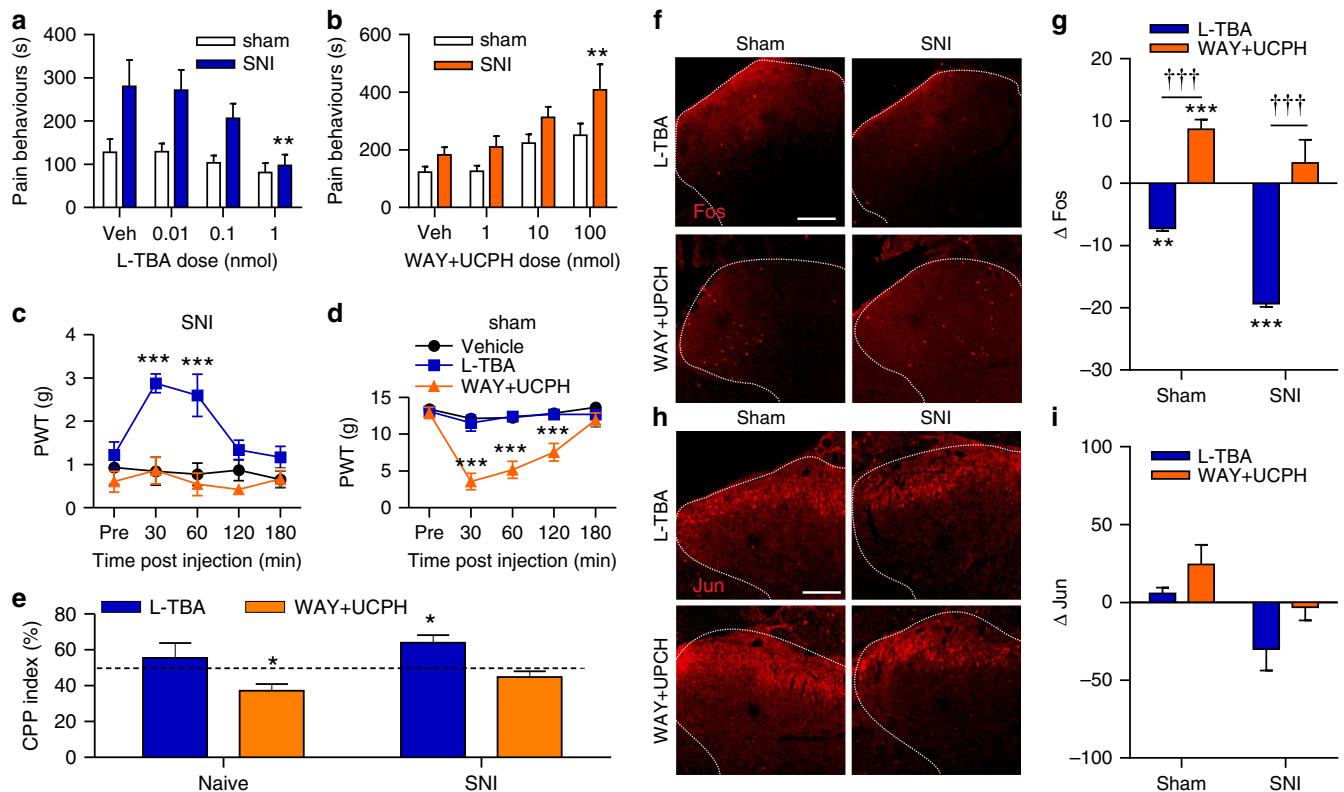


Figure 6 | Inhibition of EAAT3 reduces pain and Fos. (a) L-TBA (0.01–1 nmol) dose-dependently attenuates glutamate-induced pain in SNI (ANOVA $P=0.0069$), but not sham, rats (vehicle, veh). $N=6$ rats per group. (b) WAY + UCPH (1–100 nmol) dose-dependently potentiates glutamate-induced pain in SNI, but not sham, rats (ANOVA $P=0.003$). $N=6$ rats per group. (c) Paw-withdrawal thresholds (PWTs) of SNI rats are increased by L-TBA (1 nmol), but not WAY + UCPH (100 nmol) (ANOVA 30 min $P<0.0001$, 60 min $P=0.0004$). ($***P<0.001$ versus vehicle; legend as in d). $N=8$ rats/group. (d) PWTs of sham rats are reduced by WAY + UCPH (ANOVA 30–120 min $P<0.001$), but not L-TBA ($***P<0.001$). $N=8$ rats per group. (e) SNI, but not naive, rats show conditioned place preference (CPP) to L-TBA (1 nmol, CPP index = 64.03%, ANOVA $P=0.0099$). Naive rats exhibit conditioned place aversion to WAY + UCPH (ANOVA 100 nmol, CPP index = 37.16%, $P=0.0118$ ($*P<0.05$)). $N=8$ rats per group. (f) Representative glutamate-induced Fos in ipsilateral SCDH (outlined with dashed lines) of sham and SNI animals following spinal pretreatment with L-TBA (1 nmol) or WAY + UCPH (100 nmol). Scale bar 100 μm . (g) For both SNI and sham rats, Fos in the ipsilateral SCDH is reduced by L-TBA (ANOVA $P=0.0313$), but conversely ipsilateral Fos is increased by WAY + UCPH in sham, but not SNI rats (ANOVA $P=0.0313$). ($*P<0.05$ with respect to vehicle). In both shams and SNI rats, L-TBA attenuates Fos more effectively than WAY + UCPH. ($\dagger\dagger\dagger P<0.001$ L-TBA versus LY393053). Six to 12 sections were averaged for each animal, with $N=6$ animals per group. (h) Representative glutamate-induced Jun in ipsilateral SCDH (outlined with dashed lines) of sham and SNI animals following spinal pretreatment with L-TBA (1 nmol) or WAY + UCPH (100 nmol). Scale bar, 100 μm . (i) Neither L-TBA nor WAY + UCPH significantly affected Jun in sham or SNI rats (ANOVA). Six to 12 sections were averaged per animal, with $N=6$ animals per group. All values in figure are expressed as mean \pm s.e.m.

critical for enhanced pain behaviours to spinal glutamate in SNI rats.

Spinal injection of L-TBA (1 nmol) also attenuated ipsilateral mechanical allodynia for 1 h following injection in SNI animals (Fig. 6c), whereas no change in the PWTs was observed in sham rats (Fig. 6d). Conversely, spinal administration of WAY + UCPH produced no change in the PWTs of SNI rats (Fig. 6c), but induced a very significant reduction in PWTs (or induced allodynia) in sham rats for 2 h (Fig. 6d). CPP experiments demonstrated that 1 nmol of spinal L-TBA produced an analgesic effect (CPP Index significantly above 50%) in SNI, but not in naive, rats (Fig. 6e). In contrast, the EAAT1,2 inhibitors failed to produce a place preference in SNI rats, producing instead a significant place aversion in naive rats (Fig. 6e). Importantly, the rats in either the neuronal or glial EAAT inhibitors groups showed no BPP before drug pairings (Supplementary Fig. 5b). Taken together, these results demonstrate that intracellular transport of glutamate contributes significantly to spontaneous pain and mechanical hypersensitivity in SNI rats, consistent with our hypothesis that increased intracellular mGluR5 plays a role in neuropathic pain.

Spinal glutamate-induced changes in Fos/Jun were also tested after blockade of neuronal and glial transporters. Pretreating rats with L-TBA (1 nmol) 10 min before administering glutamate (400 μg) reduced Fos in the ipsilateral and contralateral SCDH of SNI and sham rats (Fig. 6f,g, Supplementary Fig. 5c,d). Although Jun expression is lower after L-TBA, it was not significantly reduced in any condition (Fig. 6h,i, Supplementary Fig. 5e,f). These results suggest that both spinal glutamate-induced pain and *c-fos* in SNI rats depend on the access of glutamate to intracellular mGluR5.

In contrast, increasing synaptic glutamate by spinal pretreatment with WAY + UCPH resulted in an increase in spinal glutamate-induced Fos in the ipsilateral SCDH of sham, but not SNI rats (Fig. 6f,g), and was not affected in the contralateral SCDH of either sham or SNI rats (Supplementary Fig. 5c,d). Spinal glutamate-induced Jun was not changed by pretreatment with EAAT1,2 inhibitors in either sham or SNI rats ipsi- (Fig. 6h,i) or contralaterally to the nerve surgery (Supplementary Fig. 5e,f). These results indicate that in SNI rats impeding glutamate clearance from the extracellular space by blocking EAAT1,2 induces more pain

behaviours and more *c-fos* in response to spinal glutamate injection.

To exclude the possibility that pan-EAAT inhibitors produce antinociceptive effects in neuropathic animals via previously proposed reverse-operation of glutamate transporters³¹, *in vivo* microdialysis was used in conscious behaving animals following inhibition of glial EAATs with WAY + UCPH. As would be expected with normal operation of glutamate transporters, glial EAAT inhibition produced an increase in noxious stimulus-induced glutamate concentration in the SCDH of both sham and SNI rats (Supplementary Fig. 5g).

Discussion

Some GPCRs, like mGluR5, are localized on intracellular membranes where, *in vitro*, they trigger unique signalling effects^{9,12}. Here we found that a membrane permeable agonist activating intracellular SCDH mGluR5 produced sustained Ca^{2+} responses, whereas an impermeable, non-transported agonist produced transient Ca^{2+} peaks. Identical responses were observed in SCDH neurons expressing a genetically encoded Ca^{2+} indicator restricted to the nucleus, as well as in acutely isolated SCDH nuclei. When activated, the peak amplitude of nuclear Ca^{2+} responses was ~40% higher and ninefold greater than at surface mGluR5. Akin to striatal¹⁰ and hippocampal⁷ receptors, intracellular mGluR5 uses the canonical PLC/IP₃R signalling pathway to play a dynamic role in mobilizing Ca^{2+} in a specific, localized manner. Using ultrastructural, cellular and pharmacological techniques, we also showed that nerve injury increases nuclear mGluR5 levels, along with the synaptic plasticity effectors pERK1, pERK2, Arc/Arg3.1 and *c-fos*. Behaviourally, blocking only cell-surface mGluR5 with an impermeable antagonist had little effect on neuropathic pain assays, whereas inhibiting intracellular mGluR5 using a permeable antagonist markedly reduced all pain indices and pERK1, pERK2, Arc and *c-fos* expression. Consistent with intracellular mGluR5 driving pain behaviour, blocking glutamate entry into SCDH neurons also produced analgesia and decreased *c-fos*, whereas blocking glial glutamate transporters increased pain behaviours and *c-fos*. To our knowledge, these are the first experiments demonstrating a role for an intracellular GPCR in an *in vivo* behavioural model (see schematic summary diagram in Supplementary Fig. 6).

Although many GPCRs are found on nuclear membranes (for example, receptors for epinephrine, endothelin, platelet-activating-factor and bradykinin), deducing the functional significance of such receptors remains challenging because of limited techniques to probe the nucleus *in situ*, and since most GPCRs are also present at the cell surface. One exception is the α_{1A} -adrenoceptor, which is only detected on nuclear membranes in cardiac myocytes⁴, where binding results in PKC activation and translocation leading to troponin phosphorylation and sarcomere shortening⁴. A caged cell-permeable analog of endothelin-1 was used to detect nuclear endothelin receptor-mediated increases of nucleoplasmic Ca^{2+} in cardiac myocytes after intracellular uncaging⁵. Also, activation of the GPCR F2R11 anchored at plasma membranes triggered the expression of *Ang1*, whereas nuclear-activated F2R11 induced *Vegfa* in retinal ganglion cells⁶. Despite these observations, until now *in vivo* behavioural outcomes resulting from activation of endogenous intracellular receptors have not been assessed.

Given that mGluR5 is an important target, many drugs have been optimized for mGluR5 selectivity, affinity, and pharmacokinetic parameters. Although recent compounds^{34–36} have been developed that overcome the off-target effects³⁵ and short-half-lives³⁶ of earlier drugs, little emphasis has been placed on which

receptor pool ligands act. In blocking cell surface mGluR5, the impermeable antagonist, LY393053, demonstrated only weak analgesia in pain models examined here. In contrast, the cell permeable antagonist, fenobam (a negative allosteric modulator that has both non-competitive antagonist and inverse agonist activity) significantly reduced mechanical allodynia, glutamate-induced pain and *c-fos* expression in neuropathic rats. This suggests that drugs interacting with intracellular mGluR5 are superior against neuropathic pain to those acting at cell surface mGluR5. Also, while fenobam (IC₅₀ 80 nM)³⁷ is more potent than LY393053 (IC₅₀ 1.6 μ M)^{38,39}, we did not see increased analgesic activity when the intrathecal dose of LY393053 was increased from 10 nmoles to 1 μ mole suggesting that its analgesic effects plateaued at 10 nmoles. Indeed, the reported IC₅₀ values for LY393053 may be unavoidably high, since this impermeable antagonist was assessed using an assay (PI hydrolysis) that employed the transportable mGluR5 agonist quisqualate^{38,39}. Importantly, these same investigators reported an *in vivo* ED₅₀ for LY393053 of 654–955 fmoles against DHPG-induced PI hydrolysis (that is, when the agonist is impermeable) and 9 nmoles against DHPG-induced seizures, when administered centrally as we did here. The fenobam-induced analgesic CPP in neuropathic, but not naive, rats suggests that agents acting at intracellular mGluR5 may produce analgesia with low potential for abuse. In contrast, LY393053's lowering of *c-jun* in SNI rats is consistent with its analgesic effects in acute inflammatory pain^{38,40}, and suggests a minor contribution from cell-surface mGluR5 in persistent pain. That LY393053 reduced glutamate-induced *c-jun*, but not *c-fos*, while fenobam reduced both, confirms in an *in vivo* model, our previous demonstration *in vitro* that separate intracellular cascades are triggered by cell surface and intracellular mGluR5. Specifically, we previously showed in striatal cultures^{7,9,12} that cell surface mGluR5 stimulates CAMKIV, p-CREB and *c-jun*, while intracellular mGluR5 phosphorylates ERK1/2 and Elk-1, and enhances *c-fos*, *erg-1* and Arc/Arg3.1. The importance of intracellular mGluR5 for *c-fos* induction was further supported here by the significant reduction of glutamate-induced *c-fos* following EAAT3 inhibition.

EAAT3 inhibition not only replicated the analgesic and *c-fos*-reducing effects of fenobam, but also explains the paradoxical antinociceptive effects of pan-EAAT inhibitors on persistent pain^{30–33}. Here a selective EAAT3 inhibitor produced antinociception in SNI rats, whereas EAAT1,2 inhibitors produced pronociception, with similar diverging effects on glutamate-induced pain, mechanical allodynia, CPP and glutamate-induced *c-fos* expression. Our *c-fos* studies, explain recent results showing that intracisternal TBOA significantly increased noxious heat-induced Fos immunoreactivity in the medullary dorsal horn of naive animals, while it significantly reduced this response in animals with earlier inflammation of the vibrissa pad⁴¹. Thus, TBOA's *c-fos* reducing effects in animals with persistent pain are likely due to EAAT3 blockade, while its *c-fos* enhancing effects in naive animals are likely due to inhibition of EAAT1/2. These results refute an alternative hypothesis proposing abnormal reverse-operation of EAAT1,2 in rats with persistent pain³¹. Indeed, our *in vivo* microdialysis studies demonstrated that EAAT1,2 inhibitors increased spinal extracellular glutamate concentration after noxious stimulation in both sham and SNI rats. These data provide direct evidence that neuropathic pain does not depend on reverse-operation of glutamate transporters; rather analgesia is achieved by blocking the transporters responsible for ligand uptake into SCDH neurons.

Intracellular glutamate concentrations are difficult to assess, although 10 mM is frequently used as a cytoplasmic value with levels ranging up to 100–200 mM within vesicles⁴². However,

anti-glutamate immunogold electron microscopy studies indicate that particles representing glutamate are densest in terminal fields reaching 10 mM, whereas far fewer particles are present in somas and/or dendrites and spines (1 mM)^{43,44}. The latter studies also show large numbers of gold particles over cytoplasmic organelles such as mitochondria, ER and the nucleus^{43–45}. These data, combined with glutamate's complex metabolism and the myriad of studies demonstrating that it is highly compartmentalized in neurons^{46,47}, suggest that there may be far less 'free' cytoplasmic glutamate than previously suggested. Techniques such as ¹³C-NMR, ¹³C- and/or ¹⁵N-GC/MS provide compelling evidence that glutamate has many fates within the cell^{46–48}. For example, a large proportion of extracellular glutamate is transaminated and enters the mitochondria where it serves as a substrate for the tricarboxylic acid cycle^{46–48}. Then too, there is growing precedent for many types of ER–cell surface contacts that might be specialized for given functions^{49–51}. Whether such a relationship exists between EAAT3 and mGluR5 is unknown at this moment and awaits further study.

Our electron microscopy studies would suggest that there is more nuclear mGluR5 (~55%) than there is intracellular (~25%), thus the sustained Ca²⁺ response should be largely due to a nuclear source. However, we have shown in other studies that hippocampal dendrites⁷ exhibit intracellular mGluR5 responses mirroring the sustained nuclear Ca²⁺ release seen here. Thus, it seems likely that mGluR5 associated with dendritic ER membranes can also proportionately contribute to the intracellular signal. Although it has also been proposed that glial mGluR5 may contribute to glutamate signalling, evidence for mGluR5 in glia comes mostly from studies of cultured glia⁵². Further, although mGluR5 immunostaining has been reported colocalized with markers of astrocytes or microglia in spinal cord, this typically occurs in pathological conditions such as spinal cord injury or amyotrophic lateral sclerosis, particularly when there is reactive gliosis^{53,54}. Although we see evidence of reactive astrogliosis in SCDH after SNI, we found very little colocalization of staining for mGluR5 and GFAP (astrocyte marker) in either sham or SNI rats (Supplementary Fig. 2e), consistent with an earlier finding showing no change in such colocalization in rat SCDH after nerve root compression⁵⁵.

Although our study emphasizes the physiological significance of the two pools of mGluR5, the mechanism by which nuclear mGluR5 is increased in neuropathic rats remains unknown. Altered trafficking and/or scaffolding are suggested by the significantly decreased plasma membrane and cytosolic mGluR5 and increased nuclear receptors in SNI rats (Fig. 3c). Recent studies suggest the scaffolding proteins Homer 1b/c and Preso1, which interact with mGluR5^{56–58}, may be critical. Thus, expression of Homer 1b/c is altered in neuropathic rats⁵⁶, and genetic manipulation of Homer 1b/c or Preso1 significantly affects pain and SCDH Fos^{57,58}. By further dissecting the effector proteins associated with nuclear mGluR5-dependent processes, more targeted pain therapies can be discovered.

Methods

Animals. Adult male Long Evans rats (250–400 g) were used in this study. All experiments were carried out according to ethics protocols approved by McGill University and Washington University Animal Care Committees and followed the guidelines for animal research from the International Association for the Study of Pain (IASP).

Materials. Glutamate, quisqualate, (S)-3,5-dihydroxyphenylglycine (DHPG), L-TBA, TBOA, 6-cyano-7-nitroquinoxaline-2,3-dione (CNQX), D-(–)-2-Amino-5-phosphonopentanoic acid (2S)-2-Amino-2-[(1S,2S)-2-carboxycycloprop-1-yl]-3-(xanth-9-yl) propanoic acid (LY341495), N-[4-(2-Bromo-4,5-difluorophenoxy)phenyl]-L-asparagine (WAY 213613), 2-Amino-5,6,7,8-tetrahydro-4-(4-met-hoxyphenyl)-7-(naphthalen-1-yl)-5-oxo-4H-chromene-3-carbonitrile

(UCPH), MPEP, 7-(Hydroxyimino)-cyclopropan [b]chromen-1a-carboxylate ethyl ester (CPCCOEt), and N-(3-Chlorophenyl)-N'-(4,5-dihydro-1-methyl-4-oxo-1H-imidazol-2-yl)urea (fenobam) were purchased from Tocris Bioscience (Ellisville, MO). THA was obtained from Sigma-Aldrich, (St Louis, MO). 2-Amino-2-(3-cis/trans-carboxycyclobutyl)-3-(9H-thioxanthene-9-yl) propionic acid (LY393053) was obtained from Lilly Research Laboratories, Eli Lilly and Company (Indianapolis, IN).

Cell culture and transfection. Primary cultures of SCDH neurons were prepared from postnatal day 1 rat pups as previously described²⁰. The cells were plated onto 12-mm poly-D-lysine-coated coverslips for immunostaining or Ca²⁺ imaging or 48-well plates for uptake assays. Cells were cultured in humidified air with 5% CO₂ at 37 °C for 14–18 days before use. For experiments using the microplate reader, cultures were plated at 35,000 cells per well in black-walled, clear-bottomed 96-well plates and then cultured as above. SCDH cultures were transfected with plasmid pCMV-NLS-R-GECO (Addgene, Cambridge, MA) using Mirus TransIT-X2 (Mirus Bio LLC, Madison, WI) on DIV 6 and then immunostained or imaged in real time on DIV 9.

Immunocytochemistry of neurons in culture. Spinal neurons were fixed, blocked and incubated with antibodies as described^{8–10}. Primary antibodies included polyclonal anti-C-terminal mGluR5 (1:250, Millipore, Billerica, MA, AB5675), anti-NeuN (1:100, Millipore, ABN78), and monoclonal anti-lamin B₂ (1:100, Invitrogen, Grand Island, NY, 33-2100) and anti-MAP2 (1:500, Millipore, AB5622). Secondary antibodies include goat anti-rabbit (111-165-144) or mouse (115-165-146) Cy3 (1:300, Jackson ImmunoResearch Laboratories, West Grove, PA) and goat anti-rabbit (A-11008) or mouse (A-11029) Alexa-488 (1:300, Invitrogen).

³H-labelled agonist uptake. [³H]-Quisqualate (22.0 Ci mmol⁻¹, PerkinElmer Waltham, MA) and L-[³H]-glutamate (29.0 Ci mmol⁻¹) were used for uptake assay. The SCDH cultures (5 × 10⁴ cells per well) were maintained at 37 °C for 14–18 days before use. Cultured SCDH cells were washed three times in the appropriate buffer (Krebs–Ringer solution containing the following (in mM): 137 NaCl, 5.1 KCl, 0.77 KH₂PO₄, 0.71 MgSO₄ · 7H₂O, 1.1 CaCl₂, 10 D-glucose, and 10 HEPES), Na⁺ free, Cl⁻ free or Na⁺, Cl⁻-free MNDG as described previously⁸) and then incubated at 37 °C in the presence or absence of 100 μM DHPG, 100 μM TBOA, 100 μM THA or 400 μM L-cystine for 15 min before adding labelled agonist. Uptake was terminated after 15 min. Samples were rapidly rinsed three times with ice-cold PBS, solubilized in 150 μl of 1% Triton X-100/PBS, and then analysed by liquid scintillation.

Fluorescent measurements of intracellular Ca²⁺. Days *in vitro* 14–18 SCDH neurons grown on 12-mm glass coverslips (5 × 10⁴ cells per coverslip) were loaded with Ca²⁺ fluorophore, imaged and quantitated as described⁸. SCDH neurons were treated with 100 μM DHPG or 20 μM Quis as well as 10 μM MPEP and/or 20 μM LY393053. Because Quis would also activate AMPA receptors and mGluR1, it was always bath-applied in the presence of 25 μM SYM2206, an AMPA receptor antagonist, and 20 μM CPCCOEt, an mGluR1 antagonist. For consistency SYM2206 and CPCCOEt were also added to controls and DHPG-treated samples. We also used Ca²⁺ flux measurements to assess group responses. In this case primary spinal cord cultures from 1-day-old rat pups were plated at 35,000 cells per well in black-walled, clear-bottomed 96-well plates. After 10–14 days, the cells were loaded with 0.75 μM Fura-2 AM (F14185, Invitrogen) for 30 min at 37 °C and washed with Hanks' balanced salt solution (HBSS). The cells were then preincubated with various inhibitors for 20 min at 37 °C in the assay buffer (HBSS containing 20 μM CPCCOEt and 25 μM SYM2206) before Ca²⁺ flux measurement. Fura-2 fluorescence was measured using a BioTek Synergy H4 Hybrid Microplate Reader. The baseline 340/380 nm excitation ratio for fura-2 was collected for 5 s before injecting 5.2 μM quisqualate. Data were collected for an additional 30 s and then analysed using Biotek's Gen5 analysis software. Percent inhibition of the maximal quisqualate response was calculated by comparing the normalized fold change of the indicator in inhibitor-treated wells to that of controls.

[³H]-glutamate binding assay. L-[³H]-glutamate (29.0 Ci mmol⁻¹) was obtained from GE Healthcare, Pittsburgh, PA. The fractionated plasma membrane or nuclear pellet was resuspended in buffer containing 40 mM HEPES, pH 7.5, 2.5 mM Ca²⁺, 10 μM CNQX (AMPA/kainate receptor antagonist), 10 μM APV (NMDA receptor antagonist), 20 μM CPCCOEt (mGluR1 antagonist), 100 nM LY341495 (group II & III mGluR antagonist) and protease inhibitors. Incubation was for 60 min at 25 °C, and bound label was separated from free label by fast filtration over #32 filters (Schleicher & Schuell, Keene, NH). Nonspecific binding was determined in the presence of 4 mM glutamate. The binding curves were fit using the GraphPad Prism 3.0 program (Graphpad Software, San Diego, CA, USA).

Spared-nerve injury. Rats were anaesthetized with isoflurane (2% in 95% O₂, 5% CO₂) and SNI was induced to the left sciatic nerve as previously described²¹. Sham rats received the same surgery except the sciatic nerve was only exposed and received no further manipulation. Sham and SNI rats were tested at 7 days post-surgery, unless otherwise stated.

Electron microscopy. Pre-embedding immunogold immunocytochemistry was conducted on SCDH sections as described previously¹⁴. We used a polyclonal anti-mGluR5 antibody (1:400, Millipore, AB5675, lot nos. LV1364844 and LV1416963) directed against a C-terminal sequence of the receptor (specificity and previous use can be found at http://antibodyregistry.org/AB_2295173). Omitting primary antibody was performed as a control (Supplementary Fig. 1c). Preincubation of primary antibody with increasing concentration of synthetic blocking peptide (AG 374, Chemicon) was performed using diaminobenzidine staining and light microscopy (Supplementary Fig. 1d). Subcellular distribution of silver-intensified gold grain labelling, representing mGluR5 antigenic sites, was carried out on electron microscope images of labelled neuronal somata. Grains were counted in four subcellular compartments: plasma membrane, cytoplasm, nuclear membrane and intranuclear. The results were expressed as percentage of mGluR5 in each compartment relative to the total grains in the cell.

Confocal microscopy. Double labelling of mGluR5 and GFAP was performed on lumbar free floating 50 µm thick transverse sections from SNI and sham rats perfused with 4% paraformaldehyde 2 weeks following the surgical intervention. Briefly, sections were incubated with a mixture of primary antibodies mGluR5 (1/500, Chemicon, AB5675, Lot 2585810) and GFAP (1/2,000, Cell Signaling, 3679, Lot 3) for 48 h at 4 °C. Secondary antibodies consisted of a mixture of donkey anti-rabbit IgG conjugated to Rhodamine Red (1/200, Jackson ImmunoResearch Laboratories, 711-296-152, Lot 103820) and donkey anti-mouse Alexa Fluor 488 (1/500, Molecular Probes, A21202, Lot 49728A). Images were captured with a Zeiss LSM 510 confocal scanning laser microscope using an X63 oil immersion objective and a multitrack scanning method for the detection of both signals.

Tissue isolation and western blot analysis. Dorsal regions of lumbar spinal cord (L4–L6) were dissected from sham or SNI rats at 1 week or 2 weeks after nerve injury and treatment and resuspended in 20 µl volumes of Buffer ‘A’ medium containing 2.0 mM MgCl₂, 25 mM KCl, 10 mM HEPES (pH 7.5), and protease inhibitors (Complete Tablets; Roche Applied Science, Indianapolis, IN). Tissue was homogenized and nuclei and plasma membranes were prepared as described¹¹. Aliquots from each fraction were used for gel electrophoresis as well as membrane binding. Protein concentrations were determined using the Bradford assay (Biorad, Richmond, CA). Fractionated proteins were separated by SDS–PAGE, blotted, and probed with polyclonal anti-mGluR5 (1:1,000, Millipore, AB5675), polyclonal anti-EAAT3 (1:250, Dr J. Rothstein, Johns Hopkins University), monoclonal anti-lamin B₂ (1:1,000, Invitrogen, Grand Island, NY, 33-2100), polyclonal anti-pan-cadherin (1:1,000, Cell Signaling Technology, Beverly, MA, 4068), polyclonal anti-Lactate Dehydrogenase-Biotin conjugated (1:8,000, Rockland Immunochemicals, Gilbertsville, PA, 200-1673-0100), polyclonal anti-Arc/Arg3.1 (1:500, Synaptic Systems, Germany, 156-003), monoclonal anti-ERK (1:1,000, Cell Signaling Technology, Inc., 4696) and polyclonal anti-pERK (1:2,000, Cell Signaling Technology, Inc., 9101). P-ERK1/2 was normalized to total ERK1/2 and Arc was normalized to Lamin B₂. A horseradish peroxidase conjugated with goat anti-rabbit IgG (1:2,000, Cell Signaling Technology, Inc., Beverly, MA, 7074) or anti-mouse IgG (1:2,000, Sigma-Aldrich, St Louis, MO, 7076,) was used in conjunction with enhanced chemiluminescence (Clarity Western ECL Substrate, Bio-Rad, Hercules, CA) to detect the signal. Densitometric analyses of proteins were performed using the ChemiDoc MP System together with associated software (Bio-Rad). Full-length western immunoblots are shown in Supplementary Figs 7 and 8.

Drug administration in vivo. All drugs were administered by intrathecal (i.t.) injection at the L2–L5 spinal cord level, while the rat was under isoflurane anaesthesia. Drugs were dissolved either in distilled water (glutamate or morphine) or 5% dimethyl sulfoxide + 0.1 M cyclodextrin or 25% dimethyl sulfoxide in distilled water (all other drugs). Except for morphine, which was given subcutaneously (s.c.) in a volume of 1 mg ml⁻¹, all drugs were prepared to make an injectable volume of 20 µl for spinal injection. The prepared drugs were sonicated for 45 min to generate a clear solution or a microsuspension. All drugs were prepared fresh on the day of treatment. The drug dosages for later experiments were based on the dose–response curves derived from the glutamate-induced pain behaviour experiments. Unless otherwise stated in the Results section or below, pretreatment drugs were all given 1-week post SNI or sham surgery.

Nociceptive testing. Glutamate-induced pain behaviours. One week post-SNI or sham surgery rats were habituated to an observation chamber (30 × 30 × 30 cm) fitted with a transparent floor under which was placed a mirror to allow an unobstructed view of the animal’s paws for 30 min. Following habituation, rats were given two i.t. injections 10 min apart: either a pretreatment drug or vehicle followed by an injection of 400 µg of glutamate. The rats were then returned to the

chamber and allowed to move freely. Pain behaviours were measured as the time spent licking the hind paws, lower legs and tail over a 30-min period. The behaviours were recorded starting from when the rats awoke from anaesthesia and made their first coordinated movements.

Mechanical allodynia testing. Rats were tested for mechanical allodynia between 7 and 17 days after sham or SNI surgery, following each of the five i.t. drug treatments (t-TBA, WAY + UCPH, fenobam, LY393053) or vehicle. Only one drug was tested per day with 1 day in between drug testing, with drug order counterbalanced with a Latin square design. Before each testing session, each rat was habituated to a testing box (17 × 15 × 12 cm) with a wire-mesh grid floor, for a 1-h period. Before drug administration, a baseline was established using von Frey hairs applied through the grid floor to the ventral surface of the hind paw. Each hair was applied for a 10-s period or until the animal withdrew the hind paw without ambulating. During each testing trial, the series of hairs were presented following a validated up–down procedure⁵⁹, and the 50% PWT was calculated for each rat. After a baseline score was established, rats were given either the drug or vehicle via i.t. injection and returned to the testing box. PWTs were measured 30, 60, 120 and 180 min following the injection.

Conditioned place preference (CPP). CPP procedures began on day 7 following the sham or SNI surgery. The CPP chamber consisted of two pairing chambers (22 × 38 cm) connected by a third, neutral compartment (44 × 22 cm). On the habituation and test sessions (day 7 and 12 post surgery) the neutral compartment had openings that allowed the rats to freely explore all three chambers. The pairing chambers contained salient visual cues (horizontal versus vertical black and white lines) on the chamber walls and floor. During the habituation session in which the rats were allowed to explore all chambers for 30 min, an initial measurement of BPP was taken by measuring the time spent in each chamber over 15 min. Rats spending >75% of the time in any one chamber at habituation were removed from the experiment. The next day, using a randomized block design, rats were assigned a chamber-drug pairing. Either the drug or the vehicle was administered i.t. (except morphine which was given s.c.) and the rats were restricted to one of the two pairing chambers for a period of 60 min. The following day the rats would receive the other drug in the opposite chamber. On the CPP test day, the rats placed in the CPP chamber with the open gate configuration for 15 min and the time spent in the drug- and vehicle-paired or neutral chamber was again measured. The CPP index was defined as the time spent in the drug-paired chamber divided by the time spent in both the drug- and vehicle-paired chambers multiplied by 100; a CPP >50% indicates a preference for the drug-paired chamber while a CPP <50% indicates an aversion to the drug-paired chamber.

Immunohistochemistry preparation for Fos and Jun. In Fos and Jun experiments, animals were perfused 45–60 min following glutamate injection. Twenty-micrometre thick cross sections of the lumbar spinal cord were cut using a cryostat (Leica, Wetzlar, Germany) and collected on poly-L-lysine coated superfrost plus slides (Fisher Scientific, PA, USA). The tissue sections were incubated for 1 h at room temperature in 10% normal donkey serum in 0.1% Triton-X in PBS (PBS-Tx) to block unspecific labelling. For Jun labelling, sections were incubated at 4 °C for 48 h using rabbit polyclonal to Jun (1:1,000, Abcam, ab31419). After three rinses in PBS-Tx, the sections were incubated for 72 h at room temperature with donkey polyclonal anti-rabbit IgG conjugated to Rhodamine Red (1:500, Jackson ImmunoResearch Laboratories, 711-296-152, Lot 90396) for Jun, visualization. Separate slides were labelled for Fos using rabbit polyclonal to c-fos (1:5,000, Millipore ABE 457) overnight at 4 °C. After three rinses in PBS, the sections were incubated for 4 h at room temperature with donkey polyclonal anti-rabbit IgG conjugated to Rhodamine Red (1:800, Jackson ImmunoResearch Laboratories, 711-296-152, Lot 90396). Finally, the sections were washed two times in PBS-TX then once in PBS for 10 min and cover slipped with an anti-fading mounting medium (Aqua PolyMount, Polysciences Inc., Warrington, PA). Antibodies were always diluted in PBS-Tx.

Fos and Jun cell counting. The numbers of Jun-labelled cells were estimated using ImageJ (NIH freeware, Bethesda, MD). Images were first converted into 8-bit format. The threshold command was used to segment the image into labelled cells and background, with particles <100 or >1000 pixels excluded. Fos-labelled cells were counted manually. The average number of Fos- and Jun-labelled cells per section was used as a single data point. All pretreatment + glutamate conditions were compared with vehicle + glutamate by subtracting the mean number of Fos- and Jun-labelled cells in vehicle + glutamate rats from each rat in the pretreatment + glutamate condition to yield a ΔFos and ΔJun cell count for each of the pretreatment drugs.

Microdialysis and intrathecal catheter. Microdialysis fibres and an intrathecal injection catheter were implanted into rats as described previously⁶⁰. After recovery from surgery, rats were placed in a Ratum Interactive System (Bioanalytic Systems, Inc, West Lafayette, IN, USA) with a tethering system, which allowed tubing from the microdialysis catheter to be connected to a syringe pump on one end and to a refrigerated fraction collector on the other. Sample collection was done as described⁶⁰ with collections taken every 5 min during a 30 min baseline period

(with only the final three measurements assayed), for 30 min after spinal injection of either vehicle or a 50:50 mixture of WAY + UCPH (100 nmoles), and for 30 min following intraplantar injection of 1.0% formalin.

Sampling and statistical analyses. For *in vivo* studies, sample sizes were 6–9 per group, which is commonly required to obtain statistical significance, while *in vitro* studies utilized a minimum of three experimental replicates. In all experiments, animals were randomly assigned to groups, with a randomized block design used for the CPP experiments and randomization performed after BPP measurement. In all experiments, measurements were performed with the experimenter blind to the experimental conditions. All values are expressed as mean \pm s.e.m., and no samples/animals were excluded from analysis. All statistical tests were performed using GraphPad Prism version 5 for Windows (GraphPad Software, La Jolla, CA) or Statistica 6 (Stat Soft, Tulsa, OK) and all reported statistical analyses were justified based on sample size, homogeneity of variance and normal distribution of the data. The behavioural dose–response curves were analysed using between measures two-way analysis of variances (ANOVAs; pain condition \times dose) and *post hoc* comparisons between drug dose and vehicle condition, unless stated otherwise, were performed using two-sided Dunnett's test. Paw withdrawal thresholds were similarly analysed by repeated measures ANOVA (drug \times time) followed by *post hoc* comparisons between drug conditions at each time point using the Bonferroni test. For electron microscopy quantification, the grain count in each subcellular compartment was expressed as a percentage of the total grain count for that cell. Percentage counts were grouped by animal and condition (control or SNI). A two-way nested model ANOVA was followed by Scheffé *post hoc* comparisons. Immunohistochemical data were analysed using two-way ANOVAs to identify significant changes in cell counts compared with the vehicle pretreatment condition, which was normalized to zero. CPP scores were analysed using two-way ANOVAs with Bonferroni correction for multiple comparisons used to compare CPP index to a value of 50%. All other experiments were analysed using two-way ANOVAs with Bonferroni correction and two-sided tests for multiple comparisons or two-tailed Student's *t*-test for comparing two groups.

References

- Bhattacharya, M. *et al.* Nuclear localization of prostaglandin E₂ receptors. *Proc. Natl Acad. Sci. USA* **95**, 15792–15797 (1998).
- Boivin, B., Vaniotis, G., Allen, B. G. & Hebert, T. E. G protein-coupled receptors in and on the cell nucleus: a new signaling paradigm? *J. Recept. Signal Trans. Res.* **28**, 15–28 (2008).
- Tadevosyan, A., Vaniotis, G., Allen, B. G., Hebert, T. E. & Nattel, S. G protein-coupled receptor signalling in the cardiac nuclear membrane: evidence and possible roles in physiological and pathophysiological function. *J. Physiol.* **590**, 1313–1330 (2012).
- Wu, S. C. *et al.* Nuclear localization of α 1A-adrenergic receptors is required for signaling in cardiac myocytes: an 'inside-out' α 1-AR signaling pathway. *J. Am. Heart Assoc.* **3**, e000145 (2014).
- Merlen, C., Villeneuve, L. R. & Allen, B. G. Using caged ligands to study intracrine endothelin signaling in intact cardiac myocytes. *Methods Mol. Biol.* **1234**, 31–41 (2015).
- Joyal, J. S. *et al.* Subcellular localization of coagulation factor II receptor-like 1 in neurons governs angiogenesis. *Nat. Med.* **20**, 1165–1173 (2014).
- Purgert, C. A. I. *et al.* Intracellular mGluR5 can mediate synaptic plasticity in the hippocampus. *J. Neurosci.* **34**, 4589–4598 (2014).
- Jong, Y. J., Kumar, V., Kingston, A. E., Romano, C. & O'Malley, K. L. Functional metabotropic glutamate receptors on nuclei from brain and primary cultured striatal neurons. Role of transporters in delivering ligand. *J. Biol. Chem.* **280**, 30469–30480 (2005).
- Jong, Y. J., Kumar, V. & O'Malley, K. L. Intracellular metabotropic glutamate receptor 5 (mGluR5) activates signaling cascades distinct from cell surface counterparts. *J. Biol. Chem.* **284**, 35827–35838 (2009).
- Kumar, V., Jong, Y. J. & O'Malley, K. L. Activated nuclear metabotropic glutamate receptor mGlu5 couples to nuclear Gq/11 proteins to generate inositol 1,4,5-trisphosphate-mediated nuclear Ca²⁺ release. *J. Biol. Chem.* **283**, 14072–14083 (2008).
- O'Malley, K. L., Jong, Y. J., Gonchar, Y., Burkhalter, A. & Romano, C. Activation of metabotropic glutamate receptor mGlu5 on nuclear membranes mediates intranuclear Ca²⁺ + changes in heterologous cell types and neurons. *J. Biol. Chem.* **278**, 28210–28219 (2003).
- Kumar, V., Fahey, P. G., Jong, Y. J., Ramanan, N. & O'Malley, K. L. Activation of intracellular metabotropic glutamate receptor 5 in striatal neurons leads to up-regulation of genes associated with sustained synaptic transmission including Arc/Arg3.1 protein. *J. Biol. Chem.* **287**, 5412–5425 (2012).
- Alvarez, F. J., Villalba, R. M., Carr, P. A., Grandes, P. & Somohano, P. M. Differential distribution of metabotropic glutamate receptors 1a, 1b, and 5 in the rat spinal cord. *J. Comp. Neurol.* **422**, 464–487 (2000).
- Pitcher, M. H., Ribeiro-da-Silva, A. & Coderre, T. J. Effects of inflammation on the ultrastructural localization of spinal cord dorsal horn group I metabotropic glutamate receptors. *J. Comp. Neurol.* **505**, 412–423 (2007).
- D'Mello, R. & Dickenson, A. H. Spinal cord mechanisms of pain. *Br. J. Anaesth.* **101**, 8–16 (2008).
- Dogrul, A., Ossipov, M. H., Lai, J., Malan, Jr T. P. & Porreca, F. Peripheral and spinal antihyperalgesic activity of SIB-1757, a metabotropic glutamate receptor (mGluR(5)) antagonist, in experimental neuropathic pain in rats. *Neurosci. Lett.* **292**, 115–118 (2000).
- Fisher, K., Lefebvre, C. & Coderre, T. J. Antinociceptive effects following intrathecal pretreatment with selective metabotropic glutamate receptor compounds in a rat model of neuropathic pain. *Pharmacol. Biochem. Behav.* **73**, 411–418 (2002).
- Sotgiu, M. L., Bellomi, P. & Biella, G. E. The mGluR5 selective antagonist 6-methyl-2-(phenylethynyl)-pyridine reduces the spinal neuron pain-related activity in mononeuropathic rats. *Neurosci. Lett.* **342**, 85–88 (2003).
- Fisher, K. & Coderre, T. J. Hyperalgesia and allodynia induced by intrathecal (RS)-dihydroxyphenylglycine in rats. *Neuroreport* **9**, 1169–1172 (1998).
- Hu, H. J., Alter, B. J., Carrasquillo, Y., Qiu, C. S. & Gereau, R. W. Metabotropic glutamate receptor 5 modulates nociceptive plasticity via extracellular signal-regulated kinase-Kv4.2 signaling in spinal cord dorsal horn neurons. *J. Neurosci.* **27**, 13181–13191 (2007).
- Decosterd, I. & Woolf, C. J. Spared nerve injury: an animal model of persistent peripheral neuropathic pain. *Pain* **87**, 149–158 (2000).
- Lester, H. A., Miwa, J. M. & Srinivasan, R. Psychiatric drugs bind to classical targets within early exocytotic pathways: therapeutic effects. *Biol. Psychiatry* **72**, 907–915 (2012).
- Klein, J., Iovino, M., Vakil, M., Shinozaki, H. & Löffelholz, K. Ontogenetic and pharmacological studies on metabotropic glutamate receptors coupled to phospholipase D activation. *Neuropharmacology* **36**, 305–311 (1997).
- Karim, F., Wang, C. C. & Gereau, R. W. Metabotropic glutamate receptor subtypes 1 and 5 are activators of extracellular signal-regulated kinase signaling required for inflammatory pain in mice. *J. Neurosci.* **21**, 3771–3779 (2001).
- Urca, G. & Raigorodsky, G. Behavioral classification of excitatory amino acid receptors in mouse spinal cord. *Eur. J. Pharmacol.* **153**, 211–220 (1988).
- Li, X. & Clark, J. D. Hyperalgesia during opioid abstinence: mediation by glutamate and substance P. *Anesth. Analg.* **95**, 979–984 table of contents (2002).
- Ghosh, C. *et al.* Glutamate and metabotropic glutamate receptors associated with innervation of the uterine cervix during pregnancy: receptor antagonism inhibits c-Fos in rat lumbosacral spinal cord at parturition. *J. Neurosci. Res.* **85**, 1318–1335 (2007).
- Sufka, K. J. Conditioned place preference paradigm: a novel approach for analgesic drug assessment against chronic pain. *Pain* **58**, 355–366 (1994).
- Rothstein, J. D. *et al.* Localization of neuronal and glial glutamate transporters. *Neuron* **13**, 713–725 (1994).
- Liaw, W. J. *et al.* Spinal glutamate uptake is critical for maintaining normal sensory transmission in rat spinal cord. *Pain* **115**, 60–70 (2005).
- Tao, Y. X., Gu, J. & Stephens, Jr R. L. Role of spinal cord glutamate transporter during normal sensory transmission and pathological pain states. *Mol. Pain* **1**, 30 (2005).
- Yaster, M. *et al.* Effect of inhibition of spinal cord glutamate transporters on inflammatory pain induced by formalin and complete Freund's adjuvant. *Anesthesiology* **114**, 412–423 (2011).
- Niederberger, E., Schmidtke, A., Rothstein, J. D., Geisslinger, G. & Tegeder, I. Modulation of spinal nociceptive processing through the glutamate transporter GLT-1. *Neuroscience* **116**, 81–87 (2003).
- Lindemann, L. *et al.* CTEP: a novel, potent, long-acting, and orally bioavailable metabotropic glutamate receptor 5 inhibitor. *J. Pharmacol. Exp. Ther.* **339**, 474–486 (2011).
- Lea, 4th P. M., Movsesyan, V. A. & Faden, A. I. Neuroprotective activity of the mGluR5 antagonists MPEP and MTEP against acute excitotoxicity differs and does not reflect actions at mGluR5 receptors. *Br. J. Pharmacol.* **145**, 527–534 (2005).
- Montana, M. C. *et al.* The mGluR5 antagonist fenobam is analgesic and has improved *in vivo* selectivity as compared to the prototypical antagonist MPEP. *J. Pharmacol. Exp. Ther.* **330**, 834–843 (2009).
- Porter, R. H. *et al.* Fenobam: a clinically validated nonbenzodiazepine anxiolytic is a potent, selective, and noncompetitive mGlu5 receptor antagonist with inverse agonist activity. *J. Pharmacol. Exp. Ther.* **315**, 711–721 (2005).
- Chen, Y. *et al.* Evaluation of the activity of a novel metabotropic glutamate receptor antagonist (+/-)-2-amino-2-(3-cis and trans-carboxycyclobutyl-3-(9-thioxanthyl) propionic acid) in the *in vitro* neonatal spinal cord and in an *in vivo* pain model. *Neuroscience* **95**, 787–793 (2000).
- Kingston, A. E. *et al.* Inhibition of group I metabotropic glutamate receptor responses *in vivo* in rats by a new generation of carboxyphenylglycine-like amino acid antagonists. *Neurosci. Lett.* **330**, 127–130 (2002).
- Zhang, L., Lu, Y., Chen, Y. & Westlund, K. N. Group I metabotropic glutamate receptor antagonists block secondary thermal hyperalgesia in rats with knee joint inflammation. *J. Pharm. Exp. Ther.* **300**, 149–156 (2002).

41. Yang, K. Y. *et al.* Blockade of spinal glutamate recycling produces paradoxical antinociception in rats with orofacial inflammatory pain. *Prog. Neuropsychopharmacol. Biol. Psychiatry* **57**, 100–109 (2015).
42. Kanai, Y. & Hediger, M. A. The glutamate/neutral amino acid transporter family SLC1: molecular, physiological and pharmacological aspects. *Pflugers Arch.* **447**, 469–479 (2004).
43. Bramham, C. R., Torp, R., Zhang, N., Storm-Mathisen, J. & Ottersen, O. P. Distribution of glutamate-like immunoreactivity in excitatory hippocampal pathways: a semi-quantitative electron microscopic study in rats. *Neuroscience* **39**, 405–417 (1990).
44. Ottersen, O. P., Laake, J. H., Reichelt, W., Haug, F. M. & Torp, R. Ischemic disruption of glutamate homeostasis in brain: quantitative immunocytochemical analyses. *J. Chem. Neuroanat.* **12**, 1–14 (1996).
45. De Biasi, S. & Rustioni, A. Ultrastructural immunocytochemical localization of excitatory amino acids in the somatosensory system. *J. Histochem. Cytochem.* **38**, 1745–1754 (1990).
46. Schousboe, A., Scafidi, S., Bak, L. K., Waagepetersen, H. S. & McKenna, M. C. Glutamate metabolism in the brain focusing on astrocytes. *Adv. Neurobiol.* **11**, 13–30 (2014).
47. McKenna, M. C. The glutamate-glutamine cycle is not stoichiometric: fates of glutamate in brain. *J. Neurosci. Res.* **85**, 3347–3358 (2007).
48. Olstad, E., Qu, H. & Sonnewald, U. Glutamate is preferred over glutamine for intermediary metabolism in cultured cerebellar neurons. *J. Cereb. Blood Flow Metab.* **27**, 811–820 (2007).
49. Carrasco, S. & Meyer, T. STIM proteins and the endoplasmic reticulum-plasma membrane junctions. *Annu. Rev. Biochem.* **80**, 973–1000 (2011).
50. Jackson, J. G., O'Donnell, J. C., Takano, H., Coulter, D. A. & Robinson, M. B. Neuronal activity and glutamate uptake decrease mitochondrial mobility in astrocytes and position mitochondria near glutamate transporters. *J. Neurosci.* **34**, 1613–1624 (2014).
51. Genda, E. N. *et al.* Co-compartmentalization of the astroglial glutamate transporter, GLT-1, with glycolytic enzymes and mitochondria. *J. Neurosci.* **31**, 18275–18288 (2011).
52. D'Antoni, S. *et al.* Metabotropic glutamate receptors in glial cells. *Neurochem. Res.* **33**, 2436–2443 (2008).
53. Aronica, E. *et al.* Immunohistochemical localization of group I and II metabotropic glutamate receptors in control and amyotrophic lateral sclerosis human spinal cord: upregulation in reactive astrocytes. *Neuroscience* **105**, 509–520 (2001).
54. Gwak, Y. S. & Hulsebosch, C. E. Upregulation of Group I metabotropic glutamate receptors in neurons and astrocytes in the dorsal horn following spinal cord injury. *Exp. Neurol.* **195**, 236–243 (2005).
55. Nicholson, K. J., Guarino, B. B. & Winkelstein, B. A. Transient nerve root compression load and duration differentially mediate behavioral sensitivity and associated spinal astrocyte activation and mGluR5 expression. *Neuroscience* **209**, 187–195 (2012).
56. Miletic, G., Miyabe, T., Gebhardt, K. J. & Miletic, V. Increased levels of Homer1b/c and Shank1a in the post-synaptic density of spinal dorsal horn neurons are associated with neuropathic pain in rats. *Neurosci. Lett.* **386**, 189–193 (2005).
57. Yao, Y. X. *et al.* Spinal synaptic scaffolding protein Homer 1b/c regulates CREB phosphorylation and *c-fos* activation induced by inflammatory pain in rats. *Neurosci. Lett.* **559**, 88–93 (2014).
58. Hu, J. H. *et al.* Preso1 dynamically regulates group I metabotropic glutamate receptors. *Nat. Neurosci.* **15**, 836–844 (2012).
59. Chaplan, S. R., Bach, F. W., Pogrel, J. W., Chung, J. M. & Yaksh, T. L. Quantitative assessment of tactile allodynia in the rat paw. *J. Neurosci. Methods* **53**, 55–63 (1994).
60. Kumar, N., Laferriere, A., Yu, J. S., Poon, T. & Coderre, T. J. Metabotropic glutamate receptors (mGluRs) regulate noxious stimulus-induced glutamate release in the spinal cord dorsal horn of rats with neuropathic and inflammatory pain. *J. Neurochem.* **114**, 281–290 (2010).

Acknowledgements

We thank Lilly for the generous donation of LY393053, Dr J. Rothstein for the polyclonal anti-EAAT3 antibody, Dr Terence Hébert for ultracentrifuge use and editorial comments, and Manon St Louis, Johanne Ouellette, Jacynthe Laliberte and Majid Ghahremani for technical assistance. This work was supported by grants from the Canadian Institutes of Health Research (MOP-53246 & MOP-119279), and Louise and Alan Edwards Foundation to T.J.C. and the National Institutes of Health (NINDS—NS081454) to K.O'M. K.V. and P.B. were supported by studentships from the Natural Sciences and Engineering Research Council of Canada, and V.M.C. by a fellowship from Canadian Institutes of Health Strategic Training Program in Pain: Molecules to Community.

Author contributions

V.M.C., T.J.C. and K.O'M. designed the study; K.V. conducted behavioural and immunohistochemical experiments; V.M.C. performed electron and confocal microscopy, and biochemical experiments; Y-J.I.J. conducted cell-culture, glutamate-uptake/binding, Ca^{2+} -imaging and biochemical experiments; N.K. and P.B. conducted *in vivo* microdialysis and HPLC experiments; A.L., A.M. and S.T.F. performed behavioural experiments; A.R.-d-S. supervised immunohistochemistry experiments; K.V., V.M.C., Y-J.I.J. and A.L. analysed the data; V.M.C., K.V., Y-J.I.J. and A.L. prepared figures; V.M.C., K.V., T.J.C. and K.O'M. wrote the paper. K.V. and V.M.C. contributed equally to the study.

Additional information

Supplementary Information accompanies this paper at <http://www.nature.com/naturecommunications>

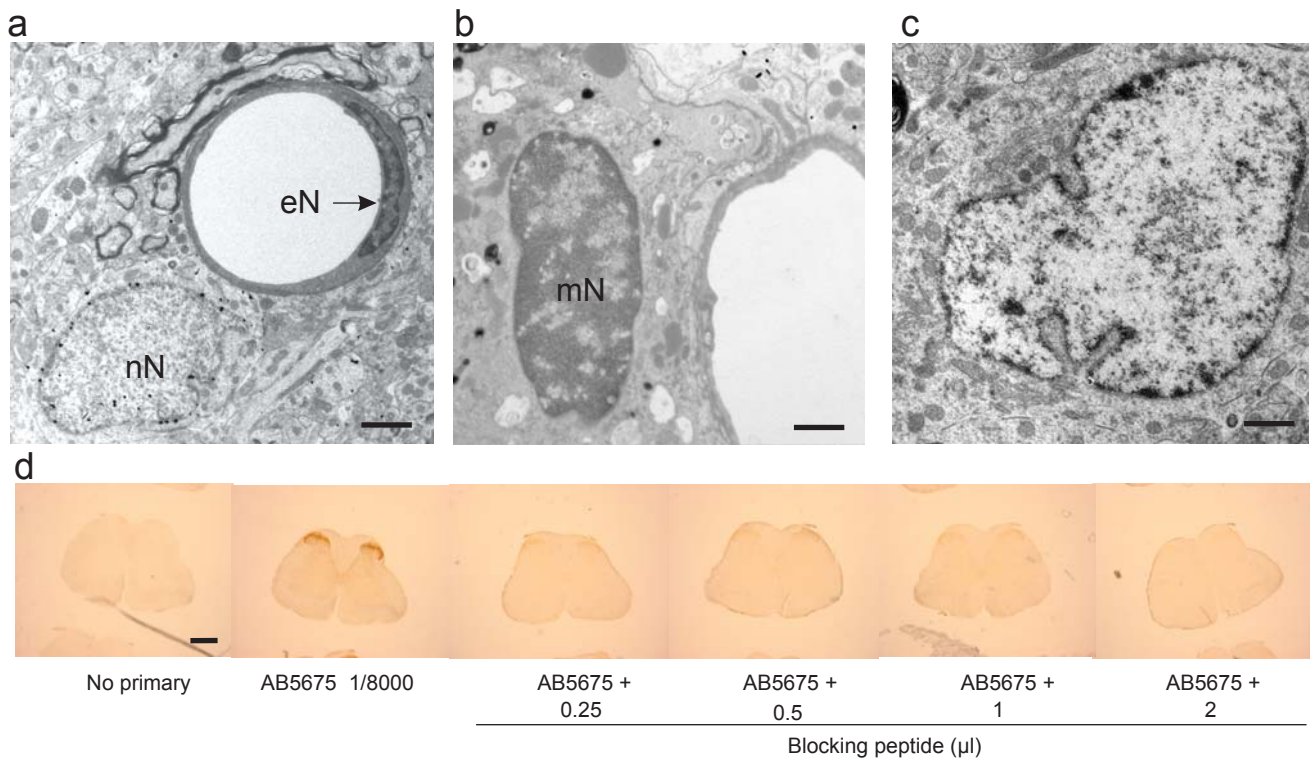
Competing financial interests: The authors declare no competing financial interests.

Reprints and permission information is available online at <http://npg.nature.com/reprintsandpermissions/>

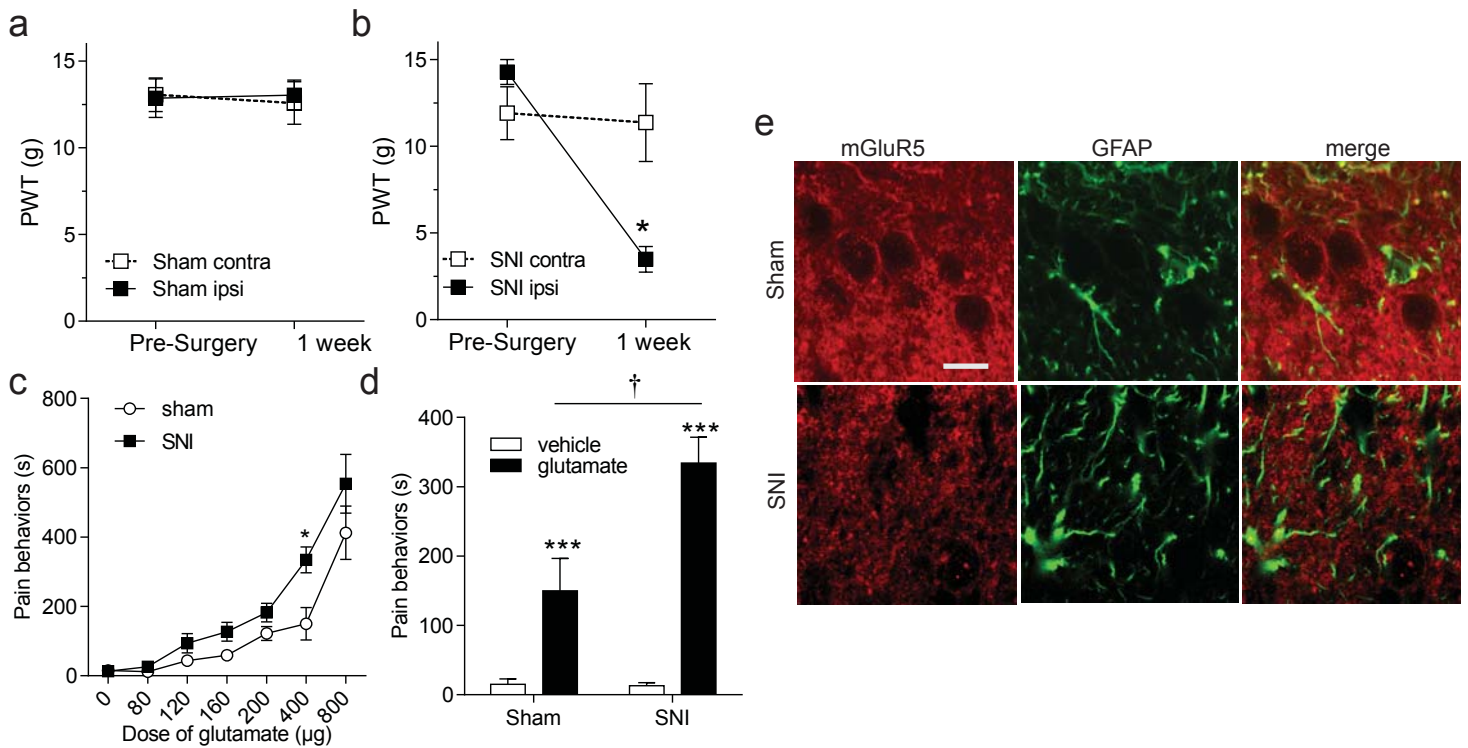
How to cite this article: Vincent, K. *et al.* Intracellular mGluR5 plays a critical role in neuropathic pain. *Nat. Commun.* 7:10604 doi: 10.1038/ncomms10604 (2016).



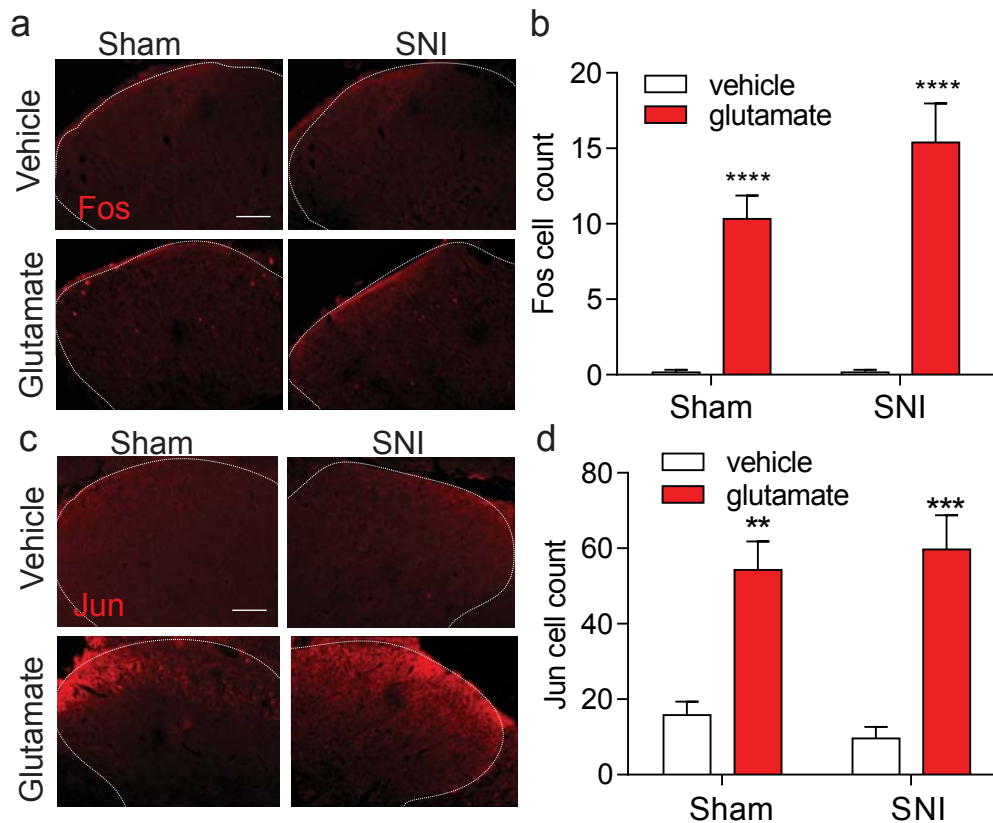
This work is licensed under a Creative Commons Attribution 4.0 International License. The images or other third party material in this article are included in the article's Creative Commons license, unless indicated otherwise in the credit line; if the material is not included under the Creative Commons license, users will need to obtain permission from the license holder to reproduce the material. To view a copy of this license, visit <http://creativecommons.org/licenses/by/4.0/>



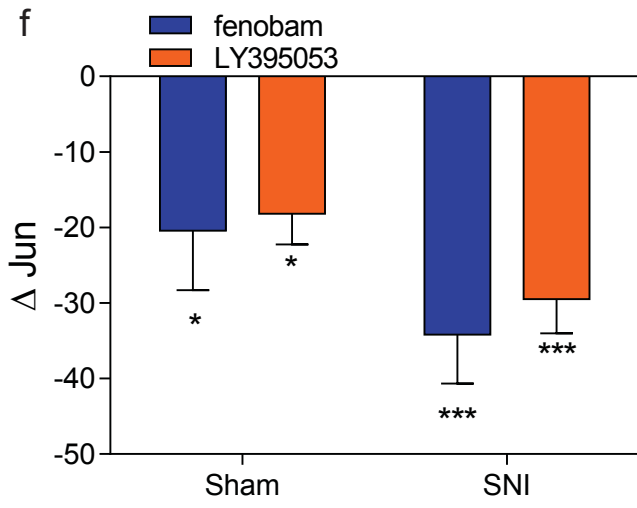
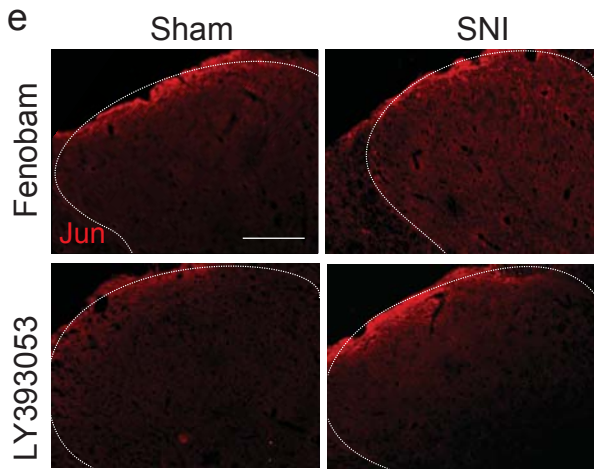
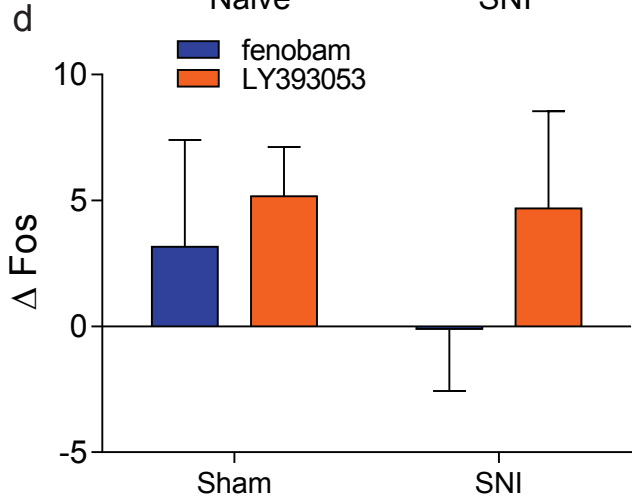
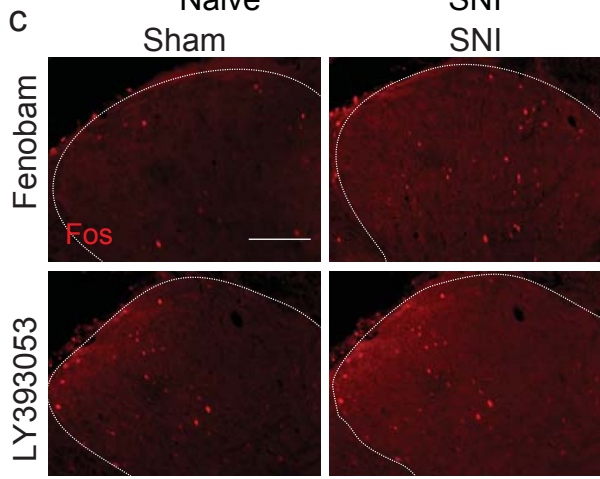
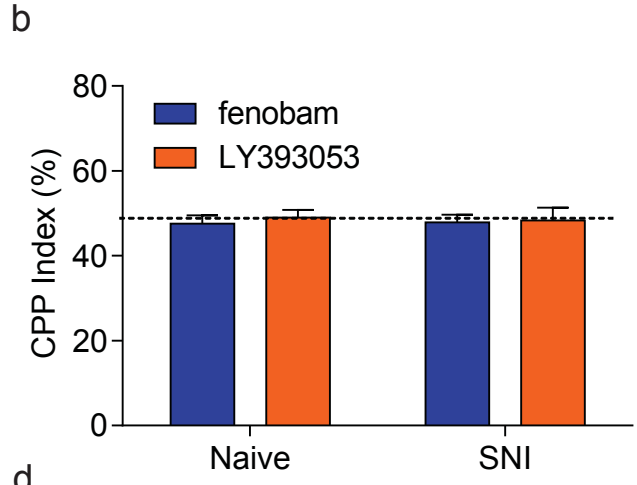
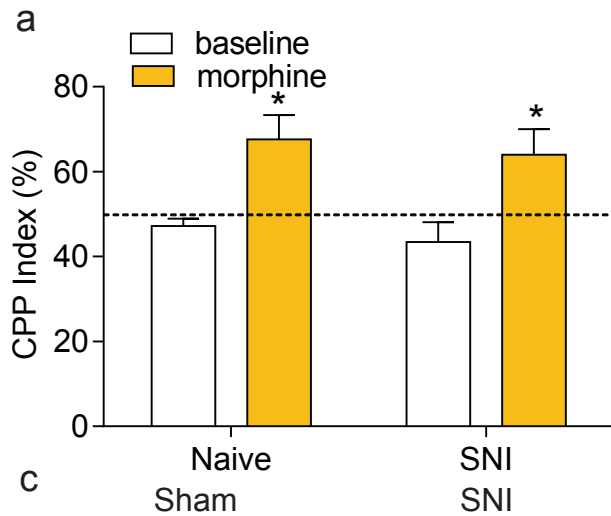
Supplementary Figure 1: EM Images of non-neuronal SCDH cells lacking mGluR5 and tests of specificity of mGluR5 antibody. (a-b) EM images showing mGluR5 immunoreactivity (as silver-intensified gold particles) in sections from SCDH. Scale bar 2 μm for a-c. (a) Gold particles are observed in a neuronal nucleus (nN), but not the nucleus of an endothelial cell (eN, endothelial cell nucleus). (b) Gold particles are not observed in a microglial nucleus (mN). (c) EM image showing no mGluR5 immunogold labelling in a neuronal nucleus in the absence of primary antibody. (d) mGluR5 diaminobenzidine staining in lumbar SCDH is decreased and ultimately abolished by preincubation of primary antibody with increasing concentration of specific blocking peptide Ag374. Scale bar 500 μm .



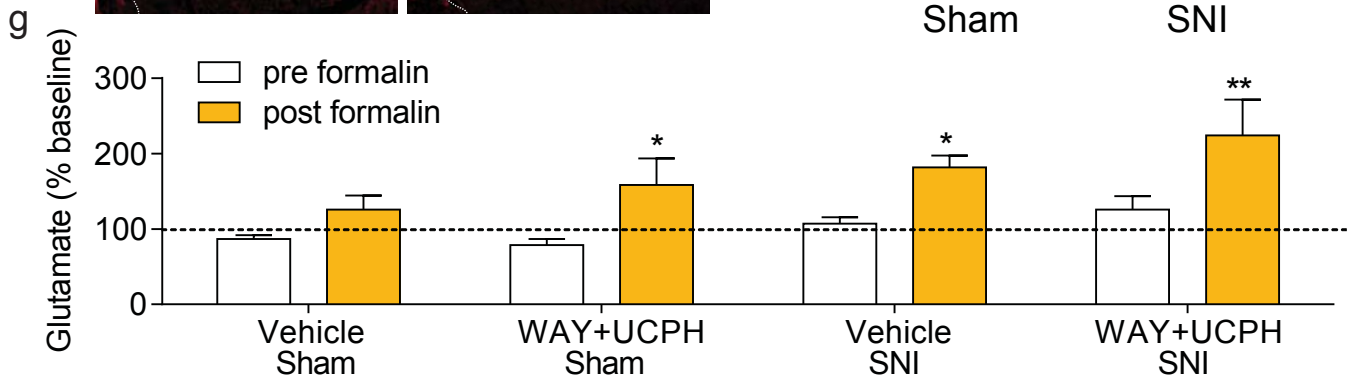
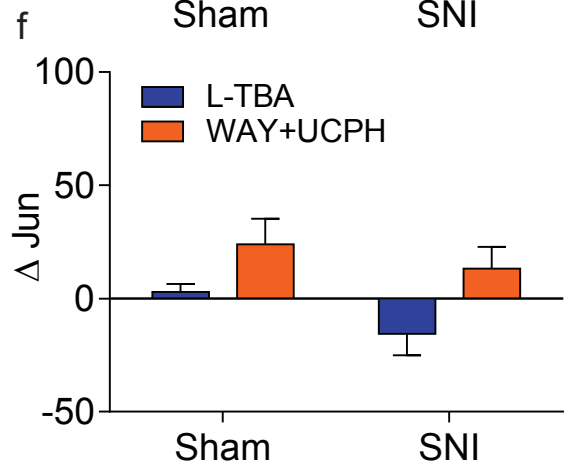
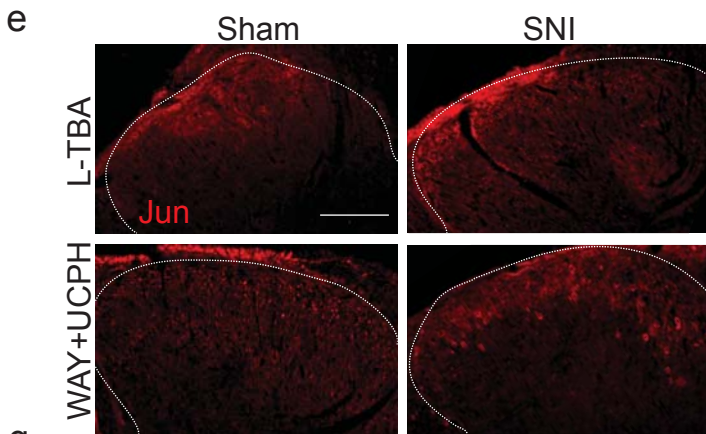
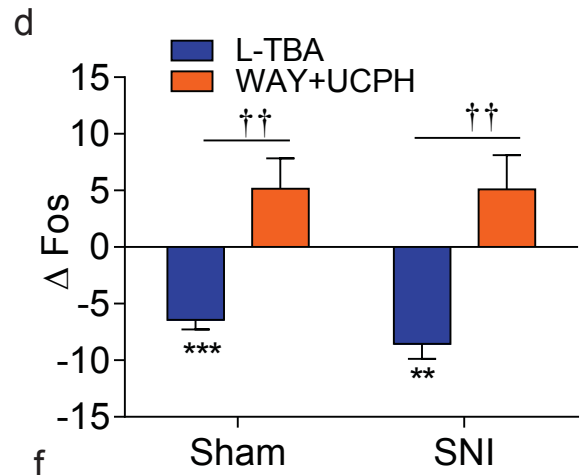
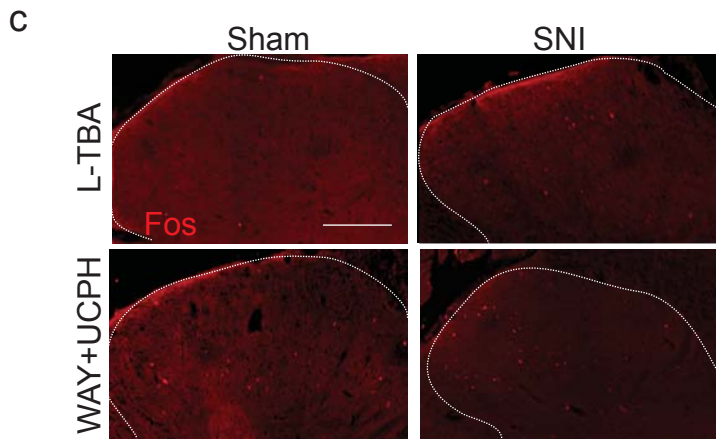
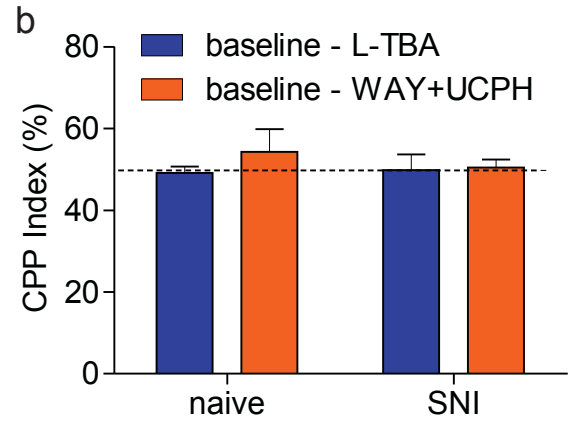
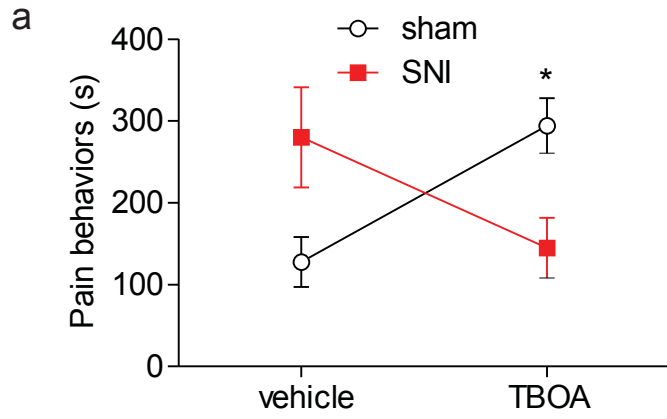
Supplementary Figure 2: Mechanical sensitivity and spinal glutamate-induced pain behaviors, and photomicrographs of mGluR5/GFAP in astrocytes, in sham and SNI rats. (a,b) Paw-withdrawal thresholds (PWTs) of sham (a) and SNI (b) rats before and one week after nerve injury. Ipsilateral, but not contralateral, PWTs are significantly reduced one week after SNI (ANOVA, $p=0.0049$), but not sham surgery). $N=5$ rats/group. (c) Dose-dependent pain behaviors induced by spinal glutamate (80-800 µg) in both sham and SNI rats. Glutamate-induced pain behaviors are higher in SNI with respect to sham rats (ANOVA, $p<0.0001$) ($*p<0.05$). $N=6$ rats/group. (d) Histogram showing pain behaviors of sham and SNI rats over a period of 30 min after spinal administration of glutamate (400 µg, black bar) or vehicle (white bar). Pain behaviors are significantly increased by glutamate in sham rats, and to a significantly greater extent in SNI rats (ANOVA, $p=0.0010$). ($***p<0.001$ with respect to vehicle; $†p<0.05$ with respect to sham). $N=6$ rats/group. (e) Immunoreactive labelling of mGluR5 (left panels, red), the astrocyte marker GFAP (centre panel, green), and double-labelling of mGluR5/GFAP (right panel) in both sham (upper panels) and SNI (lower panels) rats. Scale bar 10 µm. Note that although there is evidence of reactive astrogliosis in SNI rats, there is very little colocalization of mGluR5 and GFAP in either sham or SNI rats.



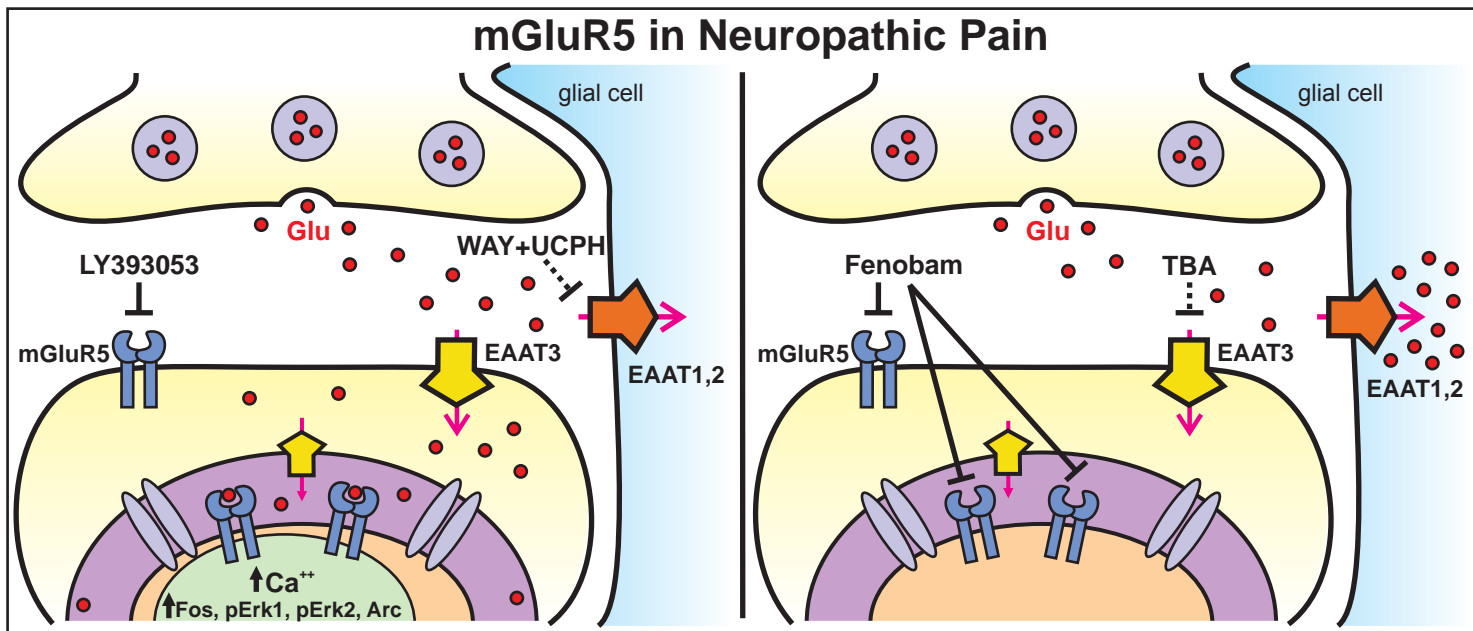
Supplementary Figure 3: Glutamate-induced gene expression in contralateral spinal cord dorsal horn of sham and SNI rats. (a) Representative Fos in contralateral SCDH (outlined with dashed lines) of sham and SNI animals following injection of vehicle or glutamate (400 μ g). Scale bar 100 μ m. (b) Glutamate significantly increases Fos in the contralateral dorsal horn in sham and SNI rats (ANOVA, $p < 0.0001$). (*** $p < 0.001$). 6-12 sections were averaged per animal, with N=6 animals/group. (c) Representative Jun in contralateral SCDH of sham and SNI animals following injection of vehicle or glutamate (400 μ g). Scale bar 100 μ m. (d) Glutamate significantly increases Jun in the contralateral dorsal horn in sham and SNI rats (ANOVA, $p < 0.0001$). (** $p < 0.01$; *** $p < 0.001$). 6-12 sections were averaged per animal, with N=6 animals/group.



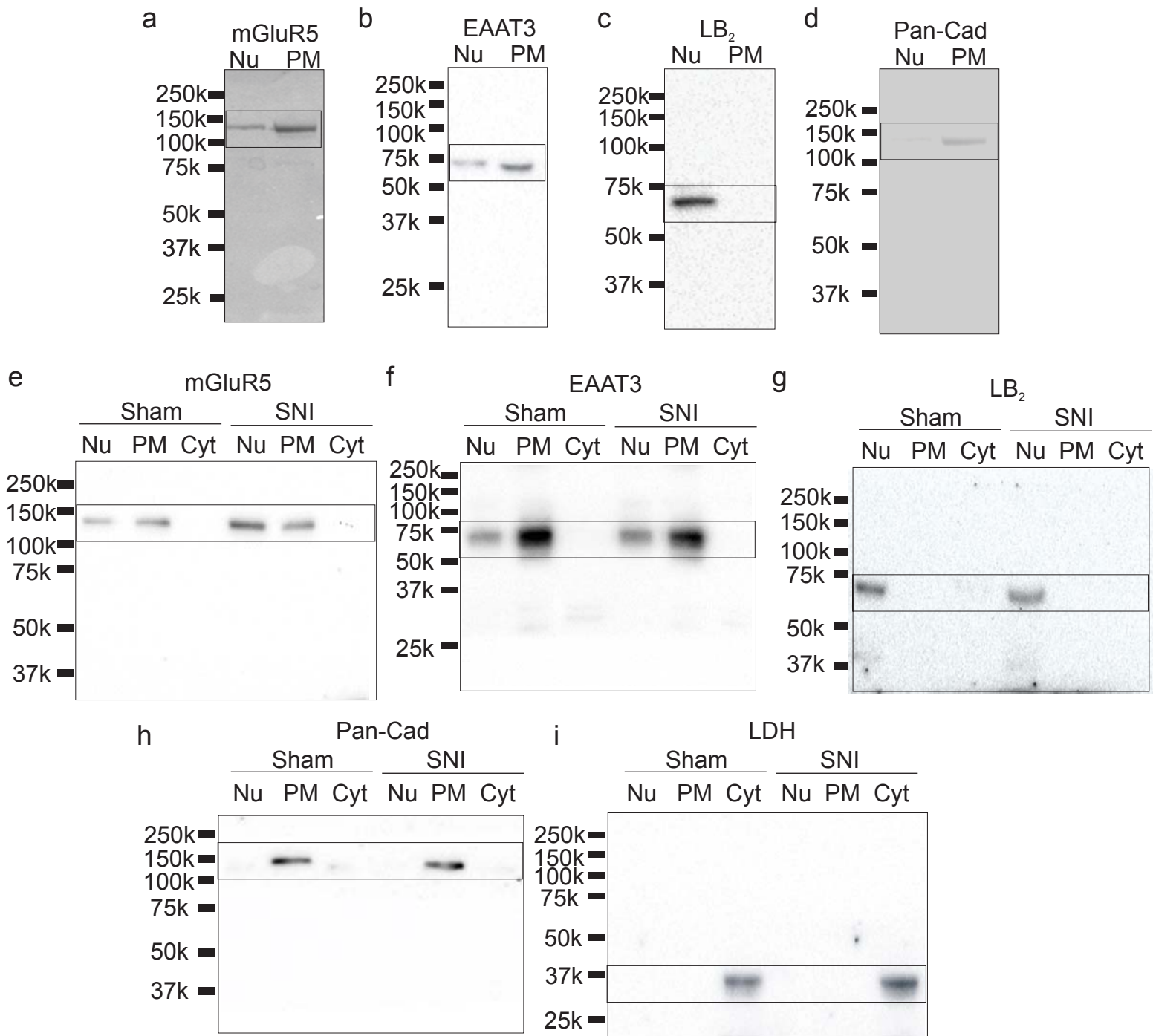
Supplementary Figure 4: Effects of fenobam and LY393053 on pain behaviors, basal PP and/or gene expression in the contralateral SCDH. (a) Morphine (10 mg/kg) produced a conditioned place preference (CPP) following two pairings in both naïve and SNI rats (naïve CPP index=67.65%, ANOVA, $p=0.0144$; SNI CPP index=63.98%, $p=0.0489$ (BPP, basal PP). N=9 rats/group. (b) Before treatment with fenobam or LY393053 (i.e., BPP), neither sham nor SNI rats differed in the time they spent in the two chambers of the apparatus. ANOVA. N=8 rats/group. (c) Representative glutamate-induced Fos in contralateral SCDH (outlined with dashed lines) of sham and SNI animals after pretreatment with fenobam or LY393053 (100 nmol each). Scale bar 100 μm . (d) Neither fenobam nor LY393053 significantly affected Fos expression in the contralateral SCDH of sham or SNI rats. ANOVA. 6-12 sections were averaged per animal, with N=6 animals/group. (e) Representative glutamate-induced Jun in contralateral SCDH (outlined with dashed lines) of sham and SNI animals following pretreatment with fenobam or LY393053 (100 nmol each). Scale bar 100 μm . (f) Jun was reduced by either fenobam or LY393053 in both SNI (fenobam $p=0.0032$; LY393053 $p=0.0013$, ANOVA) and sham (fenobam $p=0.0493$; LY393053 $p=0.0066$, ANOVA) rats. (* $p<0.05$; *** $p<0.001$). 6-12 sections were averaged per animal, with N=6 animals/group.



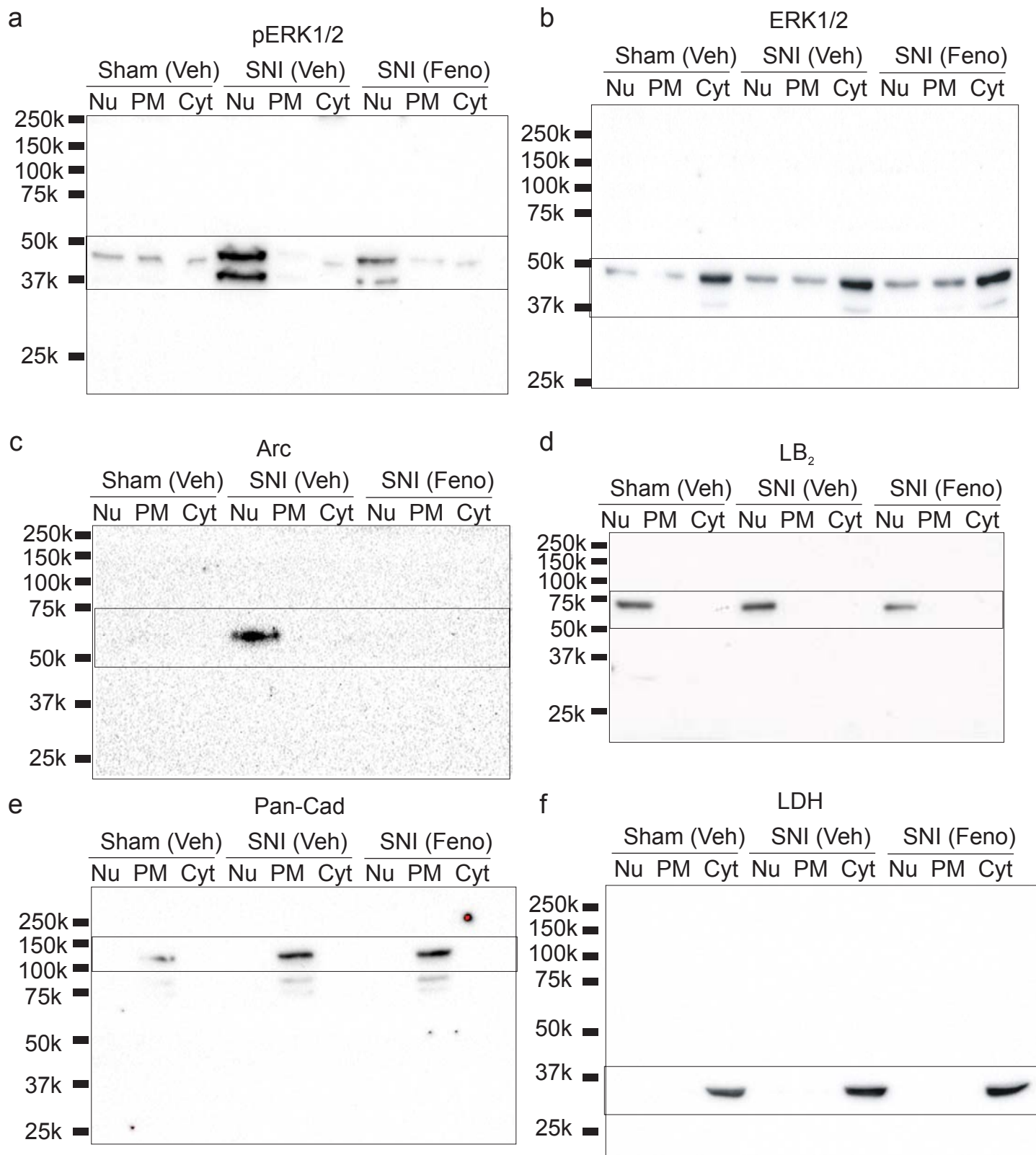
Supplementary Figure 5: Effects of L-TBA or WAY+UCPH on pain behaviors, basal CPP, and/or gene expression in the contralateral SCDH. (a) Spinal TBOA (10 nmol) has a significant interactive effect on glutamate-induced pain behaviors in sham and SNI rats (ANOVA, $p=0.0019$). Thus, TBOA significantly potentiates pain behaviors in sham animals ($p=0.0193$) and significantly reduces pain behaviors in SNI rats (ANOVA, $p=0.0317$). * $p<0.05$ with respect to glutamate alone. $N=6$ rats/group. (b) Before treatment with L-TBA or WAY+UCPH, neither naive nor SNI rats differed in the time they spent in the two chambers of the apparatus (BPP, basal place preference). (ANOVA). $N=9$ rats/group. (c) Representative glutamate-induced Fos in the contralateral SCDH (outlined with dashed lines) following pretreatment with either L-TBA or WAY+UCPH (100 nmol each). Scale bar 100 μm . (d) Fos in contralateral SCDH was decreased in both sham and SNI rats by pretreatment L-TBA (ANOVA, Sham $p=0.0006$; SNI $p=0.0014$), but was not significantly affected in either sham or SNI rats by pretreatment with WAY+UCPH. (** $p<0.01$ versus vehicle). Consequently, Fos was significantly lower in rats treated with L-TBA as compared to those treated with WAY+UCPH ($\dagger\dagger p<0.01$ L-TBA versus WAY+UCPH). 6-12 sections were averaged per animal, with $N=6$ animals/group. (e) Representative glutamate-induced Jun in contralateral SCDH (outlined with dashed lines) of sham and SNI animals following pretreatment with either L-TBA or WAY+UCPH (100 nmol each). Scale bar 100 μm . (f) Jun in contralateral SCDH was not significantly affected by either L-TBA or WAY+UCPH in either sham or SNI rats (ANOVA). 6-12 sections were averaged per animal, with $N=6$ animals/group. (g) Changes in glutamate levels following spinal treatment with vehicle or WAY+UCPH (100 nmol) and hind paw formalin injection in sham and SNI rats. In sham rats ($N=6$), formalin injection increased spinal glutamate concentrations after WAY+UCPH ($p<0.05$), but not vehicle. In SNI rats ($N=7$), formalin injection increased spinal glutamate both after vehicle (* $p<0.05$) or WAY+UCPH (** $p<0.01$). ANOVA.



Supplementary Figure 6: Schematic summary illustrating the effects of targeted mGluR5 treatments on neuropathic pain. Glutamate (Glu) is released from presynaptic terminals and binds at two pools of functional mGluR5, at the cell surface and at intracellular membranes of postsynaptic neurons in spinal cord dorsal horn (SCDH). mGluR5 at the nuclear membrane is upregulated in neuropathic pain conditions and is critical for enhanced nuclear Ca²⁺-dependent Fos, pERK1, pERK2 and Arc in SCDH. **Left panel**, Selectively blocking cell surface mGluR5 with LY393053 has little effect on neuropathic pain behaviors or Fos. Selectively blocking glutamate uptake into glial cells with excitatory amino acid transporter (EAAT) 1,2 inhibitors (WAY + UCPH) also does not reduce neuropathic pain or Ca²⁺-dependent Fos, and can even induce pronociceptive effects in neuropathic and/or non-neuropathic conditions (not depicted) due increased synaptic and extrasynaptic glutamate. **Right panel**, Blocking both intracellular and cell surface mGluR5 with fenobam dramatically reduces both neuropathic pain and Ca²⁺-dependent Fos, ERK1, ERK2 and Arc. Selectively blocking glutamate uptake into neurons with an EAAT-3 inhibitor (TBA) also dramatically reduces neuropathic pain and Fos. Together these results highlight the importance of intracellular mGluR5 in SCDH to neuropathic pain.



Supplementary Figure 7: Full length western blots for mGluR5, EAAT3 and cellular markers. Uncropped immunoblots of **a)** mGluR5, **b)** EAAT3, **c)** LB₂ (Lamin B₂), **d)** Pan-Cad (Pan-cadherin) comprising panels in Figure 1d, and uncropped immunoblots of **e)** mGluR5, **f)** EAAT3, **g)** LB₂ **h)** Pan-Cad and **i)** LDH (lactate dehydrogenase) comprising panels in Figure 3d. Molecular weights are indicated in the scale on the left (SNI, spared nerve injury; Nu, nuclear; PM, plasma membrane; Cyt, cytosolic).



Supplementary Figure 8: Full length western blots for pERK1/2, ERK1/2 and Arc/Arg3.1 (Arc) and cellular markers. Uncropped immunoblots of **a**) pERK1/2, **b**) ERK1/2, **c**) Arc, **d**) LB₂ (lamin B₂), **e**) Pan-Cad (Pan-cadherin), and **f**) LDH (lactate dehydrogenase) comprising panels in Figure 4a. Molecular weights are indicated in the scale on the left (SNI, spared nerve injury; Veh, vehicle; Feno, fenobam; Nu, nuclear; PM, plasma membrane; Cyt, cytosolic).